Université d'Ottawa · University of Ottawa

Université d'Ottawa · University of Ottawa

FACULTÉ DES ÉTUDES SUPÉRIEURES ET POSTDOCTORALES

FACULTY OF GRADUATE AND POSTDOCTORAL STUDIES

Jun YANG
AUTEUR DE LA THÈSE - AUTHOR OF THESIS

M. A. Sc. (Mechanical Engineering)
GRADE - DEGREE

Department of Mechanical Engineering
FACULTÉ, ÉCOLE, DÉPARTEMENT - FACULTY, SCHOOL, DEPARTMENT

TITRE DE LA THÈSE - TITLE OF THE THESIS

Effect of Non-uniform Axial Heat-flux Distribution on Critical Heat-flux

S.C. Chen
DIRECTEUR DE LA THÈSE - THESIS SUPERVISOR

D. Groeneveld
CO-DIRECTEUR DE LA THÈSE - THESIS CO-SUPERVISOR

EXAMINATEURS DE LA THÈSE - THESIS EXAMINERS

J. Gu

R. Milane

J.-M. De Koninck, Ph.D

LE DOYEN DE LA FACULTÉ DES ÉTUDES SUPÉRIEURES ET POSTDOCTORALES

DEAN OF THE FACULTY OF GRADUATE AND POSTDOCTORAL STUDIES

EFFECT OF NON-UNIFORM AXIAL HEAT-FLUX DISTRIBUTION ON CRITICAL HEAT FLUX

Jun Yang

A thesis submitted to the Faculty of Graduate and Postdoctoral Studies
in partial fulfillment of the requirements for the degree of

MASTER OF APPLIED SCIENCE

in Mechanical Engineering

Ottawa-Carleton Institute for Mechanical and Aerospace Engineering
University of Ottawa
Ottawa, Canada

December 2003

Your file Votre référence
ISBN: 0-494-01652-3
Our file Notre référence
ISBN: 0-494-01652-3

ABSTRACT

An experimental study of the effect of axial flux distribution (AFD) on critical heat flux (CHF) was conducted in directly heated tubes at the Freon-equivalent CANDU reactor conditions of interest. CHF measurements were obtained on test sections with four non-uniform AFD profiles as well as a uniform AFD profile using HFC-134a as a test fluid. Each of the non-uniform AFD test sections had a stepped cosine heat flux profile with approximately 16 heat flux steps. The test conditions covered a pressure range of 1662 to 2389 kPa, a mass flux range of 2827 to 4648 kg m^{-2} s^{-1} and an inlet quality range of -0.909 to -0.002.

The results showed that the AFD has a strong effect on CHF at high dryout qualities. The CHF values for non-uniform AFDs can be up to 50% lower than that for uniform AFD depending on the pressure, mass flux and the shape of the AFD profile. The AFD effect on CHF decreases with the decrease in dryout quality. At low dryout qualities, the effect of AFD on CHF is small or non-existent.

In general, the AFD effect on critical power for constant inlet conditions is small. For high inlet subcoolings, the critical powers for the four non-uniform AFD profiles are almost indistinguishable, but are slightly higher than that for the uniform heat flux profile. At low inlet subcoolings, the critical power for inlet peak AFD profile is slightly higher than that for the outlet peak AFD profile. The critical power for the uniform profile approaches to those for the non-uniform profiles as the inlet subcooling decreases and can be slightly higher than those for the non-uniform profiles for an inlet quality of about –0.2.

The boiling length average approach with the boiling length starting point at the onset of annular flow was found to give the best prediction of the AFD effect on CHF, compared with the other CHF prediction methods evaluated. This optimum method provides very good prediction for the critical power as well as for the CHF location. This conclusion was confirmed by the experimental non-uniform AFD CHF data in water.

ACKNOWLEDGEMENTS

I would like to express my deep appreciation to both my advisors, professors S.C. Cheng and D.C. Groeneveld, for their technical guidance and expertise throughout this study and I thank Dr. L.K.H. Leung of AECL CRL for his valuable comments and advice during the course of this research.

I am grateful to the Department of Mechanical Engineering of the University of Ottawa and the Ottawa-Carleton Institute for Mechanical and Aerospace Engineering for the opportunity to pursue this research in two-phase flow heat transfer. I also would like to thank my friends in the Thermalhydraulics Group of the University of Ottawa, Dr. A. Durmayaz, Dr. D. Shang, Dr. S. Peng, especially M. El Nakla, Ph.D. student, with whom I had many valuable and pleasurable discussions on science and technology.

Finally, special thanks go to my wife, Lanqin Yuan, and my son, Muyun Yang, for their patience, understanding, and encouragement.

The financial support provided by AECL and NSERC is gratefully acknowledged.

TABLE OF CONTENTS

LIST OF TABLES

LIST OF FIGURES

NOMENCLATURE

CHF	critical heat flux (kW m^{-2})
c_p	specific heat (kJ kg^{-1} K^{-1})
D	tube diameter (mm)
G	mass flux (kg m^{-2} s^{-1})
g	acceleration due to gravity (m s^{-2})
i	enthalpy (kJ kg^{-1})
i_{fg}	latent heat of vaporization (kJ kg^{-1})
Δi_{in}	inlet subcooling enthalpy (kJ kg^{-1})
h_{fo}	heat transfer coefficient for total flow assumed liquid (kW m^{-2} K^{-1})
I	electrical current (A)
j	volumetric flux (superficial velocity) (m s^{-1})
k	peaking factor ($k=q''_{max}/q''_{avg}$)
k_f	thermal conductivity of liquid phase (kW m^{-1} K^{-1})
L	length (m)
L_B	boiling length (m)
L_h	heated length (m)
$\dot{m}$	mass flow rate (kg s^{-1})
Power	power (kW)
P	pressure (kPa)
P_h	heated perimeter (m)
q''	heat flux (kW m^{-2})
R	electrical resistance
T	temperature (°C)
$T_f(z)$	bulk liquid temperature at axial position z (°C)
$T_w(z)$	wall temperature at axial position z (°C)
$\Delta T_{sat}(z)$	superheat at axial position z (°C)
$\Delta T_{sub}(z)$	subcooling at axial position z (°C)
U	electric potential difference (V)
W	mass flow rate (for the derivation of annular liquid film dryout model) (kg s^{-1})
X	thermodynamic quality (-)
z	axial location (mm)

Abbreviations

AECL	Atomic Energy of Canada Limited
AFD	axial heat flux distribution
CHF	critical heat flux
CHFPR	ratio of predicted to measured critical power
CANDU	Canadian Deuterium Uranium Reactor
DAS	data acquisition system
DC	direct current

ID	inside diameter
NSERC	Natural Sciences and Engineering Research Council of Canada
NU	non-uniform
OD	tube outside diameter
QA	quality assurance
RFD	radial heat flux distribution
RTD	resistance temperature detector
TS No. 1	non-uniform AFD test section No.1
TS No. 2	non-uniform AFD test section No.2
U of O	University of Ottawa

Greek letters

α	void fraction (-)
μ	viscosity ($N\ s\ m^{-2}$)
σ	surface tension ($N\ m^{-1}$)
ρ	density ($kg\ m^{-3}$)

Subscripts

2m	the total heated length of the actual test sections with actual stepped AFD profiles
2.4m	2.4-meters-equivalent (corresponding to the full AFD profiles for the TS No. 1 and TS No. 2 cases)
avg	average
act	actual
BLA	boiling length average
cr	critical
do	dryout
EU	uniform equivalent
exp	experimental
ext.in	imaginary inlet extension part
ext.out	imaginary outlet extension part
f	saturated liquid
g	saturated vapour
i	inside
in	inlet
loc	local conditions
m	step number
max	maximum
min	minimum
n	total step number
non	non-uniform
o	outside
OAF	onset of annular flow
ONB	onset of nucleate boiling

opt	optimum
OSV	onset of significant void fraction
out	outlet
pred	predicted
R	Freon
sat	saturation
sub	subcooled
TS	test section
U	uniform
W	water

1. INTRODUCTION

Boiling heat transfer can be encountered in many industrial applications such as in evaporators, steam boilers, and particularly nuclear reactors. One of the most important phenomena in boiling heat transfer is the critical heat flux (CHF).

CHF represents a condition after which the local heat transfer coefficient decreases sharply as a result of the replacement of continuous liquid by continuous vapour adjacent to the heat transfer surface. For a system where the surface heat flux is used as the independent variable, CHF is defined as that condition under which a small increase in the surface heat flux leads to a large increase in the surface temperature. Instead of CHF, terms such as "dryout", "departure from nucleate boiling" (DNB), "burnout', and "boiling crisis" are also used to describe this phenomenon.

The CHF condition presents an important performance limit of a thermal system in which the main mode of heat transfer is boiling. Any nuclear reactor must operate below the CHF conditions to allow sufficient safety margin during the normal or transient operation. The CHF condition may be induced during an accidental increase in power, or a sudden decrease in flow and pressure. In a nuclear reactor, one of the most serious accidents is the loss-of-coolant accident (LOCA), which may be caused by a rupture in the primary coolant system. The consequence of the CHF occurrence here implies a sharp reduction in heat transfer rate, a rapid rise in wall temperature and, at certain conditions, even physical burnout.

The importance of the critical heat flux phenomenon has led to the development of a large number of CHF prediction methods. Most of these methods were primarily developed based on results obtained from experimental studies using test sections with uniform axial heat flux distribution (AFD). However, the heat flux in a nuclear reactor is not uniform and its profile changes with fuel burn up. Figure 1.1 shows the typical axial power distribution in a reactor. Moreover, local heat flux peaking may occur for a number of reasons, e.g., end flux peaking effects in short fuel bundles, use of control or

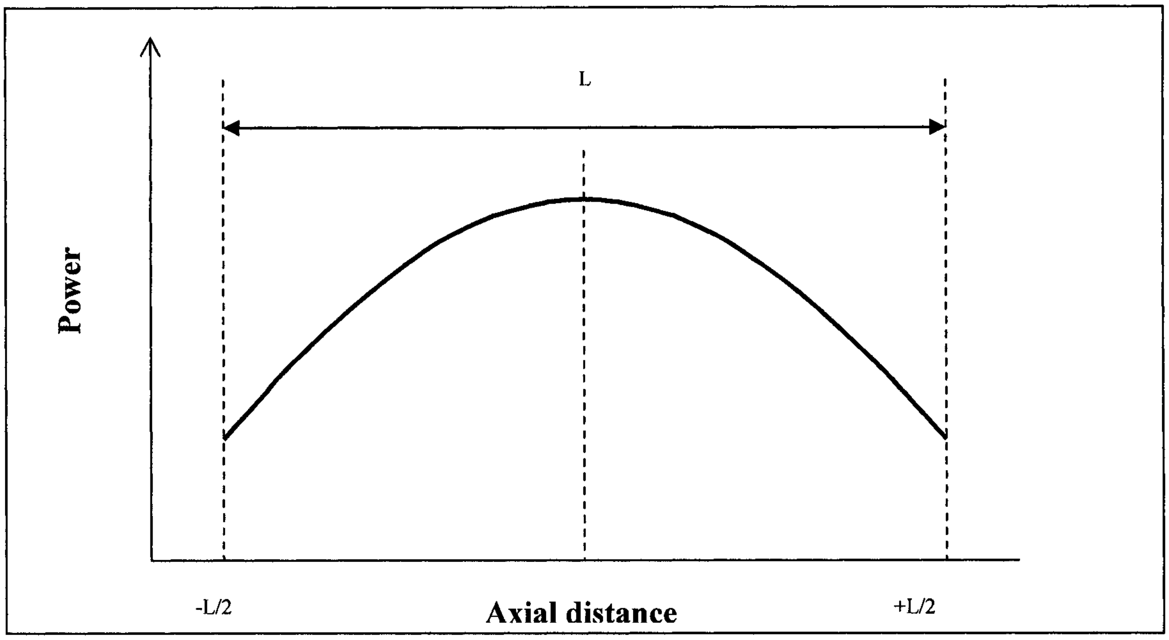

Figure 1.1 Typical Axial Power Distribution in Reactor.

booster rods, fuel densification, etc. Therefore, the effect of axial heat flux distribution on critical power needs to be considered when determining the minimum safety margin.

The primary objectives of this thesis research are: (i) to investigate the effect of axial heat flux distribution on CHF at CANDU reactor conditions of interest, and (ii) to recommend a method to determine the effect of AFD on the CHF prediction.

CHF experiments on full-scale fuel-bundle-simulators employing the same working fluid as used in CANDU reactors are very expensive. A lot of power is required to perform such experiments. The combination of high power and the actual operating conditions of a nuclear reactor could lead to dangerous and inconvenient conditions. The fluid-to-fluid modeling technique is a cost-effective alternative. It permits us to obtain water-equivalent CHF data on various AFD profiles via experimentation using the lower-temperature, lower-pressure and lower-latent-heat modeling fluid, such as HFC-134a, at a small fraction of the cost of water testing.

The experiments were performed at pressures between 1662 to 2389 kPa, and mass fluxes between 2827 and 4648 kg $m^{-2} s^{-1}$. These conditions are equivalent to 10 to 14 MPa, and 4000 to 6500 kg $m^{-2} s^{-1}$ in water. AFD profiles with inlet, middle and outlet peaks were all investigated and their CHFs and critical powers were compared with those of the uniform heat flux distribution.

Experimental results were analyzed based on both constant local conditions and constant inlet conditions. Parametric effects were studied in detail. Some well-known CHF prediction methods for non-uniform AFD in tubes were evaluated. The prediction results were compared with experimental data. The optimum CHF prediction method was determined and confirmed by the data in water from other investigators.

To explore AFD effect on CHF in tubes with flow obstruction, experiments were also conducted using the non-uniform test section with outlet peak and the reference uniform test section, all equipped with flow obstructions. These additional experiments were performed in HFC-134a, at a pressure of 1662 kPa, and mass fluxes of 2120, 2826 and 3533 kg m^{-2} s^{-1}. The corresponding water-equivalent conditions are 10 MPa, and 3000, 4000 and 5000 kg m^{-2} s^{-1}. The experimental results and the data analyses are presented in Appendix A.

The thesis work is divided into five chapters and an introduction and a conclusion. Chapter 2 reviews the existing literature on the fundamentals of critical heat flux and the effect of non-uniform axial heat flux distribution on CHF, which is pertinent to the thesis project. Chapter 3 describes the AFD CHF experiments while Chapter 4 presents the test results. Chapter 5 contains data analyses based on constant local conditions and constant inlet conditions. Chapter 6 gives a detailed assessment of the presented CHF prediction methods and determines the optimal method for the non-uniform AFD case.

2. LITERATURE REVIEW

2.1 Boiling Heat Transfer

2.1.1 Pool Boiling Heat Transfer

Pool boiling occurs on a heated surface submerged in a large volume of stagnant liquid while flow boiling occurs in internal and external forced and natural convective flow systems. In pool boiling, for a given fluid pressure, coolant temperature and heated surface configuration, the boiling curve (Figure 2.1) presents a unique relationship between the surface heat flux and the surface temperature.

On the boiling curve of Figure 2.1, four regions can be identified. In region A-B, the heat flux is low. The heat transfer process is single-phase convective heat transfer to the subcooled liquid phase. As the heat flux is increased the wall temperature exceeds the saturation temperature. The onset of nucleate boiling occurs at the active nucleation sites such as tiny pits or scratches where the wall superheat becomes sufficient to cause vapour nucleation. In region B-C, vapour bubbles created at the nucleation site grow and detach from the wall and condense before reaching the pool surface. When the liquid temperature rises to the saturation temperature, vapour bubbles no longer condense in the liquid but rise to the pool surface. The bubbles transport the latent heat of the phase change and increase the convective heat transfer by agitating the liquid near the wall; therefore, the heat transfer coefficient here is much higher than that at single-phase convection. The bubbles' population increases as the heat flux is increased. Eventually, the vapour production becomes so large isolating the heated surface from being cooled by the liquid. As a result, an unstable, and finally a stable vapour blanket over the heated surface form. The heat transfer process turns into the transition boiling (region C-D) and then the film boiling (region D-E) accompanied with a sharp decrease of heat transfer coefficient. The transition from nucleate boiling to transition boiling is defined as the critical heat flux condition, which marks the upper limit of nucleate boiling where the

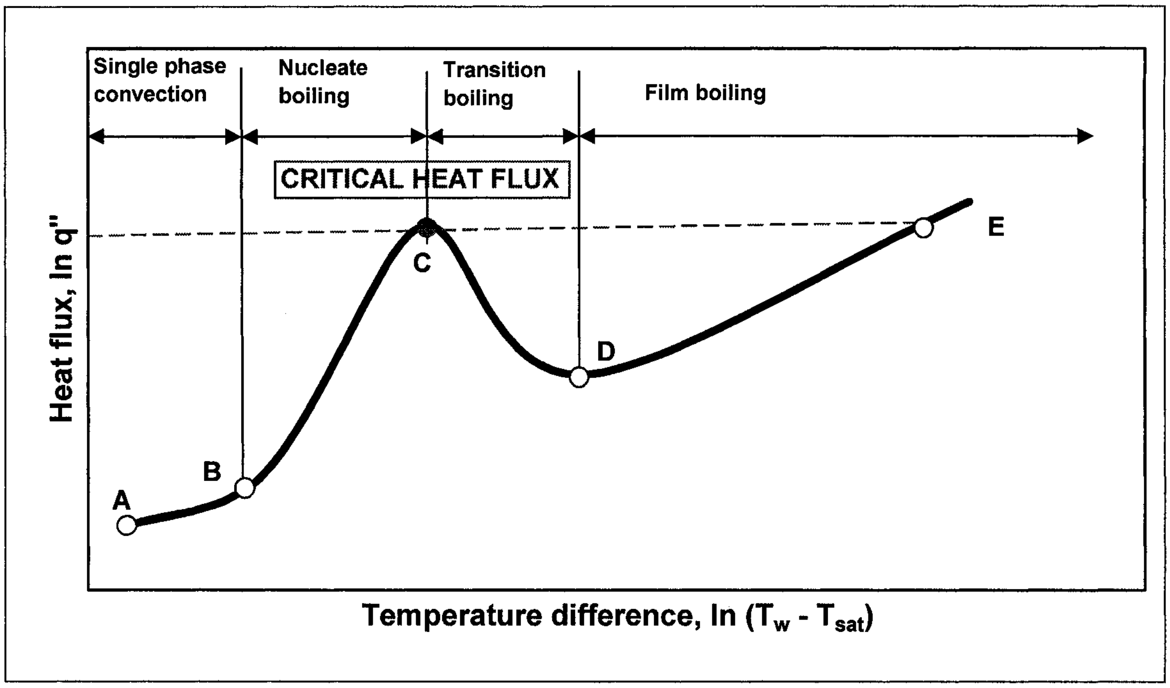

Figure 2.1 Pool Boiling Heat Transfer Curve (Collier, 1994).

interaction of the liquid and vapour steams causes a restriction of the liquid supply to the heated surface.

The boiling curves for flow boiling and pool boiling have similar general form. In the following sections, the flow boiling heat transfer, particularly for the upward flow confined in a heated vertical tube, will be discussed in detail because this type of boiling is directly related to the topic of the thesis research.

2.1.2 Flow Regimes

Compared to pool boiling, the situation of flow boiling is more complex because the liquid and the vapour generated take up a variety of configurations known as flow patterns when liquid is vaporized in a heated channel. The particular flow pattern depends on the conditions of pressure, mass flux, heat flux, and channel geometry. The main flow patterns encountered in vertical upward flow are shown schematically in Figure 2.2a. They are summarized as follows:

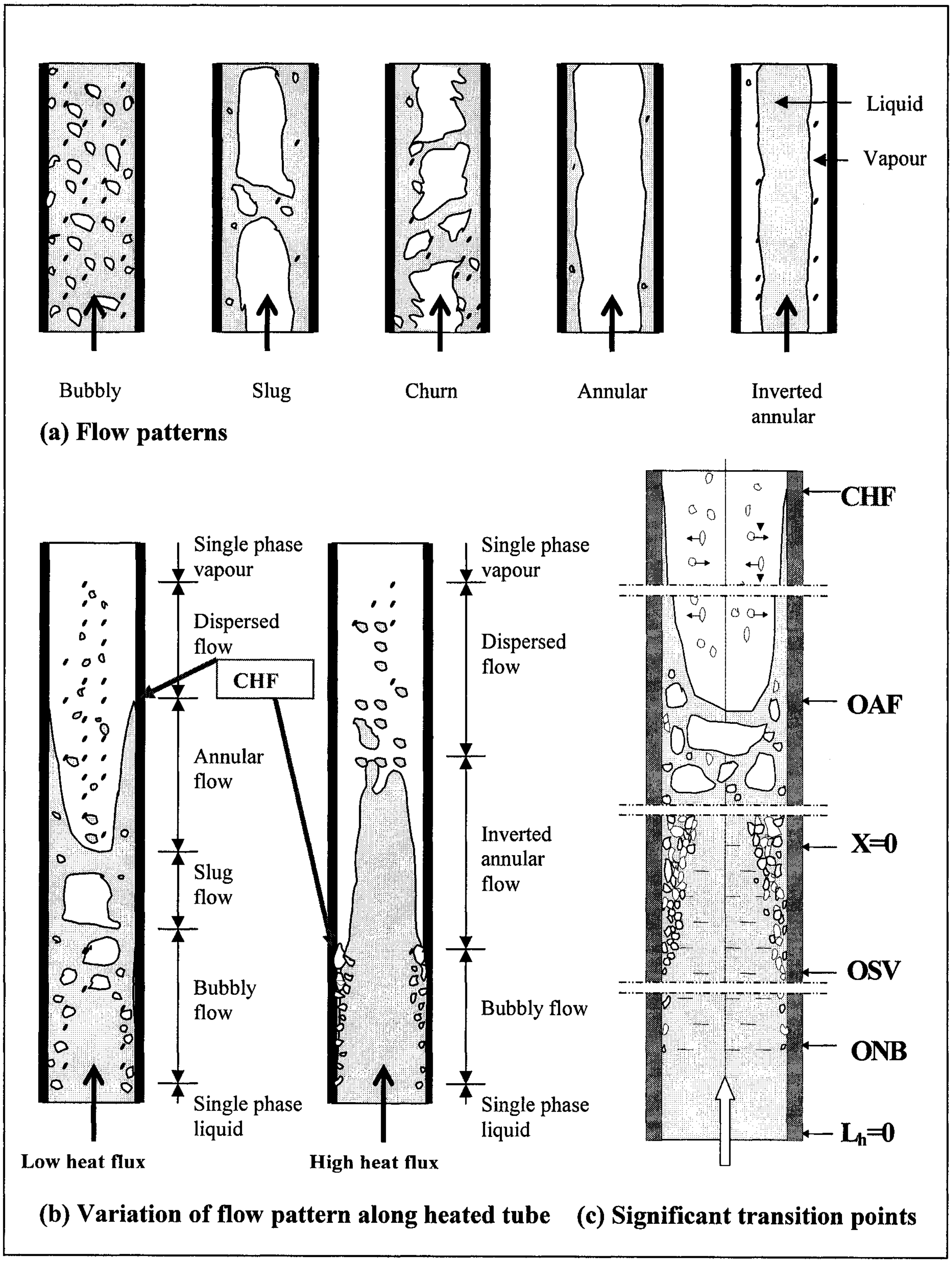

Figure 2.2 Flow Patterns in Vertical Flow (Collier, 1994).

- **Bubbly flow**. Vapour phase is distributed as discrete, basically uniform sized bubbles in a continuous liquid phase.
- **Slug flow**. Bullet-shaped vapour plugs are separated by liquid slugs. Liquid film prevents the vapour bubbles from contacting the wall.
- **Churn flow**. This flow regime is formed by the breakdown of the large vapour plugs in slug flow. The bubbles flow disorderly through the liquid. The flow has an oscillatory or time varying character.
- **Annular flow**. A liquid film forms at the channel wall. The vapour and entrained droplets flow in the central core.
- **Inverted annular flow**. A vapour blanket covers the channel wall with liquid flowing in the central core.

When a liquid flow moves upward through a heated vertical tube, the flow pattern evolves along the heated length and this change is a strong function of heat flux. Figure 2.2b shows the evolution of the flow pattern along the length of a uniformly heated vertical tube at low heat flux and high heat flux, respectively.

For low heat flux conditions, the flow patterns along the channel may be in turn the single phase liquid flow, the bubbly flow, the slug flow, the annular flow, the dispersed flow (or drop flow) and the single phase vapour. In annular flow region, the liquid film on the wall is very thin, thus the thermal conductivity is very effective. It prevents the liquid on the wall from being superheated to a temperature which would allow bubble nucleation, i.e., the nucleation is suppressed. The heat transfer process here is referred to the two-phase forced convective heat transfer. The CHF (dryout) occurs once the liquid film is totally evaporated downstream in the annular flow region accompanied with an increase in the wall temperature.

When high heat flux is present, the CHF may occur at any location along the heated length depending on the heat flux level. One case is that the CHF occurs at the end of the bubbly flow. When the bubble population increases to such a degree that the bubbles can not be carried away promptly by the flow, some areas of the heated surface are covered by vapour blanket formed by the merge of the bubbles. The heated surface will be no longer contacted by continuous liquid. As a result, the departure from nucleate boiling (DNB) occurs along with a sharp wall temperature increase (much higher than that resulting from the dryout of the liquid film); the flow pattern changes into inverted annular flow and then dispersed flow. Detailed descriptions of the flow regimes can be found in Collier (1994) and Groeneveld (1992).

2.1.3 Boiling Map for Vertical Flow

Figure 2.3 shows the various regions of two-phase heat transfer in forced-convection boiling on a plot of heat flux versus mass quality. The variation of heat transfer coefficient with quality for each heat flux level represented in Figure 2.3 is given in Figure 2.4. Curves in the figures marked with (i), (ii), etc., represent constant heat flux levels. Note that the heat flux of (ii) is higher than that of (i) and so on.

At a low heat flux (curve (i)), the flow system will follow the path from single-phase forced convective region to subcooled boiling region. As the bulk-fluid temperature reaches the saturation temperature, the system enters the saturated nucleate boiling region. With further increase in mass quality, the system enters the two-phase forced convective heat transfer region. Dryout occurs at the end of this region. The heat transfer coefficient is somewhat constant in single-phase forced convective region. When bubble nucleation occurs, the heat transfer coefficient increases rapidly until the bulk-fluid temperature reaches the saturation temperature at which it stays constant. In the two-phase forced-convective heat transfer region, the heat transfer coefficient increases with increasing mass quality, since the thickness of the liquid film decreases as the mass quality is increased. After the dryout point, the heat transfer coefficient drops abruptly from a very high value to a very low value.

At a higher heat flux (curve ii), subcooled boiling occurs at a lower quality and the heat transfer coefficient in the nucleate boiling region is higher. Dryout occurs at a lower quality than in curve (i). When the heat flux is further increased, the CHF could occur at

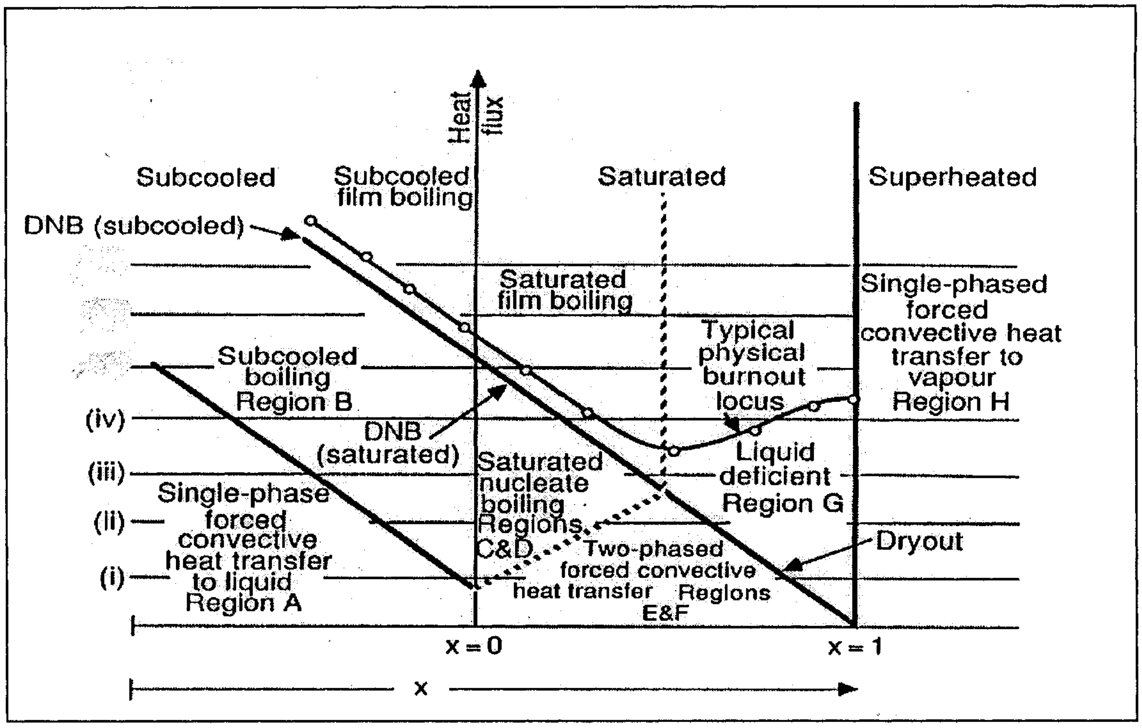

Figure 2.3 Regions of Two-Phase Forced Convective Heat Transfer as a Function of Quality with Increasing Heat Flux as Ordinate (Collier, 1994).

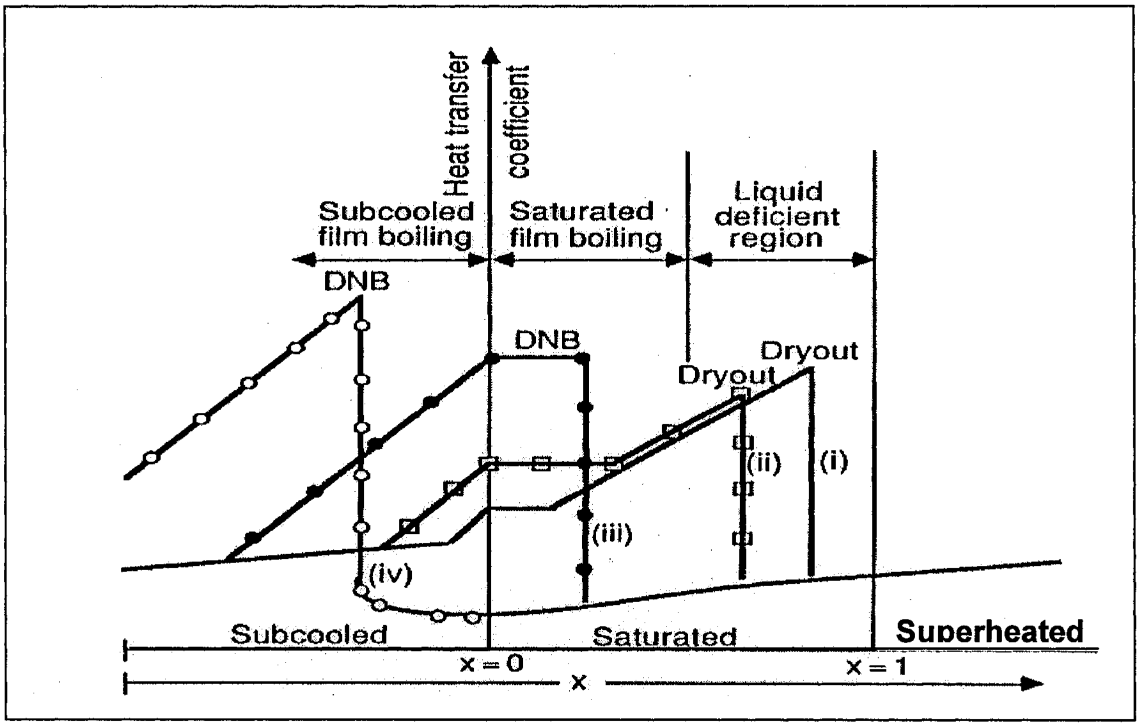

Figure 2.4 Variation of Heat Transfer Coefficient with Quality with Increasing Heat Flux as Parameter (Collier, 1994).

the end of the saturated nucleate boiling region, and even the subcooled boiling region. In this situation, the CHF is also termed "departure from nucleate boiling" (DNB).

2.1.4 Some Significant Transition Points in Boiling Heat Transfer

The points of onset of nucleate boiling (ONB), onset of significant void fraction (OSV), onset of bulk boiling (X=0) and onset of annular flow (OAF) (shown in Figure 2.2c) have physical significance, which mark the changes in heat transfer modes in flow boiling.

Onset of Nucleate Boiling. The onset of nucleate boiling occurs when the wall superheat becomes sufficient to cause vapour nucleation at the heated surface. The subcooling or the bulk temperature at ONB condition ($(\Delta T_{sub}(z))_{ONB}$ or $T_f(z)_{ONB}$) can be determined by the model of Frost and Dzakowic (1967) as

$$(T_{sat} - T_f(z)_{ONB}) = (\Delta T_{sub}(z))_{ONB} = (\Delta T_{sat}(z))_{ONB} - \frac{q''}{h_{fo}} \tag{2.1}$$

where the superheat, $(\Delta T_{sat}(z))_{ONB}$, and the heat transfer coefficient for total flow assumed liquid, h_{fo}, can be found by

$$(T_w(z) - T_{sat})_{ONB} = (\Delta T_{sat}(z))_{ONB} = \left[\frac{8\sigma q''_{ONB} T_{sat}}{i_{fg} k_f \rho_g}\right]^{0.5} Pr_f \tag{2.2}$$

$$\left[\frac{h_{fo} D_i}{k_f}\right] = 0.023 \left[\frac{G D_i}{\mu_f}\right]^{0.8} \left[\frac{c_p \mu}{k}\right]_f^{1/3} \tag{2.3}$$

Onset of Significant Void Fraction. At locations just downstream of the ONB point where the subcoolings, $\Delta T_{sub}(z)$, is less than $(\Delta T_{sub}(z))_{ONB}$, the bubbles remain attached to the surface; they are created and collapse at the wall and there is no void in the centre of the channel. At locations further downstream, bubbles will eventually detach from the surface, condensing only slowly as they move through the slightly subcooled liquid; voidage in this region is a bulk fluid effect. The onset of significant void corresponds to the detachment of bubble from the wall and the transition from very low void fraction (wall void) to the build-up of void in the core. The model of Saha and Zuber (1974) can be used to determine the subcooling or the bulk temperature at OSV condition ($(\Delta T_{sub}(z))_{OSV}$ or $T_f(z)_{OSV}$) as follows:

If Peclet number, $Pe = [GD_i c_{pf}/k_f] \leq 70{,}000$,

$$(T_{sat} - T_f(z)_{OSV}) = (\Delta T_{sub}(z))_{OSV} = 0.0022\left[\frac{q'' D_i}{k_f}\right] \quad (2.4)$$

If $Pe = [GD_i c_{pf}/k_f] > 70{,}000$,

$$(T_{sat} - T_f(z)_{OSV}) = (\Delta T_{sub}(z))_{OSV} = 153.8\left[\frac{q''}{Gc_{pf}}\right] \quad (2.5)$$

Onset of Bulk Boiling. The onset of bulk boiling point refers to the location at which bulk fluid temperature reaches saturation temperature, therefore, the thermodynamic equilibrium quality here equals to zero (X=0). Downstream from the X=0 point, the bubbles will no longer collapse but will remain in the flow and may even coalesce to form larger bubbles. This point is the transition location between the subcooled nucleate boiling and the saturated nucleate boiling.

Onset of Annular Flow. The onset of annular flow point denotes the flow pattern transition location at which bubbly or slug flow changes into annular flow. The local quality at OAF condition, X_{OAF}, can be predicted using the Taitel-Bornea-Dukler (1980) model:

$$j_g = \frac{GX_{OAF}}{\rho_g} = 3.09\rho_g^{-0.5}\left[g(\rho_f - \rho_g)\sigma\right]^{0.25} \quad (2.6)$$

2.2 CHF Mechanisms

Although the CHF phenomenon has been investigated in great detail, there presently is no complete understanding of the mechanisms leading to the CHF condition. A large number of CHF mechanisms have been proposed; they can be categorized into three

DNB mechanisms and one dryout mechanism. These four CHF mechanisms are shown in Figure 2.5 and described as follows:

Dryout under a Vapour Clot. In the high subcooled region, when a bubble grows at the heated surface, due to the evaporation of the micro-layer, a dry patch forms underneath the bubble. The wall temperature in this dry patch rises because of the poor heat transport properties of the vapour. When the bubble departs from the wall, the dry patch may be rewetted and the wall temperature goes down. At a stable situation, this process repeats itself continuously. However, if the heat flux is high, the temperature of the dry patch may become high enough to prevent rewetting. The CHF condition is therefore induced. This mechanism was proposed by Fiori and Bergles (1970) and Kirby (1966, 1967).

Near-Wall Bubble Crowding. The number of bubbles generated depends on the heat flux and bulk temperature. At moderate subcoolings, a "bubble boundary layer" may build up on the heated surface. This boundary layer restricts the vapour generated escaping from the heated surface and the liquid in the core getting contact with the heated surface. When the boundary layer becomes too crowded with bubbles, a continuous vapour layer forms adjacent to the heated surface. The CHF condition is induced consequently. This mechanism was suggested by Kutateladze and Leontev (1966) and Tong (1968). This mechanism will be discussed in more detail at Section 2.3.3.

Evaporation of Liquid Surrounding a Slug Flow Bubble. In subcooled and low quality regions, at low mass velocities the slug flow pattern may occur with a thin film of liquid separating the large vapour bubble from the wall. At high heat flux levels, the liquid film will eventually evaporate, resulting in localized overheating and hence CHF. This mechanism was proposed by Fiori and Bergles (1968).

Film Dryout in Annular Flow. In the high quality annular flow region, a thin liquid film covers the heated surface, while a vapour core mixed with droplets moves at a higher velocity in the central core. Liquid droplets are continuously entrained from the liquid film into the vapour core. Meanwhile, some of the liquid suspended droplets in the vapour core are deposited on the liquid film. The liquid film dries out due to both effects of the evaporation and the entrainment. This mechanism may further be separated into

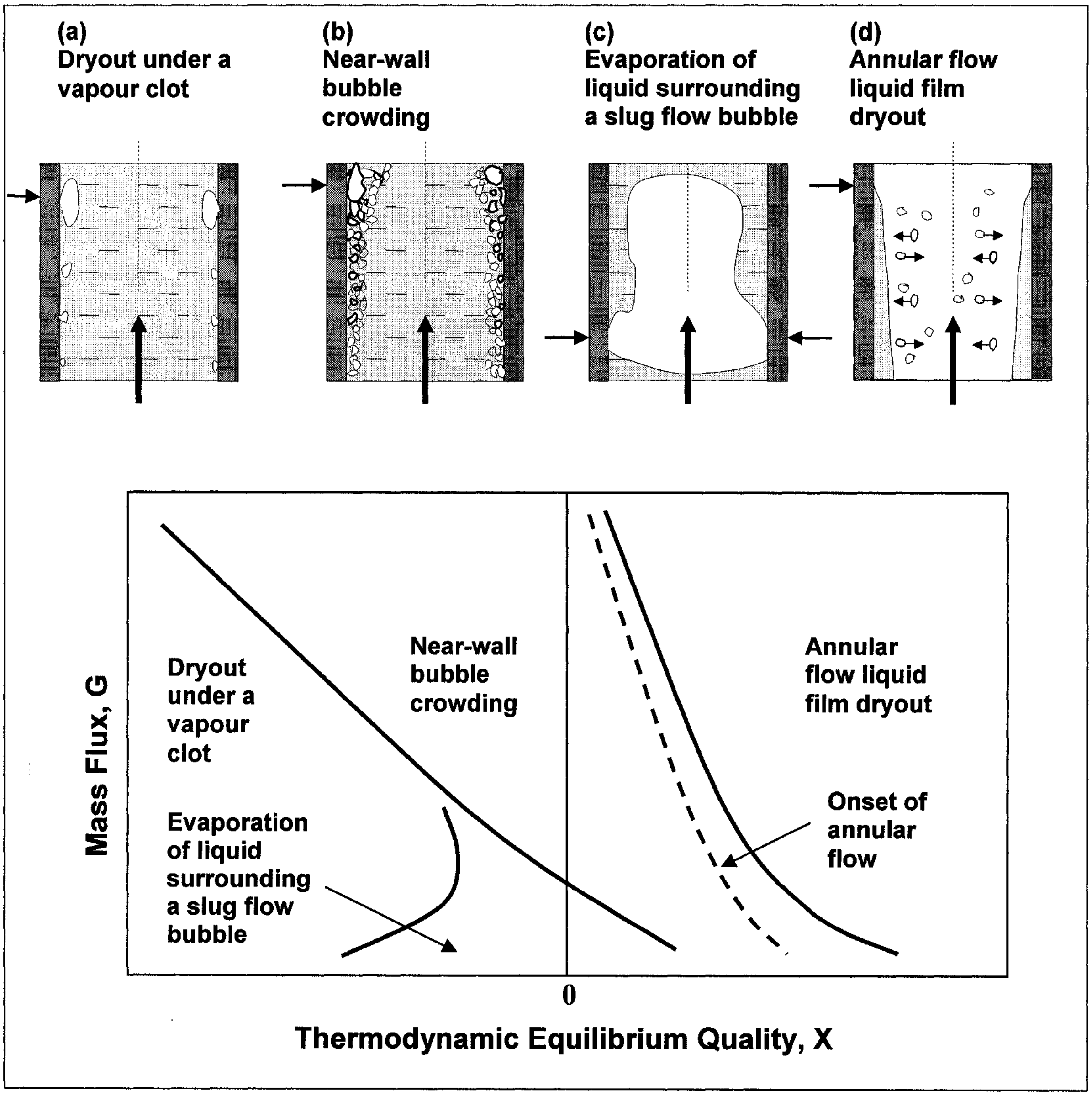

Figure 2.5 CHF Mechanisms as a Function of the Quality and Mass Flux (Semeria and Hewitt, 1972)

entrainment-controlled film dryout and deposition-controlled film dryout. The former will be discussed in more detail in Section 2.3.2. The latter is usually limited to high qualities where the liquid film is so thin that liquid entrainment is suppressed. The liquid film flow rate is then governed by evaporation and deposition: if the evaporation rate is higher than the deposition rate, dryout (CHF) will occur.

In flow boiling, the CHF mechanisms depend strongly on flow regime and phase distributions, which in turn are controlled by pressure, mass flux and quality. A qualitative chart produced by Semeria and Hewitt (1972), in which different mechanisms are set as functions of the flow rate and quality, is illustrated in Figure 2.5.

2.3 CHF Models

Currently there are more than 10 analytical models available, each of them is based on the specific physical mechanism and satisfies the conservation equations. Two models, which are widely accepted and directly related to this thesis research, will be introduced. One of them is the annular flow dryout model proposed by Whalley (1974), which is applicable to the high quality region. Another model, which corresponds to the mechanism of near-wall bubble crowding and is applicable to the subcooled and low quality regions, is the bubbly flow DNB model developed by Weisman and Pei (1983).

2.3.1 Annular Flow Film Dryout Model

In the high quality region before the occurrence of CHF, the flow is basically assumed to be annular flow. In this region, the bubble nucleation is suppressed and the process of heat transfer is the two-phase forced convective heat transfer. The CHF condition is assumed to occur at the point at which the flow rate of the liquid film on the heated surface falls to zero due to the evaporation and the interaction of the entrainment and deposition effects.

Figure 2.6a illustrates the mass balance in a control element of a heated tube. The mass balance on the liquid film may be expressed as

$$[W_{lF}]_{INFLOW} = [W_{lF}]_{OUTFLOW} + [W_{lF}]_{ACCUMULATION} \tag{2.7}$$

where $[W_{lF}]_{INFLOW}$ is the liquid flow rate entering into the liquid film element dz in length; $[W_{lF}]_{OUTFLOW}$ is the liquid flow rate getting out from the liquid film; and $[W_{lF}]_{ACCUMULATION}$

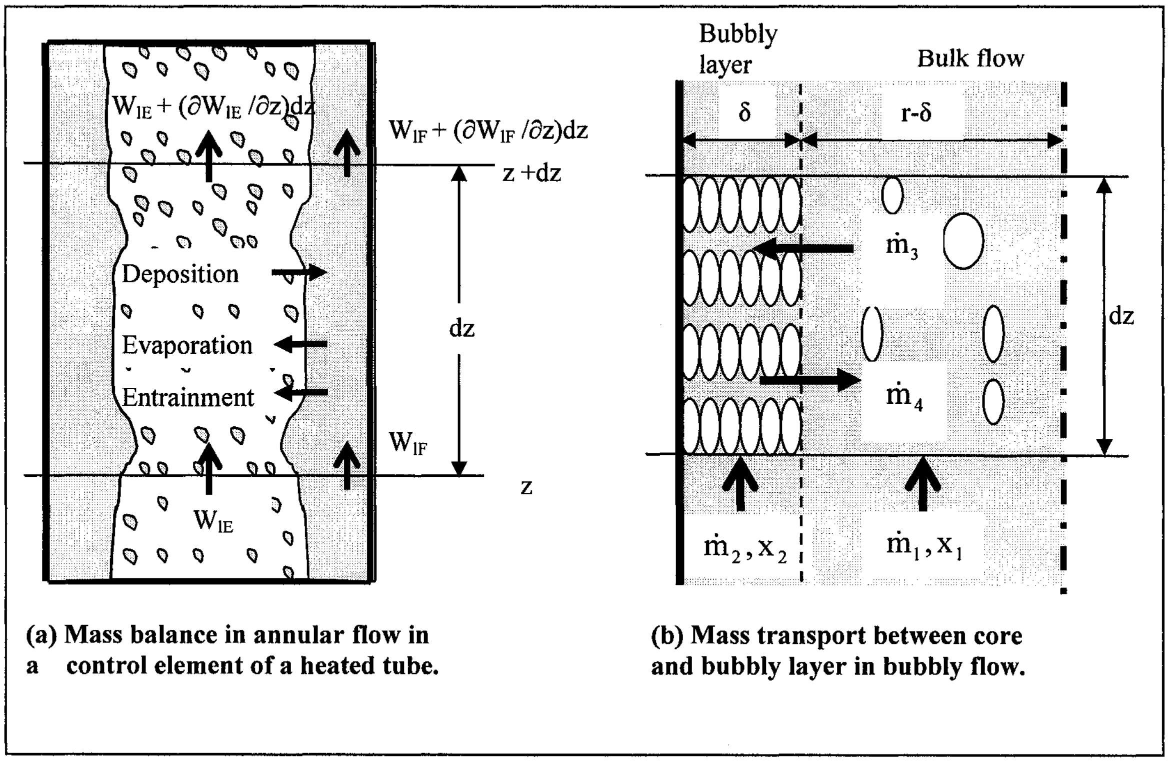

Figure 2.6 Mass Transport in a Control Element (Whalley 1974 and Weisman 1983).

is the variation in time of the mass of liquid contained in the film in the control element. They may be obtained by the following equations, respectively:

$$[W_{IF}]_{INFLOW} = W_{IF} + W_D = W_{IF} + \pi D(D_d)dz \tag{2.8}$$

$$\begin{aligned}[W_{IF}]_{OUTFLOW} &= (W_{IF} + \frac{\partial W_{IF}}{\partial z}dz) + W_{EN} + W_{EV} \\ &= (W_{IF} + \frac{\partial W_{IF}}{\partial z}dz) + \pi DEdz + \pi D\frac{q''}{i_{fg}}dz\end{aligned} \tag{2.9}$$

$$[W_{IF}]_{ACCUMULATION} = \frac{\partial M_{IF}}{\partial t}dz = \frac{\partial(\pi D\delta\rho_f)}{\partial t}dz \tag{2.10}$$

where W_{IF} is the liquid film flow rate; W_D is the flow rate of deposition in the length of dz, D is the diameter of the heated tube; D_d is the deposition rate of droplets on to the liquid film; W_{EN} is the rate of entrainment from the liquid film flow into the vapour core; W_{EV} is the evaporation rate of the liquid film; E is the entrainment rate; q" is the heat flux applying to the heated surface; i_{fg} is the latent heat of vaporization; M_{lF} is the mass of the liquid contained in the film per unit length; δ is the average film thickness and ρ_f is the liquid density.

Substituting Eq.(2.8) through Eq.(2.10) into Eq.(2.7) and setting the time derivation equal to zero, we get

$$\frac{\partial W_{lF}}{\partial z} = \pi D\left(D_d - E - \frac{q''}{i_{fg}}\right). \tag{2.11}$$

In the same way, a mass balance on the entrained liquid in the core results

$$\frac{\partial W_{lE}}{\partial z} = \pi D(E - D_d). \tag{2.12}$$

Here, the heat flux q" has been correlated to liquid film flow rate W_{lF}, deposition rate D_d and entrainment rate E. A general expression for the deposition rate is

$$D_d = kC \tag{2.13}$$

where k is the deposition or mass transfer coefficient, which has been correlated as a function of surface tension; C is the homogeneous mean droplet concentration in the vapour core. C is given by

$$C = \frac{\int_{A_c} \rho_l u_{lE} dA}{\int_{A_c} u dA} = \frac{W_{lE}}{\frac{W_{lE}}{\rho_l} + \frac{W_g}{\rho_g}} \tag{2.14}$$

where the mass flow rate of vapour, W_g can be found by

$$W_g = X(z)W = \frac{4W}{i_{fg}GD}\int_{Z_{SAT}}^{Z} q''(z)dz. \tag{2.15}$$

The entrainment rate and deposition rate are observed to be equal under the equilibrium conditions during adiabatic operation, i.e.,

$$E = D_d = kC_E . \tag{2.16}$$

The same relationship is assumed to hold even for non-equilibrium conditions. The droplet concentration under equilibrium conditions C_E can be correlated as a function of the Weber number, $\left(\frac{\tau_i \delta}{\sigma}\right)$.

To determine the interfacial shear stress, τ_i, and the liquid-film thickness, δ, the triangular relationship developed by Turner and Wallis (1965) may be used.

Eq.(2.11) can be integrated to determine the CHF value. Limits of integration are from the onset of annular flow to the onset of the CHF condition (at which the liquid film flow rate becomes zero). Onset of annular flow was assumed arbitrarily by Whalley (1974) to start at 1 per cent quality ($X = 0.01$) with 99 per cent of liquid entrained, i.e.,

$$\frac{G_{lE}}{G_l} = 0.99 \tag{2.17}$$

2.3.2 Bubbly Flow DNB Model

Weisman and Pei (1983) developed a DNB model for subcooled and low quality conditions at which the CHF mechanism is considered as near-wall bubble crowding (see Section 2.2). This model was developed based on the following assumptions:

- Under moderate subcooled and low-quality flow conditions, CHF is a local phenomenon, and is caused by the limited enthalpy transport between the bubbly layer and the core.
- The bubble layer thickness increases continuously along the channel. At the CHF condition, the turbulent eddy size in the bubbly boundary layer is insufficient to transfer the bubbles radially, with the result that the region near the wall is filled up by the bubbles.

- At the CHF conditions, the volume fraction of vapour in the bubbly layer exceeds a critical void fraction, which may be determined from the balance between the outward flow of vapour and the inward flow of liquid at the bubbly layer and fluid core interface.

- CHF is reached when the quality in the bubbly layer achieves the critical value corresponding to the critical void fraction.

Figure 2.6b illustrates the control volume element of mass transfer between the core and the bubbly layer at the location of CHF. A mass balance on the bubbly layer gives

$$\dot{m}_3 = \Delta\dot{m}_2 + \dot{m}_4 \tag{2.18}$$

where $\dot{m}_3$ is the total flow rate from the core to the bubbly layer; $\dot{m}_4$ is the total flow rate from the bubbly layer to the core; and $\Delta\dot{m}_2$ is the difference between the axial flow rates in and out of the bubbly layer control volume.

The mass balance over the liquid in the bubbly layer gives:

$$\dot{m}_3(1-\chi_1) = \frac{q''_b(2\pi r)\Delta z}{i_{fg}} - \dot{m}_2(\Delta\chi_2) + \Delta\dot{m}_2(1-\chi_2) + \dot{m}_4(1-\chi_2) \tag{2.19}$$

where X_1 and X_2 are the qualities at the core and bubbly layer, respectively; q''_b is the effective portion of the total heat flux in generating vapour, i.e.,

$$q''_b = q''\frac{i_l - i_{ld}}{i_f - i_{ld}} \tag{2.20}$$

where i_{ld} is the enthalpy of liquid at the point of bubble detachment (from Levy's model (1966)).

Omitting the second-order term, Eq. (2.19) can be simplified to a dimensionless form:

$$\frac{q''}{i_{fg}G_3}\frac{i_l - i_{ld}}{i_f - i_{ld}} = (\chi_2 - \chi_1) \tag{2.21}$$

where $G_3 = \dot{m}_3 / [2\pi\Delta z(R-\delta)]$ is the total mass flux from the core to the bubbly layer; δ is the bubbly layer thickness.

The CHF condition corresponds that X_2 reaches its critical value, $X_{2,cr}$, therefore,

$$CHF = i_{fg} G_3 (\chi_{2,cr} - \chi_1)\left(\frac{i_f - i_{ld}}{i_l - i_{ld}}\right) \quad (2.22)$$

Weisman and Pei (1983) used the following procedure to determine the critical void fraction and the corresponding $X_{2,cr}$:

- The bubbles are assumed approximately ellipsoidal, with a ratio between major and minor axes of about 3:1.
- The critical void fraction is obtained when the bubbles inside the bubbly layer are just touching, which is calculated to be α_2=0.82.
- The $X_{2,cr}$ is thus calculated from α_2 assuming that the vapour slip is negligible (i.e., homogeneous void fraction), which is believed to be a valid assumption for high mass flux (i.e., G>>875kg/m^2-s for water). The equation is in the follow form:

$$\chi_{2,cr} = \frac{1}{1 + \frac{\rho_g}{\rho_l}\left(\frac{1-0.82}{0.82}\right)} \quad (2.23)$$

G_3 corresponds to the fluctuating radial velocity component at the bubbly layer and fluid core interface and may be found by

$$G_3 = G \cdot \Psi \cdot I_b \quad (2.24)$$

where Ψ is the turbulent velocity distribution; I_b is the turbulent intensity at the bubbly layer and fluid core interface.

2.4 Limits of the CHF Condition

CHF can only occur when the heated surface temperature exceeds the saturation temperature. Hence the lower limit of CHF value can be found by

$$CHF_{min} = \frac{(\Delta T_{sub})_i}{(4z/GC_{pf}D) + (1/h_{fo})} \qquad (2.25)$$

On the other hand, The CHF condition must occur at or before all the liquid in the channel is evaporated. The upper limit of CHF value is thus given by

$$CHF_{max} = \frac{GDi_{fg}}{4z}[1 + \frac{Cp_f(\Delta T_{sub})_i}{i_{fg}}] \qquad (2.26)$$

Therefore, the actual CHF value must lie between the possible range (shown in Figure 2.7) formed by these two limits, i.e.,

$$CHF_{min} \leq CHF \leq CHF_{max} \qquad (2.27)$$

2.5 CHF Correlations

Presently there are more than 500 CHF correlations available in the literature. Each one of them is only applicable in a certain range of conditions corresponding to the range of experimental data used in derivation. Basically, two hypotheses were used in the derivation of the correlations. These are the local conditions and the overall power (inlet conditions) hypotheses. The local conditions hypothesis suggests that the local critical heat flux is solely a function of the mass quality at the point of overheating, no matter what the upstream history is, i.e., CHF = f (P, G, X_{do}, cross section geometry). Most of the correlations were developed following this hypothesis, based on the experimental data of uniformly heated round tube. The overall power hypothesis suggests that, for a given geometry and inlet conditions, the critical power is independent of axial or radial heat flux distribution, i.e., critical power = f (P_{in}, G_{in}, Δi_{in}, L_h, cross section geometry). This will permit the use of CHF correlations derived from uniformly heated

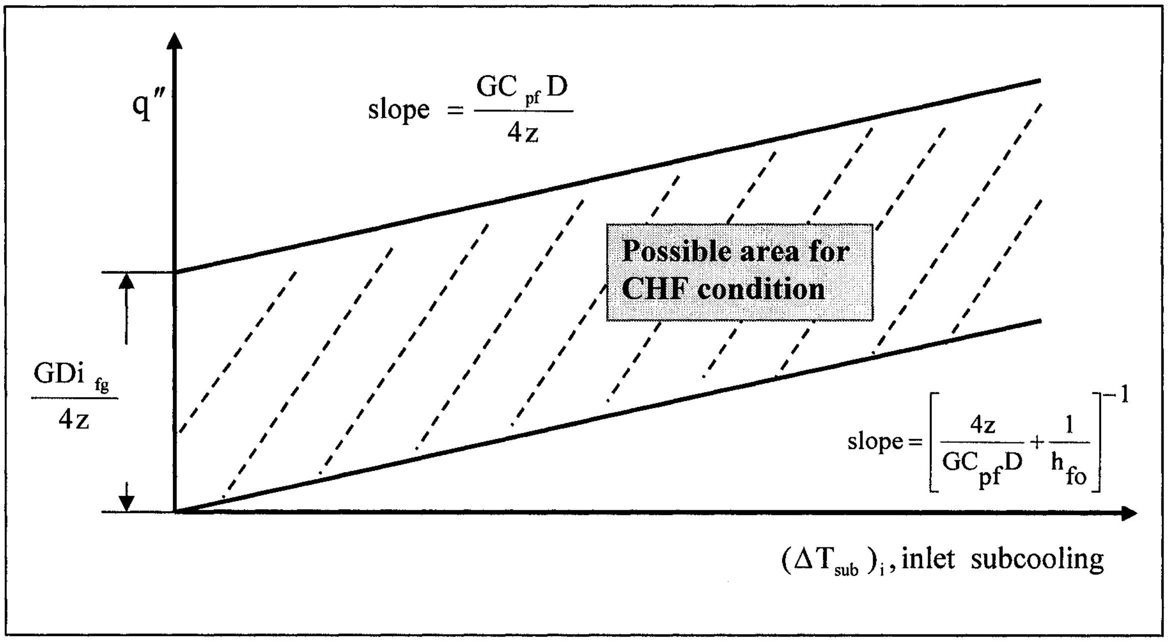

Figure 2.7 Limits of the Critical Heat Flux Condition (Collier, 1994).

channel data for the prediction of critical power in non-uniformly heated channels of identical geometry (i.e. identical cross section and heated length).

The most general one of the empirical corrections is that proposed by Macbeth (1963) based on the local conditions hypothesis, i.e.,

$$CHF = f(X(z), G, P, D) \tag{2.28}$$

Macbeth (1963) made the simplifying assumption that the critical heat flux is a linear function of inlet subcooling, thus

$$CHF = A + B(\Delta i_{SUB})_i \tag{2.29}$$

Where A and B are the functions of G, p, z, and D. Considering the heat balance equation

$$X(z) i_{fg} + (\Delta i_{SUB})_i = \frac{4q''z}{DG} \tag{2.30}$$

Macbeth (1963) finally obtained the following general equations:

$$CHF = \frac{A' + DG(\Delta i_{SUB})_i / 4}{C' + z} \tag{2.31}$$

$$CHF = \frac{A' - DGi_{fg}X(z)/4}{C'} \tag{2.32}$$

where A' and C' can be correlated in terms of G, D, and P based on experimental data.

2.6 CHF Look-up Table Method

The USSR Academy of Sciences (Doroshchuk, 1975) had developed a standard table of critical heat flux as a function of the local bulk mean water conditions and for various pressures and mass velocities for a fixed tube diameter based on 5,000 experimental data. The CHF look-up table development work has been continued at University of Ottawa and Chalk River Laboratories using a much more extensive data base (30,000 data). The CHF look-up table constructed by Groeneveld et al. (1996) provides CHF values for water-cooled 8 mm inner diameter tube, at discrete values of pressure, mass flux, and quality, covering the ranges of 0.1 to 20 MPa in pressure, 0 to 8000 kg m^{-2} s^{-1} in mass flux and –50 to 100% in mass quality, which is much wider than other prediction methods. Compared to the other available prediction methods, the CHF look-up table prediction approach has the advantages of better prediction accuracy for a wide range of flow conditions, correct asymptotic trends and less computing time. It can also easily be updated if additional data becomes available.

2.7 Fluid-to-Fluid Modeling of CHF

Fluid-to-fluid modeling is an experimental technique by which the thermalhydraulic behaviour of a prototype fluid in a given system can be modeled with a modeling fluid. Usually the prototype fluid and modeling fluid are high pressure water and refrigerant, respectively. This is because when it compares with water, the saturation temperature and latent heat of refrigerant are much lower, therefore, the cost for setting up and operating CHF test loop for refrigerant is much lower than that for water.

Using classical dimension analysis and Buckingham's Pi theorem, Ahmad (1973) deduced that the CHF (expressed in terms of CHF/Gi_{fg}) would depend on twelve dimensionless groups of which six were eliminated on inductive arguments. The remaining groups are expressed as follows:

$$\pi_1 = f(\pi_2, \pi_3, ..., \pi_7) \qquad (2.33)$$

where

$$\pi_1 = \frac{CHF}{Gi_{fg}} \quad \text{(Boiling number)} \qquad (2.34)$$

$$\pi_2 = \frac{GD_i}{\mu_f} \quad \text{(Reynolds number)} \qquad (2.35)$$

$$\pi_3 = \frac{\mu_f^2}{\sigma D_i \rho_f} \quad \text{(Weber-Reynolds number)} \qquad (2.36)$$

$$\pi_4 = \frac{\mu_f}{\mu_g} \quad \text{(Liquid/Vapour viscosity ratio)} \qquad (2.37)$$

$$\pi_5 = \frac{\Delta i_{SUB}}{i_{fg}} \quad \text{(Subcooling number)} \qquad (2.38)$$

$$\pi_6 = \frac{\rho_f}{\rho_g} \quad \text{(Liquid/Vapour density ratio)} \qquad (2.39)$$

and

$$\pi_7 = \frac{L_h}{D_i} \quad \text{(Length/diameter ratio).} \qquad (2.40)$$

The dimensionless group π_6 can be used to achieve the pressure similarity. The converted pressure of the prototype fluid should be such that the density ratio of the saturated liquid to the saturated vapour phases for the prototype fluid system is always identical to that of the modeling fluid system. Similarly, π_7 is used to realize the geometric similarity in both systems.

Consider now the heat balance equation:

$$X(z) = 4(\frac{CHF}{Gi_{fg}}) \times (\frac{z}{D_i}) - (\frac{\Delta i_{SUB}}{i_{fg}}) \tag{2.41}$$

If π_1 and π_5 are the same in both systems, then the qualities at the same length-to-diameter ratio in both systems are identical. The thermodynamic similarity is thus achieved.

In order to convert the mass flux, π_2, π_3 and π_4 are combined into a single modeling parameter Ψ_{CHF} as follows

$$\Psi_{CHF} = \pi_2 \times \pi_3^m \times \pi_4^n = \left[(\frac{GD_i}{\mu_f}) \times (\frac{\mu_f^2}{\sigma D_i \rho_f})^m \times (\frac{\mu_f}{\mu_g})^n \right] \tag{2.42}$$

Thus, Eq. (2.33) may be re-written as

$$\pi_1 = f(\Psi_{CHF}, \frac{\Delta i_{sub}}{i_{fg}}, \frac{\rho_f}{\rho_g}, \frac{L_h}{D_i}) \tag{2.43}$$

It implies that, if Ψ_{CHF}, $\frac{\Delta i_{sub}}{i_{fg}}$, $\frac{\rho_f}{\rho_g}$ and $\frac{L_h}{D_i}$ in both systems are the same, then

$$(\frac{CHF}{Gi_{fg}})_{prototype} = (\frac{CHF}{Gi_{fg}})_{model}. \tag{2.44}$$

The values of m and n in Eq. (2.42) can be determined from experimental data. After examining 7 different fluids, Groeneveld et al. (1992) concluded that the optimal values of m and n are 0.5 and 0, respectively. Thus, Eq. (2.42) becomes

$$\Psi_{CHF} = \left[(\frac{GD_i}{\mu_f}) \times (\frac{\mu_f^2}{\sigma D_i \rho_f})^{0.5} \times (\frac{\mu_f}{\mu_g})^0 \right] = \frac{GD_i^{0.5}}{(\sigma \rho_f)^{0.5}}. \tag{2.45}$$

2.8 Parametric Effects on CHF

There are seven core thermal hydraulic parameters for boiling heat transfer in a uniformly heated tube: heat flux q", pressure P, mass flux G, inlet quality X_{in} (or inlet enthalpy i_{in}), outlet quality X_{out} (or outlet enthalpy i_{out}), channel diameter D_i, and heated length L_h. The following heat balance equation shows the relationship among these parameters:

$$X_{out} - X_{in} = \frac{4q''L_h}{D_i G i_{fg}} \qquad (2.46)$$

Since the CHF basically always occurs at the exit of a uniformly heated tube, X_{out} and X_{do} are identical under CHF conditions. The parametric effects on CHF are described in the following sections based on experimental observation.

2.8.1 Critical Quality and Inlet Quality Effects

The general trend of CHF vs. X_{do} is that the CHF decreases with a decrease in channel exit subcooling or an increase in dryout quality. This trend continues until the CHF value falls to zero as the dryout quality reaches 100% (see Figure 2.8a and b). Note that, region I in Figure 2.8a is associated with the subcooled CHF mechanism, region II the entrainment-controlled film dryout and region IV the deposition-controlled film dryout. Region III, which is in between regions II and IV, corresponds to the so-called "limiting quality" effect. Although the limiting quality effect is not always observed in the whole range of flow conditions, it could be very strong at certain pressure and mass flux.

Most of the experimental studies were conducted by having subcooled liquid (negative quality value) at the channel inlet. The CHF is generally a linear function of inlet quality, and the CHF value decreases with the decrease in inlet subcooling (see Figure 2.8a and c). Non-linearity was found as the inlet quality is close to zero under the conditions of very high mass flux and / or very small tube diameters.

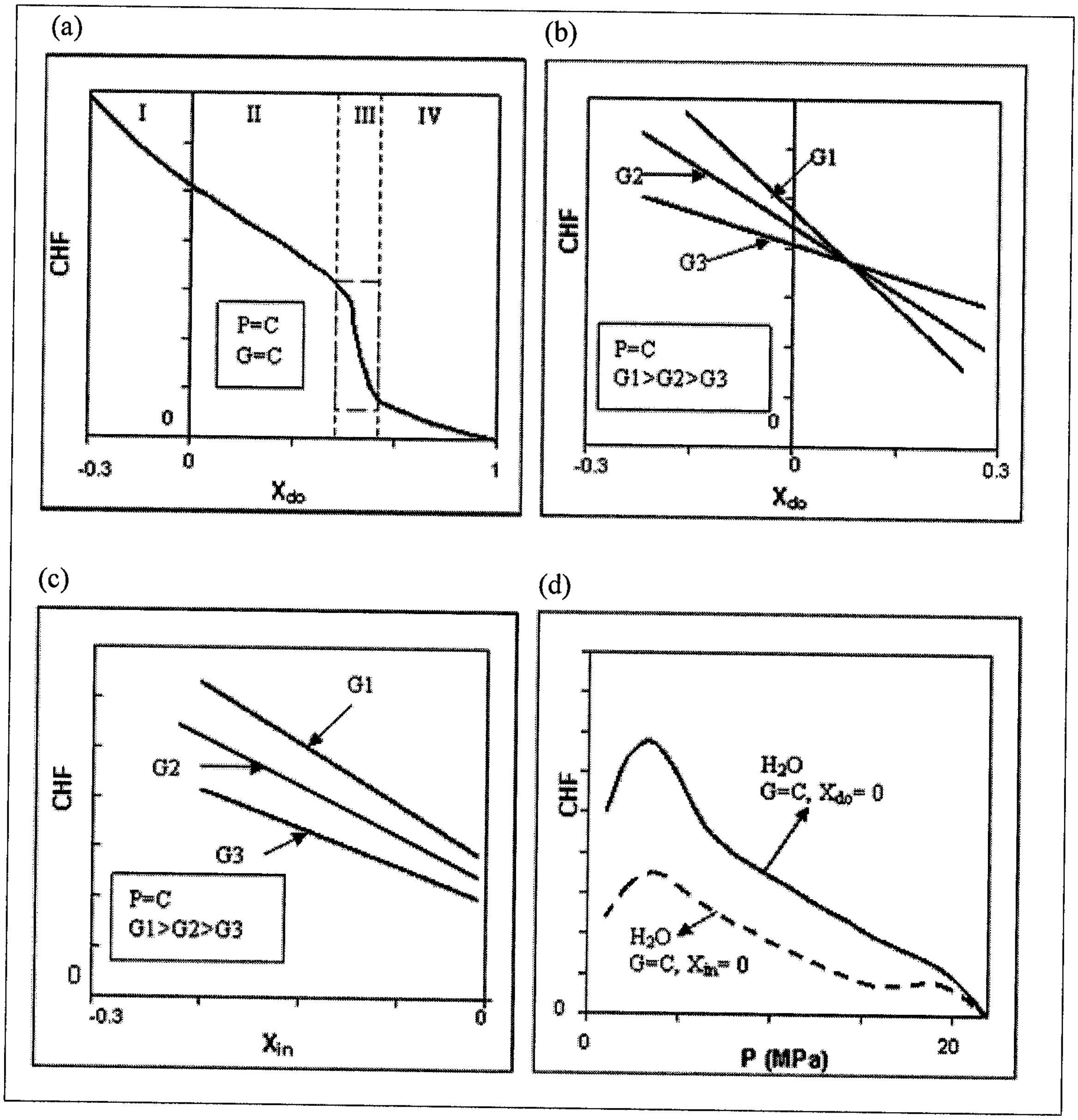

Figure 2.8 Parametric Effects on CHF (Collier, 1994).

2.8.2 Mass Flux Effect

The CHF normally increases with the increase in mass flux at constant inlet subcooling except at ultra-high mass flux, very small inlet subcooling values and low z/D_i ratios. The CHF vs. X_{do} plot (Figure 2.8b) illustrates crossovers of constant mass flux lines. CHF increases with the increase in mass flux at low dryout qualities. The opposite trend exists at high dryout qualities.

2.8.3 Pressure Effect

Figure 2.8d shows an example of the variation of CHF with pressure for water at fixed dryout quality and fixed inlet quality. In case of a constant dryout quality, at low pressure, CHF increases as the pressure increases until CHF reaches the peak value. CHF then falls sharply to approach zero when the pressure keeps increasing from the value corresponding to the peak CHF value to the critical pressure. If the inlet quality is fixed, the general trend of CHF against pressure is similar to that when dryout quality is held constant, except that in some cases, a secondary CHF peak exists at high pressure.

2.8.4 Channel Diameter and Heated Length Effects

For the condition where the dryout quality is held fixed, the CHF decreases with the increase in the channel diameter. Considering 8 mm as a standard diameter, the following correction factor was suggested by Groeneveld (1996) for CHF value conversion between the channel with 8 mm in diameter and those with other diameter values:

$$\frac{CHF_{D_i=D}}{CHF_{D_i=8mm}} = \left(\frac{D}{8}\right)^{-0.5} \tag{2.47}$$

If tube diameter, system pressure and mass flux are all held fixed, for the ratio of tube heated length to diameter larger than 75 ($L_h/D_i > 75$), the effect of heated length on CHF vs. X_{do} is quite small. For very short heated length, however, the CHF increases with decreasing heated length for a given dryout quality due to the tube entrance length effect.

2.9 Experimental Studies on the Effect of Non-Uniform Axial Heat Flux Distribution on CHF

Numerous investigations have been conducted on the effect of axial heat flux distribution on CHF because of its importance in nuclear reactor operation. Preceding experimental studies were performed usually using two types of test section: (a) the heat generation in the channel wall in the axial direction is uniform except a short length or short lengths at higher or lower level (hot patch or cold patch), and (b) the heat generation in the channel wall is smooth continuous function of the channel length.

2.9.1 Effect of Hot Patch

A hot patch experiment was performed by De Bortoli et al. (1958) using water as coolant flowing in a rectangular channel. The upstream part (L_{h1} = 67.55 cm) was operated at a uniform heat flux q''_1 and the exit part (L_{h2} = 0.95 cm) at a heat flux q''_2. The ratio (q''_2/ q''_1) was maintained at 1.98. The tests for a uniform AFD test section with the same cross section geometry and total heated length were also performed. The results suggest that the local conditions hypothesis is only approximately valid at high subcooled regions while the overall power hypothesis is roughly valid at high dryout quality regions; the critical power for the hot patch channel is basically less than that for uniform channel at low dryout qualities, and the discrepancy increases with the decrease of dryout quality or the increase of subcooling.

Experiments such as those performed by Stevens (1965) and Smith et al. 1965 show the similar result as that by De Bortoli et al. (1958). It can be concluded from their investigations that the hot patch affects the CHF condition by at least two different CHF mechanisms - one for subcooled conditions and another at high qualities, which in turn are controlled by the flow patterns just before the CHF occurrence.

Further studies explored that the hot patch effect on CHF strongly depends on the flow conditions and flux spike characteristics such as the heat flux spike length and the non-uniformity. Experiment performed by Zenkevich et al. (1969) shows that the deviation of the critical powers between the uniform AFD channel and that with hot patch increases as pressure and mass flux increase and spike length decreases. Mortimore and Beus (1979) concluded that the flux spike did not cause a reduction in critical power except for the low inlet temperature and high mass flux. The results carried out by Coeling (1978) showed that the flux spike did not have an appreciable effect on the average heat flux when CHF occurred. At given pressure and mass flux, a decrease in dryout power ratio for hot patch to uniform heating was observed as inlet temperature decreased. Experiments conducted by Bertoletti et al. (1965) and Silvestri (1966) indicated that the concept of a constant critical channel power is independent of heat flux distribution, although approximately valid at high exit qualities for moderate value of non-uniformity, becomes increasingly incorrect as the non-uniformity increase.

2.9.2 Effect of Cold Patch

Hewitt et al. (1966) conducted a cold patch test in which part of the channel was unheated. The cold patch was moved successively downstream from the location near the inlet end of the tube. When the cold patch was located near the inlet end, the critical power was close to that obtained with uniform heating for the same heated length. Nevertheless, as the cold patch was moved towards the exit end, the critical power increased sharply and could be greater than that obtained with uniform heating for the same heated length, and even for the same total length. An explanation suggested by Kinoshita et al. (1998) is that the CHF enhancement is due to the interruption and re-establishment of the bubble boundary layer just upstream of the CHF location.

2.9.3 Effect of Continuous Non-Uniform Axial Heat Flux Distribution

Many of these studies are concerned with the limitations of the critical heat flux in nuclear reactor design; the form of the axial heat flux profile is often similar to a cosine wave. Some typical axial heat flux profiles are shown in Figure 2.9. In order to relieve fabrication problem, in some of the studies, the heat flux profile is only part of cosine wave - i.e., 'choped' - and, in others, the heat flux profile has been built up in a series of

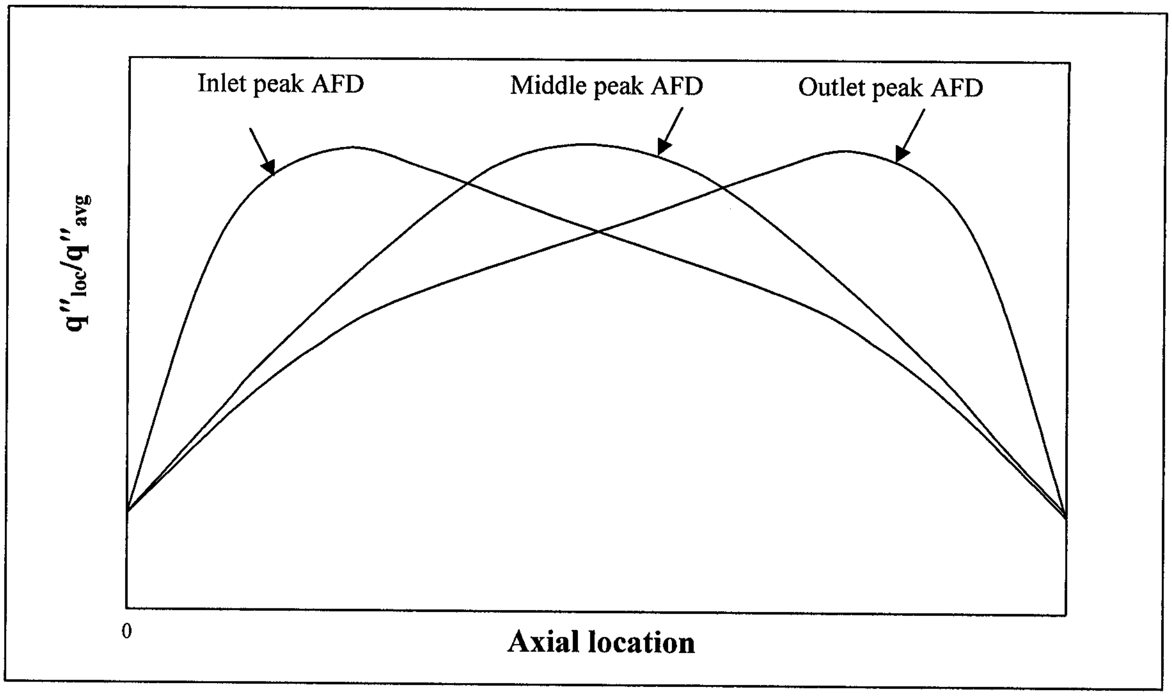

Figure 2.9 Typical AFD Profiles in the Nuclear Reactors.

steps - i.e., 'stepped'. The form factor is defined as the ratio of the maximum to average heat flux ($k = q''_{max}/q''_{avg}$).

Studies conducted by Swenson et al. (1963), Casterline and Matzer (1964) and Ornatskiy et al. (1975) showed that the no-uniform AFD has a strong effect on the local CHF. Although the local CHF for non-uniform AFD was found similar to that in uniformly heated tubes at subcooled region (DNB type of CHF), it turns out to be lower up to 80 % than that for uniform AFD with the increase of the dryout qualities (in annular flow region). The magnitude of the CHF difference between the uniform and non-uniform heat flux distributions decreased as the non-uniform heat flux distribution approaches the uniform distribution. This observation coincides with that for the hot patch.

It was also found that it is difficult to determine the precise initial CHF location for non-uniform AFD due to the fact that it could occur over a fairly broad range of sites downstream of the heat flux peak location. The initial CHF location also strongly depends on the flow conditions and the characteristic of heat flux profile. For constant inlet conditions, CHF occurs at the site close to the outlet at a low mass flux and a low form factor, and the location shifts toward the peak of the heat flux as mass flux and form factor increase.

Another interesting finding reported by Lee and Obertelli (1963) is that the heat input downstream of the CHF location had no effect on the CHF value or the initial location.

With respect to the critical power, Bertoletti and Gaspari (1963) postulated that the critical power is basically independent of the power distribution. Observations from other investigators (Casterline and Matzer 1964, Todreas and Rohsenow 1965 Ornatskiy et. al. 1975, Lee 1966, Keeys et al. 1971), however, suggested that the critical power for non-uniform AFD could be higher or lower than that for uniform AFD in a moderate scale at low mass flux depending on the inlet conditions and the location of heat flux peak, but up to 30% less than that for uniform AFD at high mass flux if the maximum heat flux occurs near the tube exit. Experiments (Swenson et al. 1963, Todreas and Rohsenow 1965) also showed that inlet peak AFD has a greater critical power than that of outlet peak AFD.

It is obvious that neither the local conditions hypothesis nor the overall power hypothesis is generally valid for the CHF prediction on non-uniform heat flux distribution. The value of the local critical heat flux for non-uniform heat flux distributions must depend, to some extent, on the heat flux profile upstream of the point.

2.9.4 Mechanistic Description of the Effect of AFD on CHF

Effect of Non-Uniform AFD on Annular Flow Film Dryout

As discussed in Section 2.3.1, at high qualities, the flow pattern before CHF occurrence is assumed to be the annular flow. The liquid film dries out due to the interaction of the effects of evaporation, entrainment and deposition. The expression of CHF resulting from a balance among these effects, can be obtained from Eq. (2.11) as

$$\frac{CHF}{i_{fg}} = G_{lF} + D_d - E \tag{2.48}$$

where G_{lF} = liquid mass flux due to the liquid film moving towards the CHF location per unit heated area

D_d = Deposition rate of droplets on to the liquid film per unit heated area

E = Entrainment rate of droplets from the liquid film per unit heated area

Hewitt et al. (1965) has carried out measurements of the annular liquid film flow rate at the exit of a heated tube and a long unheated tube. Consequently, curves for the entrained liquid flow rate as a function of local quality were built up at given mass flux, as shown in Figures 2.10a and 2.10b. The hydrodynamic equilibrium curve corresponds to the long unheated tube (under fully developed equilibrium conditions), while the boiling annular flow curve corresponds to the heated tube (departure from hydrodynamic equilibrium). Also shown is the total liquid flow rate; the difference between the total liquid flow rate and the entrained liquid flow rate is the flow rate in the liquid film.

In the boiling annular flow, the entrained liquid flow rate increases with the increase in local quality, until the hydrodynamic equilibrium curve is reached, and then begins to decrease as net deposition occurs. Dryout occurs at the quality at which the entrained liquid flow rate equals the total liquid flow rate.

Some effects observed with non-uniform AFD heating were explained by Hewitt et al. (1966) using the entrained liquid flow rate curves.

The existence of the non-uniform AFD will affect the entrained liquid flow rate, and consequently influence the CHF location and critical power. These influences depend strongly on the nature of the AFD profile. When a cold patch is located at the upstream part, Bennett et al. (1967) and Hewitt et al. (1966) demonstrated that, although the local quality remains constant across the cold patch, liquid entrainment will continue as the flow attempts to becomes 'fully developed'. As a result, the entrained liquid flow rate is increased, and the dryout quality is decreased (shown on Figure 2.10a by curve XYZ). When a cold patch is situated on the downstream part, however, the entrained liquid flow rate is decreased and the dryout quality is increased (shown on Figure 2.10a by curve UVW). This implies that extra power is required for the CHF occurrence at the tube exit. Another example given by Hewitt et al. (1966) is the boiling in a tube with a linear

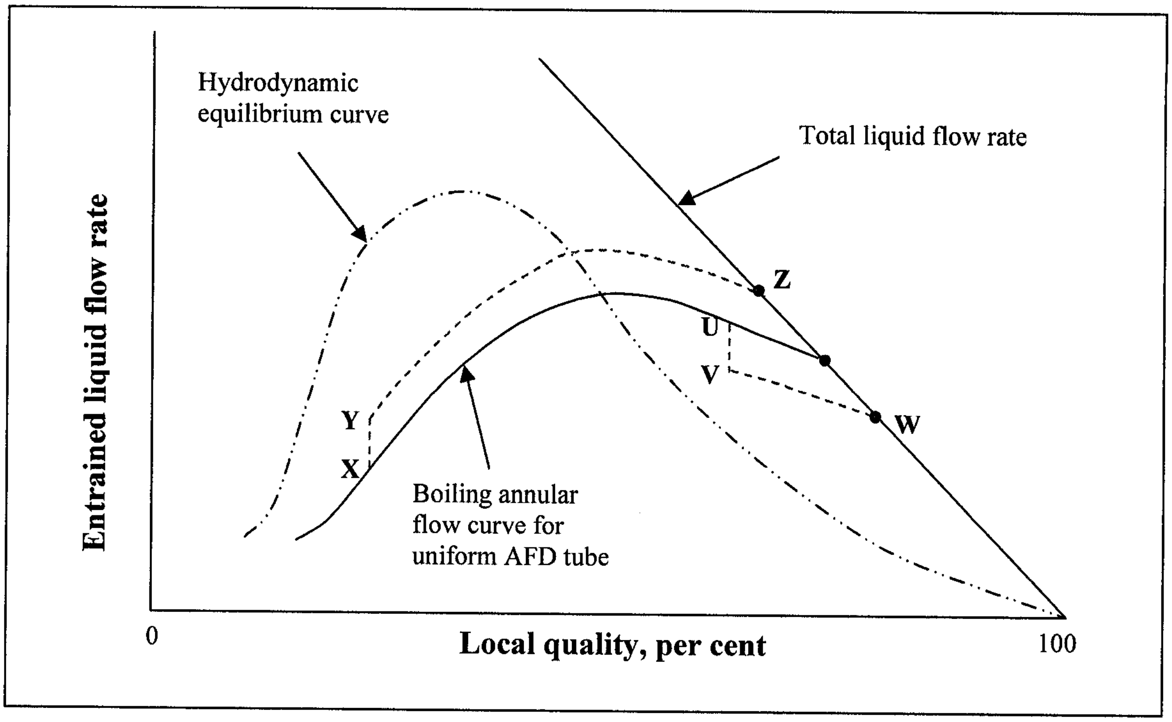

Figure 2.10a Liquid Entrainment and Cold Patch Effect (Hewitt et al., 1965).

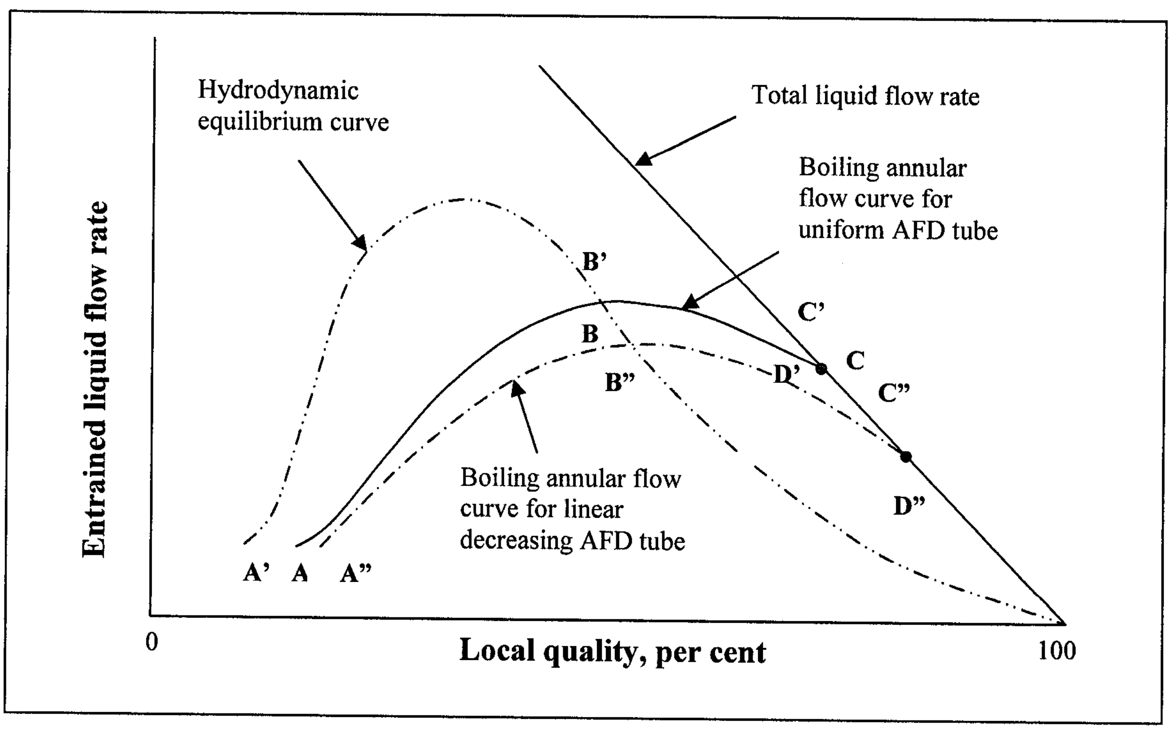

Figure 2.10b Non-Uniform AFD effect, Based on the Entrainment Curves of Hewitt et al. (1965).

decreasing heat flux profile. Hewitt et al. (1966) pointed out that the linear decreasing heat flux profile has a short length over which entrainment may take place and a long length for deposition to occur giving a higher dryout quality than a uniform AFD (shown on Figure 2.10b).

Effect of Non-Uniform AFD on Bubble Layer Thermal Shielding

In subcooled or low quality flow boiling, a bubble layer is formed on the heated surface. The bubble layer is a highly viscous layer of crowded, tiny bubbles flowing parallel to the heated surface and thus serves as a thermal shield, which restricts the vapour generated escaping from the surface and the liquid in the core cooling the heated surface. Different from the model proposed by Weisman and Pei (1983) (see Section 2.3.2), Tong et al. (1966) suggested that before CHF occurrence, the subcooled liquid coming from the core goes through the bubble layer to cool the heated surface. The liquid enthalpy in the bubble layer is reduced by mixing the subcooled liquid from the core, meanwhile the bubbles is quenched by the subcooled liquid. The subcooling of the main stream decreases and the enthalpy of the bubble layer increases along the tube in the flow direction. The CHF occurs as the enthalpy difference between the bubble layer and the main steam becomes so small that the bubble can not be quenched but be flashed to void. This model is illustrated in Figure 2.11. Tong et al. (1966) obtained the following equation by an energy balance over the control element in the bubble layer:

$$\frac{d(i-i_b)}{dz}+C(i-i_b)=C\frac{c_p q''}{h} \tag{2.49}$$

where $C = h/\rho V s c_p$ is independent of location but different form different flow regimes

ρ = average density of bubble layer

V = average velocity of bubble layer

s = thickness of bubble layer

i = average enthalpy of bubble layer

i_b = enthalpy of bulk flow

h = heat transfer coefficient from wall to bubble layer

c_p = average specific heat of bubble layer

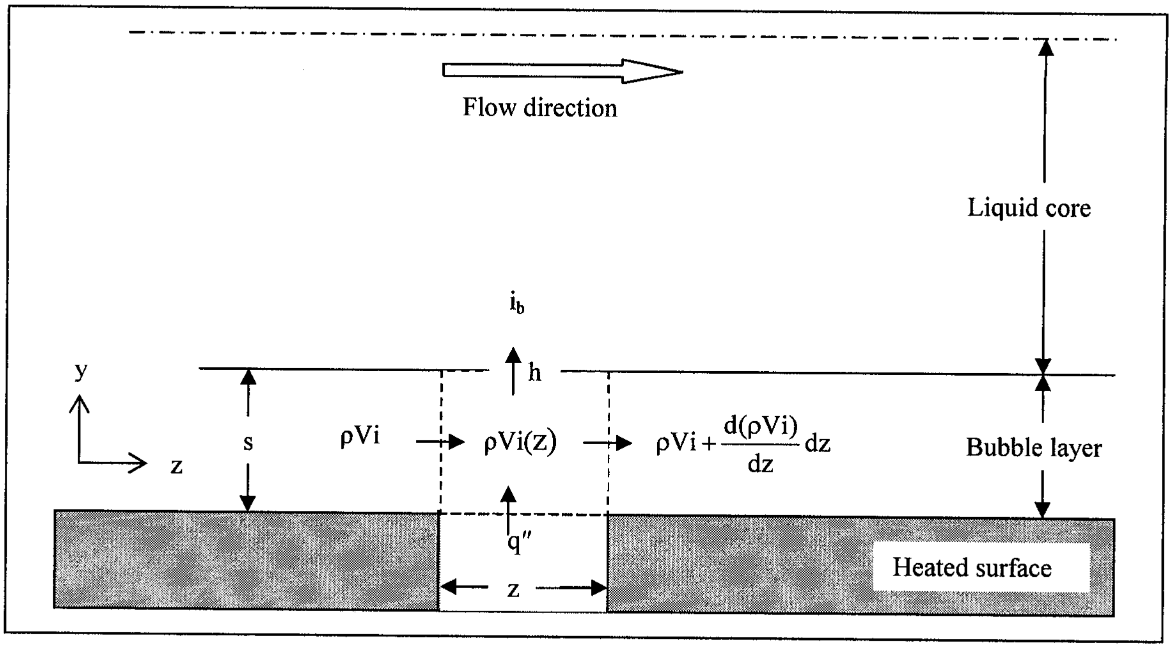

Figure 2.11 Physical Model of Heat Balance Near Wall (Tong et al., 1966).

q'' = surface heat flux

z = distance from inception of local boiling

For uniform AFD, the solution of Eq. (2.49) is

$$i(z) - i_b = \frac{c_p q''}{h}[1 - \exp(-Cz)] \tag{2.50}$$

For non-uniform AFD, the solution of Eq. (2.49) becomes

$$i(z) - i_b = C\left(\frac{c_p}{h}\right)\int_0^z q''(z')e^{-C(z-z')}dz' \tag{2.51}$$

Tong et al. (1966) postulated that the occurrence of CHF can be determined by a limiting value of the enthalpy of the bubble layer. Eq. (2.51) suggests that the bulk stream conditions alone are not sufficient for determining CHF for the case of a non-uniform AFD. The upstream history before the CHF occurrence needs to be taken into account since the enthalpy of the bubble layer at CHF location is accumulated from the upstream part of the heated channel. In other words, the upstream axial heat flux distribution effect is conveyed to the downstream bubble layer at CHF location. Eq (2.51) also suggests that the upstream heat flux distribution effect decays rapidly with the upstream distance from CHF location. In fact, at very high subcoolings, before the onset of significant void fraction (OSV), there is no effect of AFD as the bubble layer is not formed on the heated surface, thus only the local conditions determine the CHF occurrence.

2.10 Prediction Methods for CHF with Non-Uniform AFD

Unlike the uniform heated tube, of which the CHF always occurs at the exit, with non-uniform AFD, the CHF could occur at the upstream site from the channel exit. The prediction method for non-uniform AFD should predict both the critical power value and CHF location. The CHF value can be calculated from the heat flux profile if both the critical power and CHF location are known.

Generally the CHF prediction methods can be classified as (i) the analytical method derived from the CHF mechanisms (such as those based on the annular film dryout model and the bubbly clouding model), and (ii) the empirical or semi-empirical method based directly on experimental data. The analytical method is very complicated and its range of application is quite limited, thus the empirical method is therefore preferred. The empirical methods are developed based on two hypotheses: the local conditions hypothesis and the overall power hypothesis. Since none of them can be applied over the full range of flow conditions and AFDs of interest, modified local conditions approaches such as F-factor approach and boiling length average (BLA) approach were developed.

The definitions of these methods are illustrated in Figure 2.12. These methods allow us to predict the CHF conditions of a non-uniform AFD from the reference CHF conditions of a uniform AFD at the same geometry and flow conditions. Note that the variation of CHF with X_{do} for the uniform AFD may be obtained from CHF correlations, analytical models or CHF look-up table; but the one employed in this research is obtained directly by curve fitting of the experimental data.

2.10.1 Overall Power Approach

The overall power approach is based on the overall power hypothesis, which suggests that the critical power for the tube with non-uniform AFD is the same as for a uniformly heated tube of the same cross sectional geometry and heated length at given inlet conditions, i.e.,

$$\text{Power} = f(P_{in}, G_{in}, T_{in}, D_i, L_h) \tag{2.52}$$

The critical heat flux for uniform AFD can be found at the intersection of the CHF vs. X_{do} curve and the heat balance curve; thus the critical power can be calculated by simply multiplying the obtained CHF value by the heated surface area of the uniform AFD tube (see Figure 2.12a). This method is considered reasonable for obtaining a first estimate of critical power for symmetrical flux profiles and mild form factors in annular flow regime.

2.10.2 Local Conditions Approach

The local conditions approach follows the hypothesis, which states that there is a unique relationship between critical heat flux and local conditions; hence the CHF is independent of upstream history. It may be expressed as

$$\text{CHF} = f(P, G, X_{do}, D_i) \tag{2.53}$$

The prediction for the CHF magnitude, CHF location and critical power can be realized by gradually increasing the power until the local heat flux vs. local quality curve becomes tangent to the curve of CHF vs. X_{do} for uniform AFD (see Figure 2.12b). This method is found reasonable for CHF prediction at subcooled conditions.

2.10.3 F-factor Approach

As described in Section 2.9.4, Tong et al. (1966) suggested that for subcooled or low-quality flow boiling with high flow rates and at high pressures, the local conditions are not sufficient for determining CHF for the case of a non-uniform heat flux distribution since the upstream memory affects the CHF, i.e., the flow enthalpy and bubbles in the boundary layer region are accumulated from upstream surface. Accordingly, Tong et al. (1966) derived a semi-empirical method – the F-factor approach– which enables the effect of the upstream heat flux profile on the local critical heat flux value to be taken into account.

The F-factor was defined as the ratio of a uniform CHF at any local enthalpy to the CHF for a particular non-uniform AFD at the same given local enthalpy. An expression for the F-factor was derived by assuming that CHF occurs at a limiting value of the enthalpy of the bubble layer independent of the axial power distributions, i.e.,

$$[i(z) - i_b]_{cr,U} = [i(z) - i_b]_{cr,non} \tag{2.54}$$

From Eq.(2.50) and Eq.(2.51), Tong et al. (1966) obtained the expression for the equivalent uniform CHF for the case of a non-uniform AFD as

$$q''_{cr\_EU} = \frac{C}{1-\exp(-Cz_{cr})} \int_0^{z_{cr}} q''(z) \exp[-C(z_{cr} - z)] dz \tag{2.55}$$

Consequently, the general expression of F is determined as

$$F = \frac{q''_{cr\_EU}}{q''_{cr\_non}} = \frac{C}{1-\exp(-Cz_{cr})} \int_0^{z_{cr}} \frac{q''(z)}{q''(z_{cr})} \exp[-C(z_{cr} - z)] dz \tag{2.56}$$

The same form of F was also found based on a mass balance on the liquid film in the annular flow region by Smith et al. (1965). However, the coefficient, C, in the form of F was determined empirically since the heat transfer from the superheated liquid layer to the bubble layer was not sufficiently known. The empirically determined expression for C is

$$C = 0.15 \frac{(1 - X(z_{cr}))^{4.31}}{(G/10^6)^{0.478}} (in^{-1}) \tag{2.57}$$

The F-factor method modifies the critical heat flux for a uniform AFD, and predicts the CHF value as well as CHF location for a non-uniform AFD as illustrated in figure 12c.

2.10.4 Boiling Length Average Approach

In the subcooled region or at low steam qualities, C (Eq. (2.57)) is large, thus the memory effect is small, and the local heat flux primarily determines CHF condition. At high qualities, however, the upstream memory effect becomes strong for a greater upstream length from CHF location, and the average heat flux primarily determines the CHF. The boiling length hypothesis and the BLA approach are therefore proposed for the prediction of CHF in this region. Here, the boiling length is defined as a length from the onset of bulk boiling (X=0) to the CHF location, i.e.,

$$L_B = z_{cr} - z_{X=0} \tag{2.58}$$

The boiling length hypothesis can be explained by an energy balance equation in the boiling length:

$$\text{Power}_B = \int_{z_{X=0}}^{L_B + z_{X=0}} P_h q''(z)dz = GA_c i_{fg} X_{cr} \tag{2.59}$$

where Power_B is the critical power over the boiling length, P_h is the heated perimeter and A_c is the cross sectional area of the boiling channel. This equation suggests that both the Power_B and X_{cr} are the function of boiling length at fixed G, i_{fg}, $q''(z)$, and channel geometry. The boiling length hypothesis leads to the development of the CISE correlation (Bertoletti et al. 1964, 1965) by which the upstream hydrodynamic effect on CHF in quality region is expressed by a boiling length. Keeys et al. (1971) concluded that the boiling length hypothesis was more successful than a local conditions hypothesis in correlating liquid film dryout conditions when he compared the measured CHF values and dryout locations with those predicted by CISE correlation and the correlations based on the local conditions hypothesis.

Alternatively, the BLA approach was proposed by Groeneveld (1999) to meet the need for an upstream average heat flux to determine the CHF condition in the quality region. The boiling length average heat flux q''_{BLA} is defined as

$$q''_{BLA}(z_{cr}) = \frac{1}{L_B} \int_{z_{X=0}}^{z_{cr}} q''(z)dz \tag{2.60}$$

In order to determine the CHF for non-uniform AFD from the equivalent uniform CHF, a factor K_5 was defined as

$$K_5 = \frac{q''_{loc}(z_{cr})}{q''_{BLA}(z_{cr})} \tag{2.61}$$

CHF is assumed to occur at the location at which the boiling length average heat flux, q''_{BLA}, equals to the equivalent uniform CHF, q''_{cr_EU}. Thus, the CHF for non-uniform AFD can be consequently obtained by

$$q''_{cr\_non} = q''_{loc}(z_{cr}) = K_5 q''_{cr\_EU} \tag{2.62}$$

Different from Tong's F-factor method, which modifies the uniform CHF value, the BLA method modifies the local heat flux. The BLA method can be stated as that the CHF for non-uniform AFD equals to the local heat flux at the location where the q''_{BLA} reaches the value of the CHF for uniform AFD at the same local conditions (see Figure 2.12d).

Detailed computation procedure of CHF prediction for a tube with non-uniform AFD using each method is described in Appendix E.

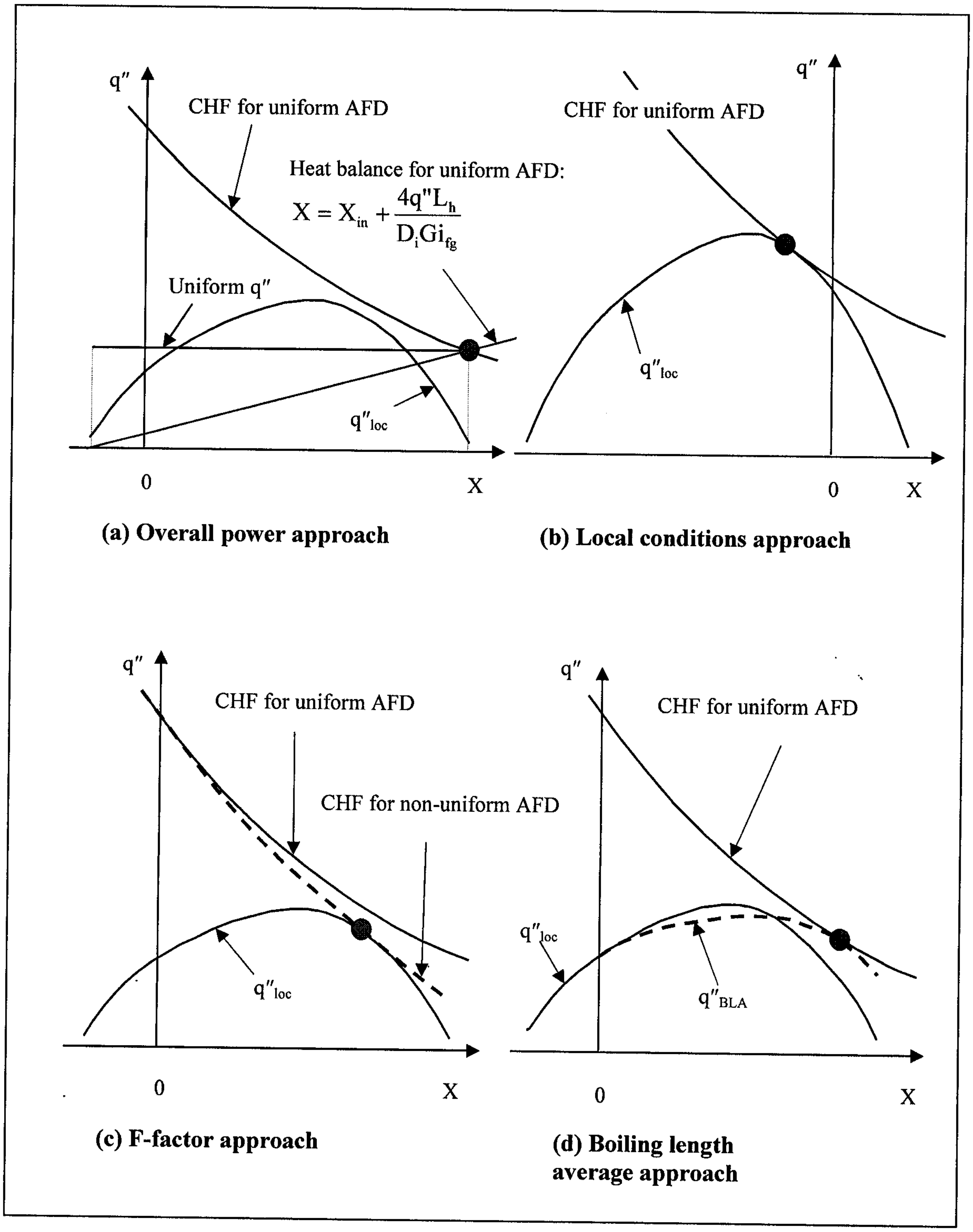

Figure 2.12 Schematic Representation of Definition of CHF Prediction Methods for Non-uniform AFD.

3. DESCRIPTION OF THE EXPERIMENT

The experiments were performed at pressures between 1662 to 2389 kPa, and mass fluxes between 2827 and 4648 kg m^{-2} s^{-1}. These are equivalent to 10 to 14 MPa, and 4000 to 6500 kg m^{-2} s^{-1} in water. AFD profiles with inlet, middle or outlet peak were all investigated and their CHFs and critical powers were compared with those of the uniform heat flux distribution.

3.1 Test Matrix

The fluid-to-fluid modeling of CHF described in Section 2.7 is employed to convert the HFC-134a parameters into water-equivalent parameters. The Katto similarities, i.e., the geometric, hydrodynamic and thermodynamic similarities are summarized in Table 3.1. If these similarities exist, the following dimensionless CHF expression for both fluids will be the same.

$$\frac{CHF}{i_{fg}G} = f\left(\frac{\rho_f}{\rho_g}, \frac{G^2 D_i}{\rho_f \sigma}, X, \frac{L_h}{D_i}\right)$$

The test conditions of HFC-134a of the experiment and corresponding water-equivalent conditions are given in Tables 3.2a and 3.2b.

3.2 Experimental Loop

The experiment was conducted in the multi-fluid test loop at University of Ottawa (Figure 3.1) using HFC-134a as the working fluid. The main components of the loop are test section, condenser, pressurizer, pumps, preheaters, power supply and related instruments.

Table 3.1 Katto Similarities

Geometric similarity	$(L_h)_R = (L_h)_W$, $(D_i)_R = (D_i)_W$
Hydrodynamic similarity	$(G^2 D_i / (\rho_f \sigma))_R = (G^2 D_i / (\rho_f \sigma))_W$ $(\rho_f / \rho_g)_R = (\rho_f / \rho_g)_W$
Thermodynamic similarity	$(X(z))_R = (X(z))_W$

Table 3.2a Test Conditions for HFC-134a

Test section	Inlet temperature range (°C)	Pressure range (kPa)	Mass flux range (kg m^{-2} s^{-1})	Heated length (m)
Uniform	18 to 73 (-0.73 to –0.03)*	1662 to 2389	2827 to 4648	0.7, 1.22, 1.5, 2.0, 2.2
TS No. 1	6 to 73 (-0.91 to –0.02)*	1662 to 2389	2827 to 4648	Forward: 1.49, 2.0 Reverse: 1.51
TS No. 2	21 to 74 (-0.73 to –0.01)*	1662 to 2389	2827 to 4648	Forward: 1.275 Reverse: 1.35

* Inlet quality range

Table 3.2b Test Conditions and Their Equivalents

Flow Parameter			
HFC134a value		Water-equivalent value	
Pressure (kPa)	Mass flux (kg m^{-2} s^{-1})	Pressure (kPa)	Mass flux (kg m^{-2} s^{-1})
1662	2827	10000	4000
	3533		5000
	4594		6500
2022	2842	12000	4000
	3552		5000
	4618		6500
2389	2861	14000	4000
	3576		5000
	4648		6500

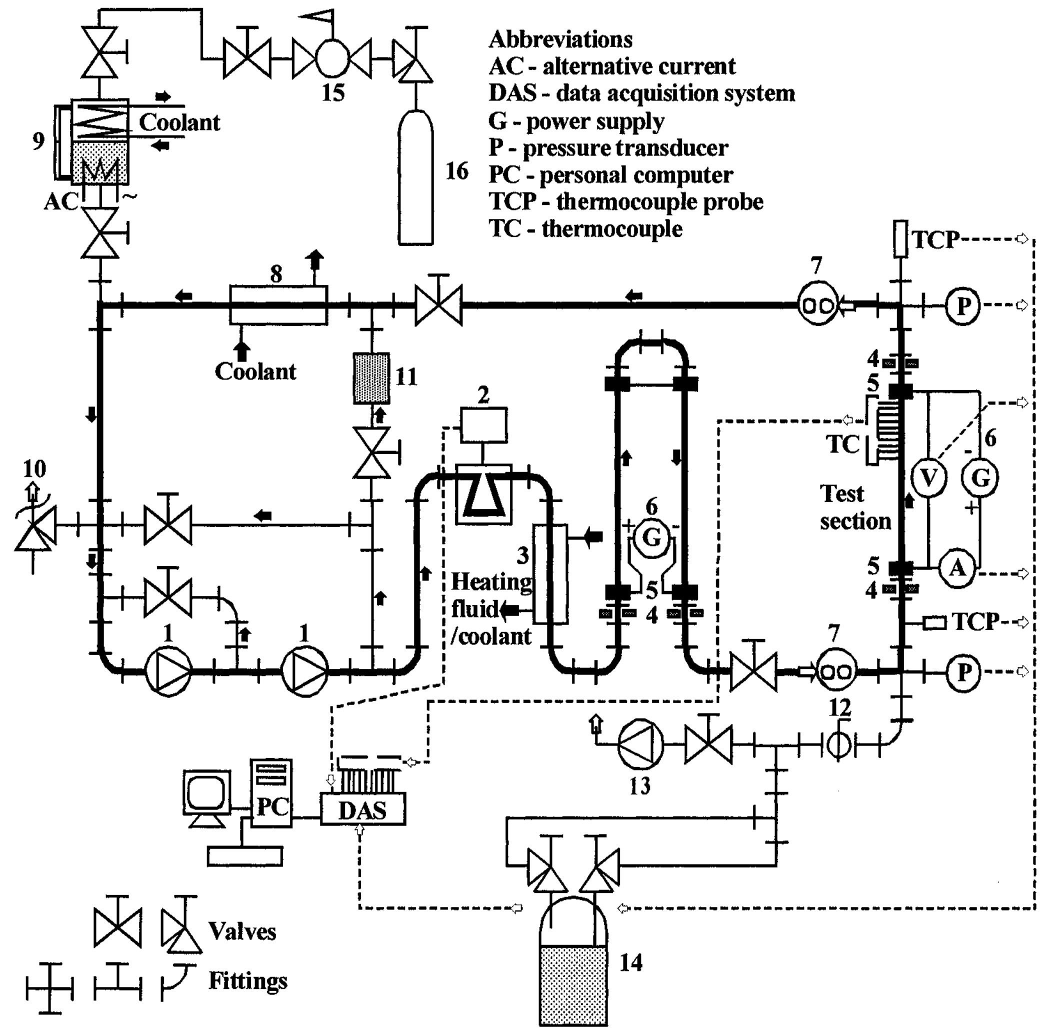

1-gear pump, 2-Coriollis type mass-flow-meter, 3-pre-heater, 4-dielectric fittings, 5-power terminals, 6-electrical pre-heater, 7-sight glass, 8-condenser, 9-pressurizer, 10-pressure relief valve, 11-refrigerant filter-dryer, 12-ball-valve, 13- vacuum pump, 14-refrigerant storage tank, 15-pressure reducer, 16-nitrogen container.

Figure 3.1 Experimental Multi-Fluid Loop (Vertical Test Section).

The test section is directly heated by a 12 kW DC power supply (40V, 300 A). The inlet and outlet fluid temperatures of the test section are measured by two RTDs. The flow is recirculated by two gear pumps, installed in series, delivering a constant mass flow rate.

A bypass system around the pumps and the test section controls the flow rate. The flow is measured by a Coriollis flow meter with an accuracy of better than 0.5% (flow range 0 – 0.34 kg s^{-1}). The pressure in the loop is controlled by the pressurizer. The pressurizer contains a heating coil, located at the bottom of the pressurizer, and a cooling coil near the top of the pressurizer. The power to the pressurizer heater (maximum 500 W) is regulated by an adjustable AC transformer. An electric pre-heater (maximum power 5 kW) and a coaxial heat exchanger (with hot water on the secondary side) are located between the pumps and the test section. They are used to adjust the test section inlet fluid temperature or inlet mass quality to the desired values. The vapour generated in the test section is condensed by a coaxial heat exchanger prior to the fluid being recirculated to the pump.

3.3 Description of the Test Sections

Three test sections (TS) were used in this investigation:

(i) the uniform AFD tube,

(ii) TS No. 1 non-uniform AFD tube and

(iii) TS No. 2 non-uniform AFD tube.

Schematic drawings of the test sections are shown in Figures 3.2, 3.3a, 3.3b, 3.4a and 3.4b. These test sections are made of Inconel 600, having an ID of 5.461 mm and 2500 mm in length. The stepped AFD profiles are realized by changing the wall thickness at each step. Because the material properties and the thin tube wall, certain machining imperfectness were present which affected the desired AFD profile. OD values were measured at each step of the test section and then compared with the design values (Tables 3.3 and 3.4). The OD profiles of the two non-uniform AFD test sections are shown in Figures 3.5 and 3.6, respectively. It can be seen that the discrepancies of the

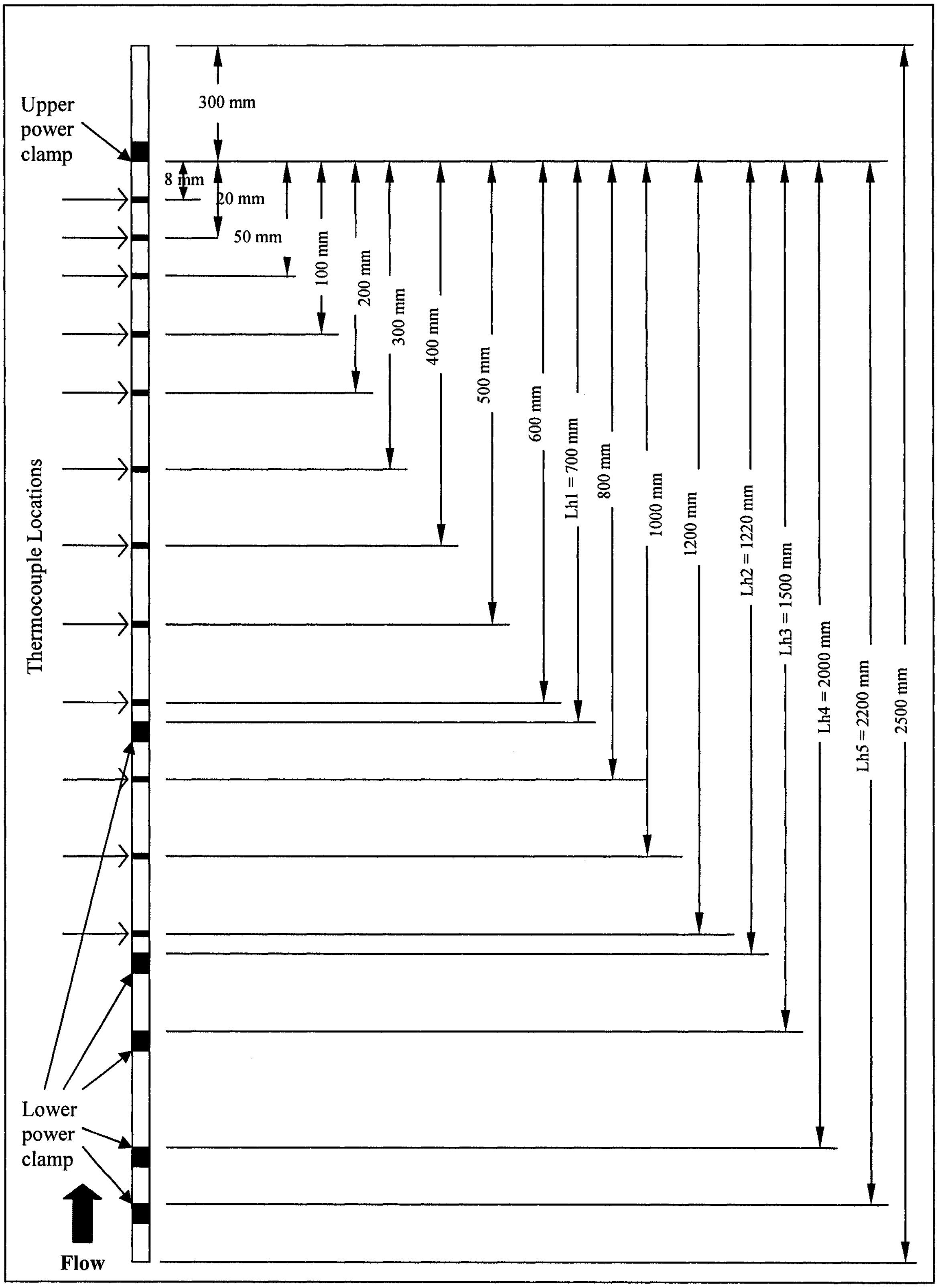

Figure 3.2 Uniform AFD Test Section.

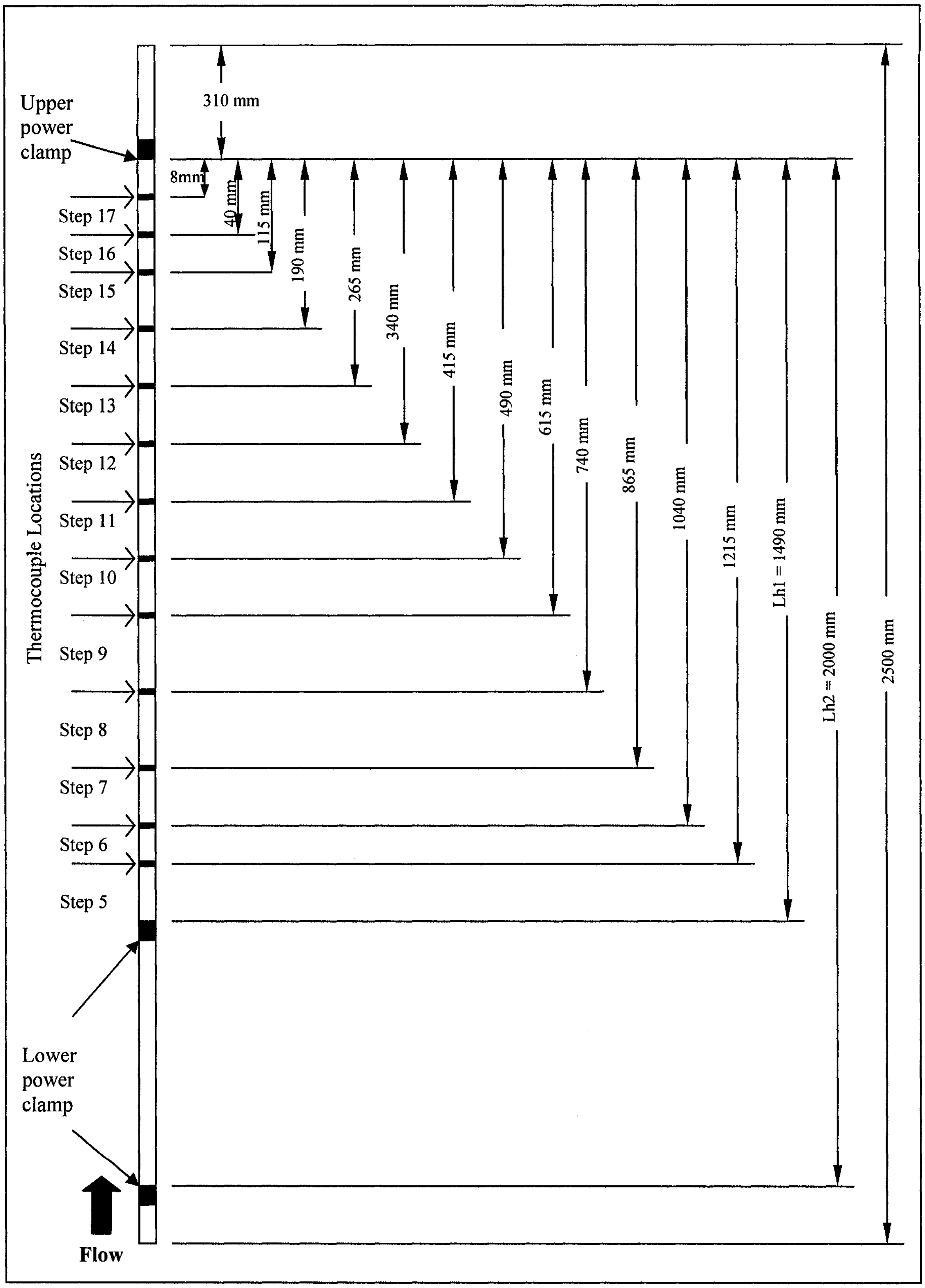

Figure 3.3a TS No. 1, Forward Flow Direction.

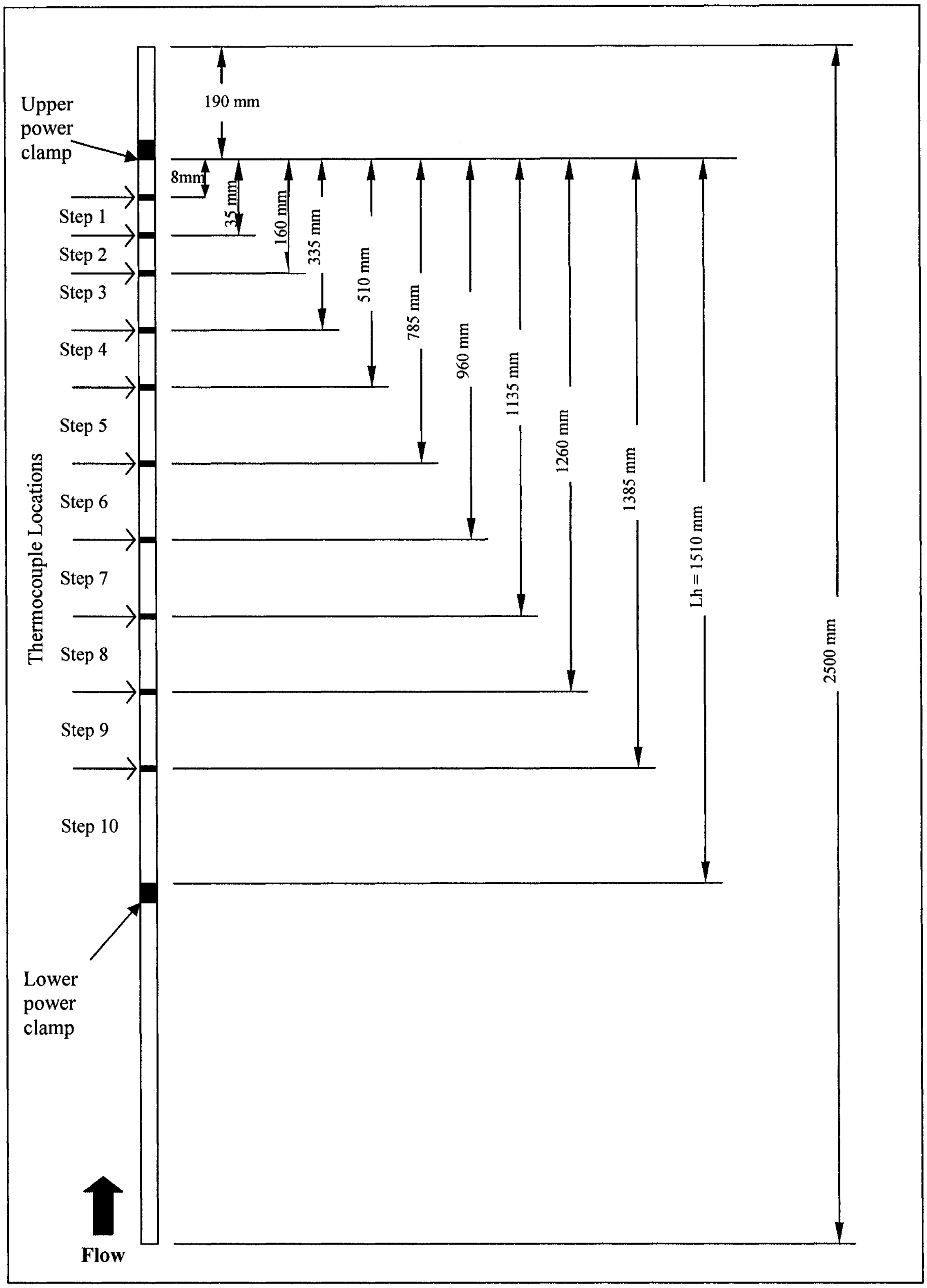

Figure 3.3b TS No. 1, Reverse Flow Direction.

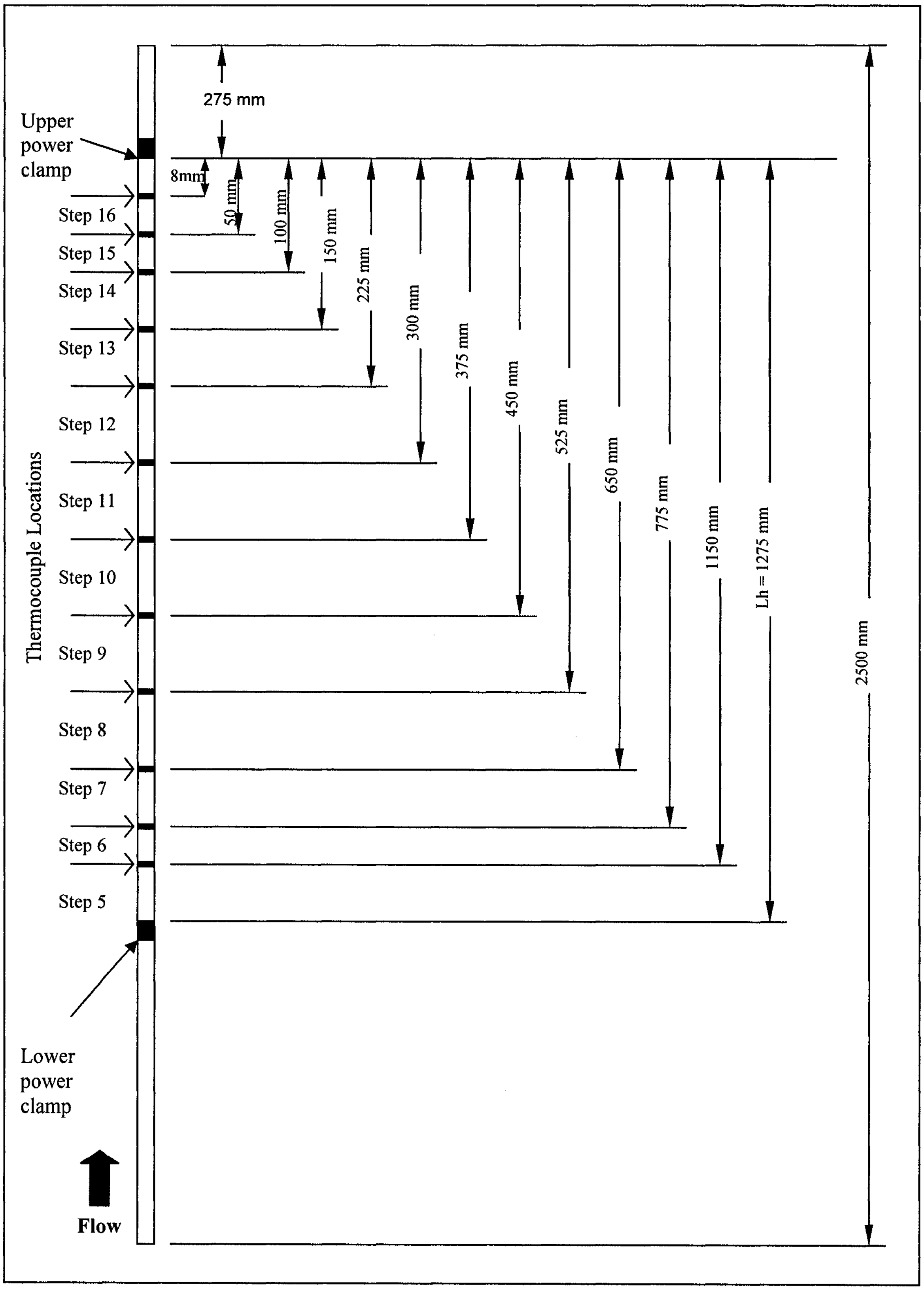

Figure 3.4a TS No. 2, Forward Flow Direction.

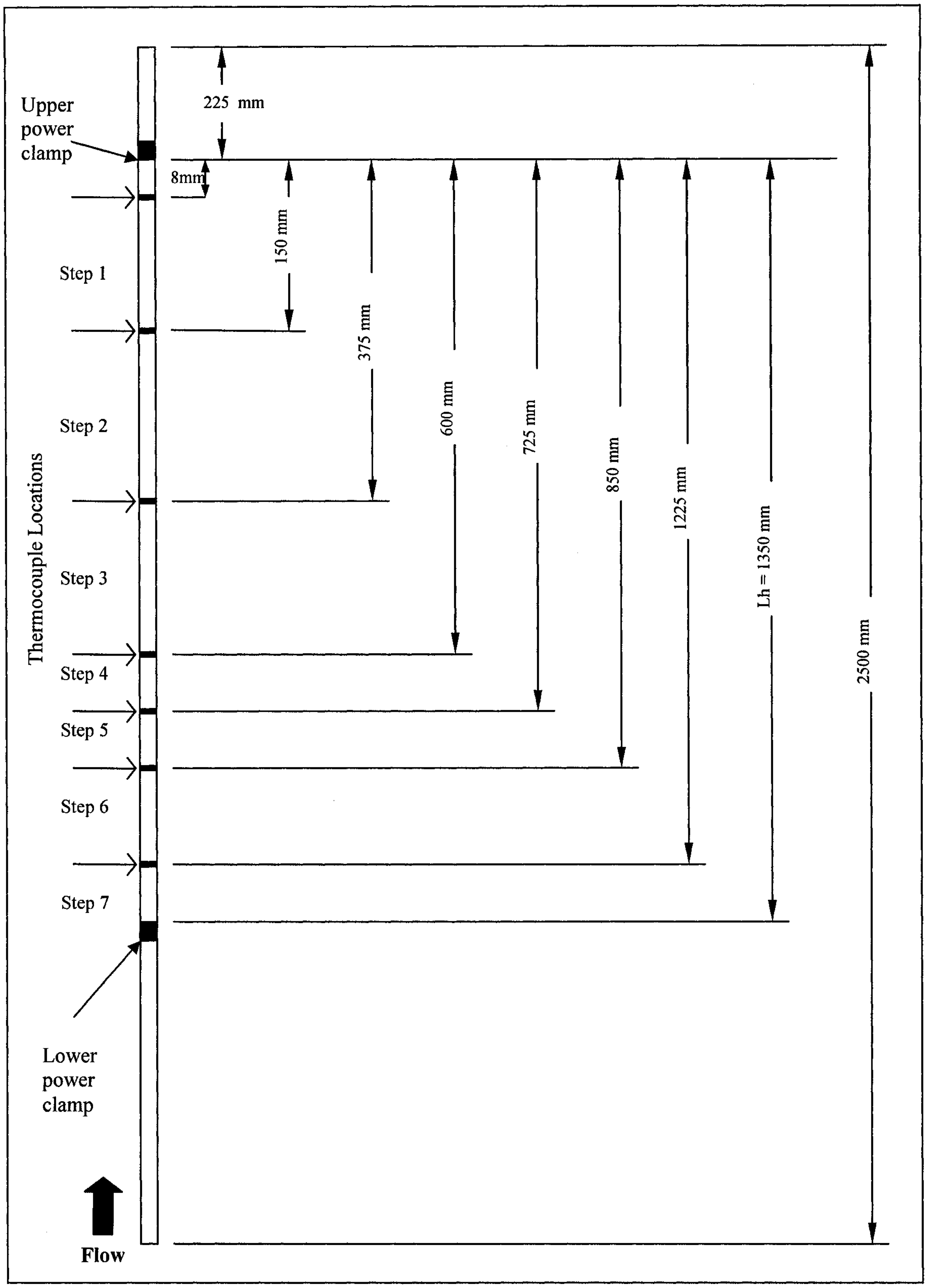

Figure 3.4b TS No. 2, Reverse Flow Direction.

Table 3.3 OD Measurements – TS No. 1

Measurement at University of Ottawa							Design	
Step No.	Axial Location of Steps	Measured Location	Measured OD	Measured OD (Turn 90°)	Average OD	Average Wall Thickness	OD	Wall Thickness
	mm	mm	mm	mm	mm	mm	mm	mm
1	from 0 to 225	50 135 220	8.034 8.034 8.034	8.032 8.034 8.034	8.034	1.286	7.938	1.239
2	from 225 to 350	230 287.5 345	7.478 7.447 7.463	7.477 7.452 7.460	7.463	1.001	7.476	1.008
3	from 350 to 525	355 437.5 520	6.899 6.922 6.927	6.901 6.920 6.921	6.915	0.727	6.916	0.728
4	from 525 to 700	530 612.5 695	6.678 6.695 6.695	6.678 6.689 6.691	6.688	0.613	6.690	0.615
5	from 700 to 975	705 837.5 970	6.652 6.647 6.607	6.650 6.651 6.610	6.636	0.588	6.634	0.587
6	from 975 to 1150	980 1062.5 1145	6.703 6.706 6.701	6.709 6.705 6.701	6.704	0.621	6.667	0.603
7	from 1150 to 1325	1155 1237.5 1320	6.774 6.764 6.764	6.770 6.765 6.764	6.767	0.653	6.721	0.630
8	from 1325 to 1450	1330 1387.5 1445	6.795 6.726 6.772	6.790 6.732 6.776	6.765	0.652	6.765	0.652
9	from 1450 to 1575	1455 1512.5 1570	6.820 6.825 6.828	6.801 6.823 6.832	6.821	0.680	6.801	0.670
10	from 1575 to 1700	1580 1637.5 1695	6.871 6.858 6.855	6.868 6.861 6.860	6.862	0.701	6.844	0.692
11	from 1700 to 1775	1705 1737.5 1770	6.922 6.914 6.922	6.920 6.916 6.921	6.919	0.729	6.893	0.716
12	from 1775 to 1850	1780 1812.5 1845	6.975 6.960 6.977	6.972 6.961 6.989	6.972	0.756	6.947	0.743
13	from 1850 to 1925	1855 1887.5 1920	7.061 7.074 7.066	7.070 7.072 7.068	7.069	0.804	7.023	0.781
14	from 1925 to 2000	1930 1962.5 1995	7.158 7.158 7.142	7.152 7.152 7.148	7.152	0.845	7.133	0.836
15	from 2000 to 2075	2005 2037.5 2070	7.305 7.310 7.308	7.311 7.320 7.307	7.310	0.925	7.293	0.916
16	from 2075 to 2150	2080 2112.5 2145	7.564 7.564 7.564	7.564 7.564 7.564	7.564	1.052	7.532	1.036
17	from 2150 to 2450	2155 2242.5 2330	8.034 8.034 8.034	8.034 8.034 8.034	8.034	1.287	7.938	1.239

Table 3.4 OD Measurements – TS No. 2

Measurement at University of Ottawa							Design	
Step No.	Axial Location of Steps	Measured Location	Measured OD	Measured OD (Turn 90°)	Average OD	Average Wall Thickness	OD	Wall Thickness
	mm	mm	mm	mm	mm	mm	mm	mm
1	from 0	50	8.006	8.001	8.001	1.270	7.938	1.239
		210	8.001	8.001				
	to 375	370	7.998	8.001				
2	from 375	380	7.122	7.036	7.093	0.816	7.139	0.839
		487.5	7.117	7.061				
	to 600	595	7.163	7.061				
3	from 600	605	6.769	6.718	6.733	0.636	6.797	0.668
		712.5	6.769	6.731				
	to 825	820	6.731	6.680				
4	from 825	830	6.680	6.528	6.607	0.573	6.692	0.616
		887.5	6.650	6.553				
	to 950	945	6.655	6.579				
5	from 950	955	6.579	6.553	6.568	0.554	6.644	0.592
		1012.5	6.609	6.553				
	to 1075	1070	6.576	6.541				
6	from 1075	1080	6.502	6.515	6.500	0.519	6.610	0.575
		1262.5	6.502	6.477				
	to 1450	1445	6.513	6.490				
7	from 1450	1455	6.655	6.604	6.617	0.578	6.644	0.592
		1512.5	6.683	6.553				
	to 1575	1570	6.629	6.579				
8	from 1575	1580	6.728	6.617	6.652	0.596	6.697	0.618
		1637.5	6.701	6.579				
	to 1700	1695	6.711	6.579				
9	from 1700	1705	6.736	6.604	6.695	0.617	6.737	0.638
		1737.5	6.782	6.629				
	to 1775	1770	6.761	6.655				
10	from 1775	1780	6.787	6.731	6.789	0.664	6.821	0.680
		1812.5	6.888	6.731				
	to 1850	1845	6.868	6.731				
11	from 1850	1855	6.934	6.807	6.854	0.697	6.912	0.726
		1887.5	6.886	6.795				
	to 1925	1920	6.896	6.807				
12	from 1925	1930	7.010	6.909	6.968	0.754	7.029	0.784
		1962.5	7.010	6.934				
	to 2000	1995	7.010	6.934				
13	from 2000	2005	7.142	7.049	7.109	0.824	7.199	0.869
		2037.5	7.125	7.051				
	to 2075	2070	7.176	7.112				
14	from 2075	2080	7.407	7.341	7.369	0.954	7.407	0.973
		2100	7.404	7.315				
	to 2125	2120	7.404	7.341				
15	from 2125	2130	7.597	7.493	7.504	1.022	7.621	1.080
		2150	7.569	7.455				
	to 2175	2170	7.493	7.417				
16	from 2175	2180	7.981	7.899	7.940	1.240	7.938	1.239
		2265	7.981	7.899				
	to 2450	2350	7.981	7.899				

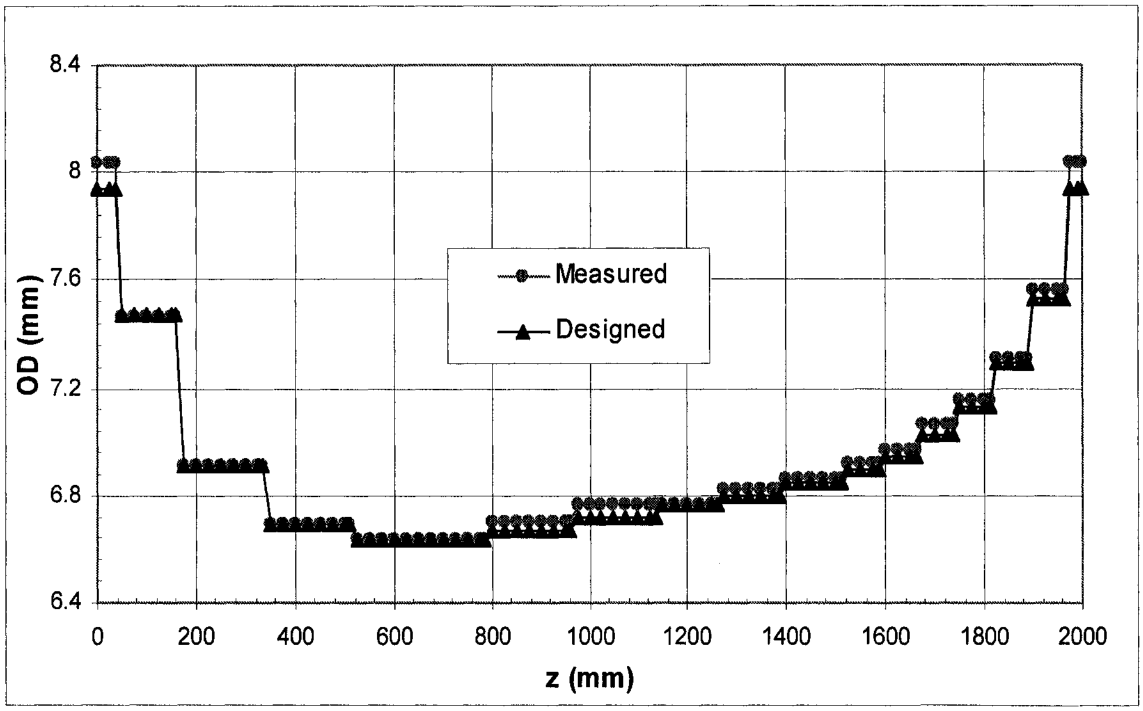

Figure 3.5 OD Variation of TS No. 1.

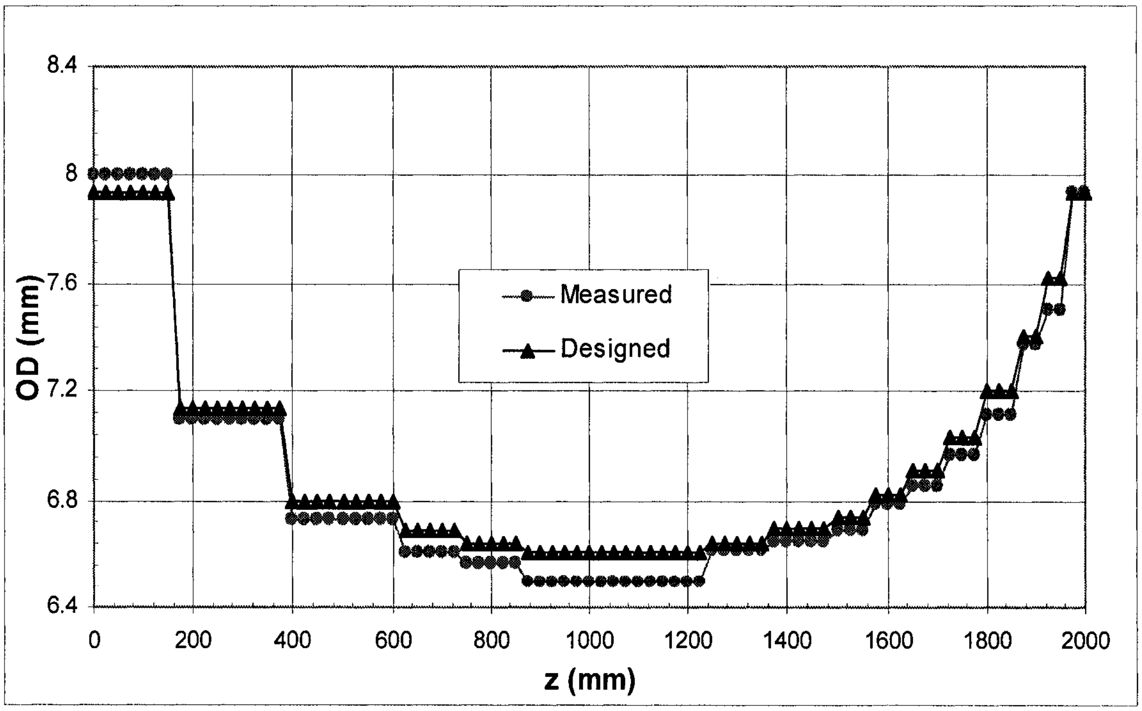

Figure 3.6 OD Variation of TS No. 2.

measured OD values exist not only in the axial direction but also in the circumferential direction in the same plane of each step, which imply that there are circumferential imperfections at several planes. The electrical resistance at each step of the test section was measured as well. The AFD profiles based on measured OD and measured electrical resistance of the two test sections were derived and compared with the ones based on designed OD (Figures 3.7 and 3.8). They are in good agreement except at step 4 of TS No. 2 tube where the local heat flux based on measured resistance is unexpectedly lower than that based on measured OD.

To investigate the effect of inlet peak versus outlet peak AFD, CHF measurements were obtained with both forward flow and reverse flow (obtained after inverting the test section) directions. CHF was detected by quick-response K-type thermocouples. In order to adjust the circumferential locations of the thermocouples at each plane, wooden clothespins were used to which two thermocouples were attached, 180° apart. The thermocouples-clothespins were installed at the planes of interest. Several heated lengths were employed to permit measuring critical powers over a broad range of critical qualities. The upper power clamp was installed at locations between 190 mm and 310 mm from the upper end of the tube. This assures that the flow pattern at the end of the heated length is unaffected by the abrupt changes in flow area because of the swagelok fitting at the outlet. Similarly sufficient unheated calming length was provided at the inlet end of the tube to establish fully developed flow. The most downstream thermocouple pair was installed 8mm upstream from the upper power clamp. 12 thermocouple pairs were used for the uniform AFD test section. For the non-uniform AFD test sections, thermocouples were installed at the sites 1-2 mm upstream from the downstream end of each step after the peak heat flux locations.

3.4 Experimental Procedure

In this experimental study, CHF tests were conducted using uniform AFD test section and two non-uniform AFD test sections. The non-uniform AFD test sections were tested in

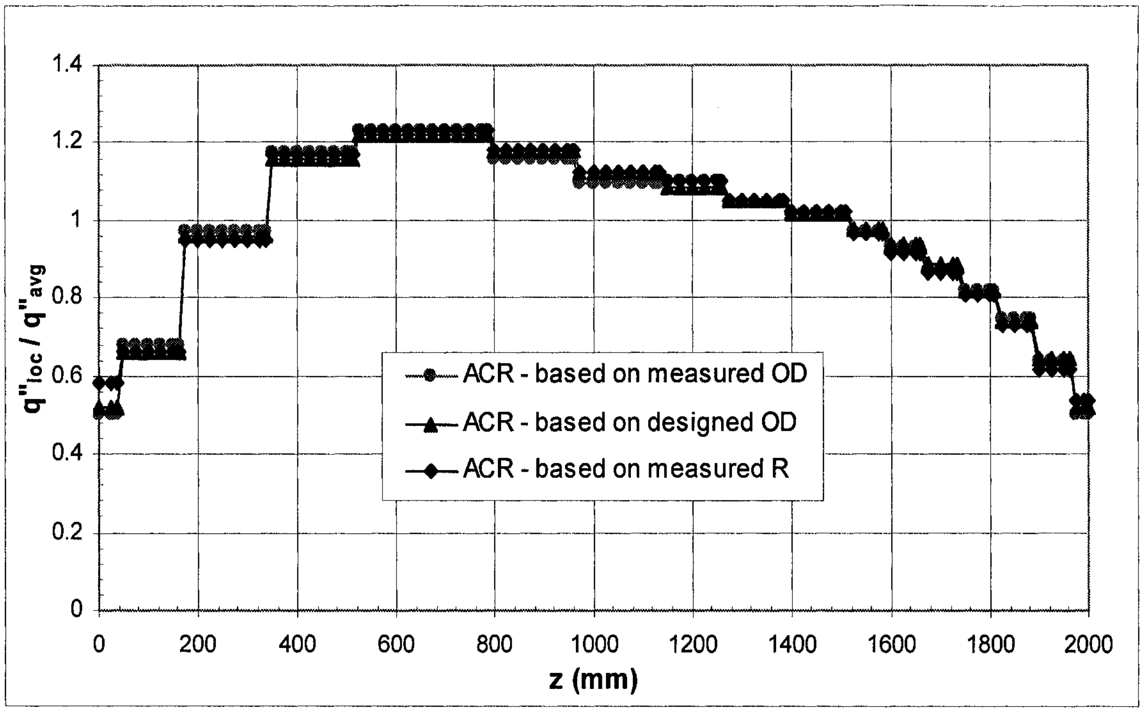

Figure 3.7 AFD Profile of TS No. 1.

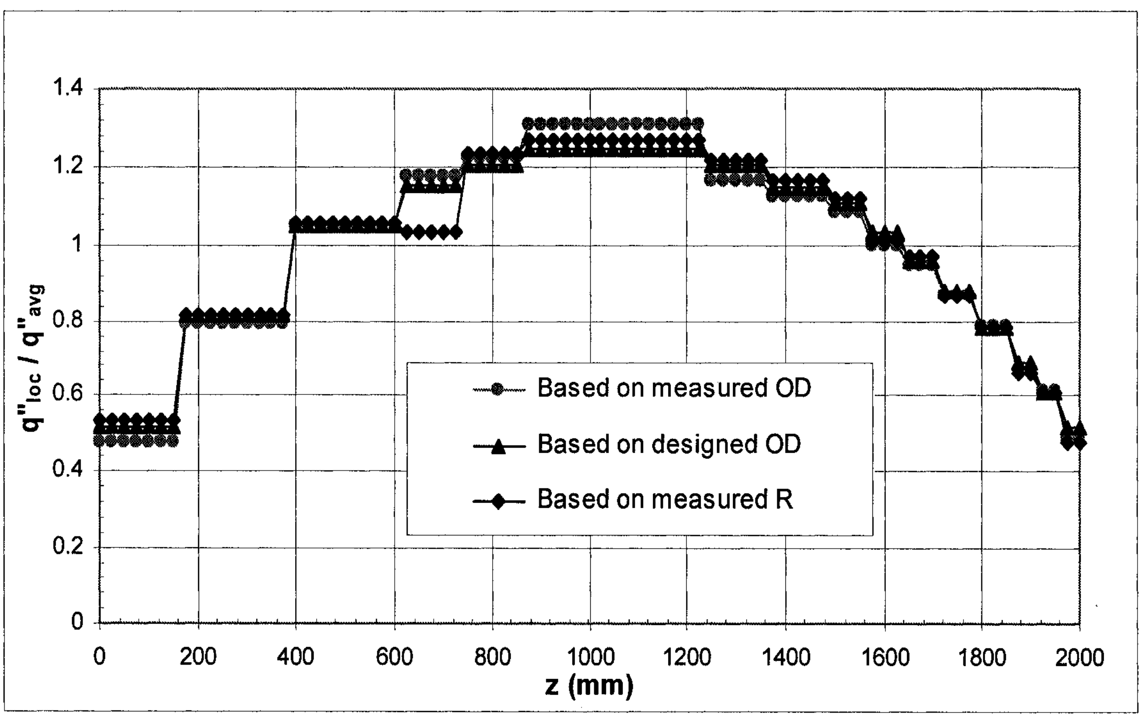

Figure 3.8 AFD Profile of TS No. 2.

both forward and reverse flow directions. The radial heat flux distribution (RFD) effect caused by machining imperfectness was investigated as well.

Various checks were performed after the test section installation but prior to the start of the CHF test program. These checks included leakage detection, transient temperature test, heat loss test, heat balance test, thermocouple calibration, pressure calibration, voltage calibration and current calibration. Detailed descriptions of these checks are presented in Appendix B.

The quality assurance (Q/A) experimental CHF point (at fixed flow conditions) was measured repeatedly during the course of this experiment. The results were compared with the value in CHF look up table (1995) at the same condition after the conversion for fluid and geometry. To further assure the repeatability of the data, the Q/A reference CHF data point was repeated following the completion of the CHF test on each test section. These repeatability results are given in Table B1.

It was found that for the uniform test section without insulation the heat loss was very small (0.037 kW at an average thermocouple temperature of 77°C). The difference between the power supplied to the test section and the enthalpy rise of the working fluid in heat balance test was less than 1%. This justified the use of an un-insulated test section.

3.4.1 CHF Test for Uniform AFD Test Section

In order to acquire CHF at stable flow conditions, pressure and mass flux were continually adjusted along with the increase of the power to the test section until the occurrence of the CHF. The power was then reduced by 1-5% depending on the flow condition (P, G and T_{in}), and then subsequently increased very slowly until the CHF was again detected at which point the CHF conditions were recorded. In general, the pressure and mass flux were quite steady before and after the CHF occurrence except for the runs at very high pressure, very high mass flux and very low inlet temperature – in this case, the pressure and mass flux fluctuated rapidly after CHF occurred. The value of the inlet temperature was varied from 2°C below the saturation temperature to the minimum available value, which depended on the cooling water temperature (separate cooling of the Freon in an ice bath was provided as well). The wide range of inlet temperatures combined with the change of heated length resulted in a wide range in critical qualities. The inlet temperature was controlled by adjusting both the water temperature in the coaxial pre-heater and the power to the electric pre-heater. CHF tests with high inlet temperatures were performed first; the inlet temperature was then reduced in steps of 2 to 5°C for the next run. This minimized the fluctuation in pressure and flow, and avoided the reduction in test section power (flow and pressure fluctuations frequently occurred if the test series started with the lowest inlet temperatures). After the completion of the CHF test for the whole range of inlet temperature, the pressure was maintained and the flow was changed to the next mass flux in the test matrix.

3.4.2 CHF Test for Non-Uniform AFD Test Section

Compared to the uniform AFD tests, the non-uniform AFD tests were more complex. The CHF could occur at multiple locations simultaneously in a non-uniform AFD test section, and the CHF locations could shift or spread in the downstream and upstream directions when the inlet temperature was changed. The local heat flux depends on the electrical resistance at each step; therefore, the electrical resistance of each step was measured before the start of the CHF test.

3.4.2.1 Resistance Measurement

A RadioShack universal meter with an accuracy of +/-0.5% of reading was used to measure the voltage drop in each step. The sum of the measured voltage drops for each step was than compared with that measured by the DAS for the complete heated length. The discrepancy of these two values was less than 0.1%. The electrical resistance in each step (see Tables 3.5 and 3.6) was then evaluated by dividing the measured voltage drop in the step by the measured electrical current through the test section, which was measured by the DAS.

Table 3.5 Electrical Resistance Measurements – TS No. 1

Step No.	Axial Position from (mm)	Axial Position to (mm)	Measured* Voltage (V)	Calculated* Resistance (Ω)	Measured** Voltage (V)	Calculated** Resistance (Ω)
1	0	35.5	0.380	0.0018	0.400	0.0018
2	35.5	160.5	1.510	0.0071	1.610	0.0072
3	160.5	335.5	3.040	0.0144	3.250	0.0144
4	335.5	510.5	3.750	0.0177	4.020	0.0179
5	510.5	785.5	6.210	0.0294	6.650	0.0296
6	785.5	960.5	3.790	0.0179	4.050	0.0180
7	960.5	1135.5	3.600	0.0170	3.850	0.0171
8	1135.5	1260.5	2.530	0.0120	2.710	0.0120
9	1260.5	1385.5	2.410	0.0114	2.590	0.0115
10	1385.5	1510.5	2.350	0.0111	2.500	0.0111
11	1510.5	1585.5	1.330	0.0063	1.420	0.0063
12	1585.5	1660.5	1.260	0.0060	1.360	0.0060
13	1660.5	1735.5	1.190	0.0056	1.270	0.0056
14	1735.5	1810.5	1.110	0.0053	1.180	0.0052
15	1810.5	1885.5	1.000	0.0047	1.070	0.0048
16	1885.5	1960.5	0.850	0.0040	0.910	0.0040
17	1960.5	2000	0.390	0.0018	0.430	0.0019
Summation in each step			36.700	0.1737	39.270	0.1745
Overall measured value (for 2000 mm)			36.46	0.1726	38.995	0.1733

* For I = 206.36 A, Power = 7.508 kW

** For I = 212.49 A, Power = 8.011 kW

Table 3.6 Electrical Resistance Measurements – TS No. 2

Axial Position			Measured* Voltage (V)	Calculated* Resistance (Ω)	Measured** Voltage (V)	Calculated** Resistance (Ω)
Step No.	from (mm)	to				
1	0	150	1.455	0.0071	1.465	0.0069
2	150	375	3.330	0.0161	3.440	0.0162
3	375	600	4.310	0.0209	4.440	0.0209
4	600	725	2.351	0.0114	2.436	0.0115
5	725	850	2.800	0.0136	2.900	0.0136
6	850	1225	8.630	0.0418	8.890	0.0418
7	1225	1350	2.763	0.0134	2.801	0.0132
8	1350	1475	2.648	0.0128	2.741	0.0129
9	1475	1550	1.522	0.0074	1.613	0.0076
10	1550	1625	1.380	0.0067	1.474	0.0069
11	1625	1700	1.321	0.0064	1.396	0.0066
12	1700	1775	1.183	0.0057	1.241	0.0058
13	1775	1850	1.062	0.0051	1.112	0.0052
14	1850	1900	0.600	0.0029	0.639	0.0030
15	1900	1950	0.552	0.0027	0.572	0.0027
16	1950	2000	0.435	0.0021	0.546	0.0026
Summation in each step			36.342	0.1761	37.706	0.1774
Overall measured value (for 2000 mm)			36.36	0.1762	37.67	0.1773

* For I = 206.36 A, Power = 7.508 kW
** For I = 212.49 A, Power = 8.011 kW

3.4.2.2 Thermocouple Location

As mentioned in Section 3.3, machining imperfections were unavoidable in the construction of the AFD test sections. This has caused some non-uniformities in the radial heat flux distribution (RFD) and possibly a hot spot. To search for the presence of hot spots, the thermocouples-clothespins were rotated until one of the thermocouple indicated the maximum value. During this search, the wall was heated to approximately 5°C below the saturation temperature at very high pressure and mass flux. Generally, when one of the thermocouples detected the highest wall temperature at a given plane, the opposite thermocouple indicated usually the lowest temperature of that plane.

3.4.2.3 RFD Effect Exploration

The RFD effect was investigated by performing subsequent CHF measurements. After the initial occurrence of CHF at a given location, the power was increased further until the CHF was detected at the opposite side of the same plane. If CHF occurred simultaneously at several axial locations, then the first occurrence of CHF at the opposite side was noted. The discrepancy between these two critical powers (corresponding to the initial CHF occurrence at opposite sides) was in the range of 0.5% to 3% depending on the flow conditions and AFD profile. Generally it was higher for low pressures, low mass flows and high inlet temperatures. Figures 3.9a and 3.9b show an example of the RFD effect by plotting CHF versus critical quality and critical power versus inlet temperature, respectively. Frequently the CHF at the opposite location occurred after the CHF spread axially to adjacent steps. For the high pressures, high mass flows and low inlet temperatures, the wall temperature increased rapidly to a very high value and the pressure and mass flux fluctuated violently when additional power was added after the occurrence of the initial CHF. This phenomenon made it impossible to measure the CHF at the opposite location. The AFD analysis described in this thesis is based on the initial CHF occurrence at a given axial plane.

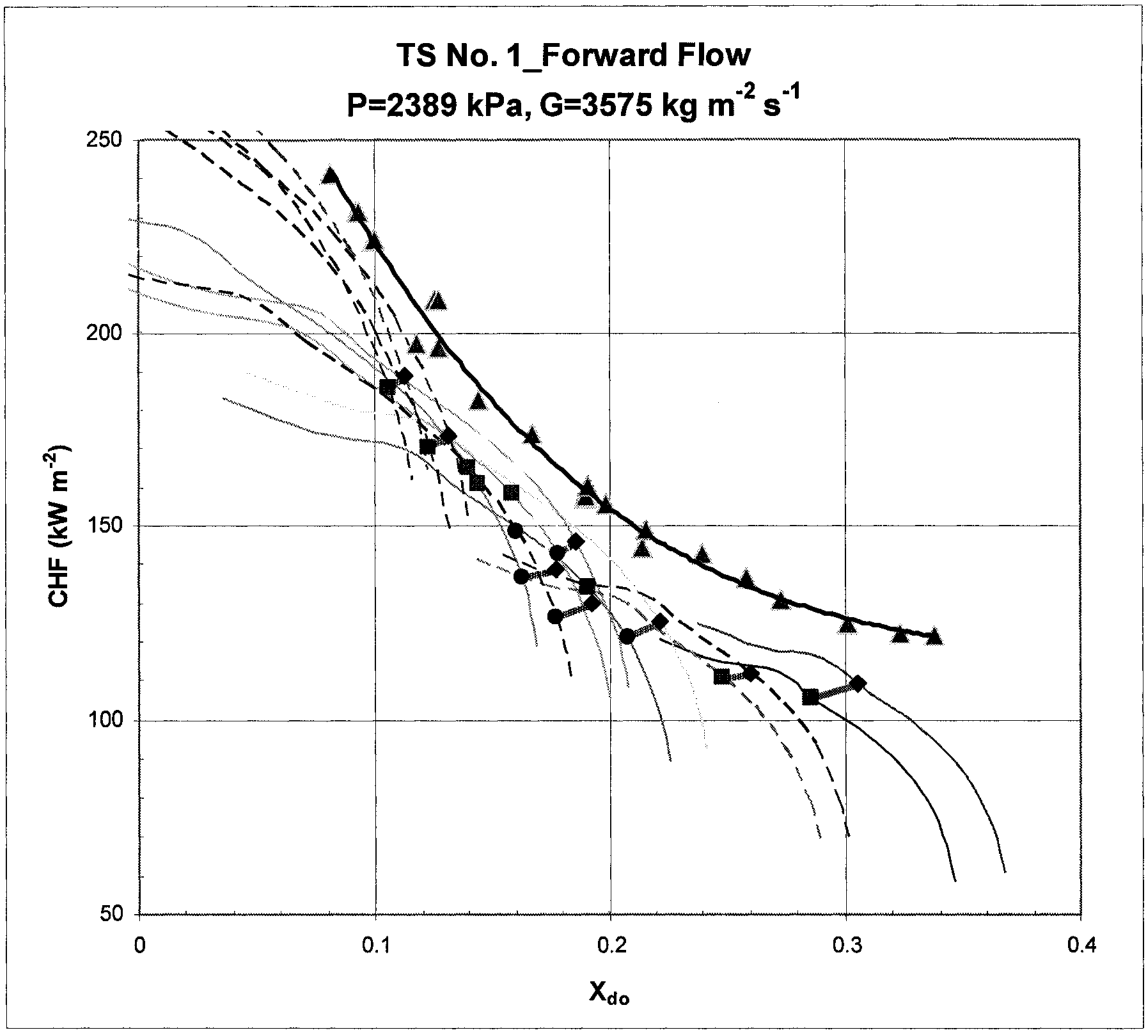

a. Thick curve – uniform CHF
b. Square point – initial CHF
c. Round point – the CHF point occurred simultaneously with the initial CHF at different axial locations
d. Diamond point – subsequent CHF occurring at the opposite side (short red line connects it to Preceding CHF)
e. Thin lines – AFD profile at different powers and different inlet temperatures (lines connected by short line were obtained at the same inlet temperature)

Figure 3.9a RFD Effect, Based on Local Conditions.

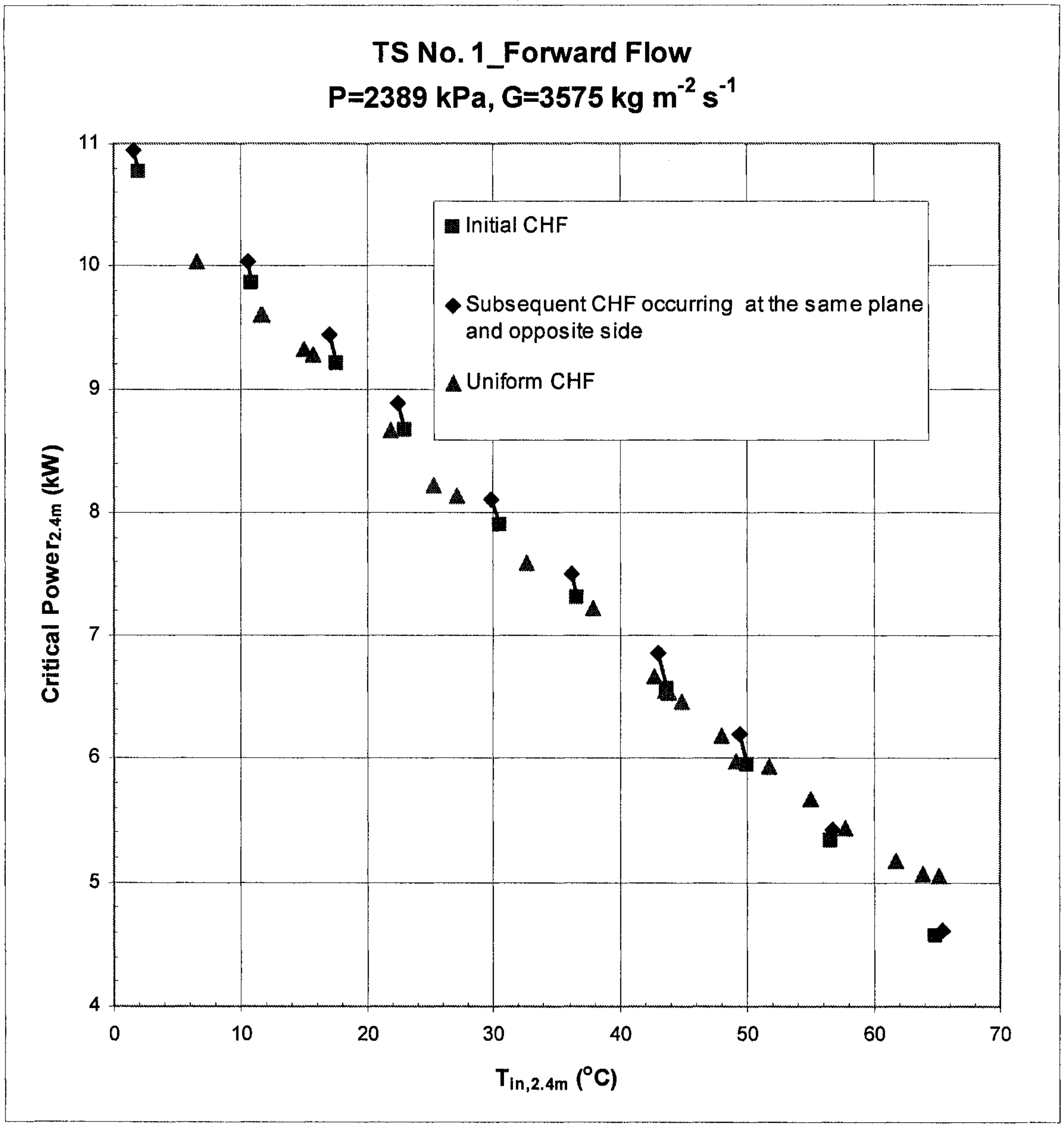

a. Points connected by line are initial CHF and subsequent CHF occurring at the same plane and opposite side of the test section

Figure 3.9b RFD Effect, Based on Inlet Conditions.

4. TEST RESULTS

The non-uniform AFD profiles of TS No. 1 and TS No. 2 were derived based on measured OD and measured electrical resistance, respectively. The CHF experimental data was obtained using HFC-134a as working fluid. Data with different heated lengths was converted into 2.4 meters equivalent value using heat balance equation. 2.4 meters is the value of the extended heated length corresponding to the complete ideal TS No. 1 and TS No. 2 non-uniform AFD profiles. The processed HFC-134a data was finally converted into the water-equivalent data related to the CANDU reactor conditions of interest.

4.1 AFD Profile Derivation

The AFD profiles based on measured OD were derived as follows:

$$\frac{q''_m}{q''_{avg}} = \frac{\dfrac{I^2 R_m}{\pi D_i L_{h,m}}}{\dfrac{I^2}{\pi D_i L_h}\left(R_1 + R_2 + \cdots + R_n\right)} = \frac{\dfrac{L_h}{D_{o,m}^2 - D_i^2}}{\dfrac{L_{h,1}}{D_{o,1}^2 - D_i^2} + \dfrac{L_{h,2}}{D_{o,2}^2 - D_i^2} + \cdots + \dfrac{L_{h,n}}{D_{o,n}^2 - D_i^2}} \tag{4.1}$$

The AFD profiles based on measured voltage drop were derived as follows:

$$\frac{q''_m}{q''_{avg}} = \frac{\dfrac{IU_m}{\pi D_i L_{h,m}}}{\dfrac{I}{\pi D_i L_h}\left(U_1 + U_2 + \cdots + U_n\right)} = \frac{L_h}{L_{h,m}} \times \frac{U_m}{\left(U_1 + U_2 + \cdots + U_n\right)} \tag{4.2}$$

The AFD profiles based on measured electrical resistance were used for the calculation of the local CHF value while the ones based on measured OD were treated as reference (see Figures 3.7 and 3.8). The calculated peaking factors k ($k = q''_{max} / q''_{avg}$) of TS No. 1 is 1.231, and that of TS No. 2 is 1.267.

The magnitude of the AFD profile changes along with the critical power but the shape remains the same. Figure 4.1 suggests that the critical power required for occurrence of the CHF condition increases as the inlet temperature decreases, consequently, the magnitude of the AFD profile increases. Another interesting fact revealed in Figure 4.1 is the existence of the difference between uniform CHF and non-uniform CHF at high qualities. This fact will be discussed in Chapter 5 in detail.

4.2 Comparison between the Reactor AFD Profile and the Actual AFD Profile of the U of O Test Sections

The actual stepped AFD profiles of the test sections are achieved by changing the wall thickness at each step, and accordingly changing the electrical resistance at each step. To make a feasible simulation of the ideal AFD profile, the start and the end parts of the complete ideal AFD profile were chopped off, because the electrical resistances there are too small to realize. Therefore, the AFD profiles used are really a truncated version of that of a longer test section that could not be accommodated in this test. The maximum heated length of the U of O test sections is about 2 meters while that corresponding to the complete ideal AFD profiles is 2.4 meters. As mentioned above, the peaking factors (i.e., maximum-to-average heat flux ratio) of the actual stepped AFD profile of TS No. 1 and TS No. 2 are 1.231 and 1.267, respectively. In certain CANDU reactors, however, the peaking factors of the complete ideal AFD profile of TS No. 1 and TS No. 2 are 1.398 and 1.437, respectively. Figures 4.2 and 4.3 show the comparison between the complete (labeled "ideal") AFD profiles of certain CANDU reactors and the actual stepped AFD profiles of U of O test sections. Table 4.1 shows the comparison of the resistances and axial heat flux distributions between the test sections with the ideal AFD profiles and the actual stepped AFD profiles.

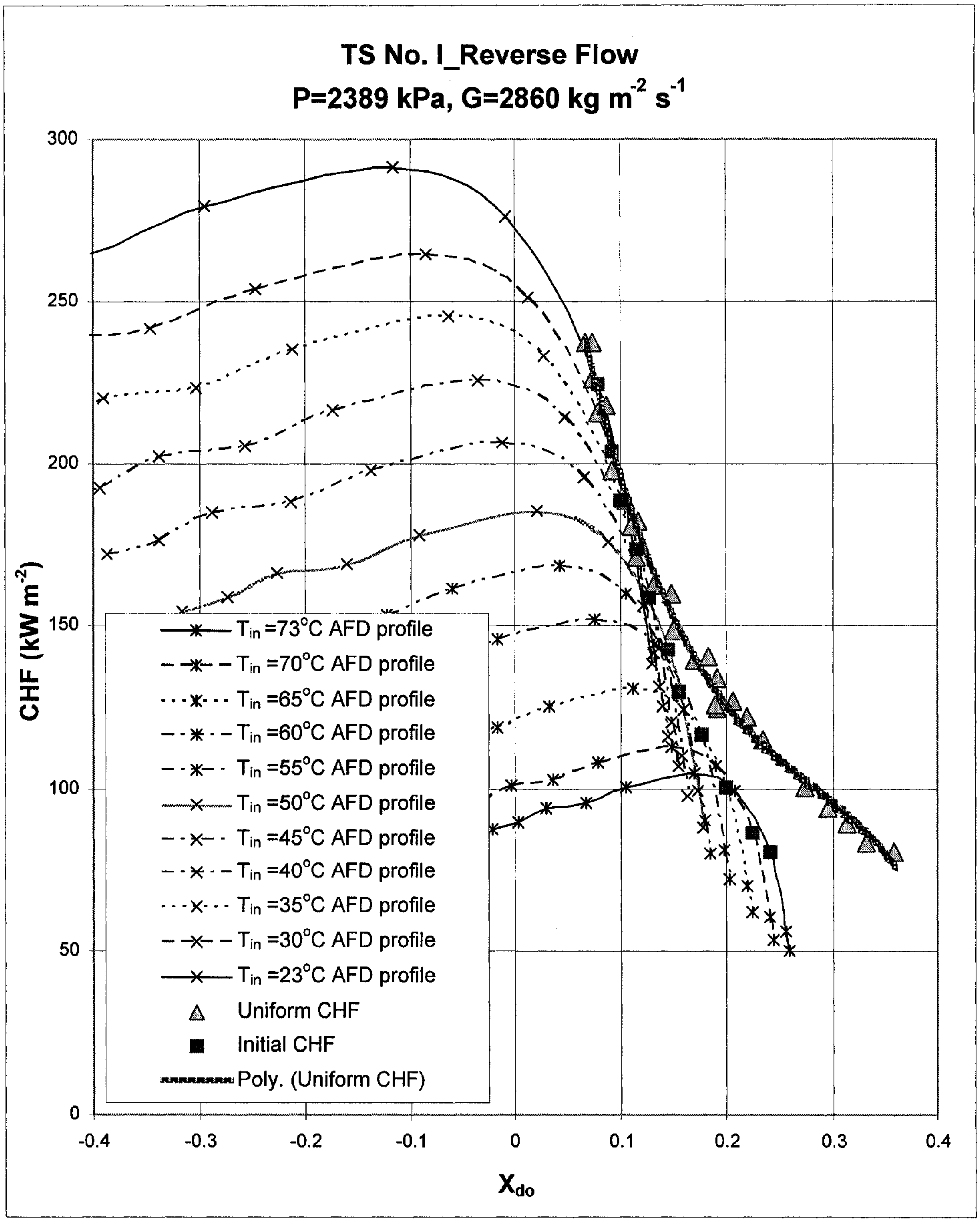

Figure 4.1 Magnitude Change of AFD Profile Along with the Change of CHF Conditions.

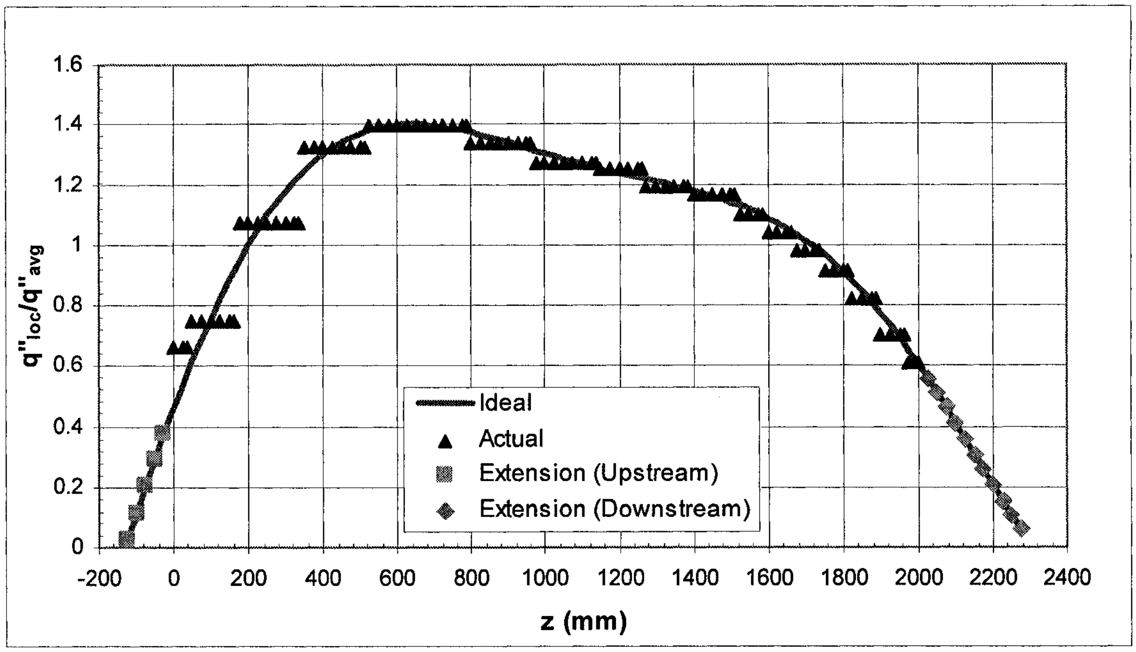

Figure 4.2 Comparison between the Complete Ideal AFD Profile and the Actual Stepped AFD Profile, TS No. 1.

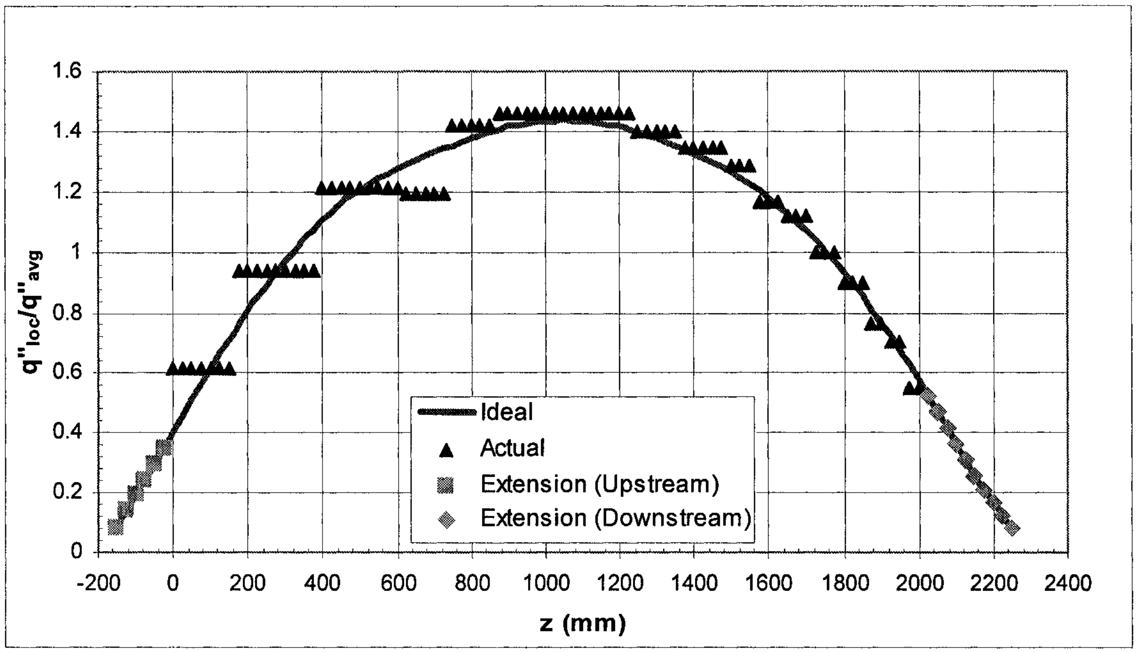

Figure 4.3 Comparison between the Complete Ideal AFD Profile and the Actual Stepped AFD Profile, TS No. 2.

Table 4.1 Resistance (in Each Step) and Axial Heat Flux Distribution of Test Sections

TS No.I					TS No. II				
z	Ideal		Actual		Z	Ideal		Actual	
(mm)	R (Ω)	q''_{loc}/q''_{avg}	R (Ω)	q''_{loc}/q''_{avg}	(mm)	R (Ω)	q''_{loc}/q''_{avg}	R (Ω)	q''_{loc}/q''_{avg}
-125	3.906E-05	0.024			-150	1.364E-04	0.082		
-100	1.895E-04	0.114			-125	2.319E-04	0.140		
-75	3.376E-04	0.203			-100	3.177E-04	0.191		
-50	4.826E-04	0.290			-75	4.003E-04	0.241		
-25	6.239E-04	0.375			-50	4.861E-04	0.292		
0	7.610E-04	0.458		0.661	-25	5.750E-04	0.346		
25	8.933E-04	0.537	0.583	0.661	**0**	6.672E-04	0.401		0.615
50	1.020E-03	0.614		0.746	25	7.529E-04	0.453		0.615
75	1.142E-03	0.687		0.746	50	8.419E-04	0.507		0.615
100	1.258E-03	0.757		0.746	75	9.308E-04	0.560		0.615
125	1.367E-03	0.823		0.746	100	1.020E-03	0.614		0.615
150	1.471E-03	0.885	0.658	0.746	125	1.102E-03	0.663		0.615
175	1.568E-03	0.943		1.072	150	1.185E-03	0.713	0.534	0.615
200	1.658E-03	0.998		1.072	175	1.264E-03	0.761		0.938
225	1.742E-03	1.048		1.072	200	1.341E-03	0.807		0.938
250	1.820E-03	1.095		1.072	225	1.411E-03	0.849		0.938
275	1.892E-03	1.138		1.072	250	1.484E-03	0.893		0.938
300	1.957E-03	1.177		1.072	275	1.550E-03	0.933		0.938
325	2.016E-03	1.213	0.947	1.072	300	1.617E-03	0.973		0.938
350	2.069E-03	1.245		1.323	325	1.674E-03	1.007		0.938
375	2.117E-03	1.273		1.323	350	1.735E-03	1.044		0.938
400	2.158E-03	1.299		1.323	375	1.785E-03	1.074	0.814	0.938
425	2.195E-03	1.320		1.323	400	1.836E-03	1.105		1.214
450	2.226E-03	1.339		1.323	425	1.884E-03	1.133		1.214
475	2.252E-03	1.355		1.323	450	1.932E-03	1.162		1.214
500	2.274E-03	1.368	1.168	1.323	475	1.967E-03	1.183		1.214
525	2.292E-03	1.379		1.394	500	2.001E-03	1.204		1.214
550	2.305E-03	1.387		1.394	525	2.036E-03	1.225		1.214
575	2.315E-03	1.393		1.394	550	2.068E-03	1.244		1.214
600	2.321E-03	1.397		1.394	575	2.097E-03	1.261		1.214
625	2.324E-03	1.398		1.394	600	2.125E-03	1.279	1.054	1.214
650	2.325E-03	1.399		1.394	625	2.151E-03	1.294		1.192
675	2.322E-03	1.397		1.394	650	2.173E-03	1.307		1.192
700	2.318E-03	1.394		1.394	675	2.192E-03	1.319		1.192
725	2.311E-03	1.390		1.394	700	2.214E-03	1.332		1.192
750	2.302E-03	1.385		1.394	725	2.233E-03	1.344	1.035	1.192
775	2.292E-03	1.379	1.231	1.394	750	2.252E-03	1.355		1.420
800	2.281E-03	1.372		1.337	775	2.271E-03	1.367		1.420
825	2.268E-03	1.365		1.337	800	2.291E-03	1.378		1.420
850	2.255E-03	1.357		1.337	825	2.306E-03	1.388		1.420
875	2.241E-03	1.348		1.337	850	2.322E-03	1.397	1.233	1.420
900	2.226E-03	1.339		1.337	875	2.338E-03	1.407		1.458
925	2.211E-03	1.330		1.337	900	2.354E-03	1.416		1.458
950	2.196E-03	1.321	1.180	1.337	925	2.364E-03	1.422		1.458
975	2.181E-03	1.312		1.270	950	2.373E-03	1.428		1.458
1000	2.166E-03	1.303		1.270	975	2.380E-03	1.432		1.458
1025	2.151E-03	1.294		1.270	1000	2.383E-03	1.433		1.458
1050	2.137E-03	1.286		1.270	1025	2.386E-03	1.435		1.458

(Continued)

Table 4.1 Resistance (in Each Step) and Axial Heat Flux Distribution of Test Sections (Continued)

TS No.I					TS No. II				
Z	Ideal		Actual		Z	Ideal		Actual	
(mm)	R (Ω)	q"loc /q"avg	R (Ω)	q"loc /q"avg	(mm)	R (Ω)	q"loc /q"avg	R (Ω)	q"loc /q"avg
1075	2.123E-03	1.277		1.270	1050	2.389E-03	1.437		1.458
1100	2.109E-03	1.269		1.270	1075	2.386E-03	1.435		1.458
1125	2.095E-03	1.260	1.121	1.270	1100	2.383E-03	1.433		1.458
1150	2.082E-03	1.252		1.249	1125	2.380E-03	1.432		1.458
1175	2.069E-03	1.245		1.249	1150	2.373E-03	1.428		1.458
1200	2.056E-03	1.237		1.249	1175	2.364E-03	1.422		1.458
1225	2.044E-03	1.230		1.249	1200	2.354E-03	1.416		1.458
1250	2.032E-03	1.222	1.103	1.249	1225	2.338E-03	1.407	1.266	1.458
1275	2.020E-03	1.215		1.190	1250	2.325E-03	1.399		1.401
1300	2.008E-03	1.208		1.190	1275	2.306E-03	1.388		1.401
1325	1.995E-03	1.200		1.190	1300	2.291E-03	1.378		1.401
1350	1.983E-03	1.193		1.190	1325	2.271E-03	1.367		1.401
1375	1.970E-03	1.185	1.051	1.190	1350	2.252E-03	1.355	1.216	1.401
1400	1.956E-03	1.177		1.161	1375	2.230E-03	1.342		1.343
1425	1.942E-03	1.168		1.161	1400	2.208E-03	1.328		1.343
1450	1.927E-03	1.159		1.161	1425	2.183E-03	1.313		1.343
1475	1.911E-03	1.149		1.161	1450	2.157E-03	1.298		1.343
1500	1.893E-03	1.139	1.025	1.161	1475	2.132E-03	1.282	1.166	1.343
1525	1.874E-03	1.127		1.095	1500	2.106E-03	1.267		1.286
1550	1.853E-03	1.115		1.095	1525	2.071E-03	1.246		1.286
1575	1.830E-03	1.101	0.966	1.095	1550	2.040E-03	1.227	1.117	1.286
1600	1.805E-03	1.086		1.037	1575	2.001E-03	1.204		1.166
1625	1.778E-03	1.070		1.037	1600	1.963E-03	1.181		1.166
1650	1.749E-03	1.052	0.916	1.037	1625	1.919E-03	1.154	1.013	1.166
1675	1.716E-03	1.033		0.979	1650	1.874E-03	1.128		1.116
1700	1.681E-03	1.011		0.979	1675	1.827E-03	1.099		1.116
1725	1.643E-03	0.988	0.865	0.979	1700	1.782E-03	1.072	0.969	1.116
1750	1.602E-03	0.964		0.914	1725	1.728E-03	1.040		1.000
1775	1.557E-03	0.937		0.914	1750	1.674E-03	1.007		1.000
1800	1.509E-03	0.908	0.807	0.914	1775	1.614E-03	0.971	0.868	1.000
1825	1.458E-03	0.877		0.823	1800	1.557E-03	0.937		0.897
1850	1.403E-03	0.844		0.823	1825	1.490E-03	0.896		0.897
1875	1.345E-03	0.809	0.727	0.823	1850	1.423E-03	0.856	0.779	0.897
1900	1.283E-03	0.772		0.700	1875	1.347E-03	0.810		0.760
1925	1.218E-03	0.733		0.700	1900	1.274E-03	0.766	0.660	0.760
1950	1.150E-03	0.692	0.618	0.700	1925	1.201E-03	0.722		0.700
1975	1.078E-03	0.649		0.610	1950	1.125E-03	0.677	0.608	0.700
2000	1.003E-03	0.604	0.538	0.610	1975	1.042E-03	0.627		0.551
2025	9.261E-04	0.557			2000	9.594E-04	0.577	0.479	0.551
2050	8.462E-04	0.509			2025	8.705E-04	0.524		
2075	7.643E-04	0.460			2050	7.815E-04	0.470		
2100	6.807E-04	0.410			2075	6.926E-04	0.417		
2125	5.959E-04	0.358			2100	6.004E-04	0.361		
2150	5.104E-04	0.307			2125	5.115E-04	0.308		
2175	4.250E-04	0.256			2150	4.257E-04	0.256		
2200	3.403E-04	0.205			2175	3.495E-04	0.210		
2225	2.572E-04	0.155			2200	2.764E-04	0.166		
2250	1.765E-04	0.106			2225	2.033E-04	0.122		
2275	9.925E-05	0.060			2250	1.334E-04	0.080		

In order to convert the experimental data with the actual heated length into that for the 2.4 meters heated length, i.e., 2.4-m-equivalent data (corresponding to the complete ideal AFD profile), imaginary extension parts were added to the start and the end of the heated length. After including these imaginary extensions to our analysis, the peaking factors of TS No. 1 and TS No. 2 became 1.394 and 1.458, respectively. The electrical resistance of the TS No. 1 with the actual stepped profile is 0.173703 Ω; the electrical resistances of the imaginary start and end extension parts are 0.001673 Ω and 0.005622 Ω, respectively. The electrical resistance of the TS No. 2 with actual stepped profile is 0.17611 Ω; the electrical resistances of the imaginary start and end extension parts are 0.002147 Ω and 0.004845 Ω, respectively.

4.3 CHF Location

For the non-uniform AFD test section, the CHF could occur at a single location or at multiple locations simultaneously. The CHF location could also shift along with the change of flow condition. Tables 4.2 to 4.5 show the CHF locations at given pressure, mass flux and inlet temperature for each test section and flow conditions.

4.4 Experimental Data Processing

Variables such as outlet pressure, mass flow rate, inlet and outlet fluid temperatures and wall temperature were measured directly in the experiment while critical power, critical heat flux, inlet quality, critical quality, 2.4-m-equivalent critical power and 2.4-m-equivalent inlet enthalpy were calculated as follows:

Critical Power

$$\text{Power} = I \times U \qquad (4.3)$$

Critical Heat Flux

For uniform AFD,

Table 4.2 Initial CHF Locations; Test Section AFD: TS No. 1, Forward Flow (CHF Occurred at the Downstream End Edge of the Specified Step. Step Numbers are Defined in Figure 3.3a)

P (k Pa)	G (kg m^{-2} s^{-1})	T_{in} (°C)									
		70	65	60	55	50	45	40	35	30	25
		Step Number									
1662	2826				13, 14	16, 17	16, 17	16	15, 16	15, 16	15, 16
	3533				13, 14, 15, 16	16	14, 15, 16	14, 15, 16	15, 16	15, 16	15, 16
	4593				13, 14	14	14	14	14, 15	15	15, 16
2022	2841		13, 14, 15, 16	14, 15, 16, 17	16	15, 16	15, 16	15, 16	15, 16	15, 16	15, 16
	3552		13, 14	14	15, 16	14, 15, 16	14, 15, 16	14, 15, 16	15, 16	15, 16	15, 16
	4617		11	11	13, 14	14	14	14	14, 15	15	15, 16
2389	2860	13, 14	15, 16	15, 16	15, 16	15, 16	15, 16	15, 16	15, 16	15, 16	15, 16
	3575	11, 12, 13, 14	14	14, 15, 16	14, 15, 16	14, 15, 16	14, 15, 16	14, 15, 16	15, 16	15, 16	15, 16
	4648	10, 11	11	11, 12	12, 13, 14	13, 14	14	14, 15	15, 16	15, 16	

Table 4.3 Initial CHF Locations; Test Section AFD: TS No. 1, Reverse Flow (CHF Occurred at the Downstream End Edge of the Specified Step. Step Numbers are Defined in Figure 3.3b)

P (k Pa)	G (kg m^{-2} s^{-1})	T_{in} (°C)									
		70	65	60	55	50	45	40	35	30	25
		Step Number									
1662	2826				3	3	3	3	3	3	3
	3533				3	3	3	3	3	3	3
	4593				3	4, 3	4, 3	4, 3	4, 3	4, 3	4, 3
2022	2841		3, 2	3, 2	3	3	3	3	3	3	3
	3552		3	3	3	3	3	3	3	3	3
	4617		4, 3	4, 3	4, 3	4, 3	4, 3	4, 3	4, 3	4, 3	4, 3
2389	2860	3, 2	3	3	3	3	3	3	3	3	3
	3575	3	3	3	3	3	3	3	3	3	3
	4648	4, 3	4, 3	4, 3	3	3	3	3	3	3	3

Table 4.4 Initial CHF Locations; Test Section AFD: TS No. 2, Forward Flow (CHF Occurred at the Downstream End Edge of the Specified Step. Step Numbers are Defined in Figure 3.4a)

P (k Pa)	G (kg m^{-2} s^{-1})	T_{in} (°C)									
		70	65	60	55	50	45	40	35	30	25
		Step Number									
1662	2826				13, 14, 15, 16	13, 14, 15	13, 14, 15, 16	13, 14, 15, 16	13, 14, 15, 16	13, 14, 15	13, 14, 15, 16
	3533				13	13	13, 14	13, 14, 15	13	13	13, 14, 15
	4593				12, 13	12, 13	13	13, 14	13, 14, 15	13, 14, 15	14, 15, 16
2022	2841		13, 14, 15	13, 14, 15	13, 14, 15	13	13	13	13, 14, 15	13, 14, 15	13, 14, 15
	3552		11, 12, 13, 14, 15	11, 12, 13, 14, 15	13	13	13	13	13, 14, 15	13, 14, 15	13, 14, 15
	4617		11	11, 12, 13	11, 12, 13	13	13	13, 14	13, 14, 15	14, 15	15
2389	2860	13, 14, 15, 16	12, 13, 14, 15	12, 13, 14	13	13	13	13, 14, 15	13, 14, 15	13, 14, 15	14, 15
	3575	11, 12, 13	11, 12, 13	11, 12, 13	11, 12, 13	13	13	13, 14, 15	14, 15	14, 15, 16	14, 15, 16
	4648	10, 11, 12	10, 11, 12, 13	12, 13	12, 13	13, 14, 15	13, 14, 15	13, 14, 15, 16	14, 15, 16	14, 15, 16	15, 16

Table 4.5 Initial CHF Locations; Test Section AFD: TS No. 2, Reverse Flow (CHF Occurred at the Downstream End Edge of the Specified Step. Step Numbers are Defined in Figure 3.4b)

P (k Pa)	G (kg m^{-2} s^{-1})	T_{in} (°C)									
		70	65	60	55	50	45	40	35	30	25
		Step Number									
1662	2826				1	1	1	1	1	1	1
	3533				2	2, 1	1	1	1	2, 1	2, 1
	4593				2	2	2	2	2	2	2
2022	2841		2, 1	1	1	1	1	2, 1	2, 1	2, 1	2
	3552		2	2	2	2	2	2	2	2	2
	4617			2	2	2	2	2	2	2	2
2389	2860	2	1	2, 1	2	2	2	2	2	2	2
	3575	2	2	2	2	2	2	2	2	2	2
	4648	7	2	2	2	2	2	2	2	2	2

$$CHF = \frac{Power}{\pi D_i L_h} \quad (4.4)$$

For non-uniform AFD,

$$CHF = \frac{Power_k}{\pi D_i z_k} \quad (4.5)$$

where k is the number of the step at which the initial CHF was detected, $Power_k$ is the power received by Step k, z_k is the length of Step k.

<u>Critical Quality</u>

$$X_{do} = \frac{\dot{i}_{in} - \dot{i}_f + \frac{Power}{\dot{m}}}{\dot{i}_{fg}} \quad (4.5)$$

<u>Inlet Quality</u>

$$X_{in} = \frac{(\dot{i}_{in} - \dot{i}_f)}{\dot{i}_{fg}} \quad (4.6)$$

<u>2.4-m-Equivalent Critical Power</u>

$$Power_{2.4m} = Power_{act} \times \frac{R_{2.4m}}{R_{act}} \quad (4.7)$$

where,

$$R_{2.4m} = R_{2m} + \Delta R_{ext.in} + \Delta R_{ext.out} \quad (4.8)$$

<u>2.4-m-Equivalent Inlet Enthalpy</u>

$$\dot{i}_{in,2.4m} = \dot{i}_{in,act} - \frac{(Power_{2.4m} - Power_{act} - Power_{ext.out})}{\dot{m}} \quad (4.9)$$

The CHF data obtained during this study are summarized in Appendix D and is also available in electronic form. An uncertainty analysis has been performed and is presented in Appendix C.

5. ANALYSIS OF THE EXPERIMENTAL RESULTS

5.1 AFD Profile of Non-Uniform AFD Test Section

Figures 4.2 and 4.3 show that TS No. 1 forward direction had an inlet peak AFD profile while its reverse direction had an outlet peak AFD profile. Note also that the actual stepped AFD is an excellent simulation of the ideal AFD. TS No. 2 is almost symmetric and has a middle peak AFD profile, however, because of machining difficulties, the wall thickness of step 4 is larger than the design value and consequently the local heat flux at step 4 is approximately 10% less (see Figure 3.8) than the design value. This had no effect on the forward flow CHF or critical power results as the initial CHF location is far away from this machining flaw and the overall resistance is close to the design value. Since this step was near the expected CHF locations for reverse flow test, its lower heat flux could have an effect on the CHF.

5.2 Effect of Flow Condition on CHF Location for Non-Uniform AFD Test Section

Tables 4.2 to 4.5 show that the CHF location changes with flow conditions as well as AFD profiles. This can best be observed for the AFDs with forward flow since there are more heat flux steps in the area where CHF was expected to occur (i.e. the downstream part of the test section) (see Figures 3.3 and 3.4). The CHF locations were observed near the exit of the test section at low inlet temperatures, but shifted upstream towards the peak heat flux location with an increase of inlet temperatures. A change in mass flux did not affect the CHF location at low inlet temperatures; however at high inlet temperatures, a decrease in mass flux shifted the CHF location towards the outlet of the test section. The pressure did not have a significant effect on the CHF location in this investigation.

5.3 Analysis of the Experimental Results Based on Inlet Conditions

5.3.1 HFC-134a Experimental Data

If the impedance of the test section and power supply are properly matched, the test section would receive the maximum power (12 kW) from a 12 kW DC power supply (40 V, 300 A). This requires different heated lengths ("optimum heated length") for the uniform and non-uniform AFD test sections because the wall thickness of the non-uniform AFD test sections is less than that of the uniform AFD test section except at the first step and the last step. The calculated optimum heated length for uniform AFD test section is around 3.05 m, while those for TS No. 1 forward and reverse flows are approximately 1.49 m and 1.51 m, respectively, and those for TS No. 2 forward and reverse flows are approximately 1.275 m and 1.35 m, respectively. Because of the limitation of the testing facilities, the maximum heated length is 2.2 m, which is less than the optimum value for the uniform AFD test section. Therefore, the maximum power attainable for the uniform AFD case is about (2.2/3.05) times 12 kW or 8.65 kW, which is well below 12 kW of the non-uniform AFD case.

Since the ideal AFDs correspond to a heated length of 2.4 m, all of the experimental data were converted into 2.4-m-equivalent data using the relationships of Section 4.5. Figures 5.1a and 5.1b illustrate the differences between 2.4-m-equivalent data and the data with actual heated length (L_h) for both the uniform and non-uniform AFD test sections. Note the increase in critical power and inlet subcooling for the 2.4-m-equivalent case. Figures 5.1a and 5.1b suggest that, at given flow conditions (P, G, T_{in}), the critical power increases with an increase in heated length. However, after conversion to a 2.4-m-equivalent heated length conditions the length effect disappears. This, thus, supports the transformation methodology to 2.4-m-equivalent length of Section 4.5, which resulted in a broader range of inlet subcoolings.

The AFD effect on the critical power is illustrated in Figures 5.2 to 5.10, which show the 2.4-m-equivalent critical powers vs. 2.4-m-equivalent inlet quality for different test sections for each pressure and mass flux tested.

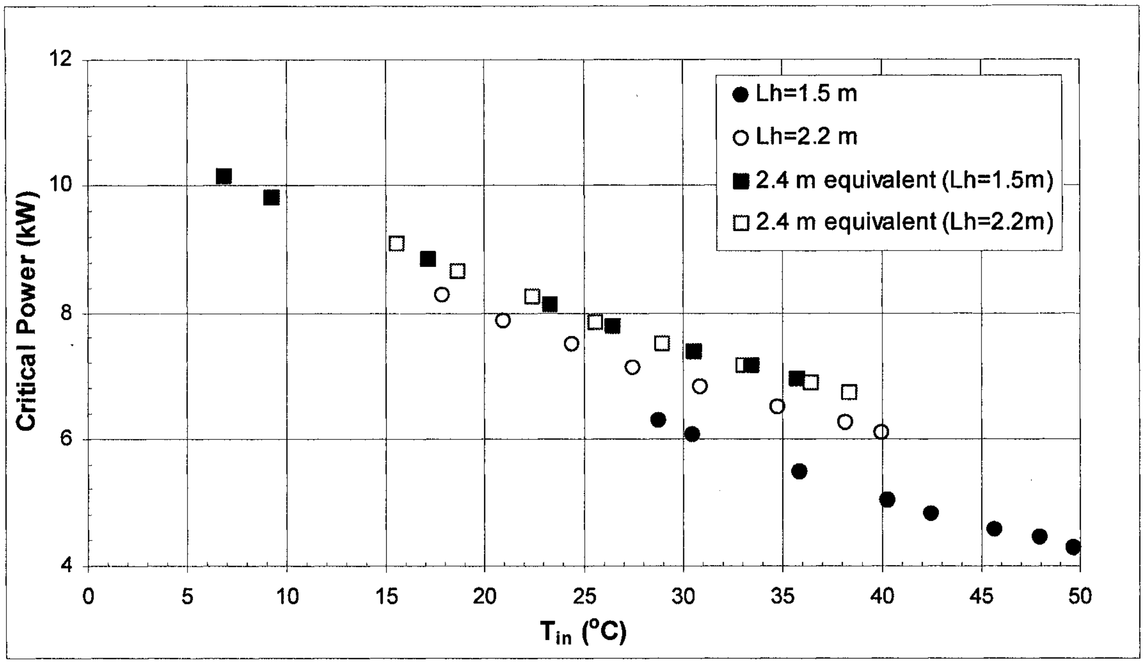

Figure 5.1a Difference between 2.4-m-Equivalent Data and the Data with Actual Heated Length, Uniform AFD Test Section at P=1662 kPa, G=4593 kg m^{-2} s^{-1}.

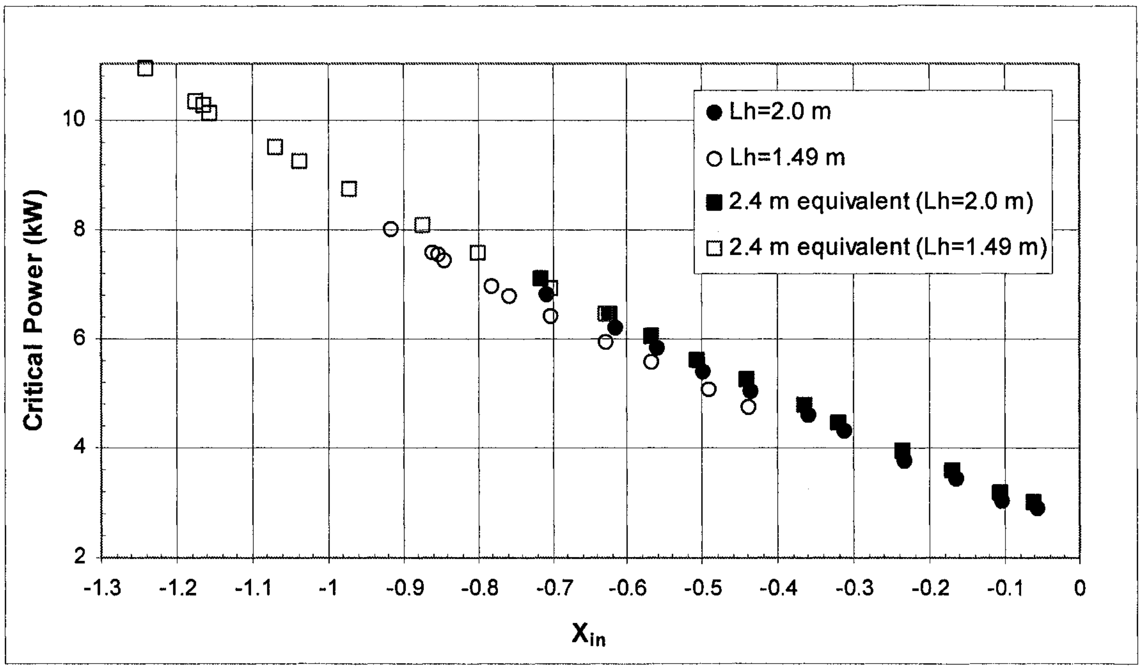

Figure 5.1b Difference between 2.4-m-Equivalent Data and the Data with Actual Heated Length, Non-Uniform Test Section (TS No. 1, Forward Flow) at P=2389 kPa, G=2860 kg m^{-2} s^{-1}.

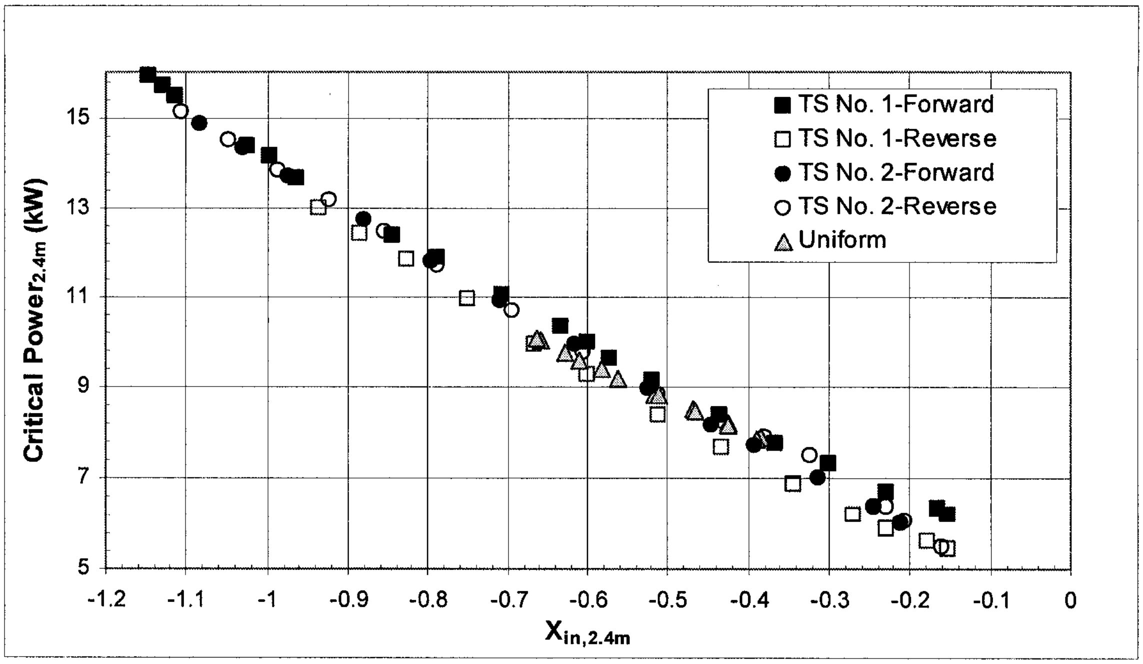

Figure 5.2 Critical Power versus Inlet Quality, HFC-134a, P=2389 kPa, G=4648 kg m^{-2} s^{-1}.

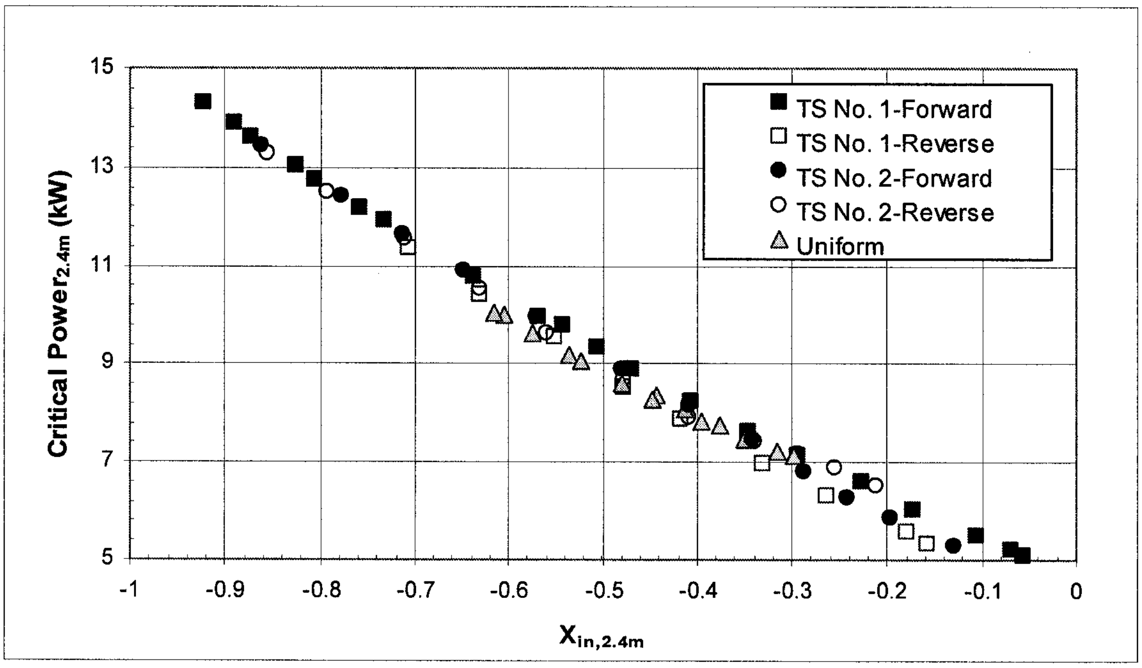

Figure 5.3 Critical Power versus Inlet Quality, HFC-134a, P=2022 kPa, G=4617 kg m^{-2} s^{-1}.

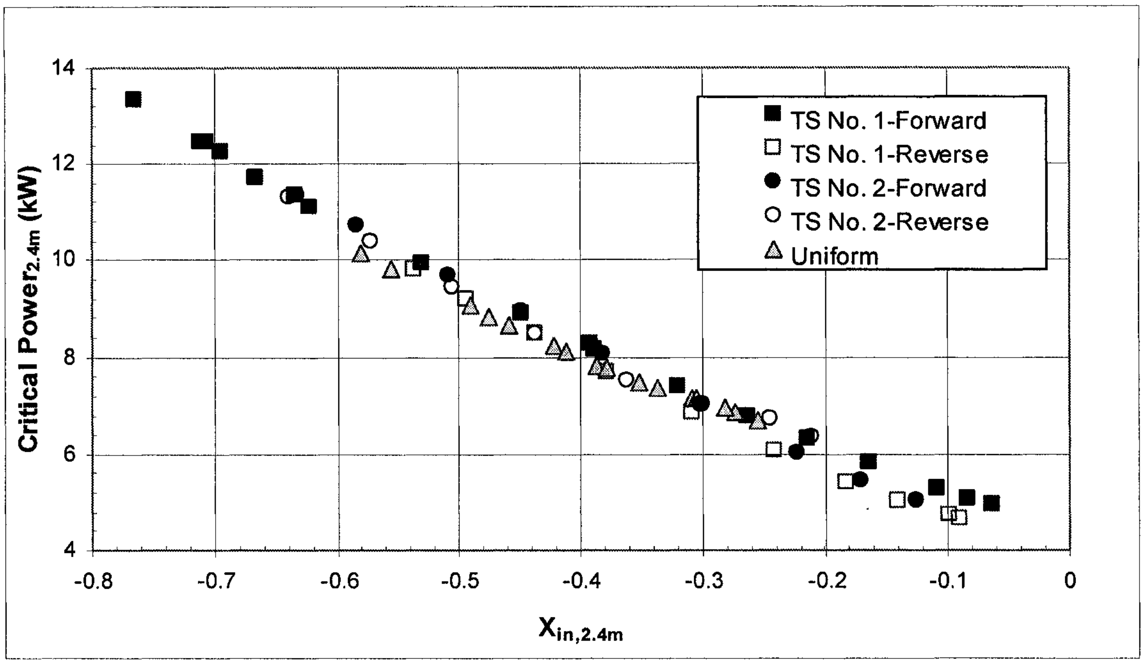

Figure 5.4 Critical Power versus Inlet Quality, HFC-134a, P=1662 kPa, G=4593 kg m^{-2} s^{-1}.

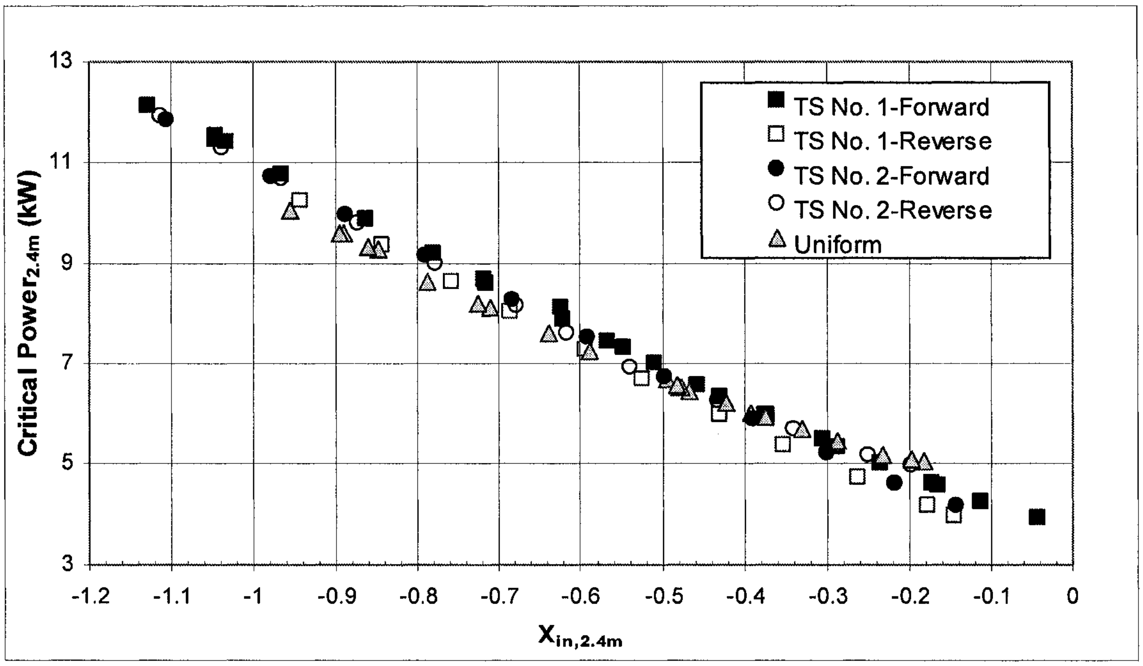

Figure 5.5 Critical Power versus Inlet Quality, HFC-134a, P=2389 kPa, G=3575 kg m^{-2} s^{-1}.

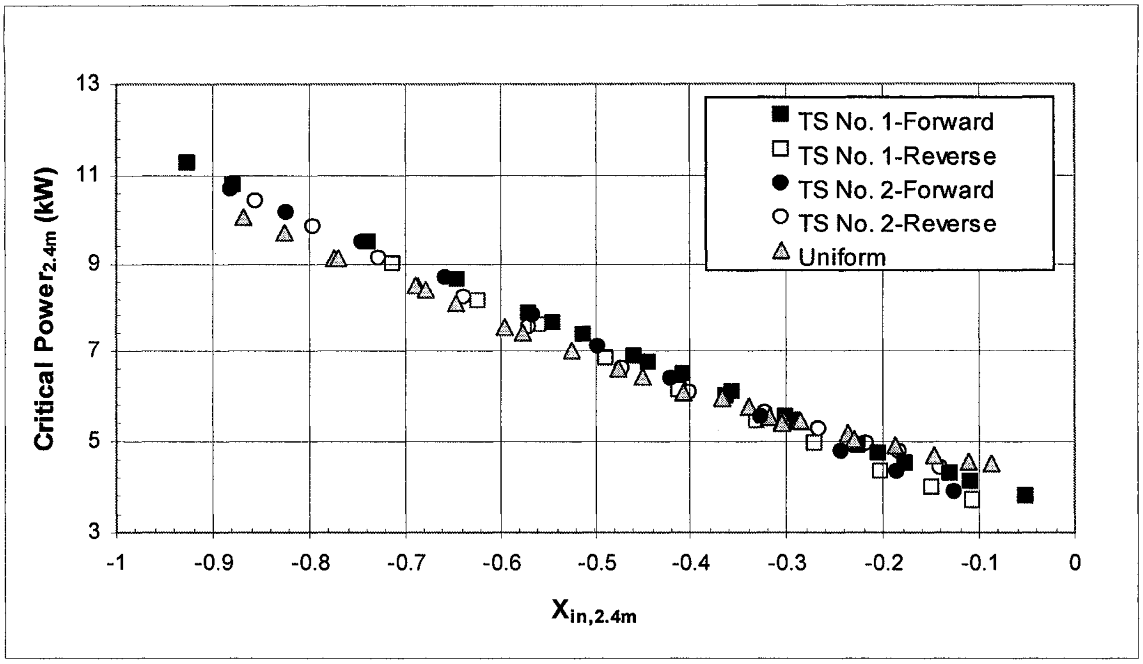

Figure 5.6 Critical Power versus Inlet Quality, HFC-134a, P=2022 kPa, G=3552 kg m^{-2} s^{-1}.

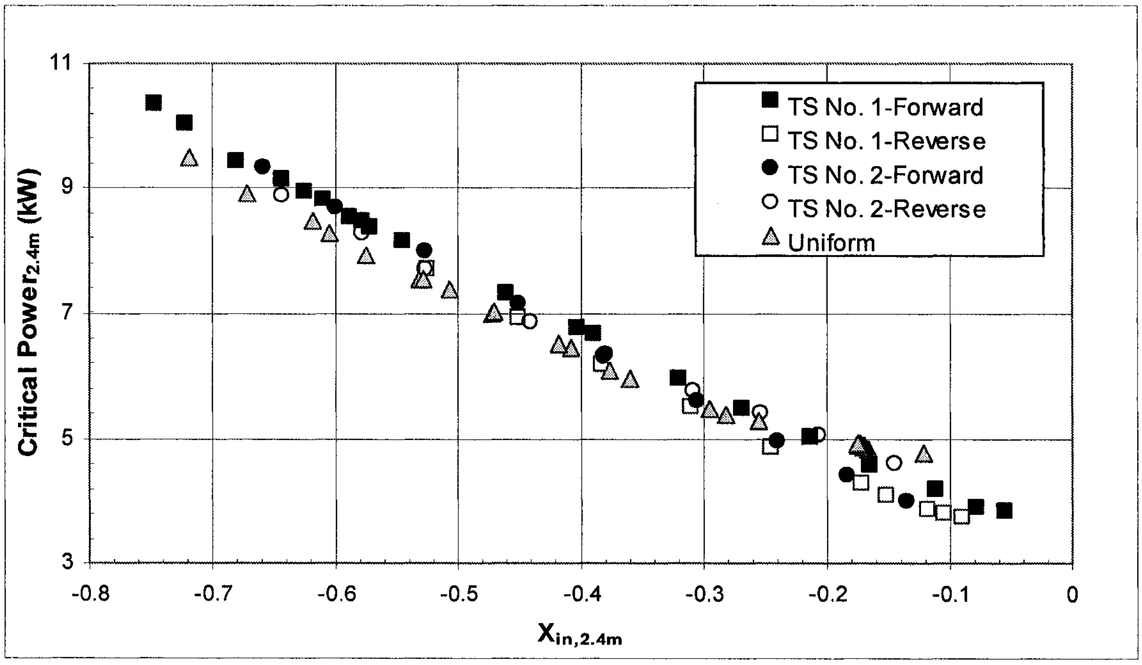

Figure 5.7 Critical Power versus Inlet Quality, HFC-134a, P=1662 kPa, G=3533 kg m^{-2} s^{-1}.

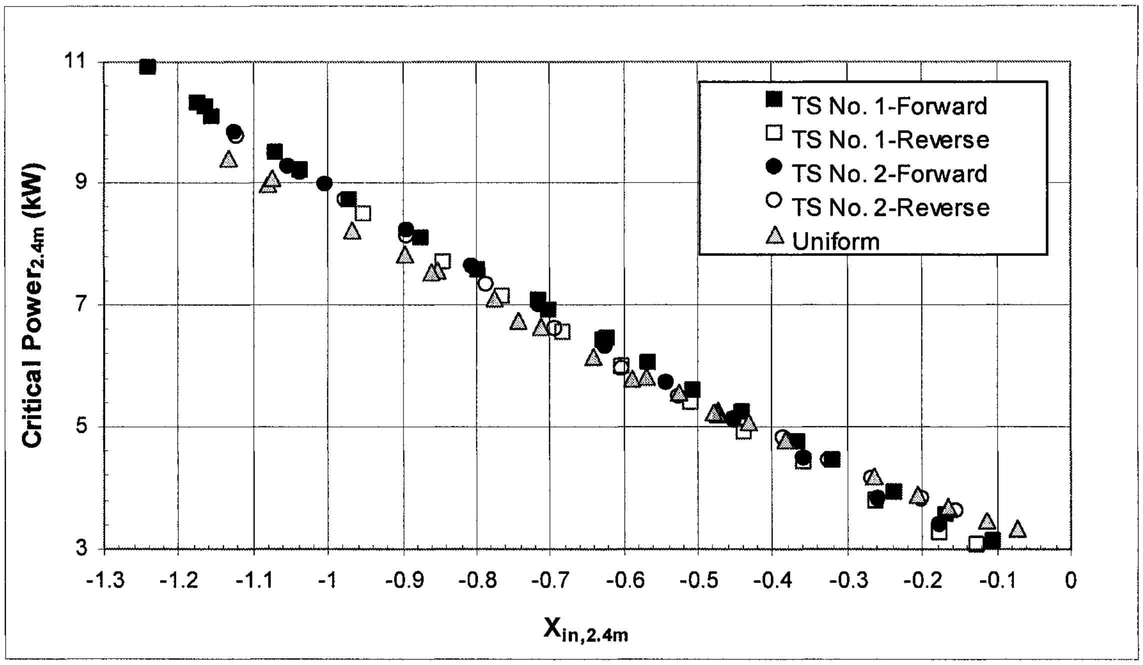

Figure 5.8 Critical Power versus Inlet Quality, HFC-134a, P=2389 kPa, G=2860 kg m^{-2} s^{-1}.

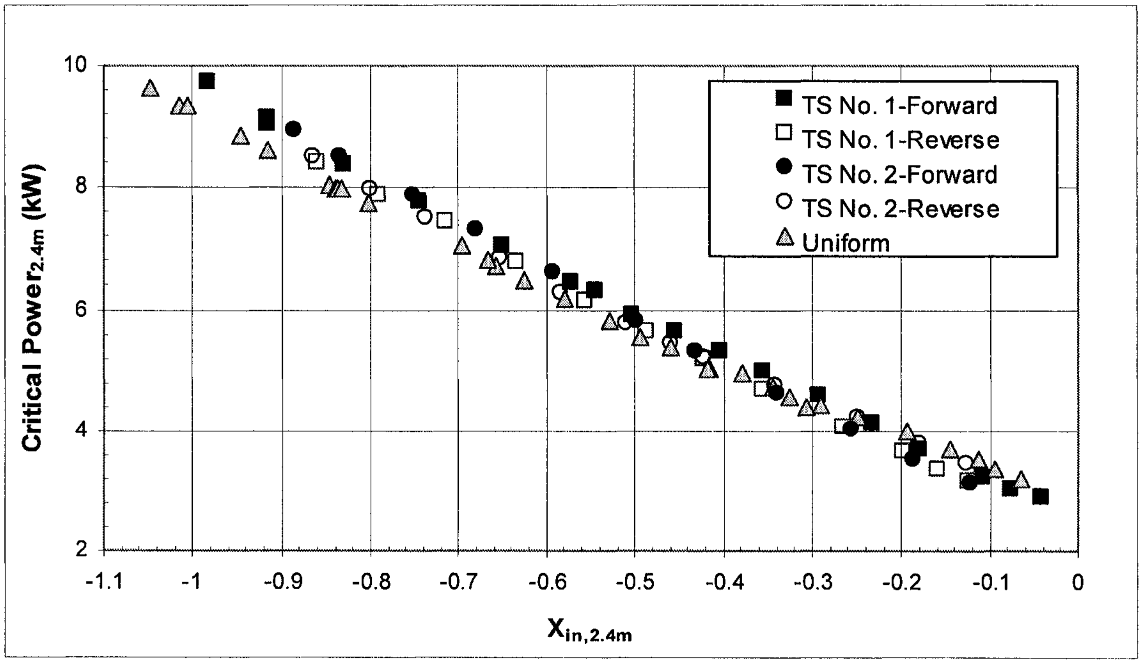

Figure 5.9 Critical Power versus Inlet Quality, HFC-134a, P=2022 kPa, G=2841 kg m^{-2} s^{-1}.

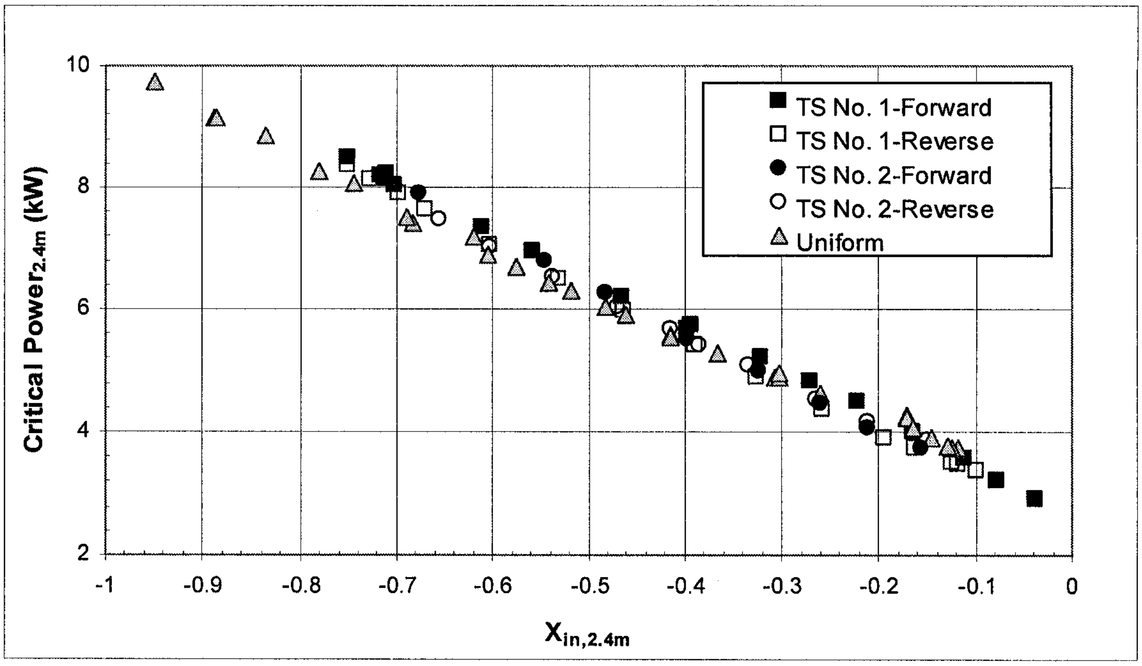

Figure 5.10 Critical Power versus Inlet Quality, HFC-134a, P=1662 kPa, G=2826 kg m^{-2} s^{-1}.

5.3.2 Water Equivalent Data

The HFC-134a data was converted into water-equivalent values using the CHF fluid-to-fluid modeling relationships of Section 3.1. Figures 5.11 to 19 show the plots of the critical power versus inlet quality with 2.4-m-equivalent heated length for all the AFDs for each pressure and mass flux.

5.3.3 Discussion for the Experimental Results Based on Inlet Conditions

It was found that the relationship between critical power and inlet quality is quite linear for all of the test sections and flow conditions, except for the uniform AFD test section at high mass flux and very high inlet temperatures (or inlet qualities greater than -0.2). This exception was referred to by Collier et al. (1994) as "the anomalous effect due to ultra-high mass velocity".

The main finding of this investigation (see Figures 5.2 to 5.19) is the absence of a strong effect of AFD on critical power. When looking closely at the results, one notices that the uniform AFD test section tends to give a slightly lower critical power at the lower inlet qualities ($X_{in} < -0.5$). For the higher inlet qualities the uniform data tends to fall within the range of all AFDs. They cross over or represent an upper bound to all AFDs for $X_{in} > -0.2$. The curves of critical power versus inlet quality for the non-uniform AFDs match each other very well at high inlet subcoolings, and begin to separate as inlet quality increases to around -0.8 to -0.45 depending on flow conditions. Frequently this separation in the curves moves to the high inlet quality region with a decrease in mass flux or pressure. At the high inlet qualities, the critical power for the outlet peak AFD test section is lower than that for the inlet peak AFD by 3% to 15% depending on the flow conditions. This deviation generally increases with an increase in pressure and mass flux. The critical power for the middle peak AFD (TS No. 2) is in between that for inlet and outlet peak AFD profiles. It appears that the critical powers for all non-uniform and uniform AFD profiles approach each other again as inlet quality approaches to zero at low mass flux.

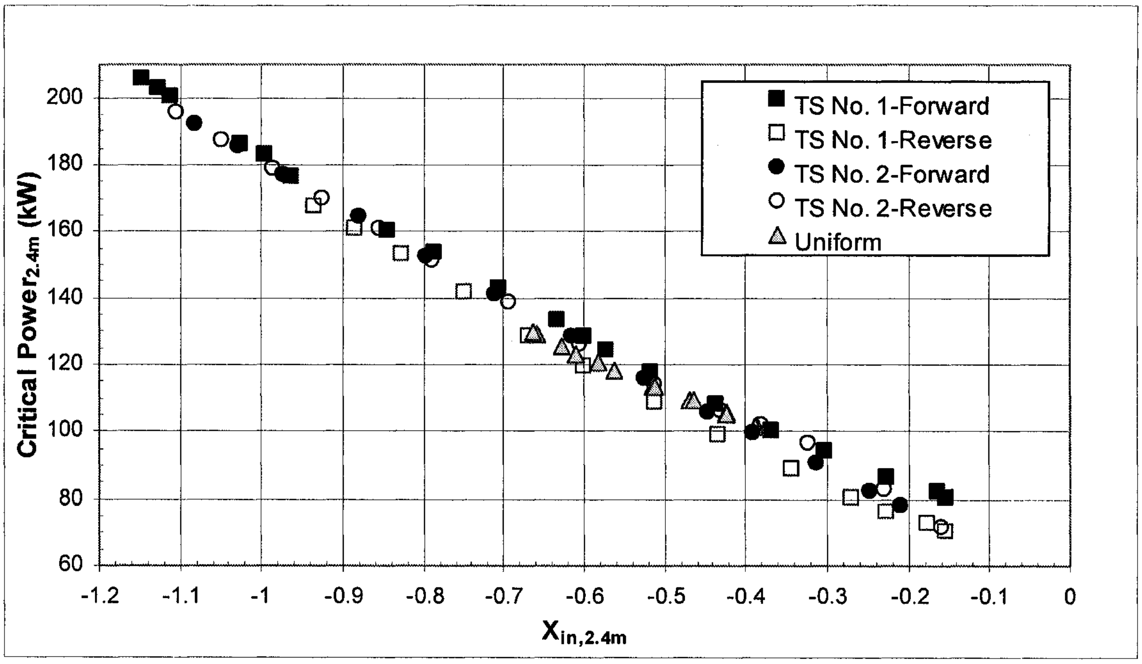

Figure 5.11 Critical Power versus Inlet Quality, Water, P=14 MPa, G=6500 kg m^{-2} s^{-1}.

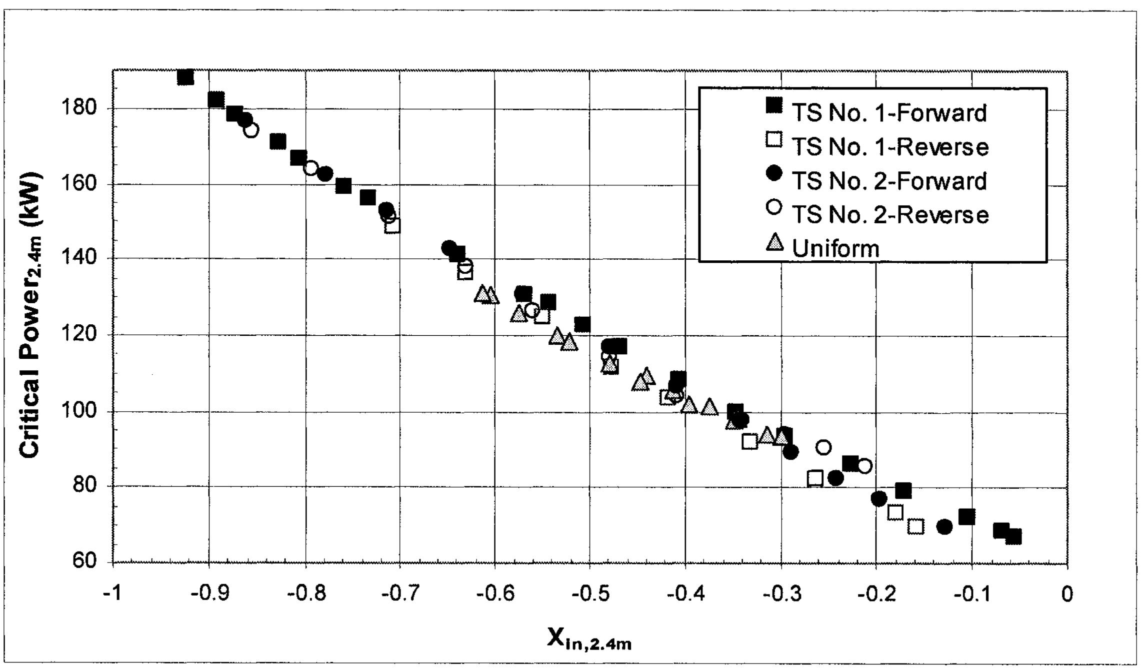

Figure 5.12 Critical Power versus Inlet Quality, Water, P=12 MPa, G=6500 kg m^{-2} s^{-1}.

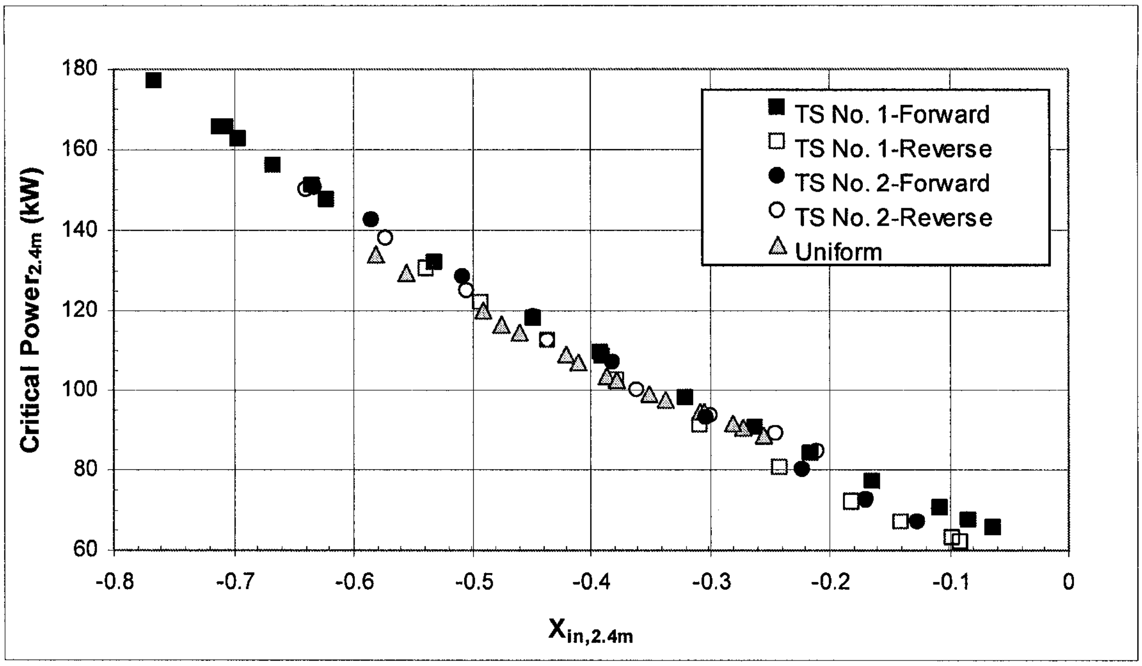

Figure 5.13 Critical Power versus Inlet Quality, Water, P=10 MPa, G=6500 kg m^{-2} s^{-1}.

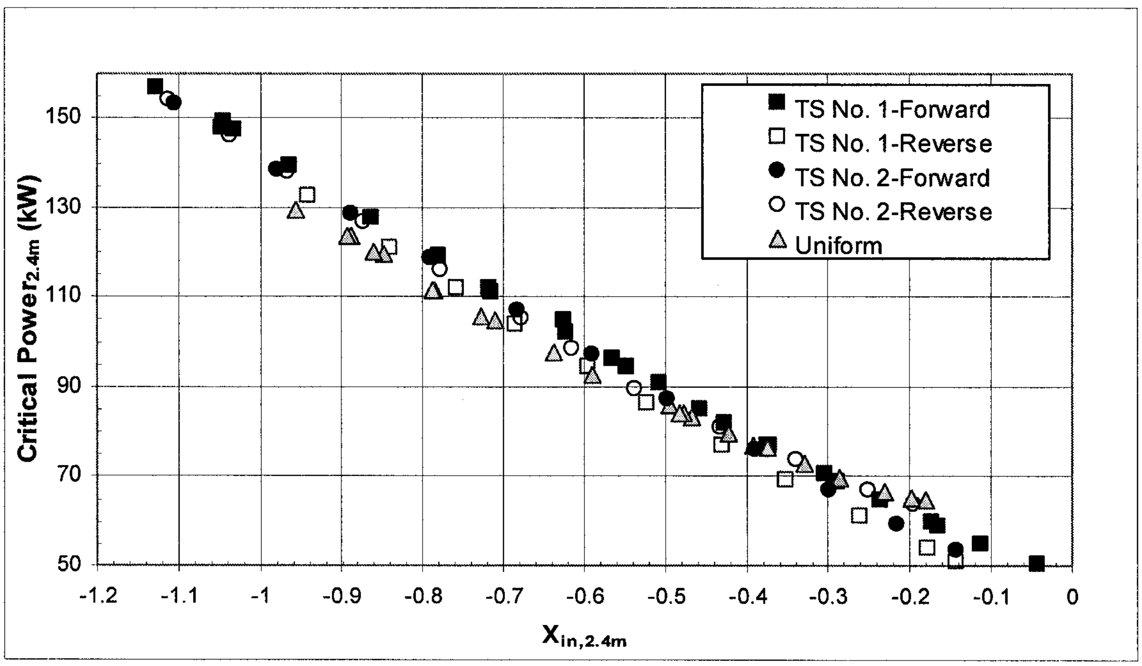

Figure 5.14 Critical Power versus Inlet Quality, Water, P=14 MPa, G=5000 kg m^{-2} s^{-1}.

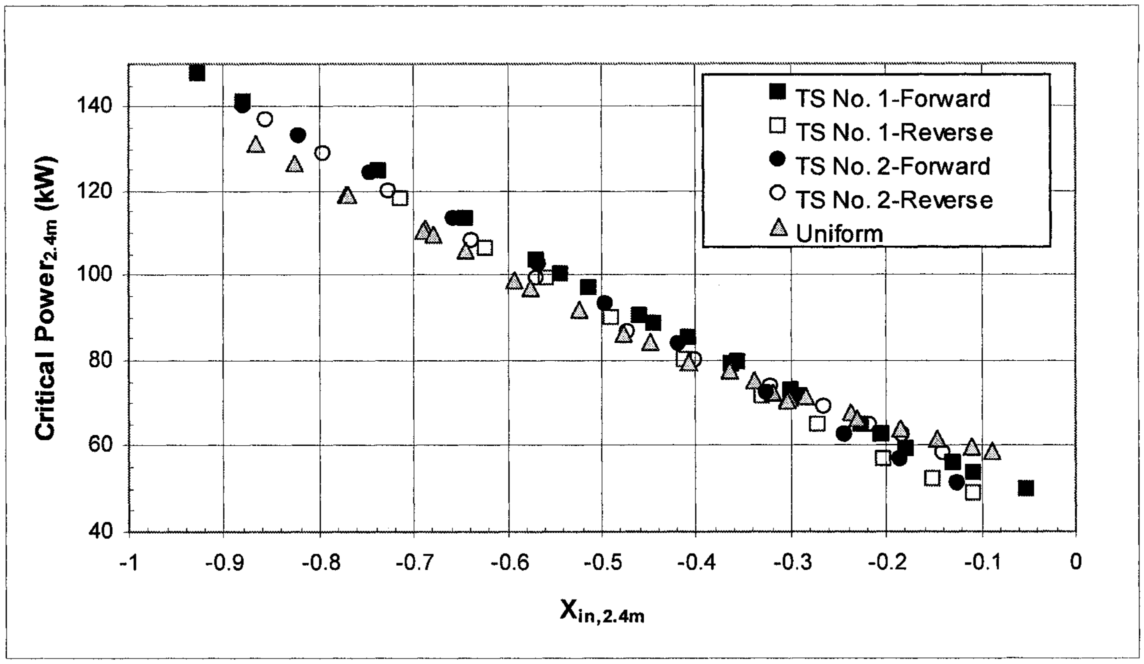

Figure 5.15 Critical Power versus Inlet Quality, Water, P=12 MPa, G=5000 kg m^{-2} s^{-1}.

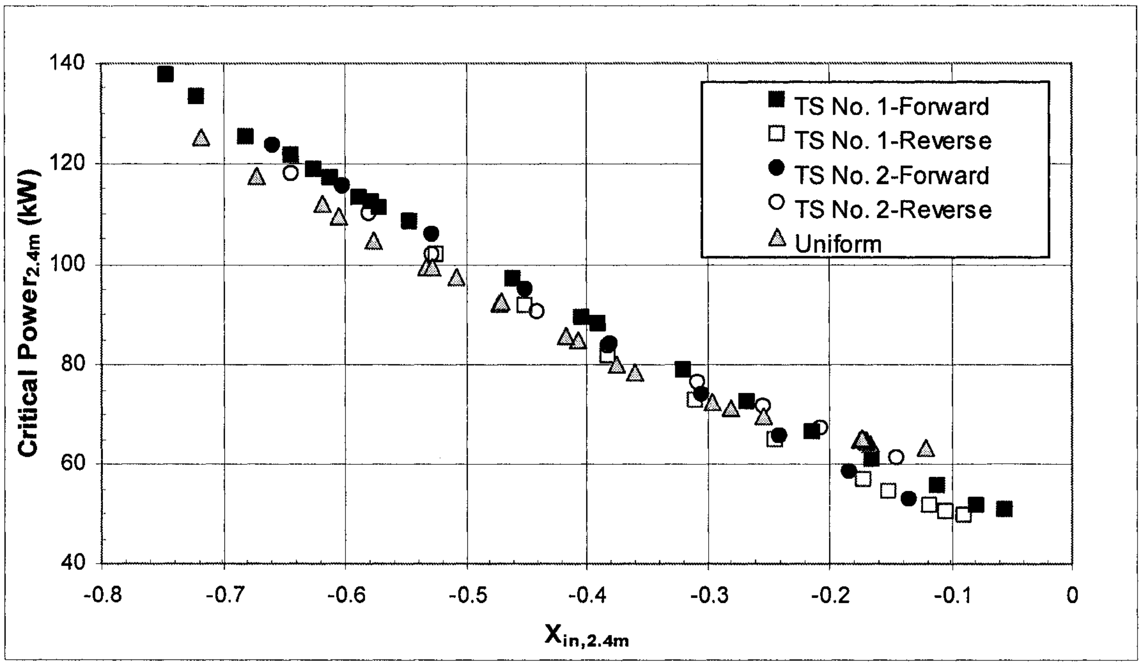

Figure 5.16 Critical Power versus Inlet Quality, Water, P=10 MPa, G=5000 kg m^{-2} s^{-1}.

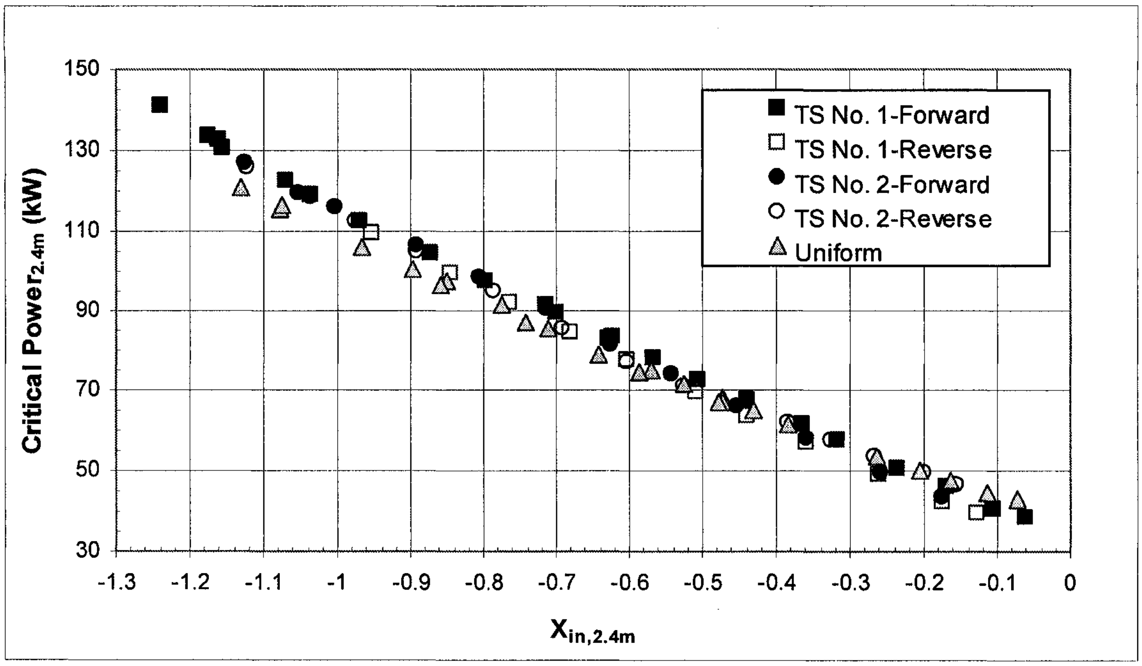

Figure 5.17 Critical Power versus Inlet Quality, Water, P=14 MPa, G=4000 kg m^{-2} s^{-1}.

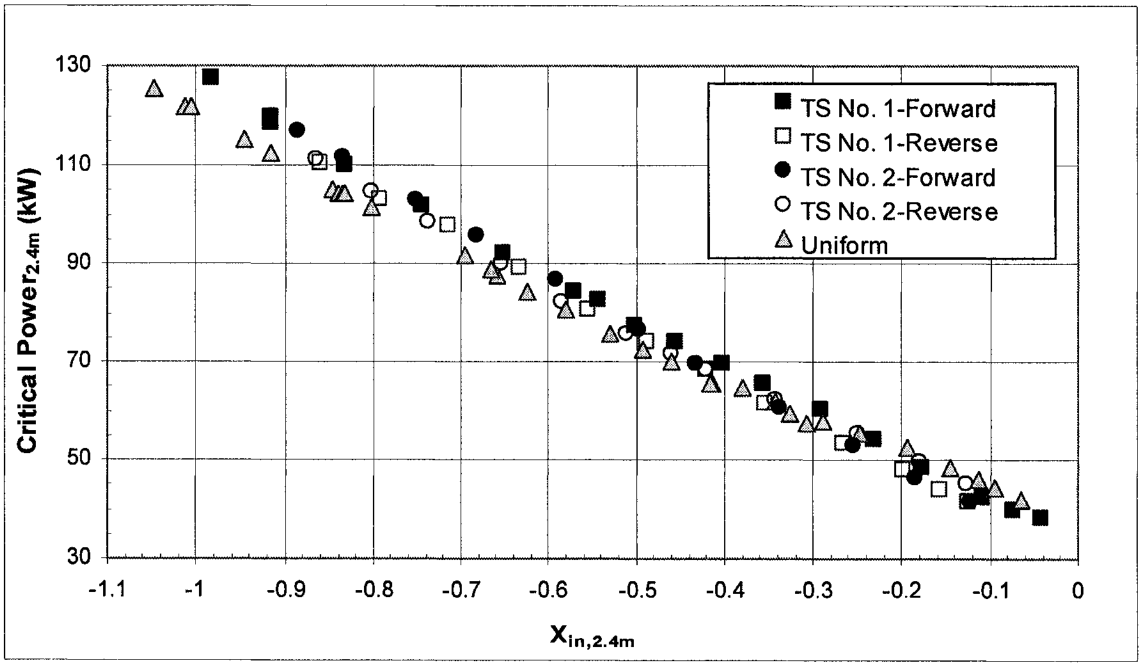

Figure 5.18 Critical Power versus Inlet Quality, Water, P=12 MPa, G=4000 kg m^{-2} s^{-1}.

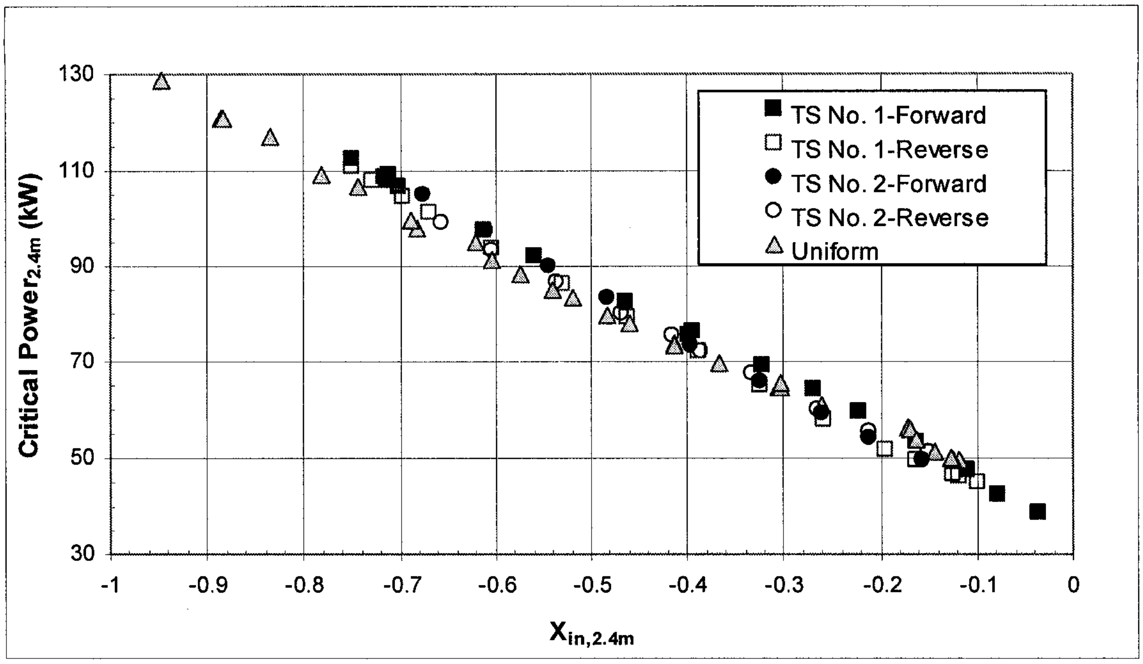

Figure 5.19 Critical Power versus Inlet Quality, Water, P=10 MPa, G=4000 kg m^{-2} s^{-1}.

5.4 Analysis of the Experimental Results Based on Local Conditions

The analysis of experimental results based on inlet conditions shows how the non-uniform axial heat flux distribution affects the critical power at given inlet conditions (X_{in}, P, G). Alternatively, the analysis based on local conditions conducted in this section reveals the variation of the local critical heat flux for the various axial heat flux distributions at given local conditions (X_{do}, P, G).

5.4.1 Definition of Initial CHF

For a uniform AFD test section, the CHF always occurs initially at the exit of the channel. However, as mentioned before, for a non-uniform AFD test section, the CHF could occur at a single location or at multiple locations simultaneously, and the CHF location could also shift or spread along with a change in flow conditions. Therefore, in order to analyze the effect of non-uniform AFD on the CHF, the initial CHF needs to be defined for the non-uniform AFD when CHF occurred at two or more locations. If the CHF occurred at two locations, the one with lower quality was selected as the initial CHF, while if the number of the CHF location is three or more, the one in the middle, or in the middle and with lower quality, was chosen.

5.4.2 Discussion for the Experimental Results Based on Local Conditions

The AFD effect on critical heat flux is illustrated graphically in Figures 5.20 to 5.28, which show the critical heat fluxes vs. dryout quality for uniform and non-uniform test sections at given pressures and mass fluxes. Because of the limitation of the power supply, the uniform AFD data does not cover the same dryout quality region as that of non-uniform AFD data at the high mass flux. In this case, the variation of CHF with X_{do} for the uniform AFD given by CHF look-up table (1995) was also illustrated in Figures 5.26 to 5.28.

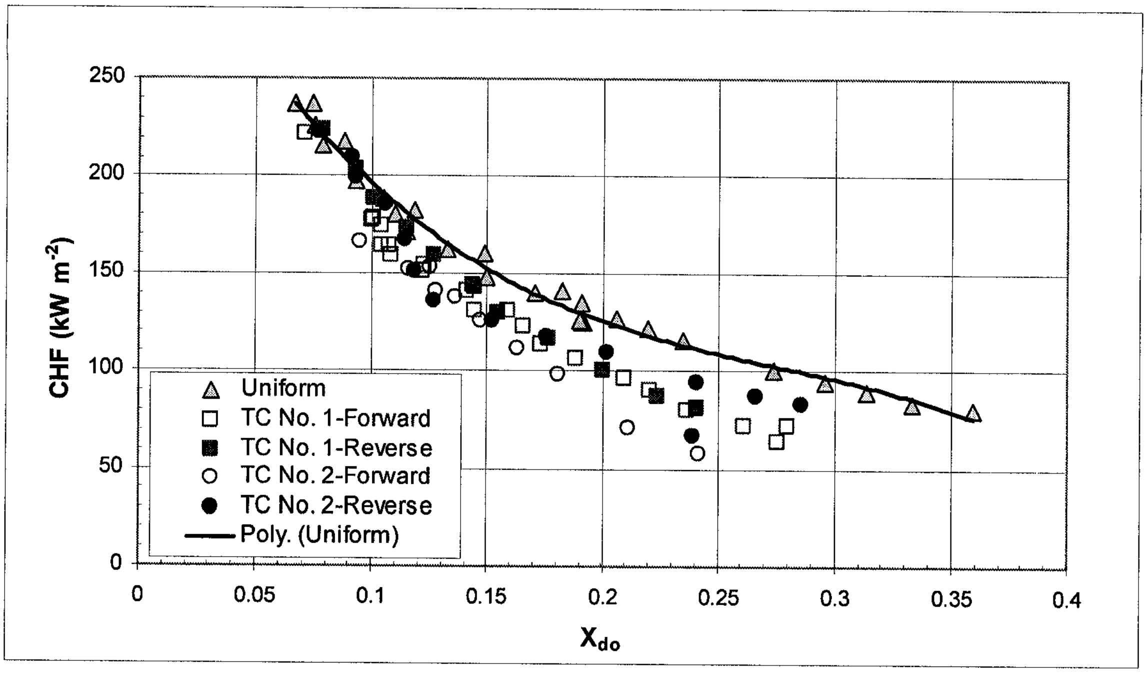

Figure 5.20 Critical Heat Flux versus Dryout Quality for Each AFD, P=2389 kPa, G=2860 kg m^{-2} s^{-1}.

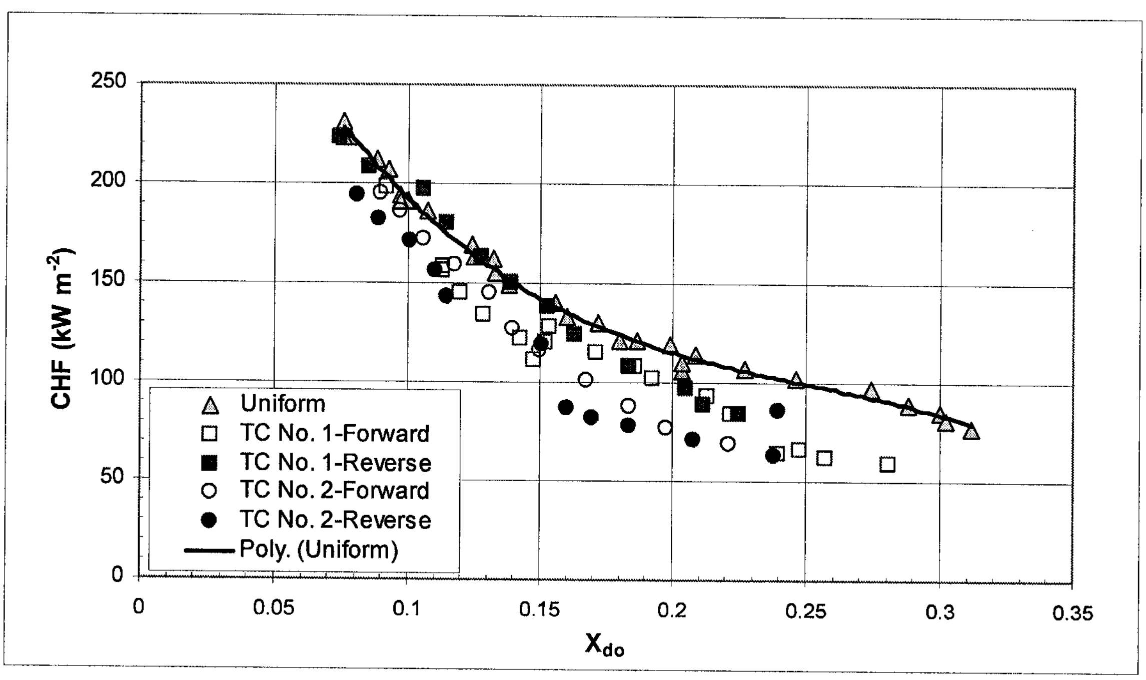

Figure 5.21 Critical Heat Flux versus Dryout Quality for Each AFD, P=2022 kPa, G=2841 kg m^{-2} s^{-1}.

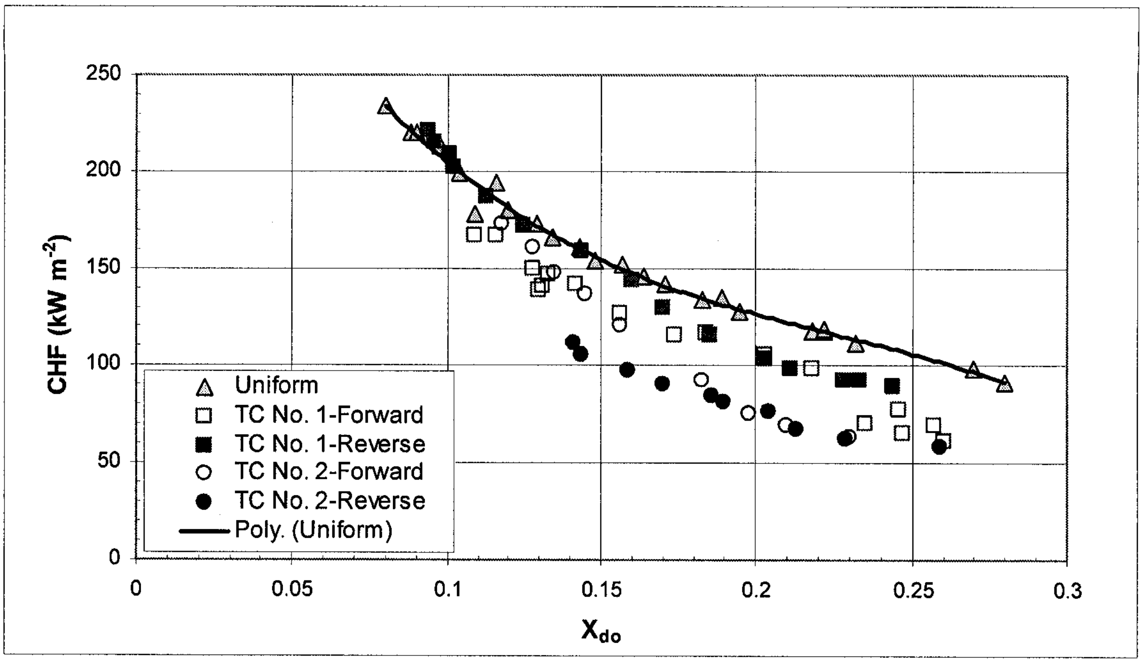

Figure 5.22 Critical Heat Flux versus Dryout Quality for Each AFD, P=1661 kPa, G=2826 kg m^{-2} s^{-1}.

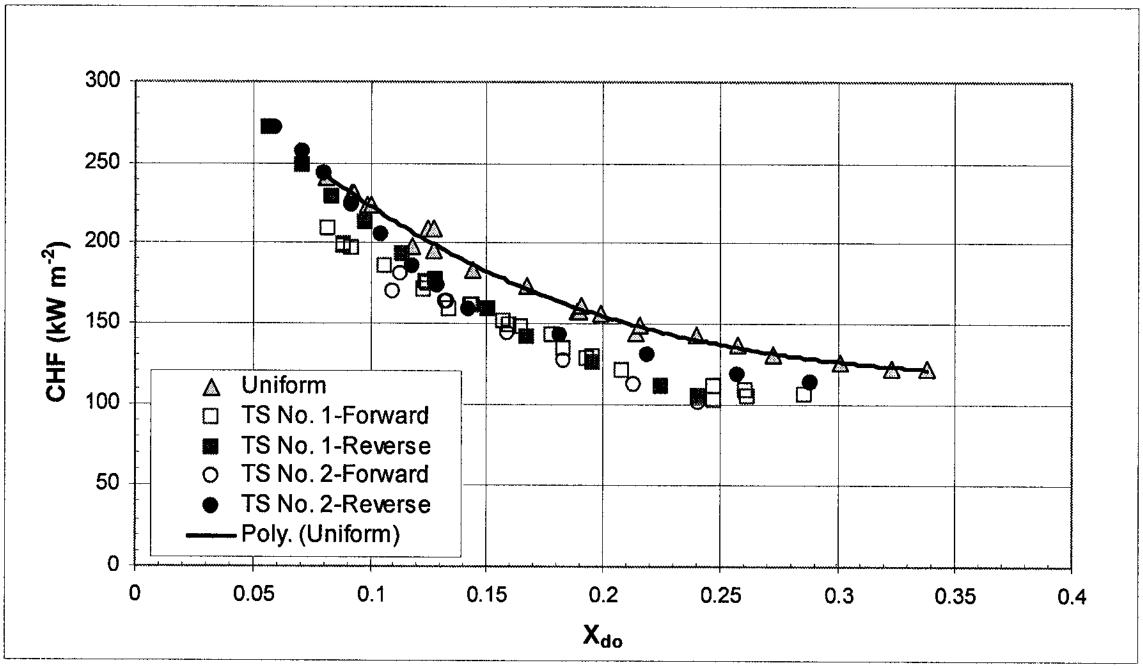

Figure 5.23 Critical Heat Flux versus Dryout Quality for Each AFD, P=2389 kPa, G=3575 kg m^{-2} s^{-1}.

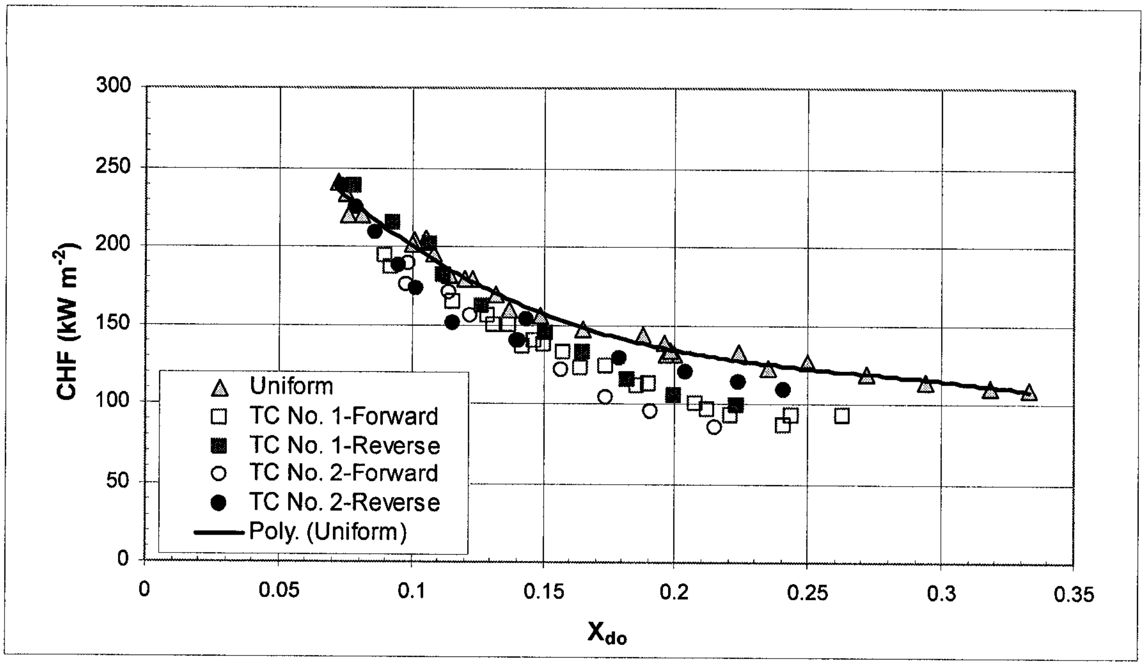

Figure 5.24 Critical Heat Flux versus Dryout Quality for Each AFD, P=2022 kPa, G=3552 kg m^{-2} s^{-1}.

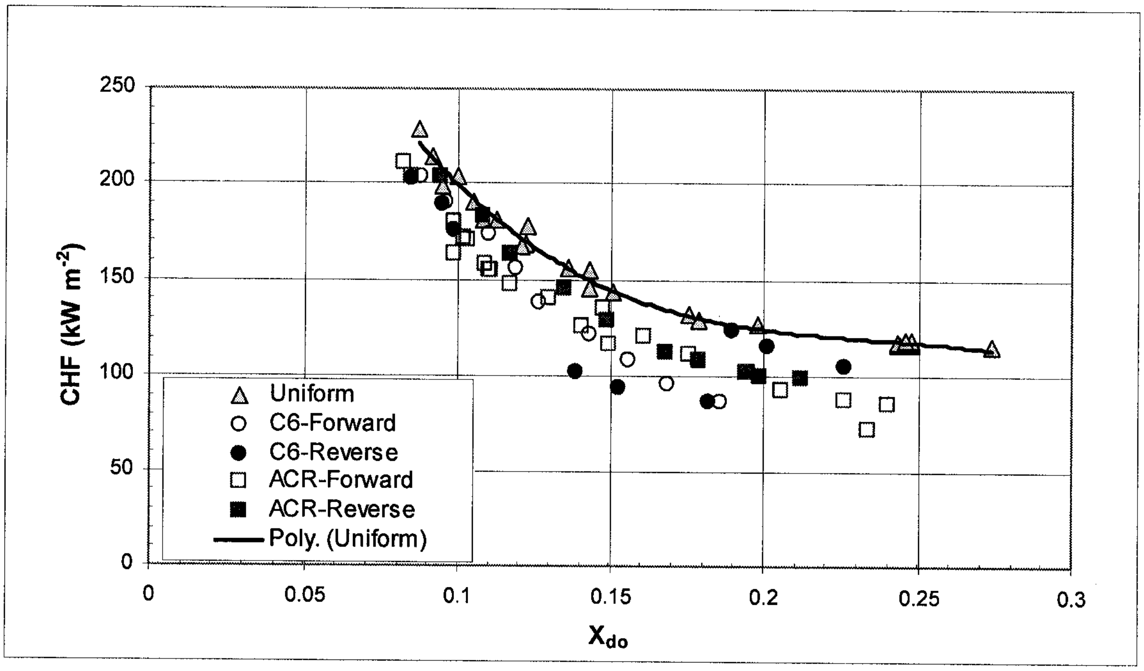

Figure 5.25 Critical Heat Flux versus Dryout Quality for Each AFD, P=1662 kPa, G=3533 kg m^{-2} s^{-1}.

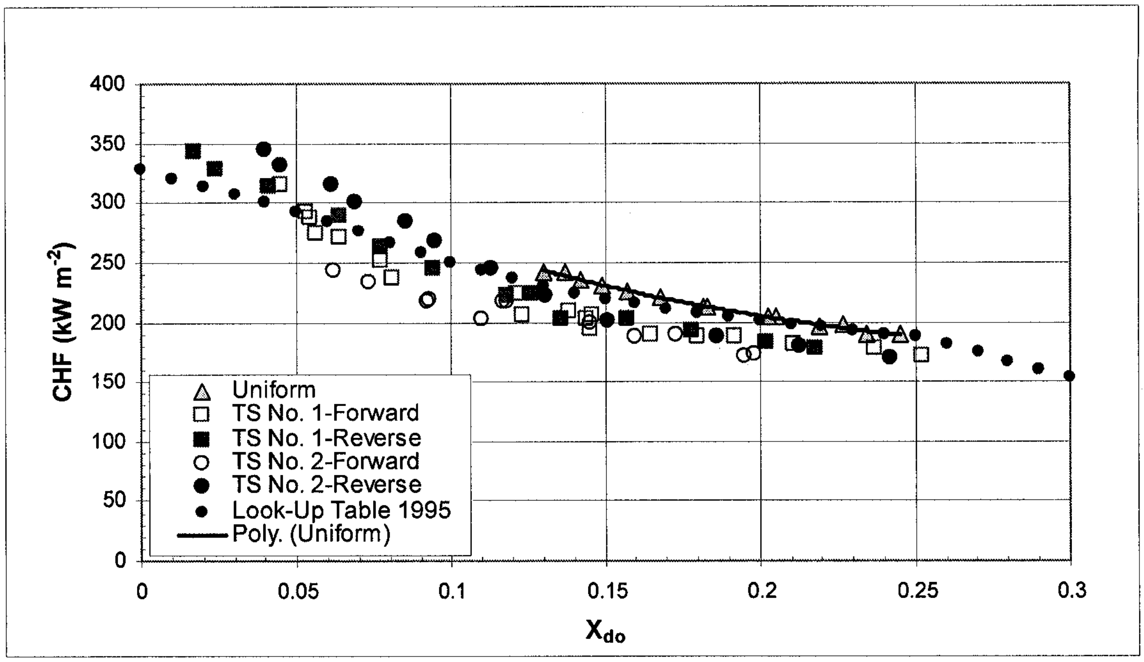

Figure 5.26 Critical Heat Flux versus Dryout Quality for Each AFD, P=2389 kPa, G=4648 kg m^{-2} s^{-1}.

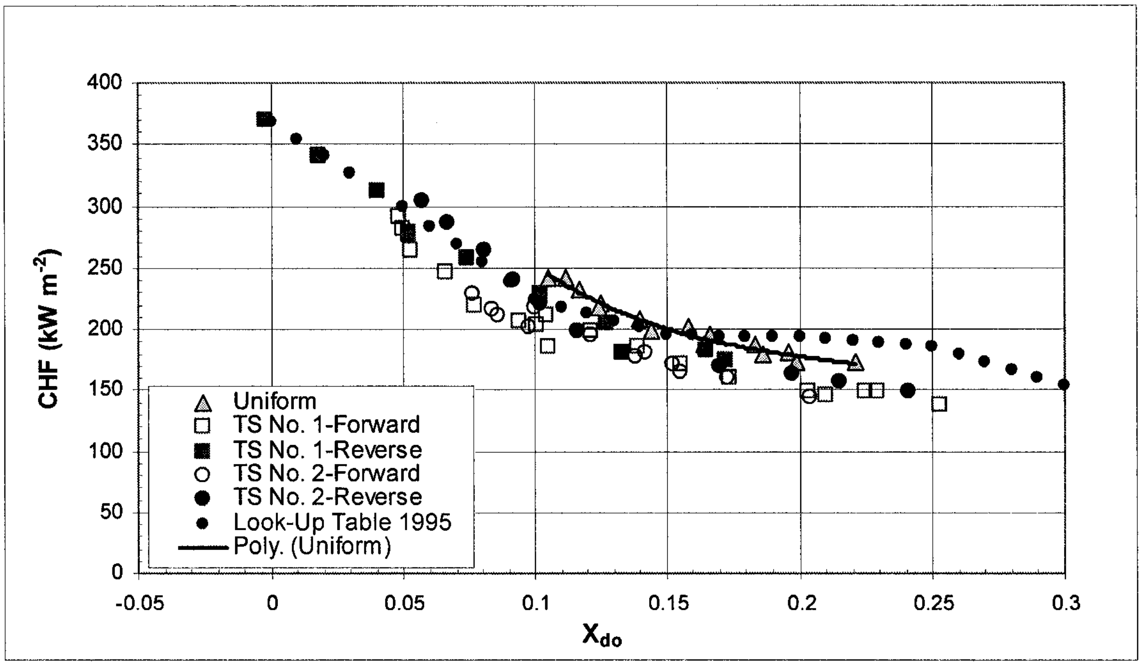

Figure 5.27 Critical Heat Flux versus Dryout Quality for Each AFD, P=2022 kPa, G=4617 kg m^{-2} s^{-1}.

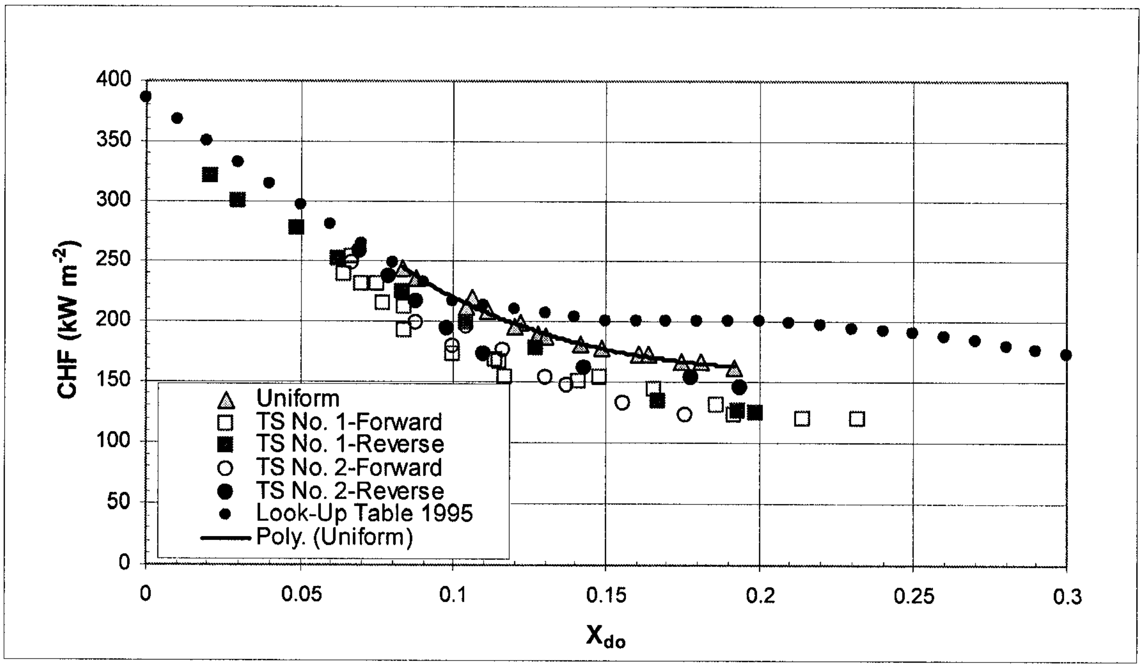

Figure 5.28 Critical Heat Flux versus Dryout Quality for Each AFD, P=1662 kPa, G=4593 kg m^{-2} s^{-1}.

Note that, in some cases, the curve of CHF against dryout quality for non-uniform AFD is not always smooth continuously. This fluctuation can be caused by the variation of the initial CHF location resulting from the change of the inlet temperature.

The general trend presented in the figures is that the AFD has a strong effect on CHF at high dryout qualities: here the CHF values for non-uniform AFDs can be up to 50% lower than that for uniform AFD depending on the pressure, mass flux and the shape of the AFD profile. The AFD effect on CHF decreases with a decrease in dryout quality. At low dryout qualities, the effect of AFD on CHF is small or non-existent. This observation implies that the local conditions hypothesis may be approximately valid at low dryout qualities. It appears that, at given dryout qualities, the discrepancy of the CHF values between the uniform and non-uniform AFDs decreases as either the pressure increases or mass flux increases.

The effect of the heat flux peak location in the non-uniform AFD profile is not clearly shown in the figures. The unavoidable fluctuation of the CHF vs. dryout quality curve caused by the variation of the CHF location, the arbitrary nature of the initial CHF definition, and the step heat flux distribution character makes it difficult to further identify the physical trend of CHF for each AFD profile.

For TS No.1 reverse direction, at low mass flux, CHF occurred at only one or two locations, and the initial CHF situated always at the downstream end of step 3. Therefore, the CHF vs. X_{do} curve for this AFD is basically continuously smooth. For the TS No.1 forward direction and TS No.2 forward direction, however, CHF occurred at up to five locations simultaneously depending on the flow conditions. The initial CHF location varied with inlet temperature. Consequently, the CHF vs. X_{do} curve fluctuates unavoidably. Considering also the effect of the machining flaw in TS No.2 reverse direction, which enhanced CHF at high inlet temperature at certain flow conditions, the effect of the heat flux peak location in the non-uniform AFD profile is not clearly observed in this study.

5.5 Mechanistic Explanation of the Observed AFD Effect

It was observed that AFD has strong effect at high dryout quality at which the corresponded CHF mechanism is annular flow liquid film dryout. The entrained liquid flow rate curves described in Section 2.9.4 are employed to explain this phenomenon in this section.

Curve ABC shown in Figure 5.29 represents the entrained liquid flow rate under hydrodynamic equilibrium conditions corresponding to that at the end of a long unheated tube. The entrainment rate is assumed to be equal to the deposition rate under these conditions. The entrained liquid flow rate for a boiling annular flow corresponding to a uniformly heated tube (departure from hydrodynamic equilibrium) follows curve A'B'C'. Dryout occurs at point C', at which the entrained liquid flow rate equals to the total liquid flow rate. These two curves were proposed by Hewitt et al. (1965) based on the experimental results. Recall Eq.(2.12), i.e.,

$$\frac{dW_{lE}}{dz} = \pi D_i (E - D_d) \tag{2.12}$$

where W_{lE} is the entrained liquid flow rate, E is the entrainment rate of droplets from the liquid film per unit heated area and D_d is the deposition rate of droplets on to the liquid film per unit heated area. For a uniformly heated tube, a heat balance equation yields

$$dX = \frac{4q''}{D_i G i_{fg}} dz \tag{5.1}$$

therefore,

$$\frac{dW_{lE}}{dX} = \frac{\pi D_i^2 G i_{fg}}{4q''} (E - D_d) \tag{5.2}$$

This equation suggests that the slope of the entrained liquid flow rate curve (dW_{lE}/dX) for a heated tube depends on the heat flux and the difference between E and D_d at given flow conditions. It can be deduced form the trend of the entrained liquid flow rate curve A'B'C'

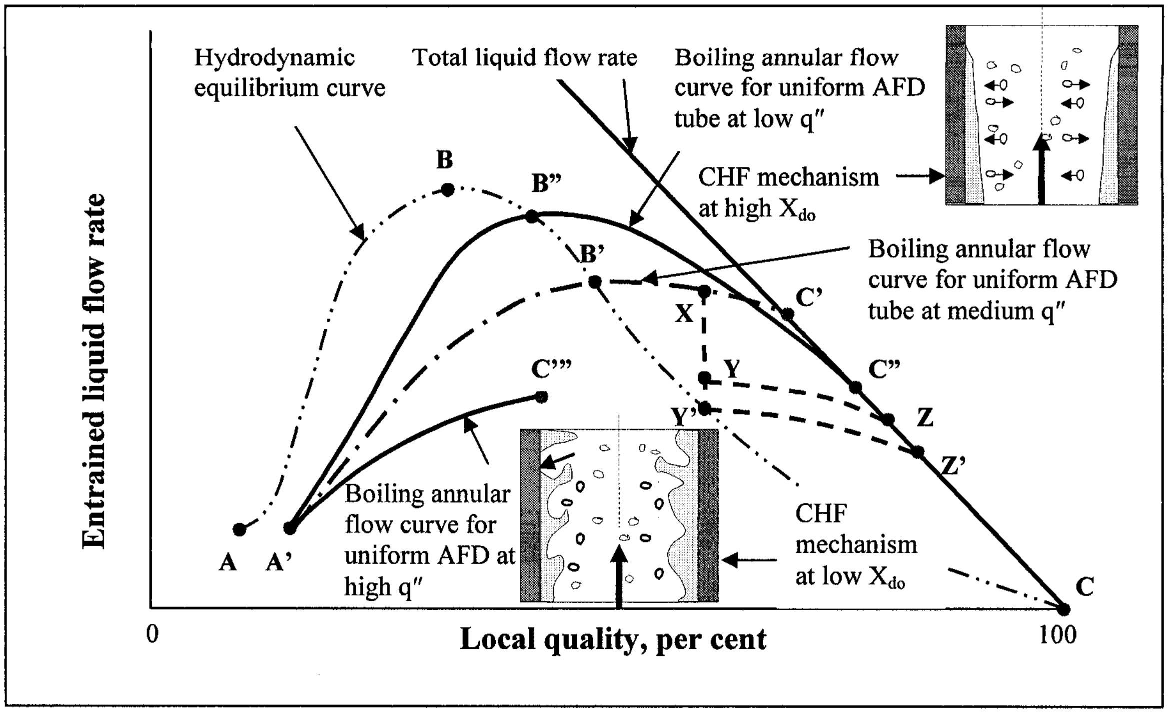

Figure 5.29 Heat Flux Effect on the Entrained Liquid Flow Rate for Uniform AFD and the Cold Patch effect on CHF. Based on the Entrainment Curves of Hewitt et al. (1965).

that, before the maximum W_{lE} point of B', E is larger than D_d (entrainment domain) and after the maximum W_{lE} point, D_d is larger than E (deposition domain). At the maximum W_{lE} point, $D_d = E$. The behavior of the heat flux affecting the dW_{lE}/dX is quite complex, since E-D_d may also change with the change in the heat flux. A study of the cold patch phenomenon may be helpful to understand the heat flux effect.

When a cold patch is located at the downstream part of a heated tube, the local quality remains constant along the cold patch. Since q″ equals to zero, dW_{lE}/dX approaches minus infinite, thus, W_{lE} decreases sharply following the vertical line XY as shown in Figure 5.29. Then W_{lE} follows curve YZ after the cold patch. This results in a higher dryout quality at point Z than that at point C'. D_d can be obtained by

$$D_d = kC = k\frac{W_{lE}}{\frac{W_{lE}}{\rho_l} + \frac{W_g}{\rho_g}} = k\frac{W_{lE}}{\frac{W_{lE}}{\rho_l} + \frac{WX(z)}{\rho_g}}. \qquad (5.3)$$

where k is the deposition coefficient. Note that D_d decreases with a decrease in W_{IE} as W_{IE} curve A'B'C' moves towards the equilibrium curve ABC. If the cold patch is very long, the flow could reach the hydrodynamic equilibrium conditions at Y' at which D_d = E. In this case, the W_{IE} curve could follow XY'Z' in Figure 5.29 instead of XYZ.

If the heat flux corresponding to curve A'B'C' is reduced to a lower value, then a higher dryout quality will result. The entrained liquid flow rate curve corresponding to a uniformly heated tube for a lower heat flux will follow A'B"C" in Figure 5.29, because the flow would attempt to become 'fully developed' as the heat flux is decreased.

When a very high heat flux is applied to a uniformly heated tube, however, W_{IE} is small compared to that corresponding to curve A'B'C'. Then the CHF conditions may be reached at a low quality point (C'" in Figure 5.29) before the W_{IE} curve reaches the total liquid flow rate curve. W_{IE} at the CHF location is less than the total liquid flow rate. The CHF mechanism in this case is not the dryout of liquid layer on the heated surface at the end of the annular flow regime. Instead, the dryout is caused by liquid–layer disruption due to surface wave instability (see the CHF mechanisms for low and high X_{do} in Figure 5.29).

If a decreasing heat flux profile exists near the tube exit, then a higher dryout quality will result. Consequently more power is required to induce the CHF conditions compared with that for a uniformly heated tube. For a linearly decreasing heat flux profile, the W_{IE} curve follows XY in Figure 5.30. For a slope-changed decreasing heat flux profile, however, the W_{IE} curve may follow XY'Z', and the dryout may occur at a point (for example, Y') before the end point Z' if the slope of the heat flux profile changes suddenly at Y'. This is because the slope of the entrained liquid flow rate curve, dW_{IE}/dX, is a function of heat flux profile.

When a hot patch is located at the downstream end of a heated tube, a lower dryout quality will result; the W_{IE} curve will follow XY or even a horizontal line XY' (shown in Figure 5.31). The latter case corresponds to the situation of a very high heat flux in the hot patch. CHF here is induced by the very quick evaporation process. When a hot patch is located at the upstream part of a heated tube, the slope, dW_{IE}/dX, over the hot patch is

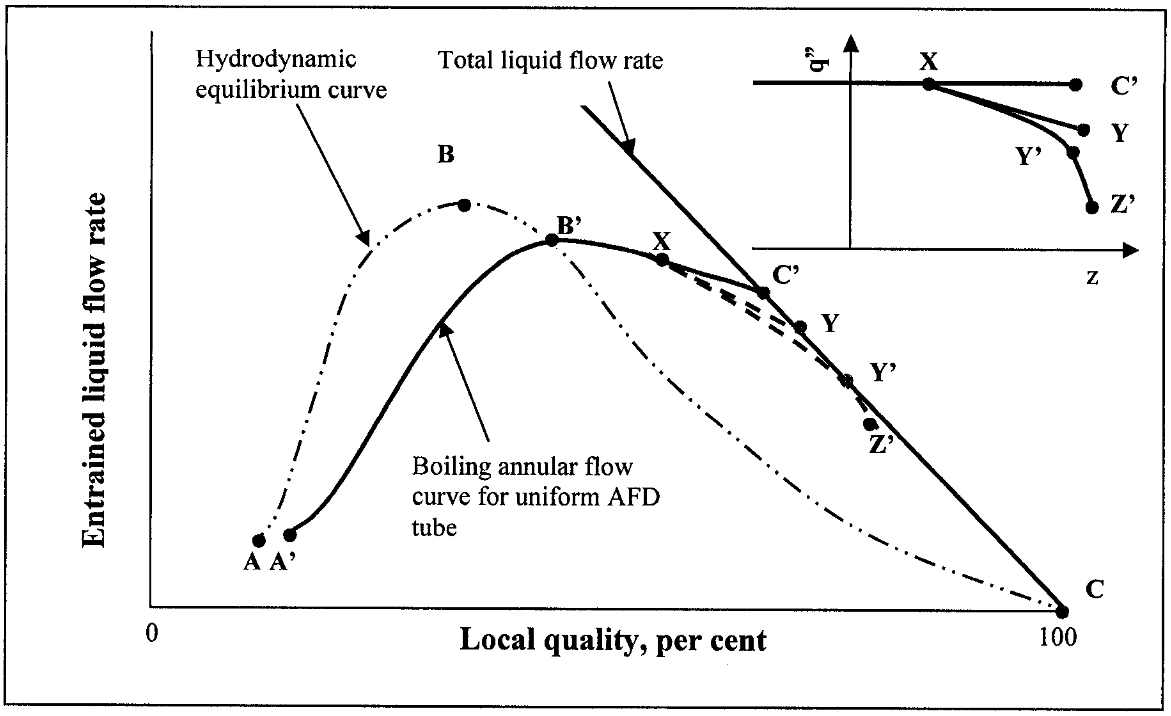

Figure 5.30 Effect of Gradually Decreasing Heat Flux Distribution Near the Tube Exit on CHF. Based on the Entrainment Curves of Hewitt et al. (1965).

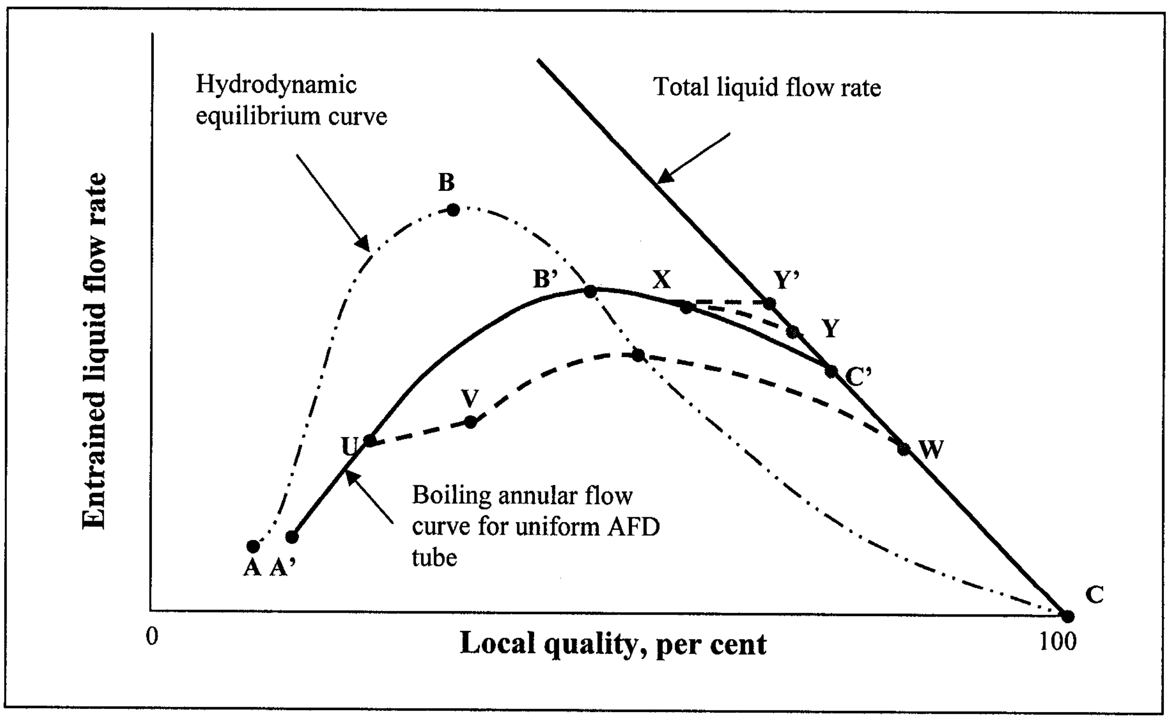

Figure 5.31 Hot Patch Effect on CHF. Based on the Entrainment Curves of Hewitt et al. (1965).

reduced corresponding to the higher q″, hence the W_{IE} follows UV (over the hot patch) and then VW (after the hot patch).

The continuous non-uniform AFD effect on CHF is complex because local heat flux and hence the corresponding CHF mechanism depends strongly on the inlet conditions. At high mass fluxes and low inlet qualities, the CHF mechanisms may be DNB in bubbly flows ($X_{cr}<X_{OAF}$) or the dryout caused by liquid–layer disruption due to surface wave instability ($X_{do}>X_{OAF}$). At high inlet qualities, however, the CHF mechanism is the dryout of liquid layer on the heated surface at the end of the annular flow regime.

Figure 5.32 shows the difference between the heat flux profiles at a high inlet quality and a low inlet quality at CHF conditions. It is found from Figure 5.32 that the dryout location for the high inlet quality is upstream to that for the low inlet quality. The critical power, and hence the local heat flux at high inlet quality are much smaller than those at low inlet quality.

For a uniform AFD, CHF occurs at the quality at which the heat flux line contacts the uniform CHF vs. X_{do} curve. In the case where a uniform AFD has the same average heat flux and the same inlet conditions (P, G, T_{in}, L_h and D_i) as those of a non-uniform AFD, the exit qualities are the same for both AFDs. Figure 5.32 shows that at high inlet quality, the average heat flux line contacts the uniform CHF vs. X_{do} curve at a quality higher than the exit quality of the non-uniform AFD. This phenomenon suggests that either an additional L_h (q″=constant) or an additional q″ (L_h=constant) is required to induce the CHF conditions. Therefore, at the same inlet conditions, the average heat flux of the non-uniform AFD is less than the CHF for the uniform AFD. In other words, the critical power ($=q''_{avg}*\pi D_i L_h$) for the non-uniform AFD is lower than that for the uniform AFD. In addition, Figure 5.32 shows that CHF for the non-uniform AFD is seriously less than that for the uniform AFD at constant local conditions; thus, the local conditions hypothesis is not valid at high inlet qualities.

At low inlet quality, the average heat flux line contacts the uniform CHF curve at a quality lower than the exit quality of the non-uniform AFD. Hence, the average heat flux

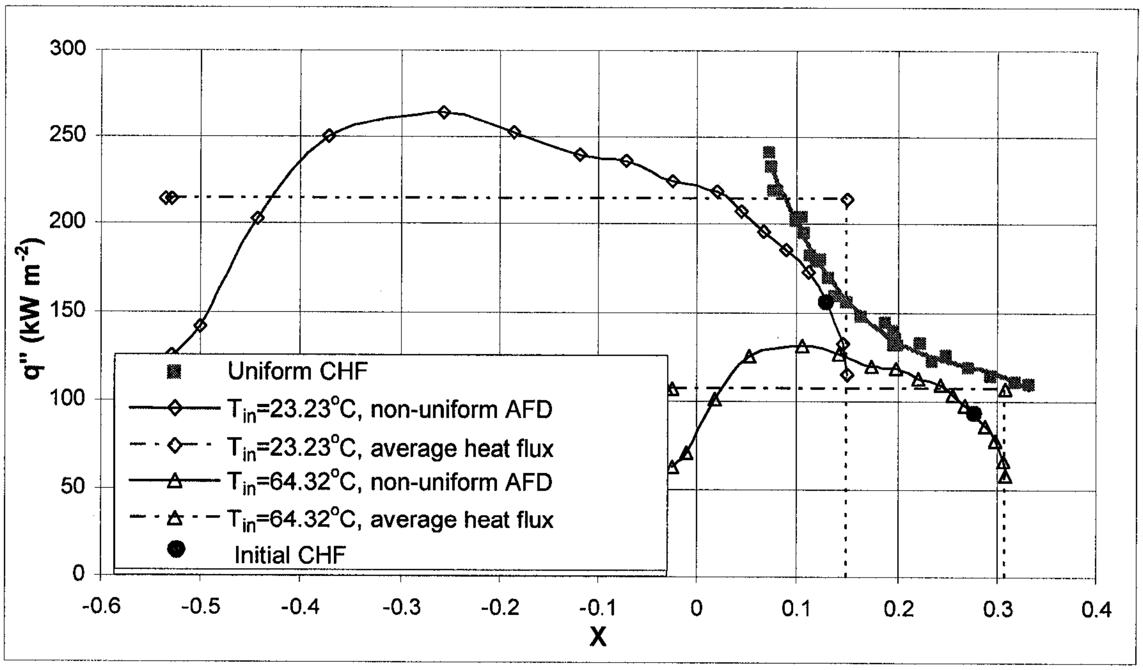

Figure 5.32 Heat Flux Profile at High Inlet Quality and Low Inlet Quality, TS No.1 Forward Direction, P=2022 kPa, G=3533 kg m^{-2} s^{-1}, L_h= 2 m.

of the non-uniform AFD is higher than the CHF of a uniform AFD at the same flow conditions of P, G, T_{in}, D_i and L_h. Therefore, the critical power for the uniform AFD is lower than that for the non-uniform AFD. The CHF for the non-uniform AFD matches reasonably the uniform CHF curve. Thus the local conditions hypothesis is valid at low inlet conditions.

The quality at the onset of annular flow calculated by Eq (2.6) for these flow conditions is 0.02. At high inlet quality, the OAF occurs near the tube entrance while at low inlet quality that occurs at the downstream part of the tube near the average heat flux location. The dryout quality for T_{in}=23.23°C and T_{in}=64.32°C are 0.13 and 0.27, respectively. It is most likely that, the CHF mechanism corresponding to the low inlet quality may be the dryout caused by liquid–layer disruption due to surface wave instability, while that corresponding to the high inlet quality is the dryout of liquid film on the heated surface at the end of the annular flow regime. Based on these observations, Figure 5.33 was produced to illustrate the AFD effect for the high and low inlet qualities.

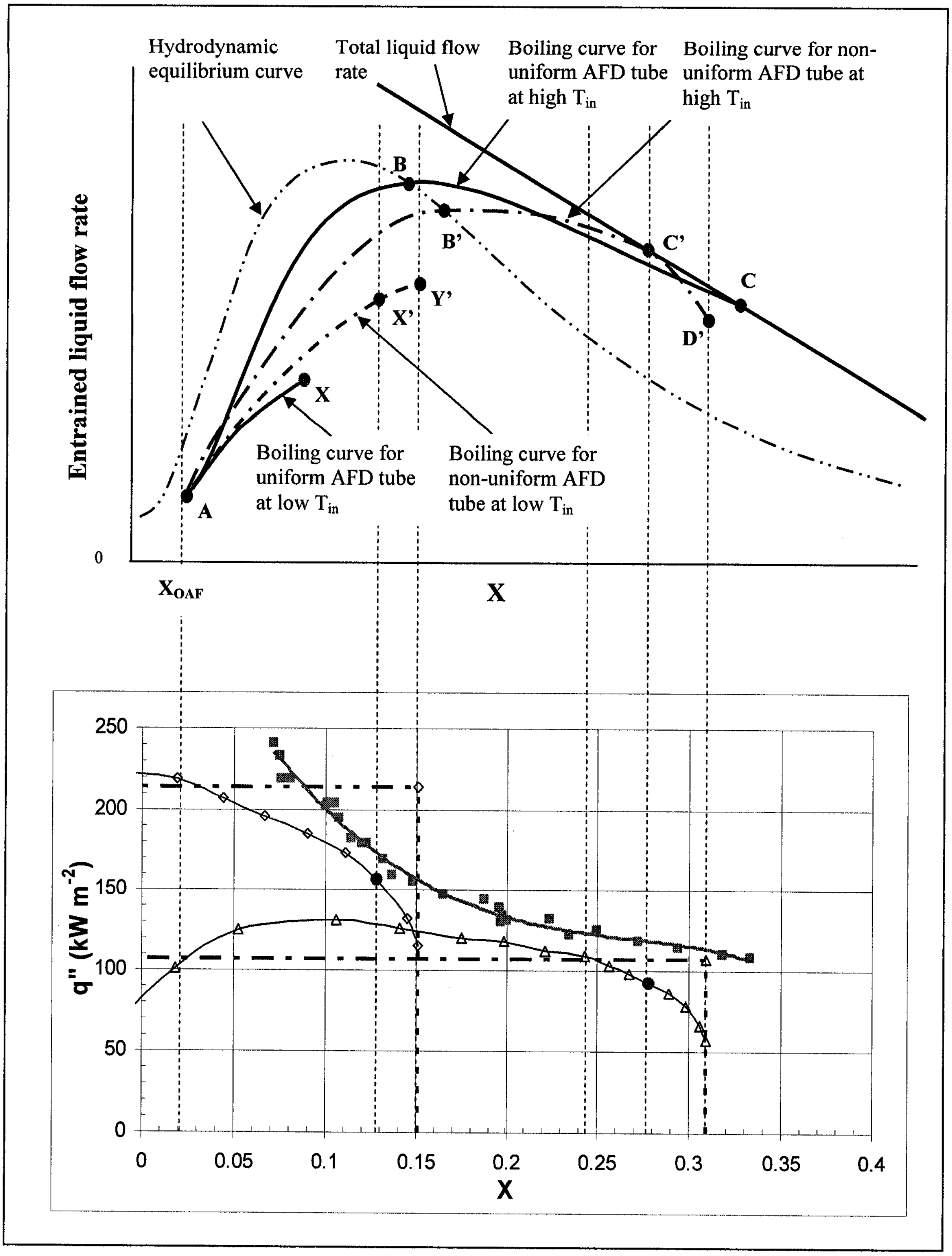

Figure 5.33 Continuous non-uniform AFD Effect on CHF. Based on the Entrainment Curves of Hewitt et al. (1965).

The effect of AFD peak location on the critical power at high inlet qualities can be explained by Figure 5.34. At the upstream part of the tube, the heat flux of an inlet peak AFD is higher than that of an outlet peak AFD. The opposite trend exists at the downstream part. Therefore, the entrained liquid flow rate for the inlet peak AFD may always be lower than that for the outlet peak AFD in the case where the onset of entrainment occurs near the tube entrance (at high inlet qualities) resulting in a higher dryout quality and hence a higher critical power for the inlet peak AFD.

It may be concluded that the AFD effect on CHF depends strongly on the CHF mechanism. AFD has strong effect on CHF if the CHF mechanism is the liquid film dryout on the heated surface at the end of the annular flow regime. For the CHF mechanism of the dryout caused by liquid–layer disruption due to surface wave instability, however, the local conditions hypothesis is approximately valid. It is also noticed that the AFD effect depends on the AFD profile as well.

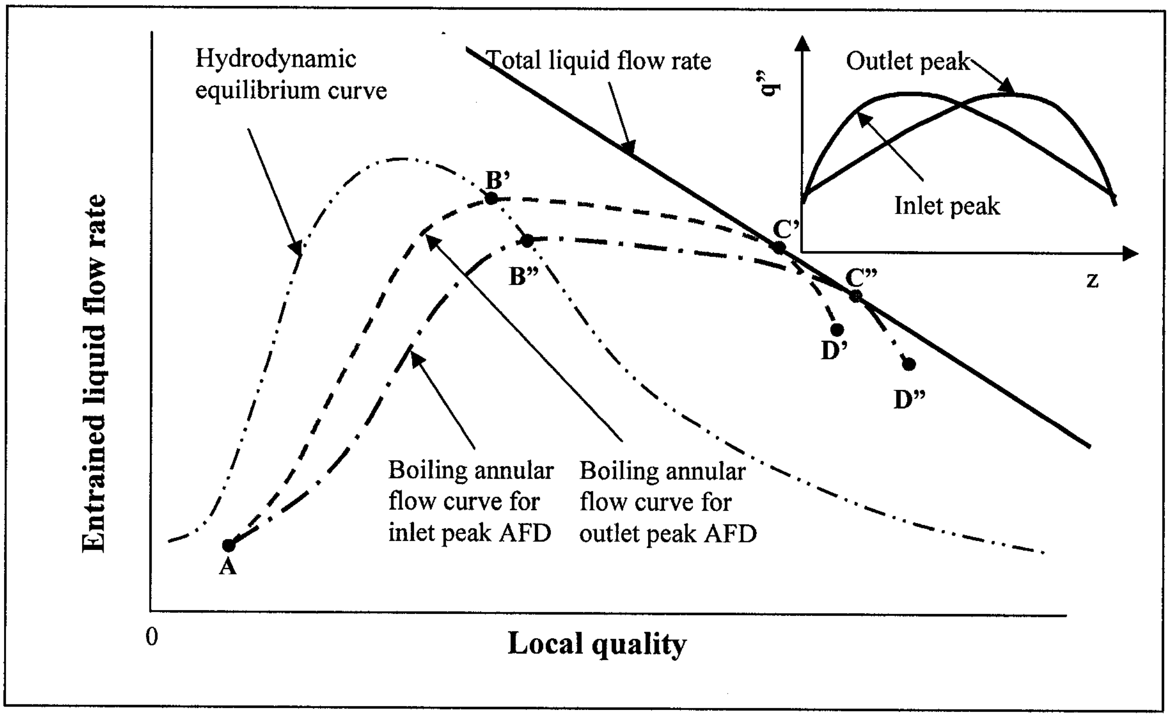

Figure 5.34 Heat Flux Peak Location Effect on CHF at High Inlet Quality. Based on the Entrainment Curves of Hewitt et al. (1965).

6. CHF PREDICTION AND DISCUSSION

6.1 CHF Prediction Methods for Non-Uniform AFD

The CHF prediction methods assessed in this study include the overall power approach, the local conditions approach, the F-factor approach, and the BLA approach. Details on these methods were described in Section 2.10. The definitions of these methods are illustrated in Figure 2.12. Note that the variation of CHF with X_{do} for the uniform AFD employed in this research (see Table 6.1) is obtained directly by the curve fitting of the experimental data.

In the case of F-factor approach, since Eq. (2.57) was correlated from experimental data in water, ideally, the mass flux in this equation should also be the value in water. Considering that the experiments were performed using HFC-134a as working fluid, both the mass fluxes in Freon and water equivalent were used for the calculation of the factor, F.

Besides using X=0, as the starting point for the boiling length, there are some other possible definitions for the start of the boiling length, such as the channel inlet, the onset of nucleate boiling (ONB), the onset of significant void fraction (OSV), and the onset of annular flow (OAF) locations (see Section 2.1.4). The impact of different definitions for the boiling length on the BLA approach was also assessed in this investigation.

6.2 CHF Prediction for Non-Uniform AFD in HFC-134a

The prediction errors were evaluated using the following definitions:

$$\text{Error} = \frac{\text{Value}_{pred} - \text{Value}_{exp}}{\text{Value}_{exp}} \qquad (6.1)$$

$$\text{Average\_Error} = \frac{1}{n}\sum_{i=1}^{i=n} \text{Error}_i \qquad (6.2)$$

$$\text{RMS\_Error} = \sqrt{\frac{1}{n}\sum_{i=1}^{i=n} \text{Error}_i^2} \qquad (6.3)$$

Table 6.1 Critical Heat Flux as a Function of Dryout Quality for the Uniform AFD Derived by Curve Fitting of the Experimental Data

P (kPa)	G (kg m^{-2} s^{-1})	CHF = f(X_{do})
1662	2827	CHF = $-17664X_{do}^3 + 12491X_{do}^2 - 3299.3X_{do} + 427.54$
	3533	CHF = $-26697X_{do}^3 + 18782X_{do}^2 - 4516.3X_{do} + 489.92$
	4594	CHF = $-10625X_{do}^3 + 8355.1X_{do}^2 - 2414.1X_{do} + 390.43$
2022	2842	CHF = $-15201X_{do}^3 + 11426X_{do}^2 - 3135.5X_{do} + 406.76$
	3552	CHF = $-10446X_{do}^3 + 8629.3X_{do}^2 - 2522.2X_{do} + 376.41$
	4618	CHF = $-35453X_{do}^4 + 16803X_{do}^3 + 1107.5X_{do}^2 - 1717.3X_{do} + 395.27$
2389	2861	CHF = $-8886.3X_{do}^3 + 7381.7X_{do}^2 - 2297.7X_{do} + 360.65$
	3576	CHF = $-3768.7X_{do}^3 + 4264.4X_{do}^2 - 1700.7X_{do} + 354.25$
	4648	CHF = $1021.1X_{do}^3 + 608.2X_{do}^2 - 855.79X_{do} + 346$

The prediction errors for the critical power by each method are shown in Table 6.2.

It was found that the BLA approach with boiling length starting point at the onset of annular flow gives the best critical power prediction. The prediction results presented as a ratio of the predicted to measured critical power (CHFPR) and a comparison of the predicted to measured CHF location by each method are illustrated in Figures 6.1 to 6.10 and will be discussed in the following sections.

6.2.1 CHF Prediction Results by Overall Power Approach

This method generally under-predicts the critical power for a non-uniform AFD. This is especially true at high inlet subcooling. Figure 6.1 shows that the prediction accuracy increases as the inlet subcooling decreases. The pressure does not apparently affect the prediction accuracy, but the discrepancy between the predicted and the measured critical powers increases with an increase in mass flux. As mentioned previously, the overall power approach is incapable of predicting the CHF location.

6.2.2 CHF Prediction Results by Local Conditions Approach

The local conditions approach generally over-predicts the critical power for non-uniform AFD (see Figure 6.2). At high inlet subcooling (X_{in}<-0.4), this method provides excellent

Table 6.2 Prediction Errors for Critical Power by Each Method (Based on All 481 HFC-134a Data Points)

Method		Average Error	RMS Error
Overall Power Approach		-0.061	0.077
Local Conditions Approach		0.040	0.054
F-factor Approach	$G = G_R$	-0.027	0.043
	$G = G_W$	-0.031	0.047
BLA Approach with Boiling Length Starting Point at	Tube Inlet	-0.058	0.074
	ONB*	-0.058	0.074
	OSV*	-0.034	0.046
	X=0	-0.014	0.030
	OAF	-0.008	0.026

* In case the calculated local quality at the boiling length starting point is lower than that at the tube inlet, the tube inlet is used as the boiling length starting point.

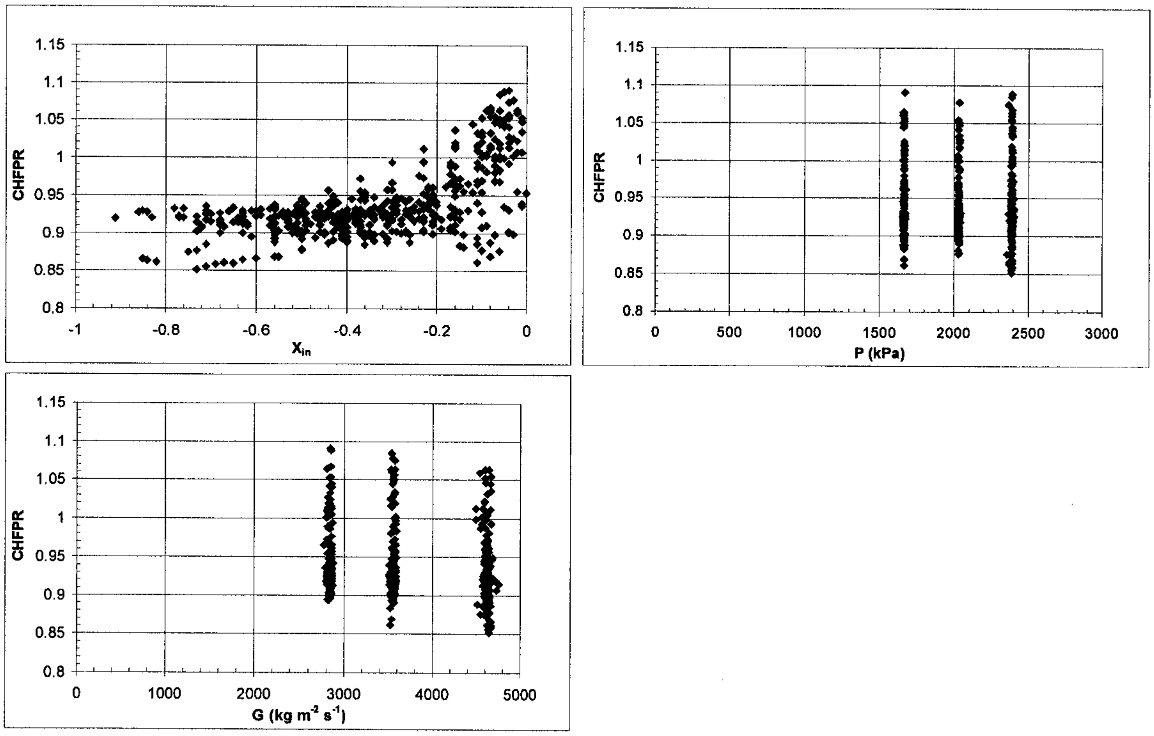

Figure 6.1 CHF Prediction Results by Overall Power Approach.

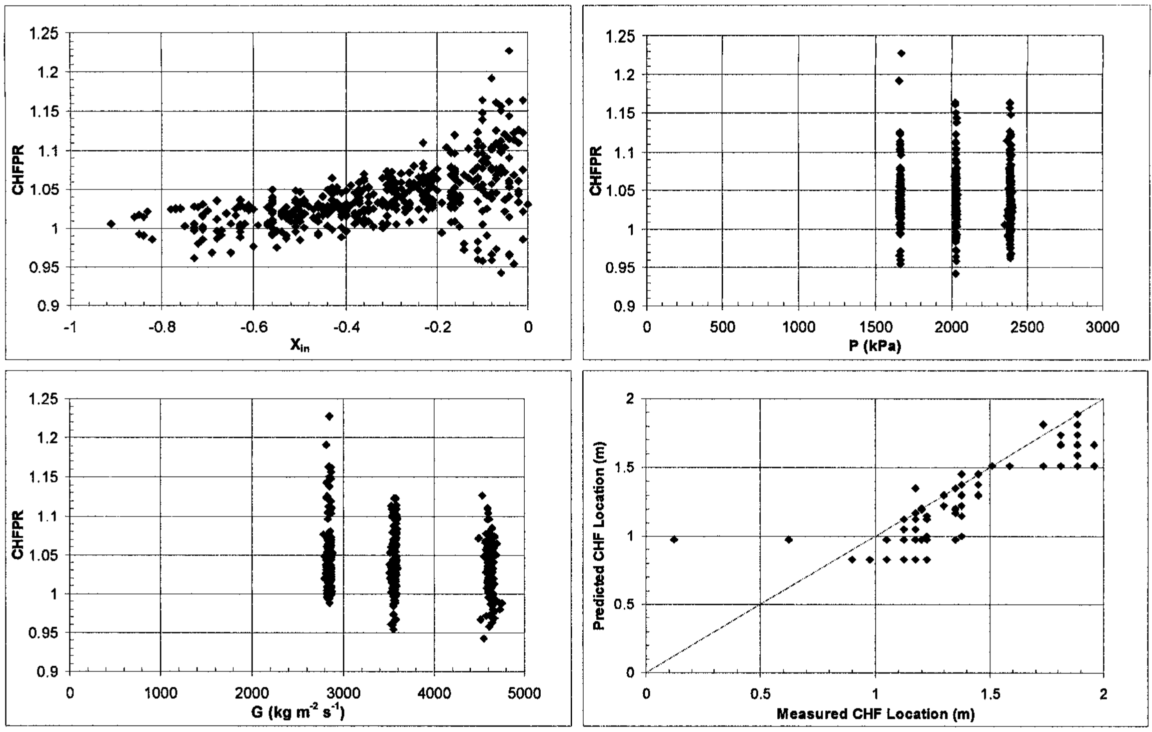

Figure 6.2 CHF Prediction Results by Local Conditions Approach.

critical power predictions but the scatter in the predictions increases with an increase in quality and/or a decrease in mass flux. The pressure does not appear to have a strong effect on the prediction accuracy. The predicted CHF locations are generally closer to the channel inlet than the measured ones.

6.2.3 CHF Prediction Results by the F-factor Approach

The results illustrated in Figures 6.3 to 6.4 show that the F-factor approach is more accurate than the local conditions approach, and the one using mass flux in Freon is better than that using water equivalent mass flux. Unlike the local conditions approach, which over-predicts the critical power at low inlet subcooling, the F-factor approach generally under-predicts the critical power, especially at high inlet subcooling. This is because the uniform CHF does not need to be corrected and/or the correction factor provided by the F-factor approach is stronger than required for the high subcooling region. Once again, the pressure does not appear to affect the prediction accuracy, and this method gives better prediction results for lower mass flux. The CHF locations are reasonably well predicted by this method.

6.2.4 CHF Prediction Results by Boiling Length Average Approach

The results indicate that the boiling length starting point, which is used for the computation of the $q''_{BLA,}$ has a strong effect on the prediction accuracy. The BLA approach with the boiling length starting point at the channel inlet seriously under-predicted the critical power, and gives the highest prediction error comparing with the other points. The prediction accuracy increases as the boiling length starting point shifts successively in the flow direction from the channel inlet to the points of the onset of nucleate boiling, the onset of significant void fraction, X=0 and the onset of annular flow (see Figures 6.5 to 6.9). The BLA approach with the boiling length starting point at the onset of annular flow gives the most accurate predictions. This finding corroborates the theoretical analysis. Almost all of the experimental data are found with positive critical quality, and the CHF condition for the majority occurs in the annular flow region. The

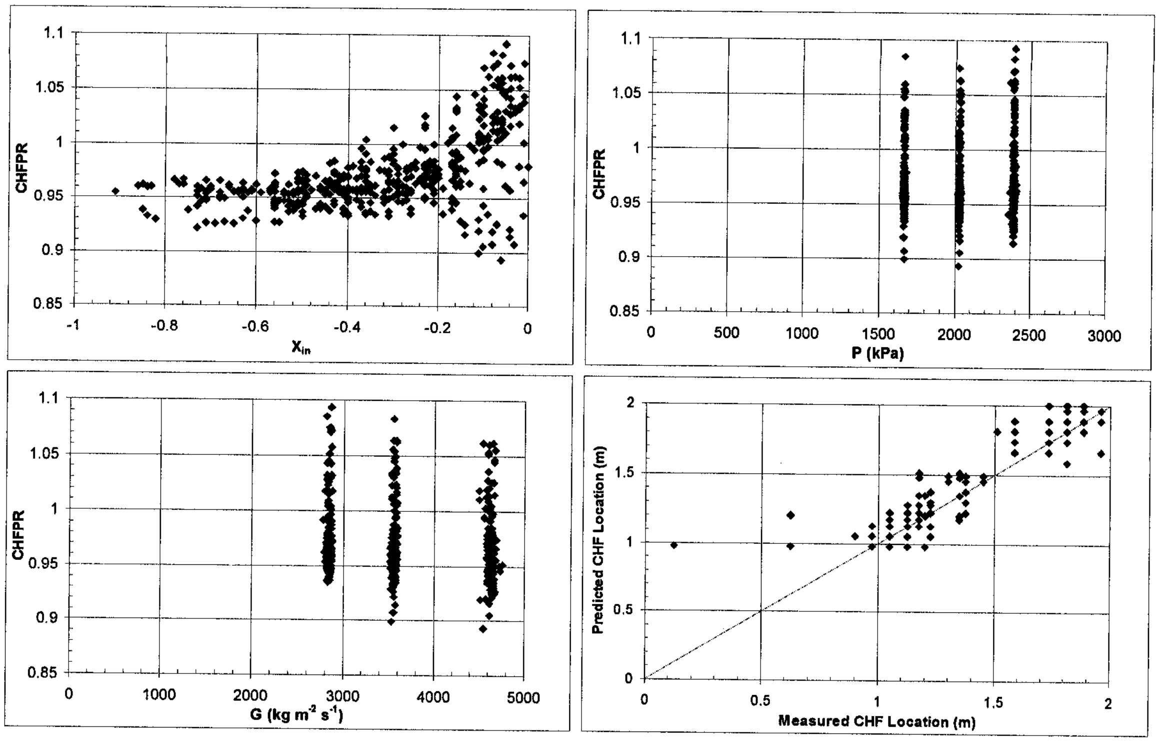

Figure 6.3 CHF Prediction Results by F-factor Approach Using Freon Conditions.

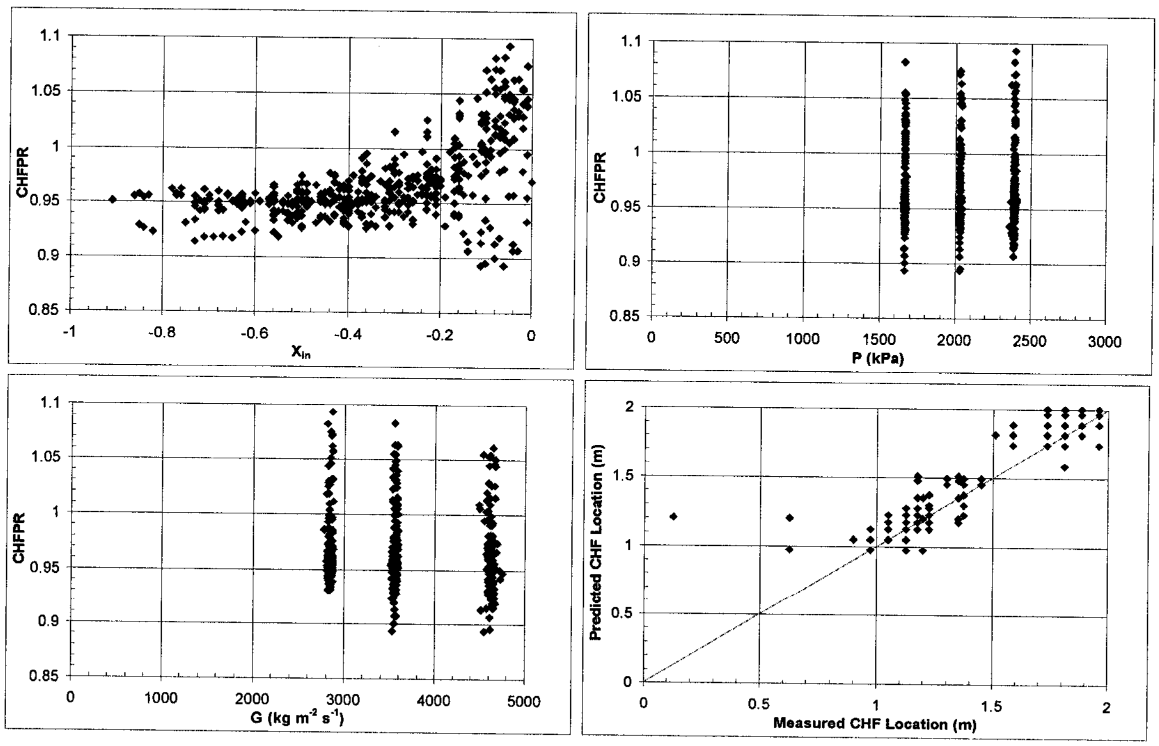

Figure 6.4 CHF Prediction Results by F-factor Approach Using Water Equivalent Conditions.

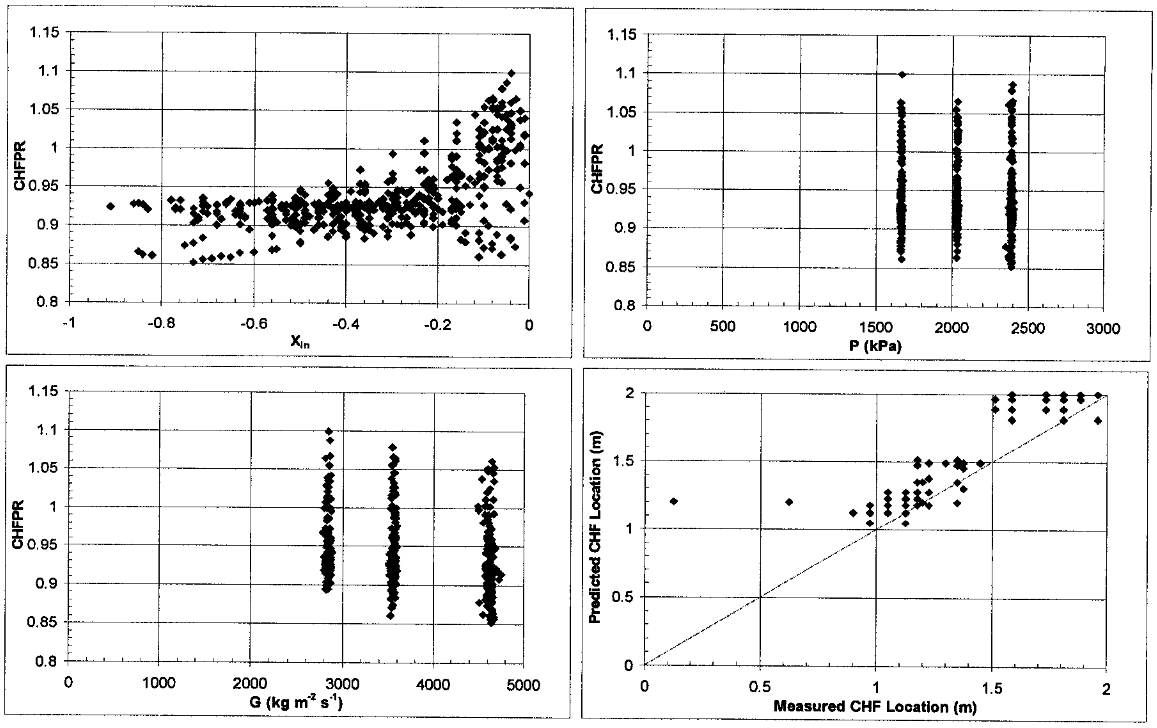

Figure 6.5 CHF Prediction Results by BLA Approach with the Boiling Length Starting Point at Channel Inlet.

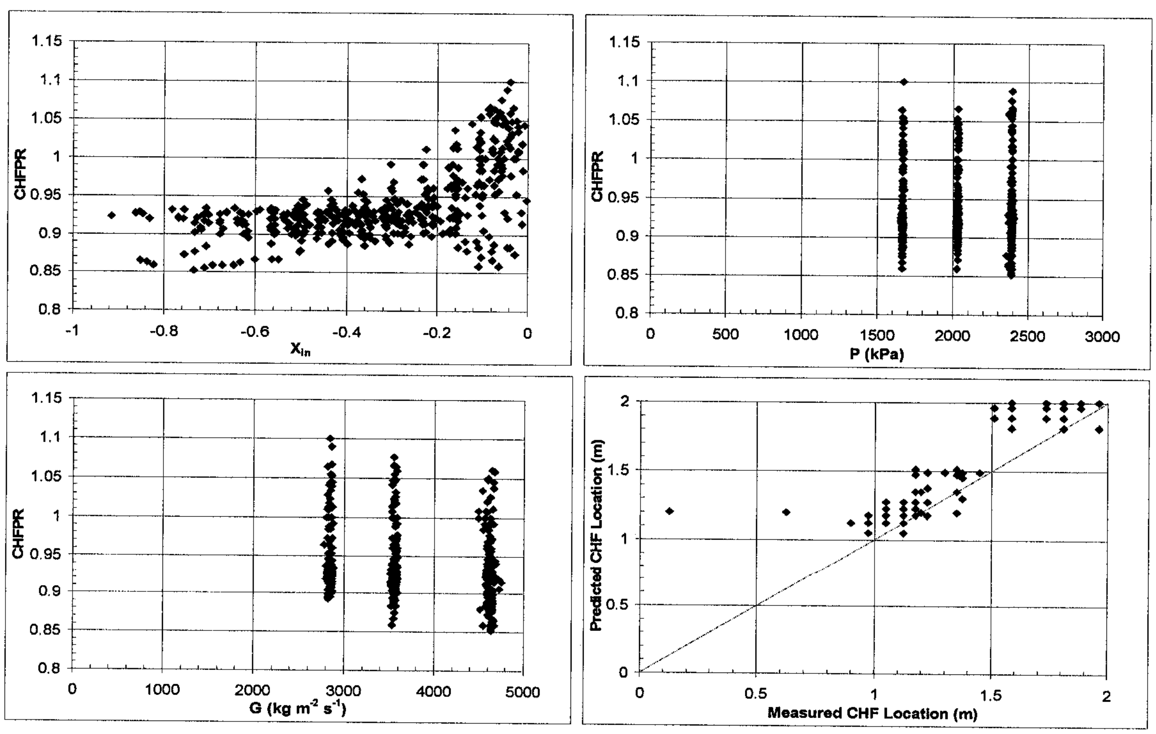

Figure 6.6 CHF Prediction Results by BLA Approach with the Boiling Length Starting Point at the Onset of Nucleate Boiling.

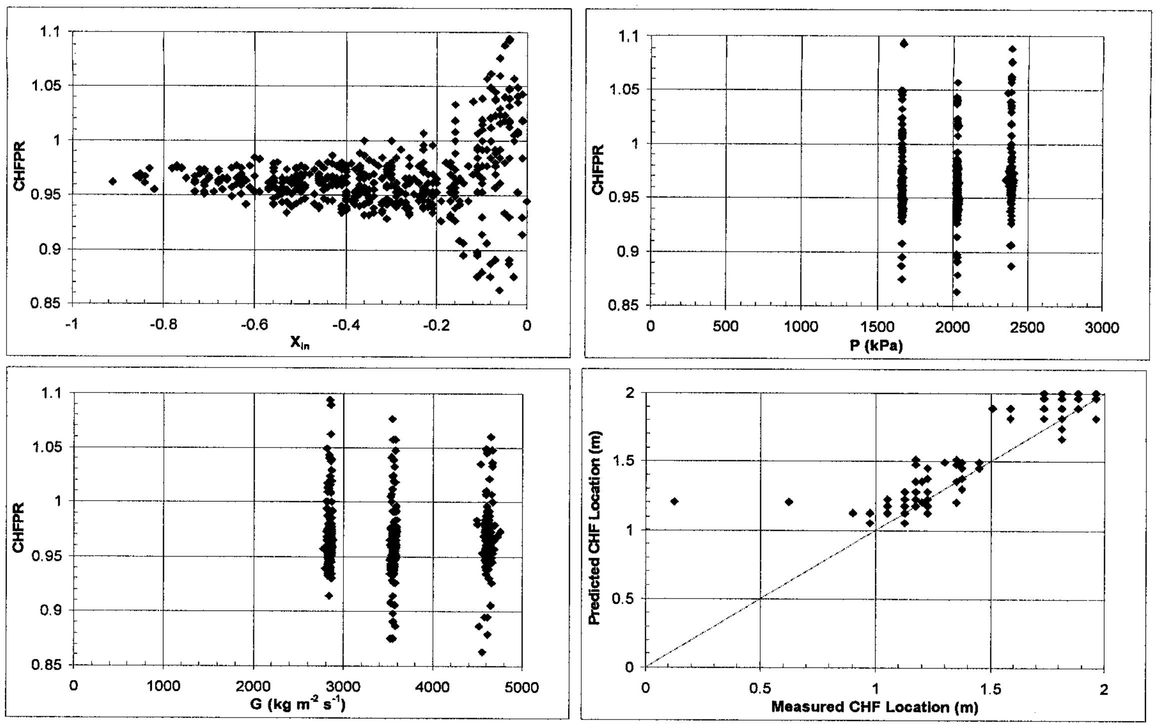

Figure 6.7 CHF Prediction Results by BLA Approach with the Boiling Length Starting Point at the Onset of Significant Void Fraction.

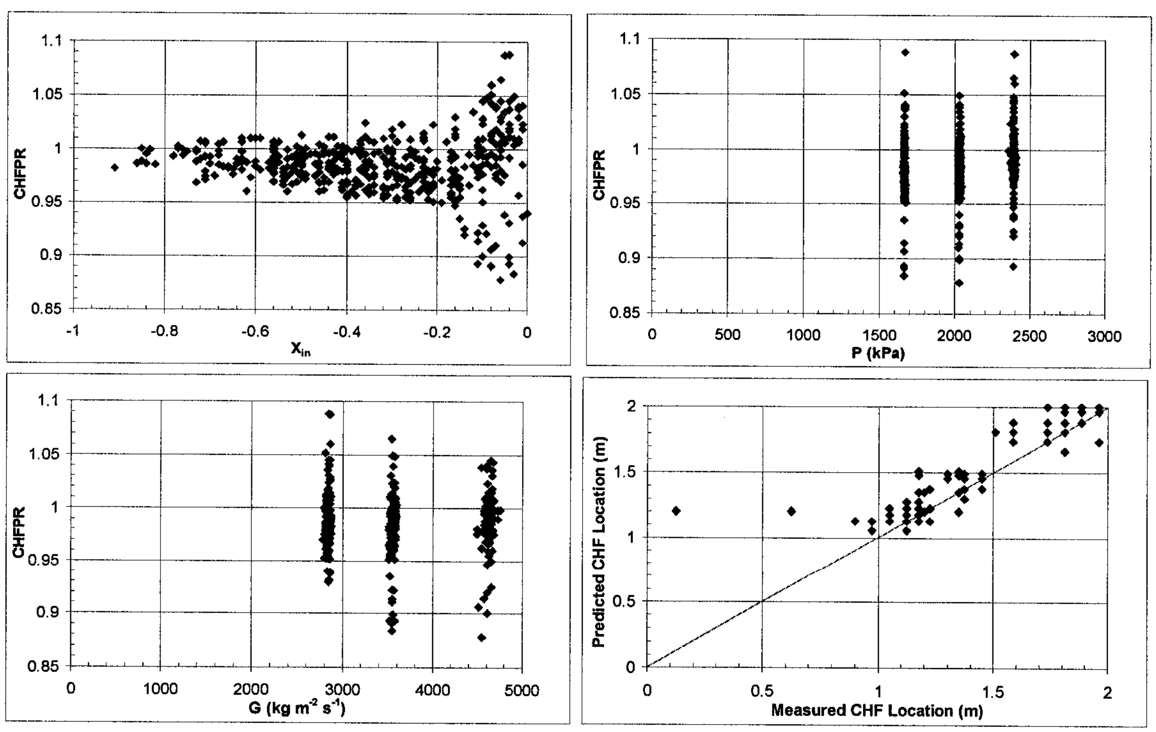

Figure 6.8 CHF Prediction Results by BLA Approach with the Boiling Length Starting Point at X=0.

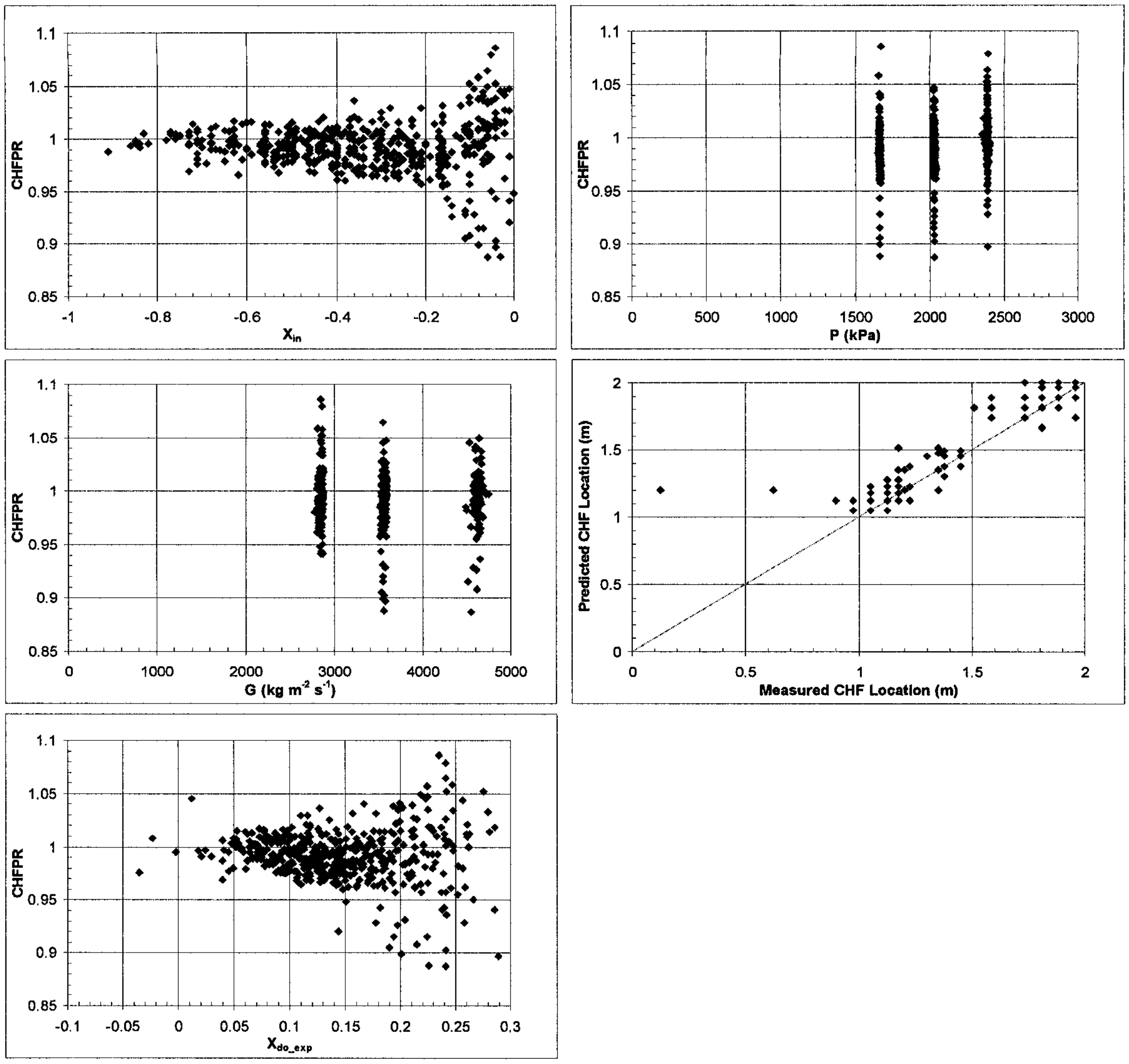

Figure 6.9 CHF Prediction Results by BLA Approach with the Boiling Length Starting Point at the Onset of Annular Flow.

onset of annular flow is the location most directly related to the CHF condition when the CHF mechanism is the liquid film dryout in the annular flow region. Therefore, this location is most suited as the boiling length starting point.

The optimum method, the BLA approach with the boiling length starting point at the onset of annular flow, gives an average error of 0.9%, and an RMS error of 2.6% for the prediction of critical power for all of the 481 data points. These errors are much smaller than those corresponding to the overall power, local conditions and the F-factor approach. This method also provides a very good prediction for the CHF location. The parametric error trends for all data are shown graphically in Figure 6.9. Note the good agreement of the predicted and measured critical powers except at low inlet subcoolings, where the predicted and measured critical power ratio varies from 0.89 to 1.08.

In order to obtain a closer look at this quality region, plots of the prediction results were produced for each AFD profile separately as shown in Figures 6.10a to 6.10e. The prediction errors for each AFD profile are also presented separately in Table 6.3. It was found that the RMS error for the TS No. 2 reverse direction is 4%, which is much larger than those for the other three AFD profiles of which with the values varying from 1.3% to 2.6%. The critical power prediction errors for TS No. 1 forward and reverse direction and TS No. 2 forward direction basically fall in a band of ± 5%, except for a few data (7 of all the 378 data) with low mass flux and very low inlet subcooling (close to zero). The CHF locations predicted for these three AFD profiles are in very good agreement with that measured as well. With respect to the TS No. 2 reverse direction, the prediction of critical power is also very accurate at high subcooling. When inlet quality becomes higher than around –0.2, however, this prediction method seriously under-predicts the critical power, especially for the data with high mass flux. Large deviations between the predicted and measured CHF location are also detected in some cases with high mass flux and high inlet quality, in which the measured CHF locations are much close to the tube inlet than that predicted. It is felt that this disagreement is probably due to the machining flaw in step 4 of the TS No. 2. The local heat flux at this step is approximately 10% less than the design value. Since this step was near the expected CHF locations for reverse

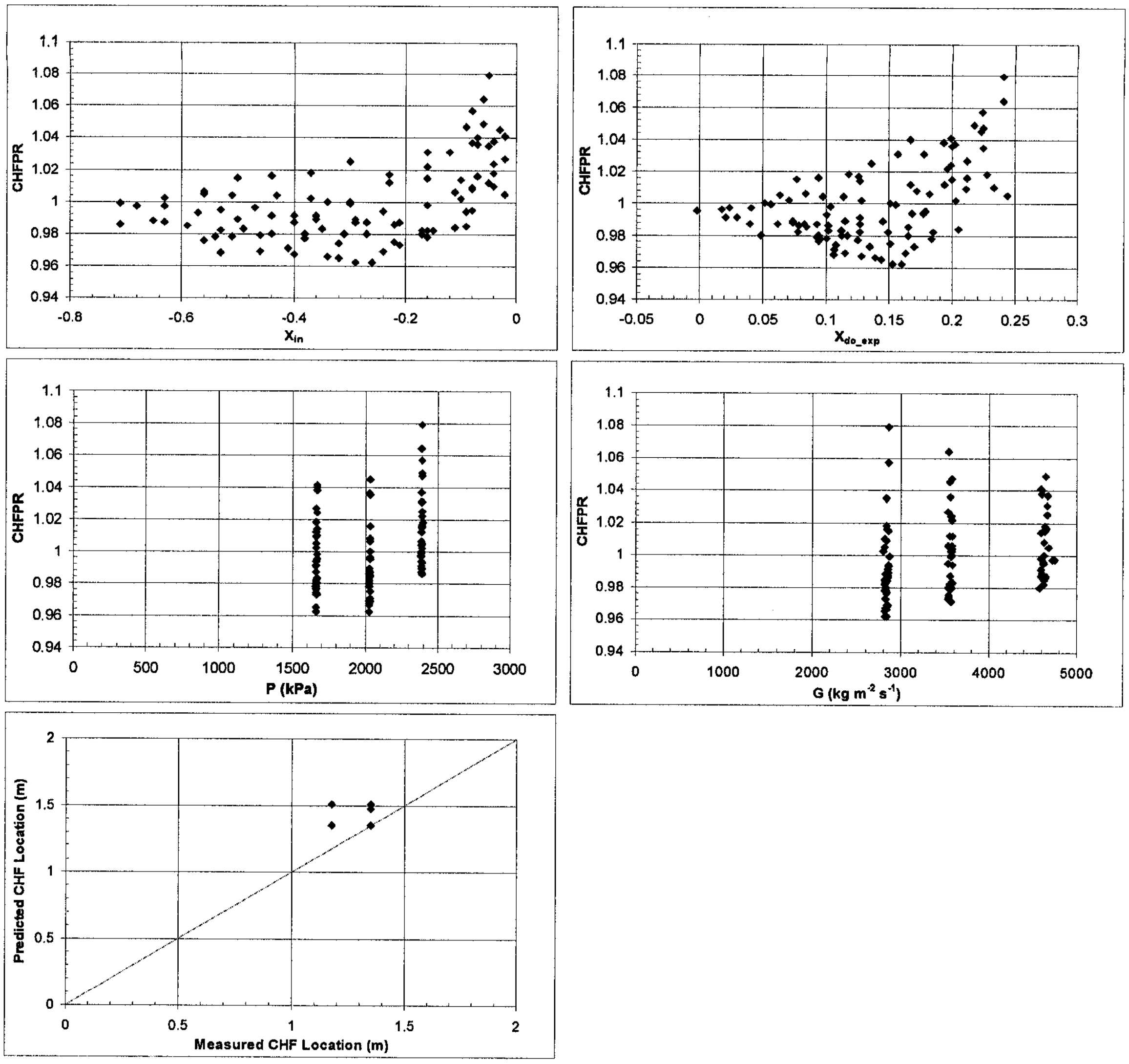

Figure 6.10a CHF Prediction Results by BLA_{OAF} Approach for TS No. 1, Reverse Direction.

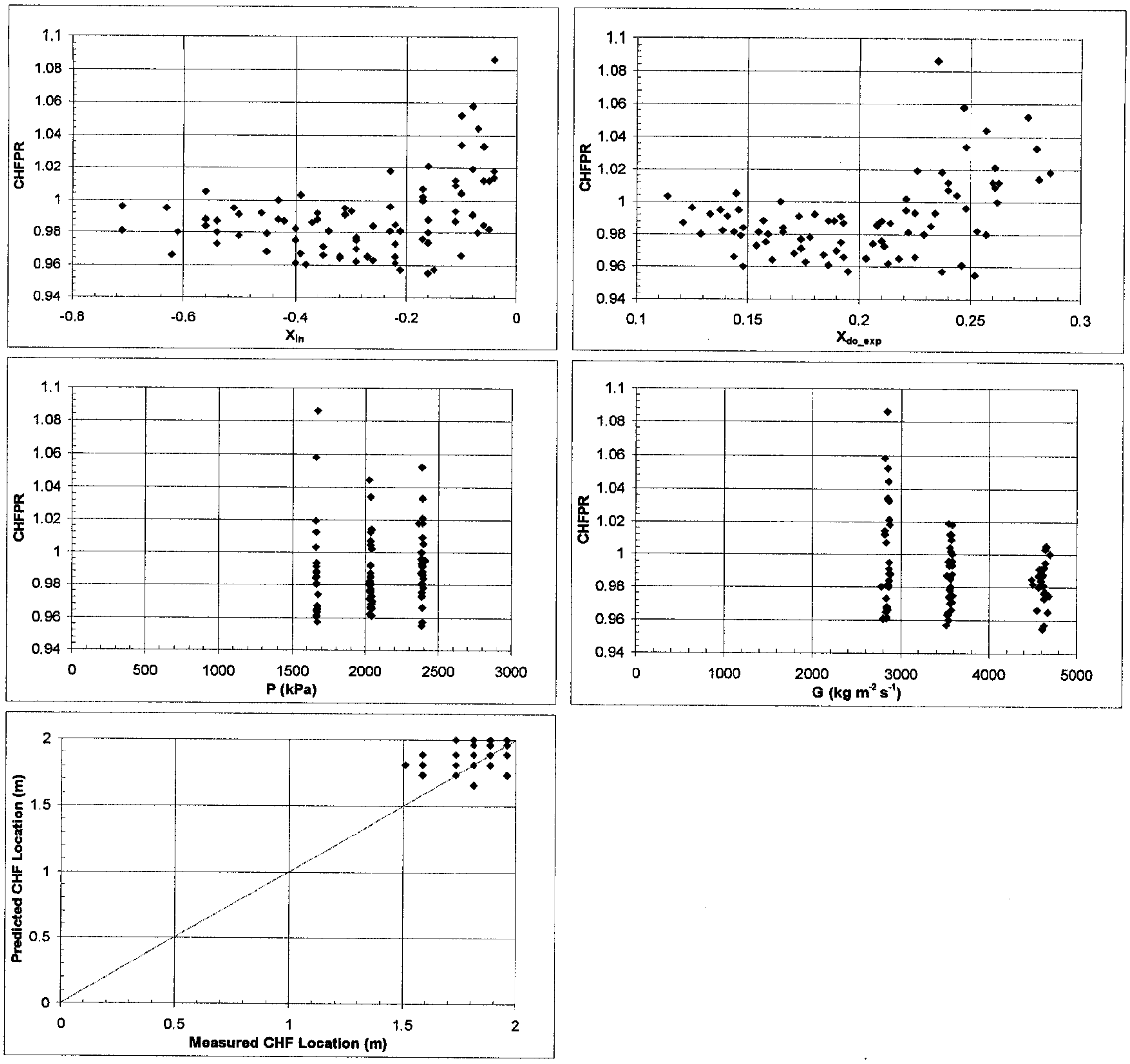

Figure 6.10b CHF Prediction Results by BLA_{OAF} Approach for TS No. 1, Forward Direction, L_h = 2m.

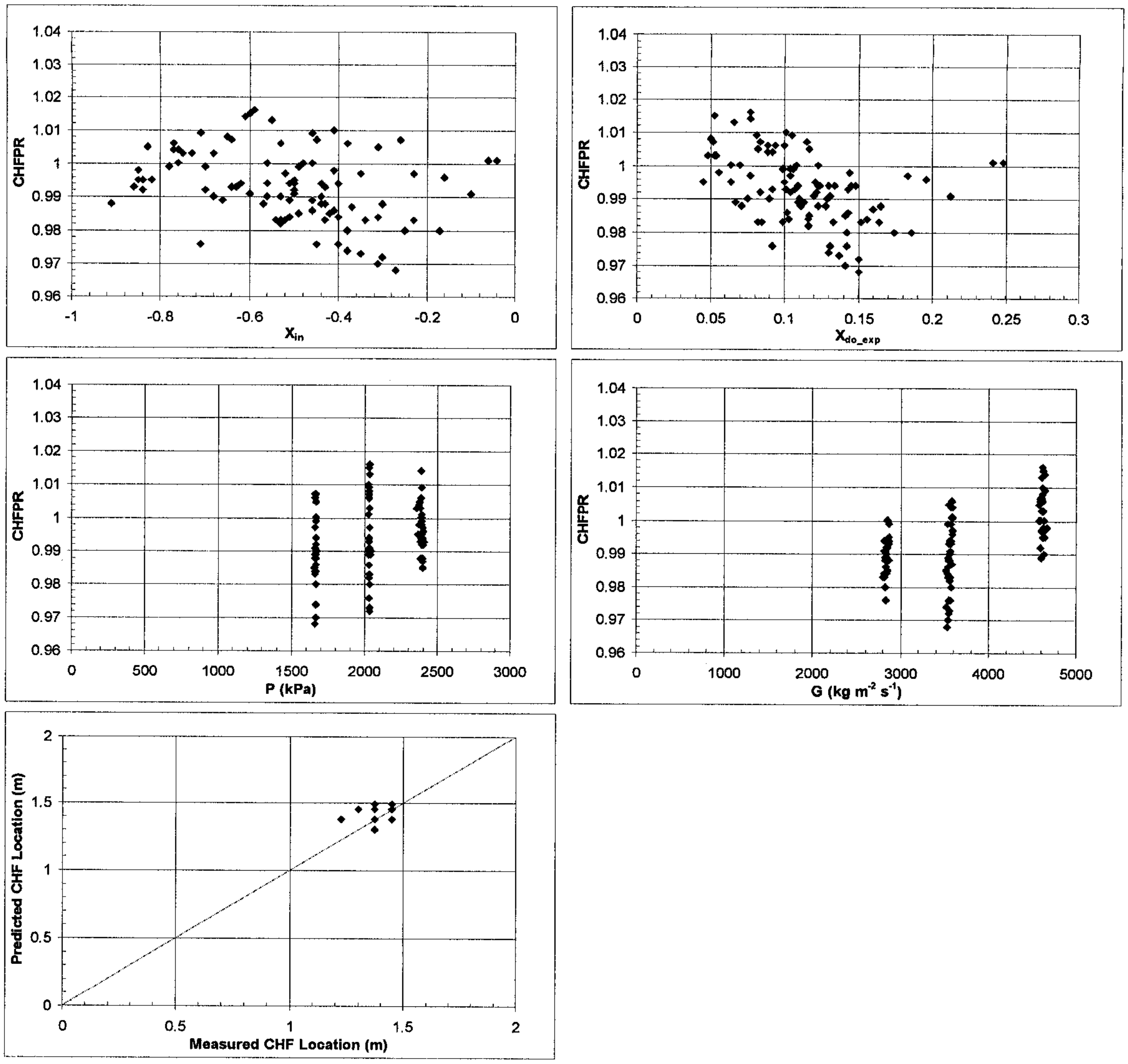

Figure 6.10c CHF Prediction Results by BLA_{OAF} Approach for TS No. 1, Forward Direction, L_h = 1.49m.

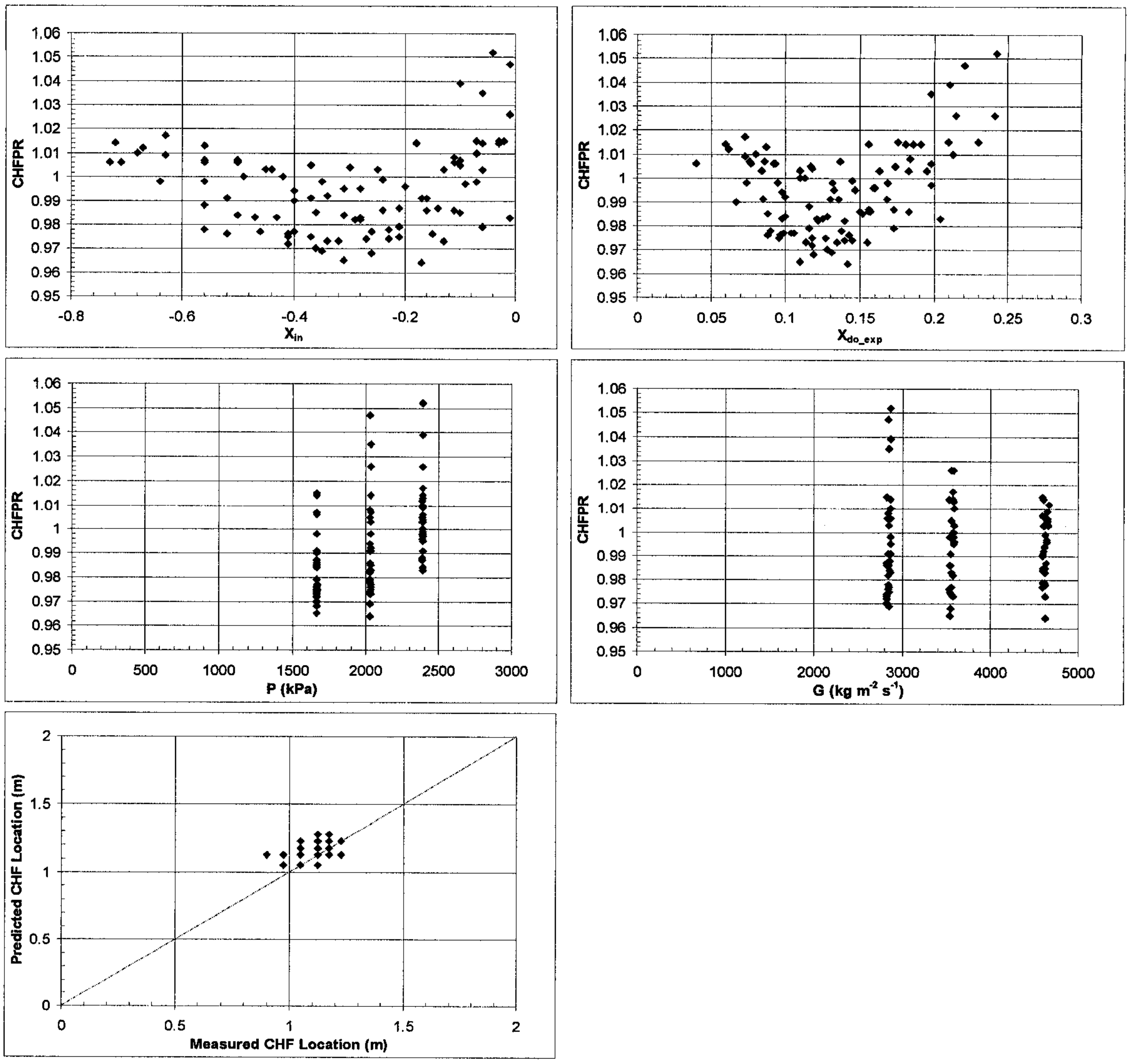

Figure 6.10d CHF Prediction Results by BLA_{OAF} Approach for TS No. 2, Forward Direction.

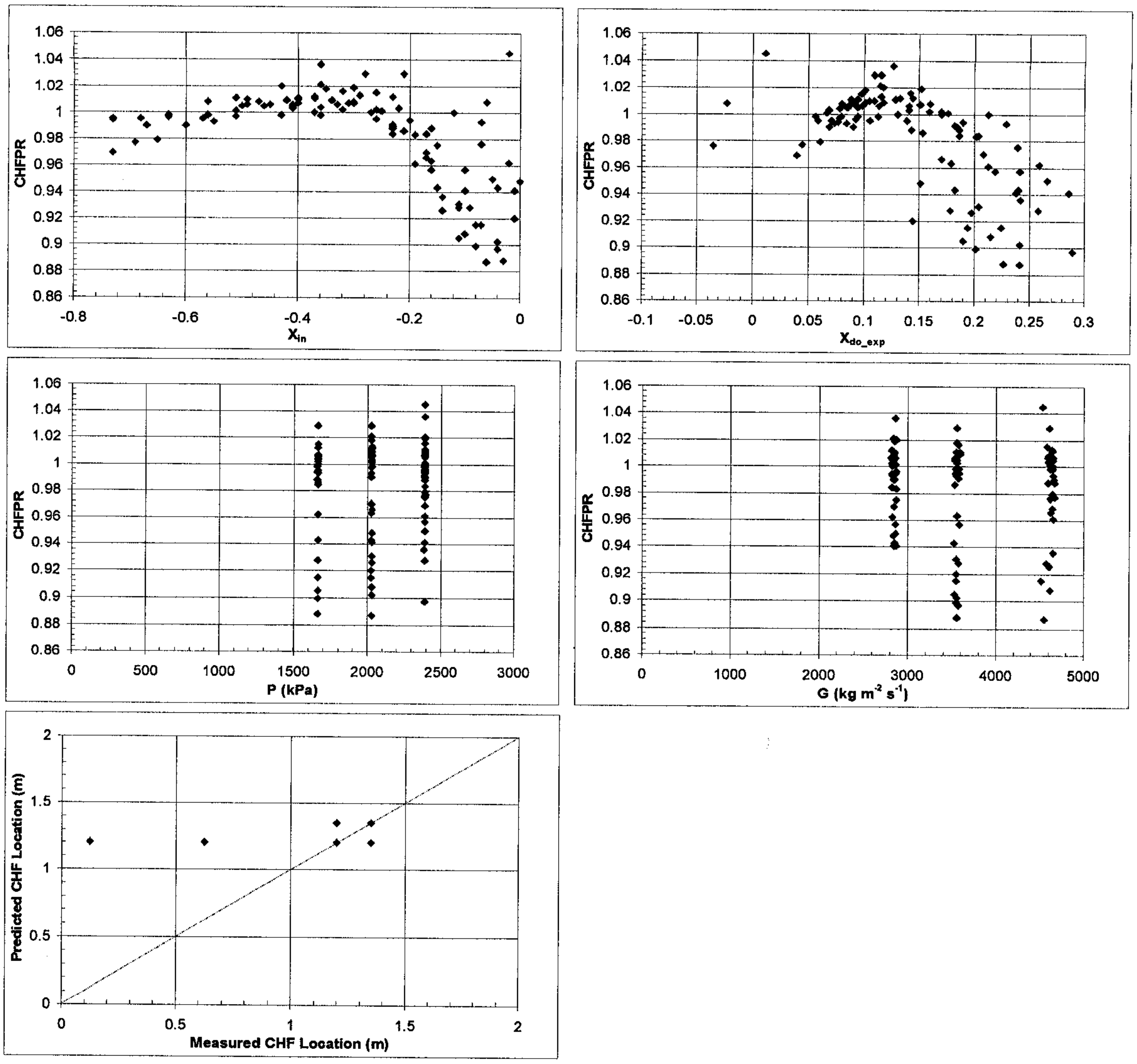

Figure 6.10e CHF Prediction Results by BLA_{OAF} Approach for TS No. 2, Reverse Direction.

Table 6.3 Prediction Errors for Critical Power by BLA_{OAF} Approach for Each AFD (Based on HFC-134a Data Points)

Method		Average Error	RMS Error
BLA Approach with Boiling Length Starting Point at OAF	All Data (481)*	-0.008	0.026
	TS No. 1_Reverse (101)	-0.001	0.024
	TS No. 1_Forward, Lh=2m (84)	-0.011	0.026
	TS No. 1_Forward, Lh=1.49m (96)	-0.007	0.013
	TS No. 2_Forward (97)	-0.005	0.019
	TS No. 2_Reverse (103)	-0.017	0.040

* Value in ( ) is the number of data points.

flow test, its lower heat flux exerted an effect on the CHF similar to a cold patch effect, which enhanced the critical power and affected the CHF location at certain conditions.

6.2.5 Comparison between Boiling Length Average Heat Flux and Local Heat Flux

The previous comparisons show that the BLA approach with the boiling length starting point at the onset of annular flow gives an excellent CHF prediction for tubes with a non-uniform AFD. An analysis of the q''_{BLA} has provided the explanation for this conclusion. Figure 6.11 shows an example of the comparison between the q''_{BLA} profile with the boiling length starting point at the onset of annular flow and the local heat flux profile at CHF conditions. It is evident that the q''_{BLA} is higher than the local heat flux at the same dryout quality, and the q''_{BLA} vs. local quality curve approximately tangents to the uniform CHF vs. X_{do} curve at the measured CHF location. Figures 6.12 to 6.14 display the uniform CHF vs. X_{do} curve, the measured local CHF and the q''_{BLA} with the boiling length starting point at the onset of annular flow at the measured CHF location for each test section at different flow conditions. Plots, which show the q''_{BLA} with the boiling length starting point at X=0, were also produced and are illustrated in Figures 6.15 to 6.17 as the reference cases. It is observed that, unlike the measured CHF for non-uniform AFD, which is generally lower than the uniform CHF, especially at high qualities, the q''_{BLA} with the boiling length starting point at the onset of annular flow at the measured CHF location matches the uniform CHF reasonably well in the whole dryout quality region. These observations support the application of the BLA approach with the boiling length starting point at the onset of annular flow for the CHF prediction for tubes with non-uniform axial heat flux distribution.

6.2.6 Effect of Void Fraction at Boiling Length Starting Point on Prediction Accuracy

In annular flow a liquid film forms at the channel wall with a continuous central vapor core. Sufficient void fraction is required for the transition from intermittent (churn) flow

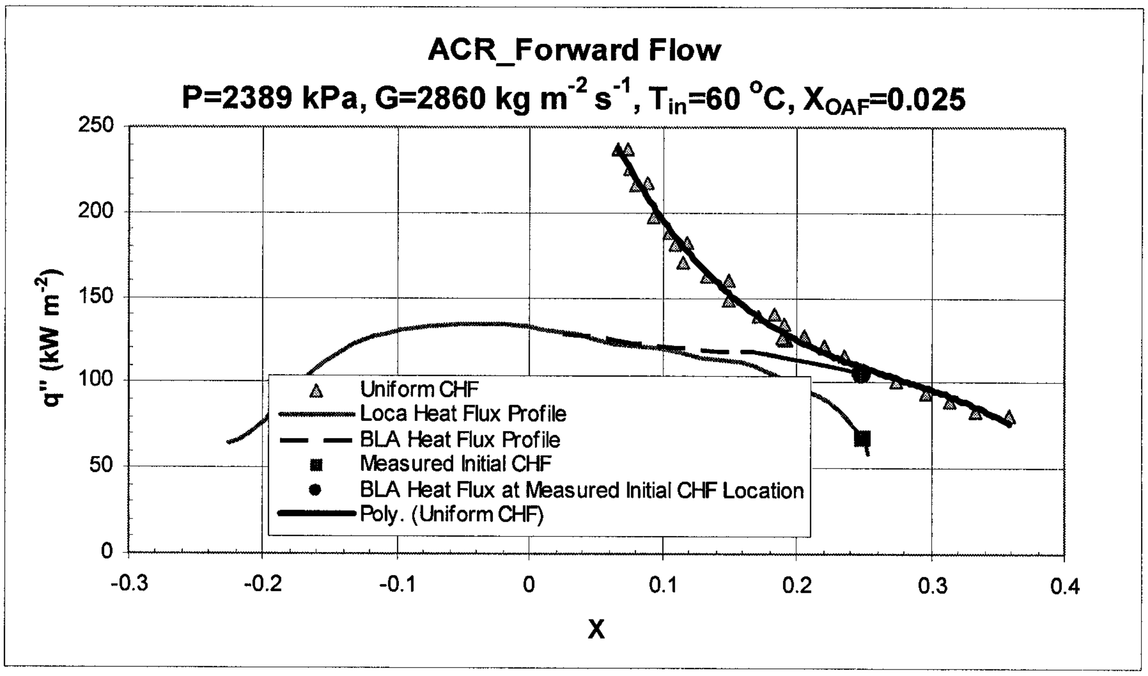

Figure 6.11 Comparison between the Boiling Length Average Heat Flux Profile with the Boiling Length Starting Point at the Onset of Annular Flow and the Local Heat Flux Profile at CHF Conditions.

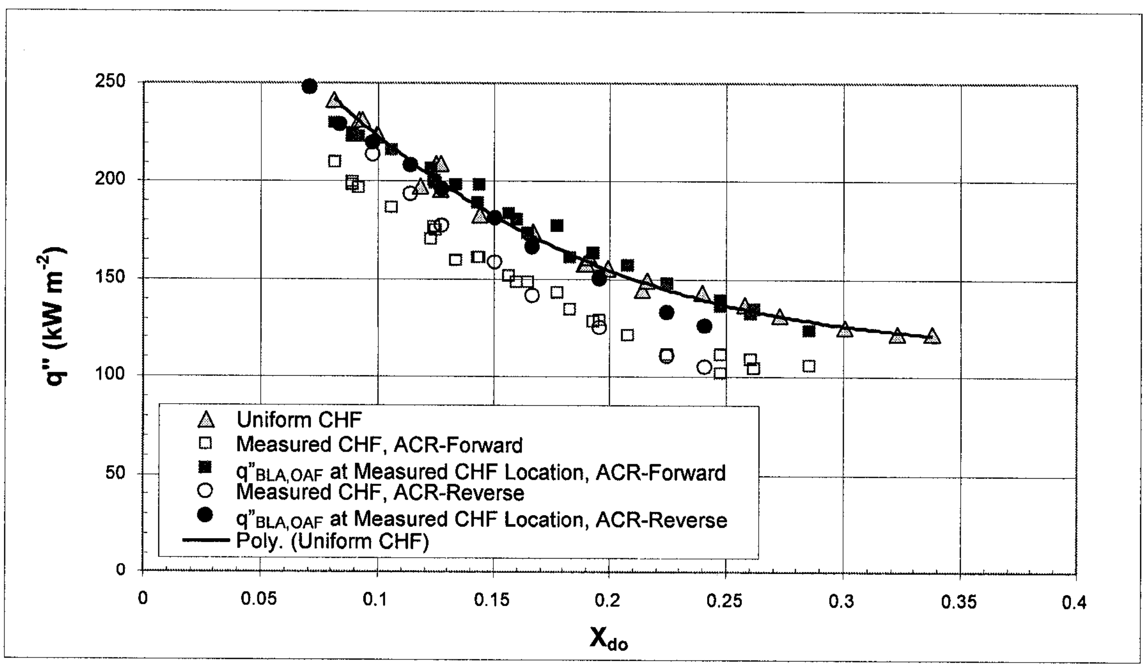

Figure 6.12a Comparison between the Local CHF and the Boiling Length Average Heat Flux with the Boiling Length Starting Point at OAF at the Measured CHF Location, P=2389 kPa, G=3575 kg m^{-2} s^{-1}, X_{OAF}=0.02, TS No. 1.

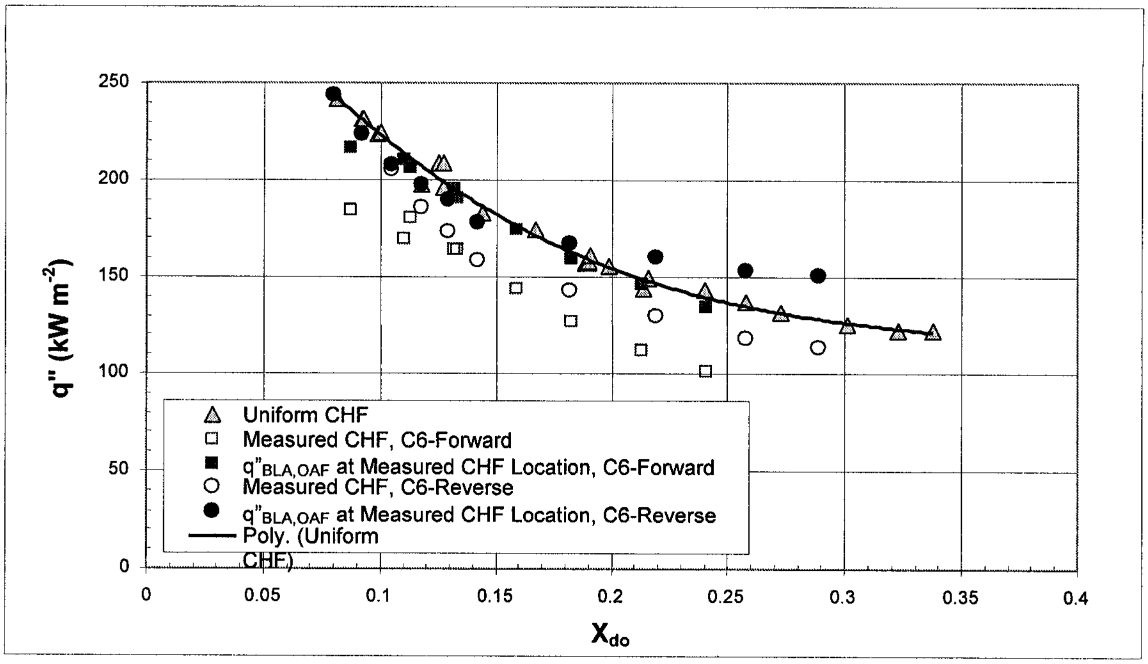

Figure 6.12b Comparison between the Local CHF and the Boiling Length Average Heat Flux with the Boiling Length Starting Point at OAF at the Measured CHF Location, P=2389 kPa, G=3575 kg m^{-2} s^{-1}, X_{OAF}=0.02, TS No. 2.

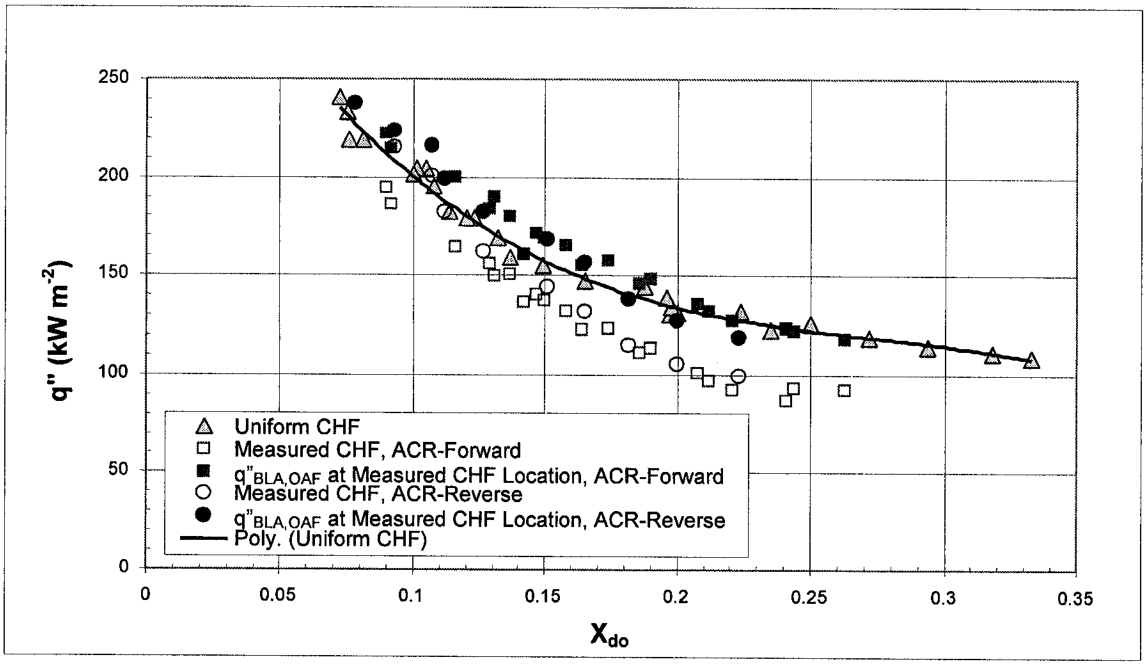

Figure 6.13a Comparison between the Local CHF and the Boiling Length Average Heat Flux with the Boiling Length Starting Point at OAF at the Measured CHF Location, P=2022 kPa, G=3552 kg m^{-2} s^{-1}, X_{OAF}=0.02, TS No. 1.

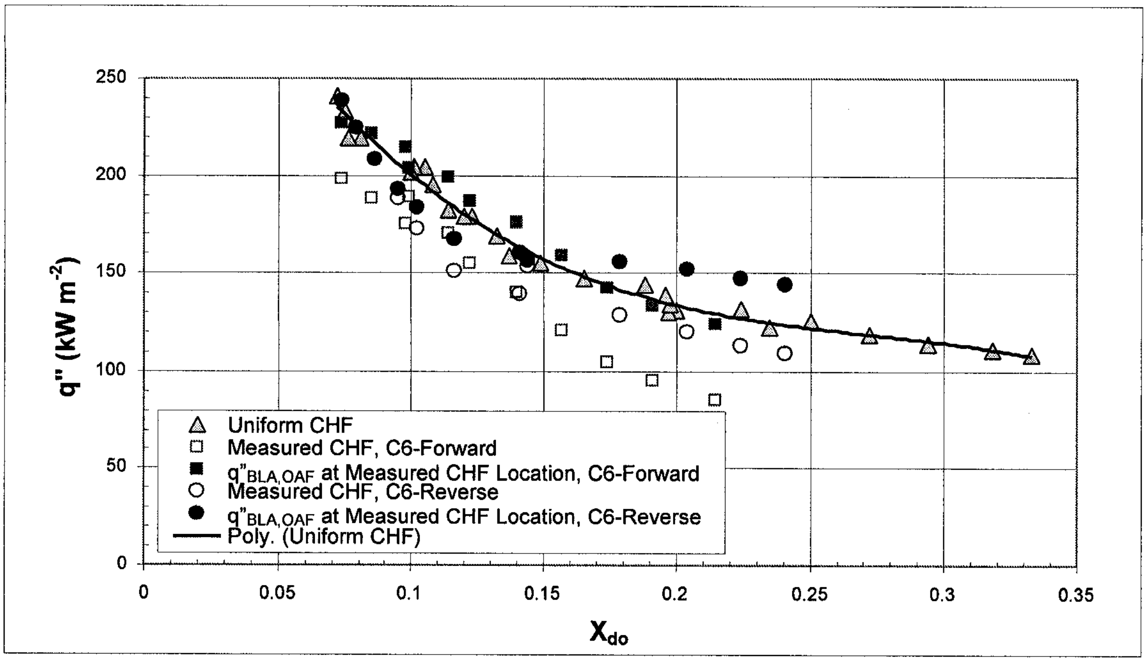

Figure 6.13b Comparison between the Local CHF and the Boiling Length Average Heat Flux with the Boiling Length Starting Point at OAF at the Measured CHF Location, P=2022 kPa, G=3552 kg m^{-2} s^{-1}, X_{OAF}=0.02, TS No. 2.

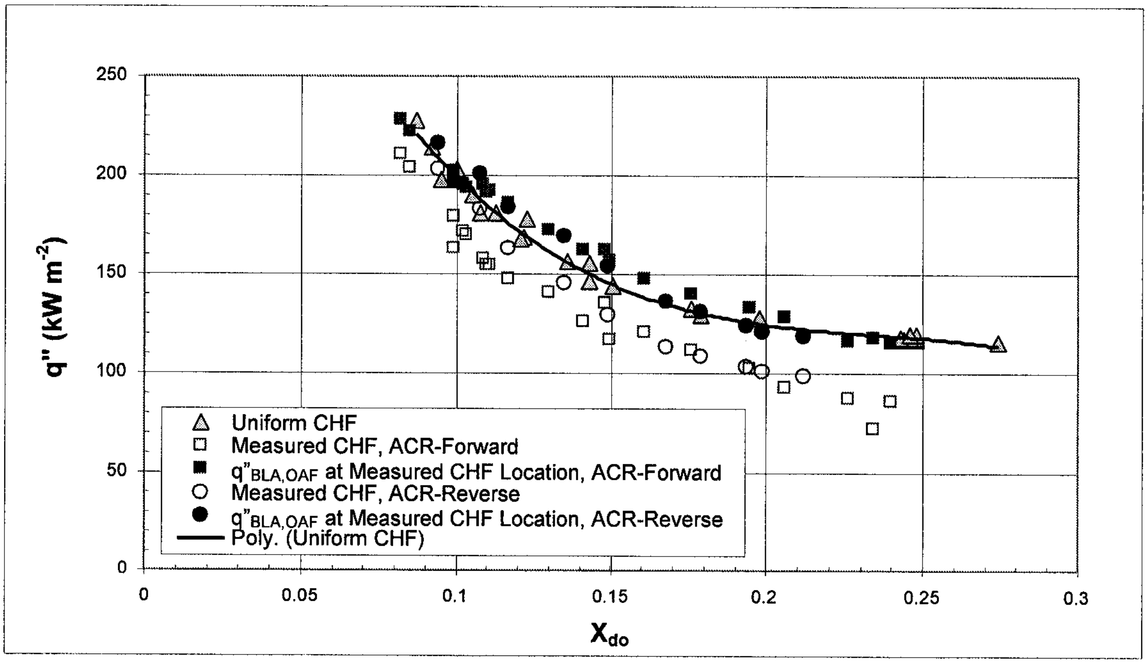

Figure 6.14a Comparison between the Local CHF and the Boiling Length Average Heat Flux with the Boiling Length Starting Point at OAF at the Measured CHF Location, P=1662 kPa, G=3533 kg m^{-2} s^{-1}, X_{OAF}=0.02, TS No. 1.

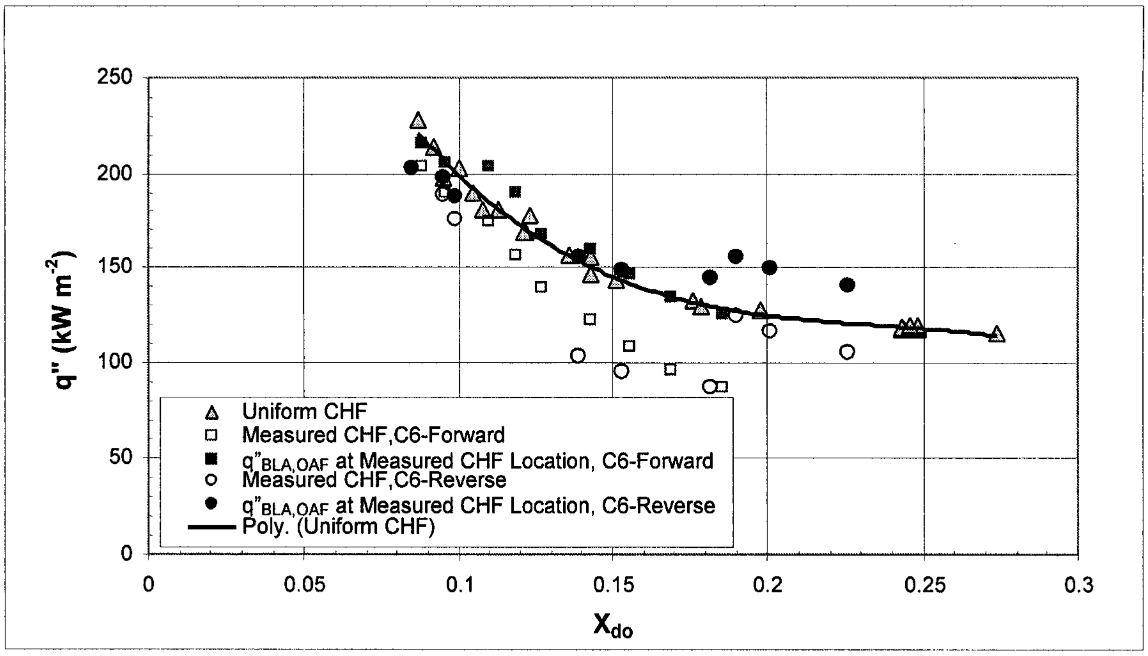

Figure 6.14b Comparison between the Local CHF and the Boiling Length Average Heat Flux with the Boiling Length Starting Point at OAF at the Measured CHF Location, P=1662 kPa, G=3533 kg m^{-2} s^{-1}, X_{OAF}=0.02, TS No. 2.

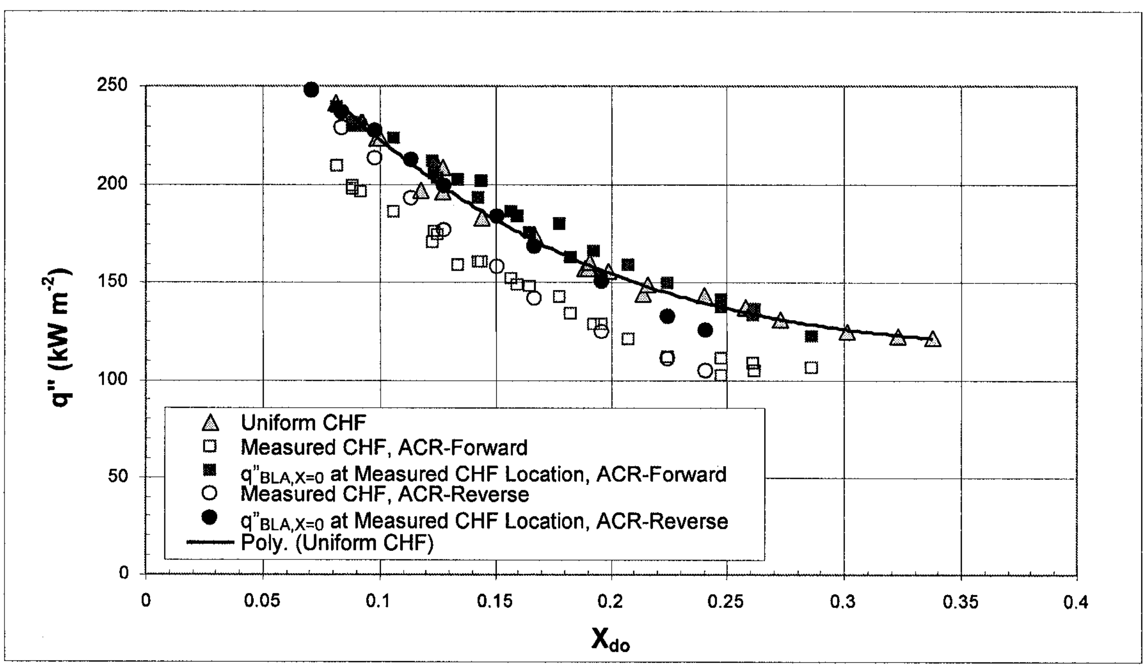

Figure 6.15a Comparison between the Local CHF and the Boiling Length Average Heat Flux with the Boiling Length Starting Point at X=0 at the Measured CHF Location, P=2389 kPa, G=3575 kg m^{-2} s^{-1}, TS No. 1.

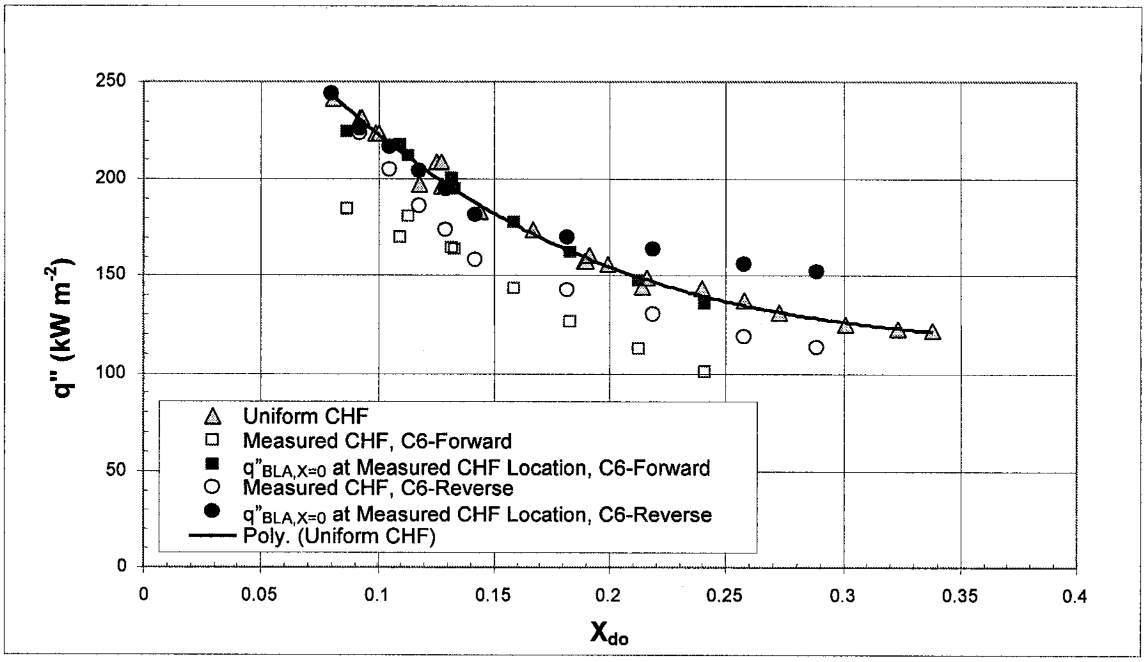

Figure 6.15b Comparison between the Local CHF and the Boiling Length Average Heat Flux with the Boiling Length Starting Point at X=0 at the Measured CHF Location, P=2389 kPa, G=3575 kg m^{-2} s^{-1}, TS No. 2.

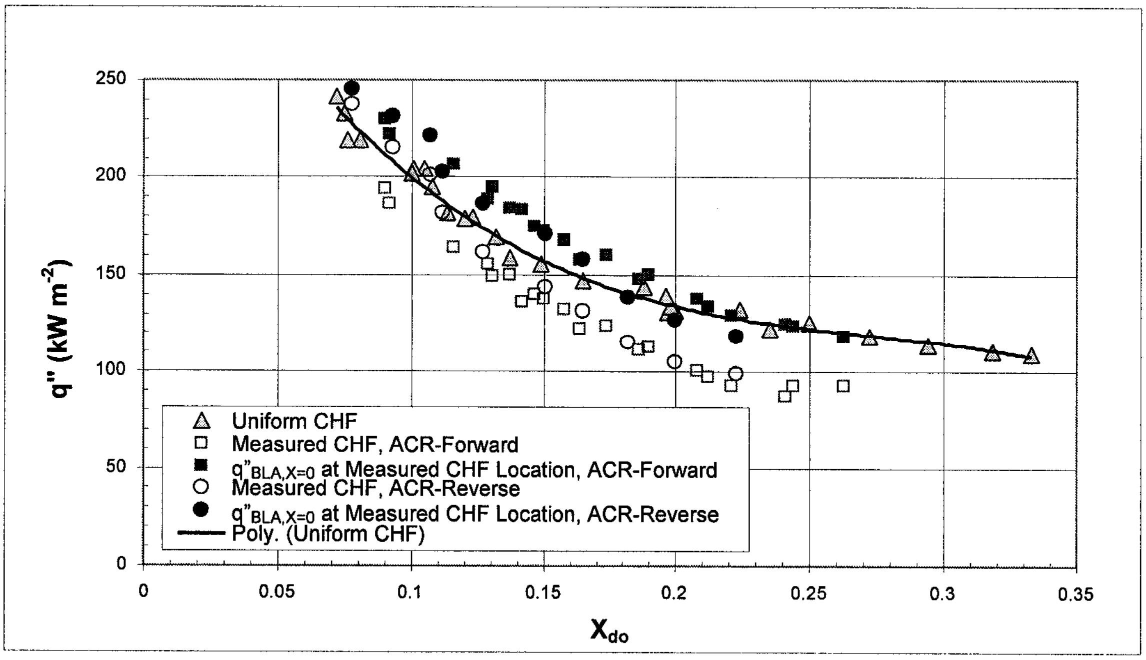

Figure 6.16a Comparison between the Local CHF and the Boiling Length Average Heat Flux with the Boiling Length Starting Point at X=0 at the Measured CHF Location, P=2022 kPa, G=3552 kg m^{-2} s^{-1}, TS No. 1.

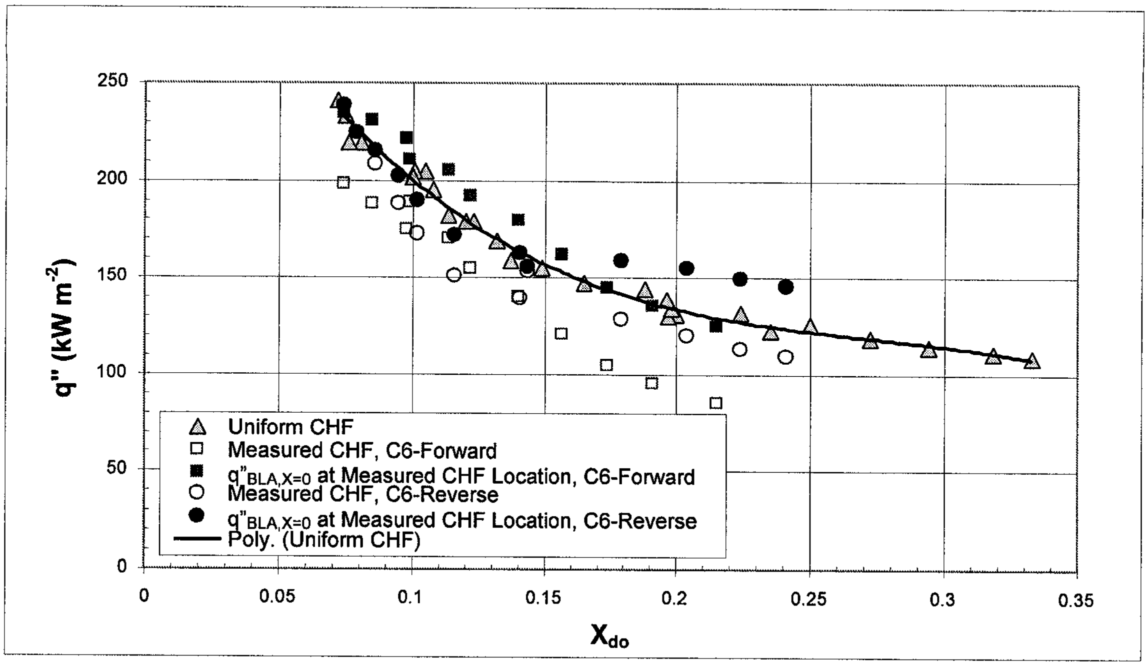

Figure 6.16b Comparison between the Local CHF and the Boiling Length Average Heat Flux with the Boiling Length Starting Point at X=0 at the Measured CHF Location, P=2022 kPa, G=3552 kg m^{-2} s^{-1}, TS No. 2.

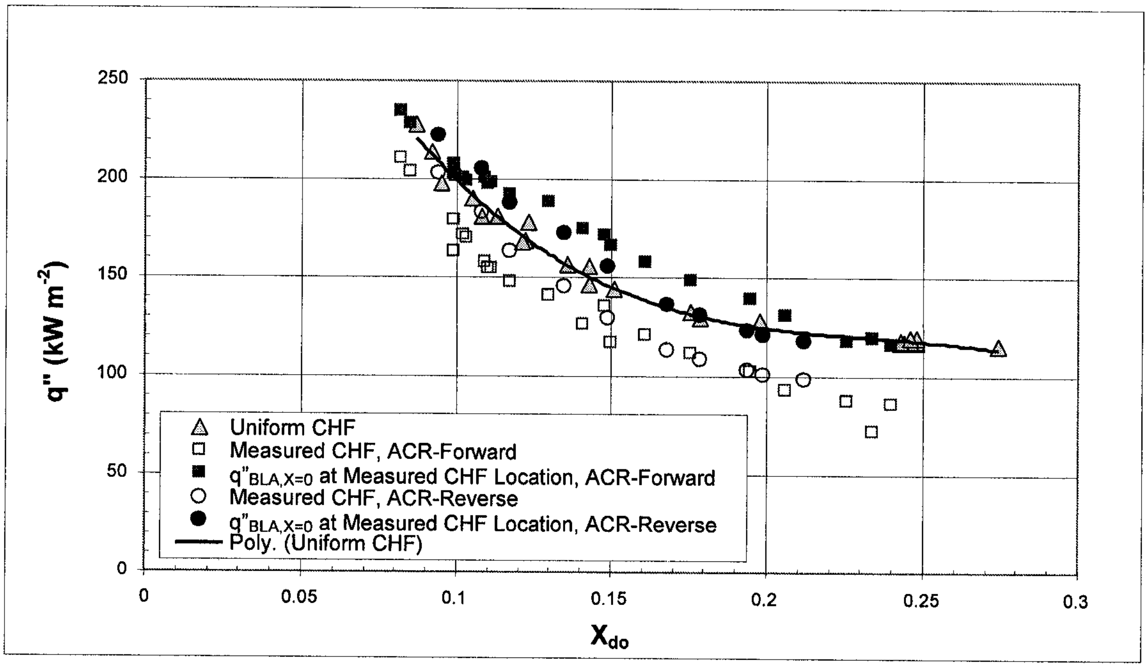

Figure 6.17a Comparison between the Local CHF and the Boiling Length Average Heat Flux with the Boiling Length Starting Point at X=0 at the Measured CHF Location, P=1662 kPa, G=3533 kg m^{-2} s^{-1}, TS No. 1.

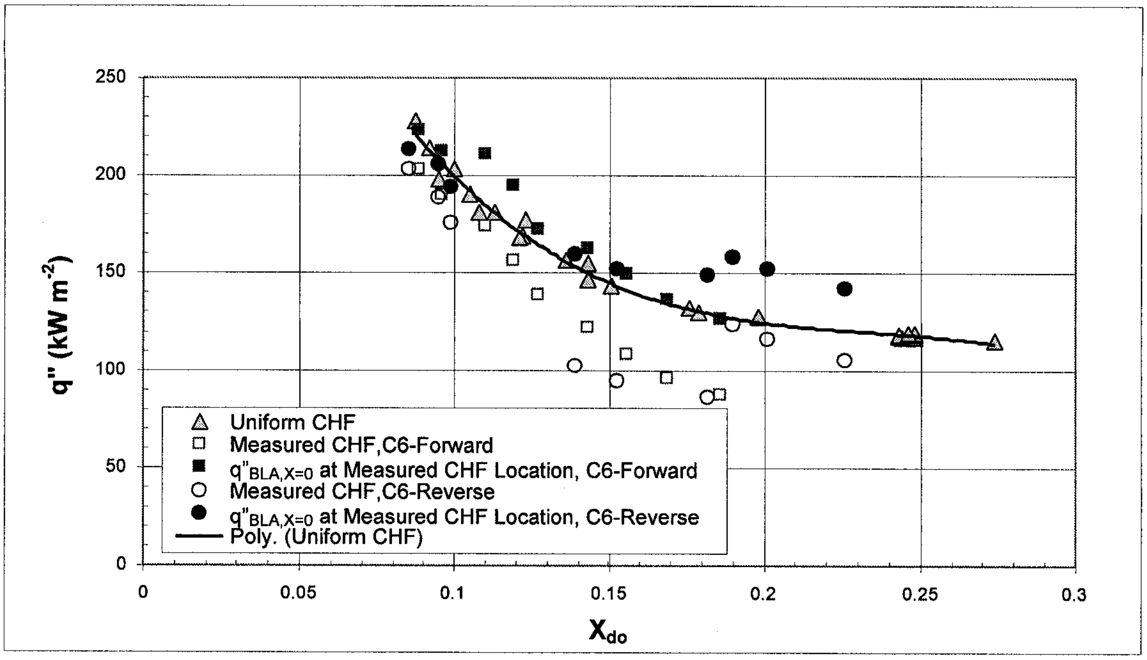

Figure 6.17b Comparison between the Local CHF and the Boiling Length Average Heat Flux with the Boiling Length Starting Point at X=0 at the Measured CHF Location, P=1662 kPa, G=3533 kg m^{-2} s^{-1}, TS No. 2.

to annular flow. Using the homogeneous model, the void fraction can be obtained by

$$\alpha = \frac{X}{X + \frac{\rho_g}{\rho_f}(1 - X)}. \tag{6.13}$$

The calculated void fraction value at the onset of annular flow (from Eq. (2.6)) varies from 0.1 to 0.24, depending on the pressure and the mass flux. It seems that these values are quite small. In order to further investigate the void fraction effect on the prediction accuracy, the sites with different void fraction values were set as the boiling length starting point. The prediction results are illustrated in Table 6.4. It was found that the prediction accuracy for critical power is not quite sensitive to the void fraction. The value of void fraction, $\alpha = 0.3$, which is higher than those at OAF locations, gives the lowest prediction errors: an average error of 0.001 and an RMS error of 0.025. These are marginally lower than those obtained by BLA_{OAF} approach (average error = -0.008, RMS error = 0.026). This observation suggests that the local quality at OAF location obtained by Eq. (2.6) is a little lower than the optimum quality for the boiling length starting point which would give the lowest RMS error. Subsequently, the optimum quality, which provides an average error of -0.001 and an RMS error of 0.024, was found by trial and error (see Table 6.5) as

$$X_{opt} = X_{OAF} + 0.02 \tag{6.14}$$

The improved BLA_{OAF} approach, i.e., the one using X_{opt} as the boiling length starting point instead of X_{OAF} gives the best prediction accuracy. However the improvement is marginal; hence the BLA approach with the boiling length starting point at the onset of annular flow is still recommended for the CHF prediction for tubes with R-134a coolant and non-uniform AFDs.

Table 6.4 Prediction Errors for Critical Power by BLA Approach with Boiling Length Starting Point at Different Void Fraction (Based on All 481 HFC-134a Data Points)

Method		Average Error	RMS Error
BLA Approach with Boiling Length Starting Point at	$\alpha = 0.10$	-0.011	0.028
	$\alpha = 0.15$	-0.008	0.027
	$\alpha = 0.20$	-0.006	0.026
	$\alpha = 0.25$	-0.003	0.025
	$\alpha = 0.30$	0.001	0.025
	$\alpha = 0.35$	0.006	0.026
	$\alpha = 0.40$	0.011	0.028
	$\alpha = 0.45$	0.017	0.032

Table 6.5 Prediction Errors for Critical Power by BLA Approach with Boiling Length Starting Point at $X = X_{OAF} + \Delta X$ (Based on All 481 HFC-134a Data Points)

Method		Average Error	RMS Error
BLA Approach with Boiling Length Starting Point at $X = X_{OAF} + \Delta X$	$\Delta X = 0.01$	-0.005	0.025
	$\Delta X = 0.02$	-0.001	0.024
	$\Delta X = 0.03$	0.003	0.024
	$\Delta X = 0.04$	0.007	0.025
	$\Delta X = 0.05$	0.011	0.026

6.3 Validation of the Optimum AFD Prediction Method Using Water Data

6.3.1 Water Data

The optimum method is based only on the HFC-134a experimental data; hence, it is necessary to verify the validity of this method using relevant water data. Water data is available from a number of sources, of which Becker's data is considered to be more reliable, and therefore selected in this study. Compared to other non-uniform AFD data obtained in water, those reported by Becker et al. (1992) are more recent and obtained from a very reliable source (the KTH laboratory in Stockholm is one of the best in the world). Also Becker's study covered many AFD profiles, and was obtained over a wide range of flow conditions (P, G, X_{do}).

Becker et al. (1992) reported the CHF conditions obtained as part of a PDO experiment. To use these data for CHF analysis, the heated length, $L_{h,CHF}$, was set as the distance between the tube entrance and the measured CHF location (i.e. the section in film boiling is removed from the test section length). The total power applied to $L_{h,CHF}$ and the AFD profile were thus modified accordingly.

Becker's non-uniform data covers the following range of variables:

Inner diameter	$D_i = 0.015$ m
Heated length	$L_{h,CHF} = 1.5 - 6.7$ m
No. of heat flux distributions	$N = 5$
Pressure	$P = 1 - 16$ MPa
Mass flux	$G = 500 - 3000$ kg m^{-2} s^{-1}
Inlet subcooling	$\Delta T_{in} = 10$ °C
Heat flux	$q'' = 90 - 3060$ kW m^{-2}

The AFD profiles studied by Becker et al. (1992) are listed in Table 6.6 and illustrated in Figure 6.18.

The uniform CHF data reported by Becker et al. (1983) was obtained using uniformly heated 7 meters long round tubes with inner diameters of 0.01, 0.0149 and 0.0247 m, a pressure range of 3 to 20 MPa, a mass flux range of 500 to 3000 kg m^{-2} s^{-1} and surface heat fluxes between 100 and 1250 kW m^{-2}.

Table 6.6 AFD Profiles Studied by Becker et al. (1992)

	Shape	Peaking factor ($k = q''_{max} / q''_{avg}$)	q''_{max} / q''_{min}
1	Inlet peak	1.60	3.64
2	Middle peak	1.60	3.64
3	Outlet peak	1.60	3.64
4	Inlet narrow peak	2.04	3.78
5	Middle narrow peak	1.97	3.68

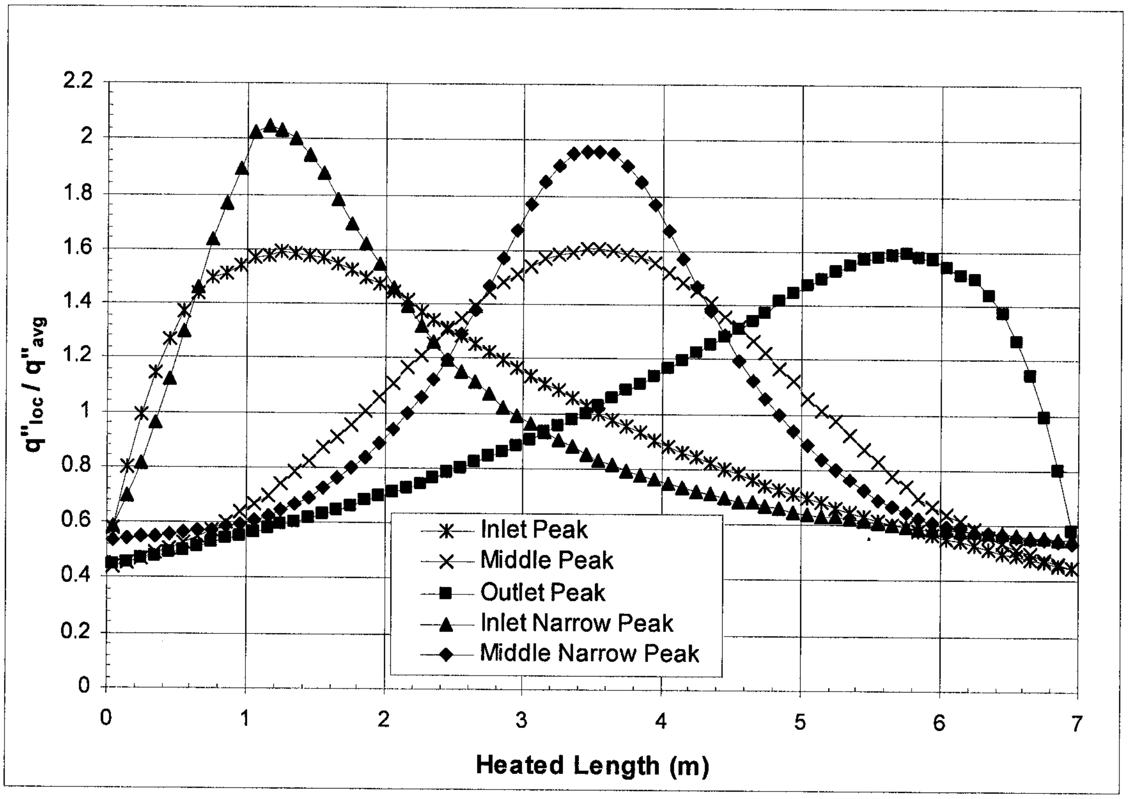

Figure 6.18 AFD Profiles Studied by Becker et al. (1992).

The water data with low pressure (less than 5 MPa) and low mass flux (less than 1500 kg m^{-2} s^{-1}) were well outside the range of our water-equivalent HFC-134a data and were therefore not used in this comparison. The uniform water data with the inner diameter other than 0.015 m was also not used to avoid potential errors caused by diameter correction. The flow conditions of Becker's uniform data are shown in Figure 6.19. Since the uniform CHF data does not cover the whole quality range of that of the non-uniform data, the Groeneveld CHF look-up table (1996) was used as the reference for the CHF prediction for non-uniform AFD. The calculated average error and RMS error for the experimental uniform CHF data based on local condition using the look-up table are 5.41% and 27.77%, respectively. In order to eliminate the discrepancy, the following correction factor was derived by curve fitting, and the average error and RMS error are reduced to -1.77% and 13.13%, respectively, by applying this factor to the look-up table:

$$F^{-1} = 2.97 - 1.973(\frac{P}{10000}) - 0.343(\frac{G}{1000}) + 0.647(\frac{P}{10000})^2 + 0.038(\frac{G}{1000})^2 \quad (6.15)$$

This correction factor may only be applied to the range of flow parameters for which it was developed. Despite this limitation 180 uniform CHF data and 281 non-uniform data could be employed from Becker's data base.

6.3.2 Prediction Results and Discussion

All prediction methods described in Section 6.1 were evaluated by comparing with experimental data in water. The prediction errors for the critical power by each of the methods are shown in Table 6.7. The prediction results presented as a ratio of the predicted to measured critical power (CHFPR) and a comparison of the predicted to measured CHF location for all data by the methods, which give relatively lower prediction errors, i.e., the F-factor approach, the BLA approach with boiling length starting point at the onset of significant void fraction, X=0 and the onset of annular flow, are shown in Figures 6.20 to 6.23. It is again found that the BLA approach with boiling length starting point at the onset of annular flow results in the best critical power prediction.

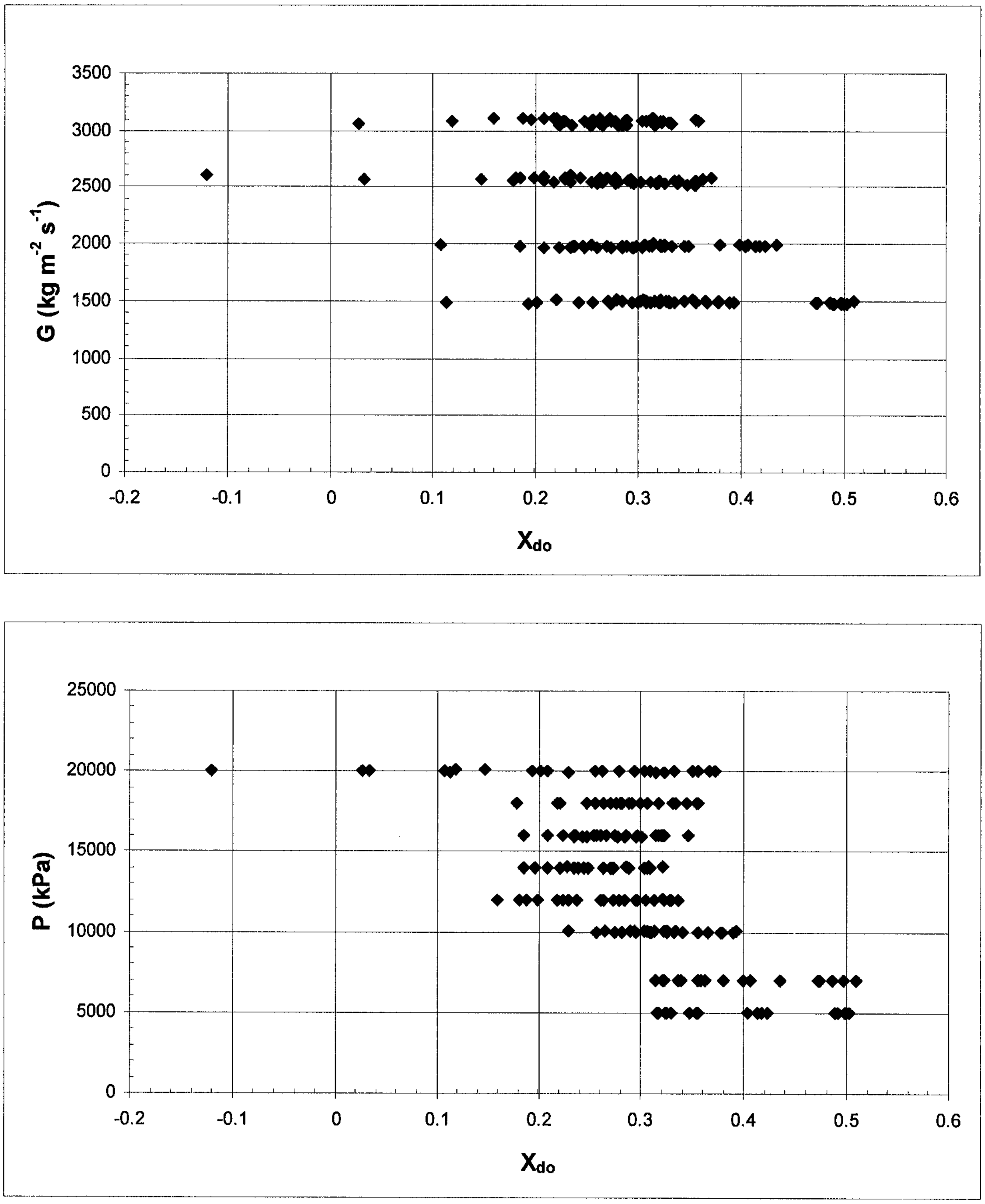

Figure 6.19 Flow Conditions of Becker's Uniform Data.

Table 6.7 Prediction Errors for Critical Power by Each Method (Based on All 281 Water Data Points)

Method		Average Error	RMS Error
Overall Power Approach		0.081	0.131
Local Conditions Approach		-0.002	0.090
F-factor Approach		-0.003	0.070
BLA Approach with Boiling Length Starting Point at	Tube Inlet	0.081	0.131
	ONB*	0.081	0.131
	OSV*	0.077	0.129
	X=0	0.026	0.080
	OAF	0.004	0.067

* In case the calculated local quality at the boiling length starting point is lower than that at the tube inlet, the tube inlet is used as the boiling length starting point.

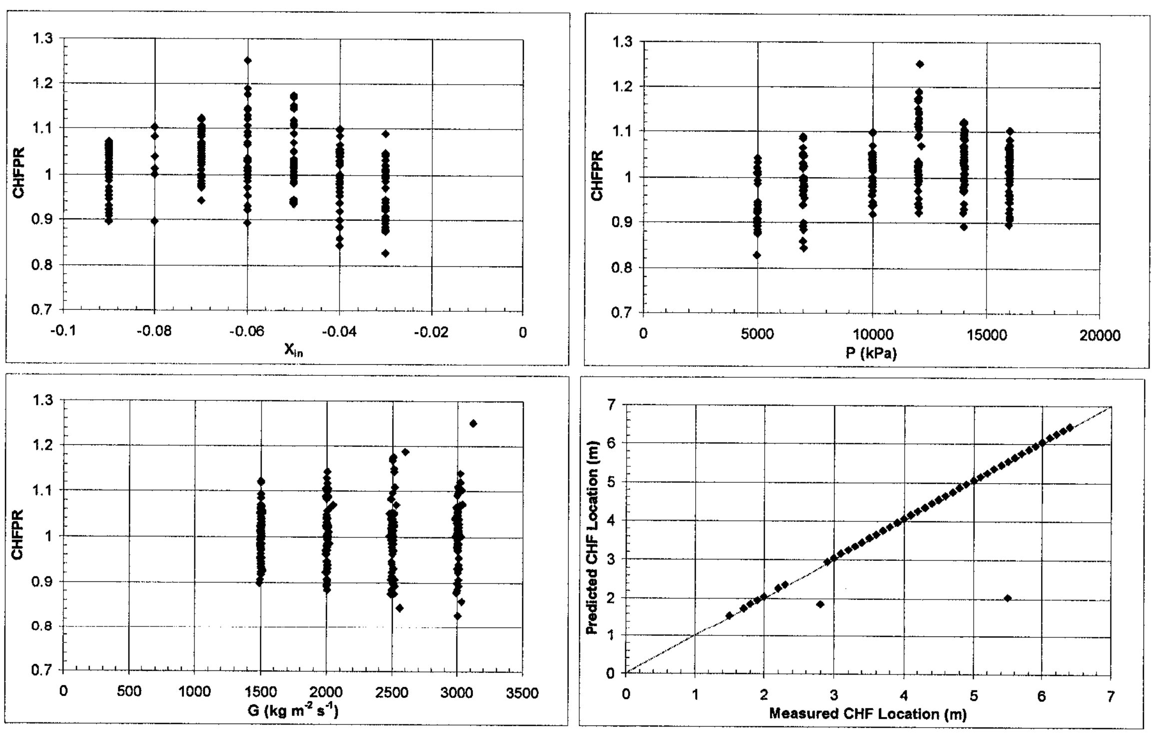

Figure 6.20 CHF Prediction Results by F-factor Approach (Based on All Water Data Points).

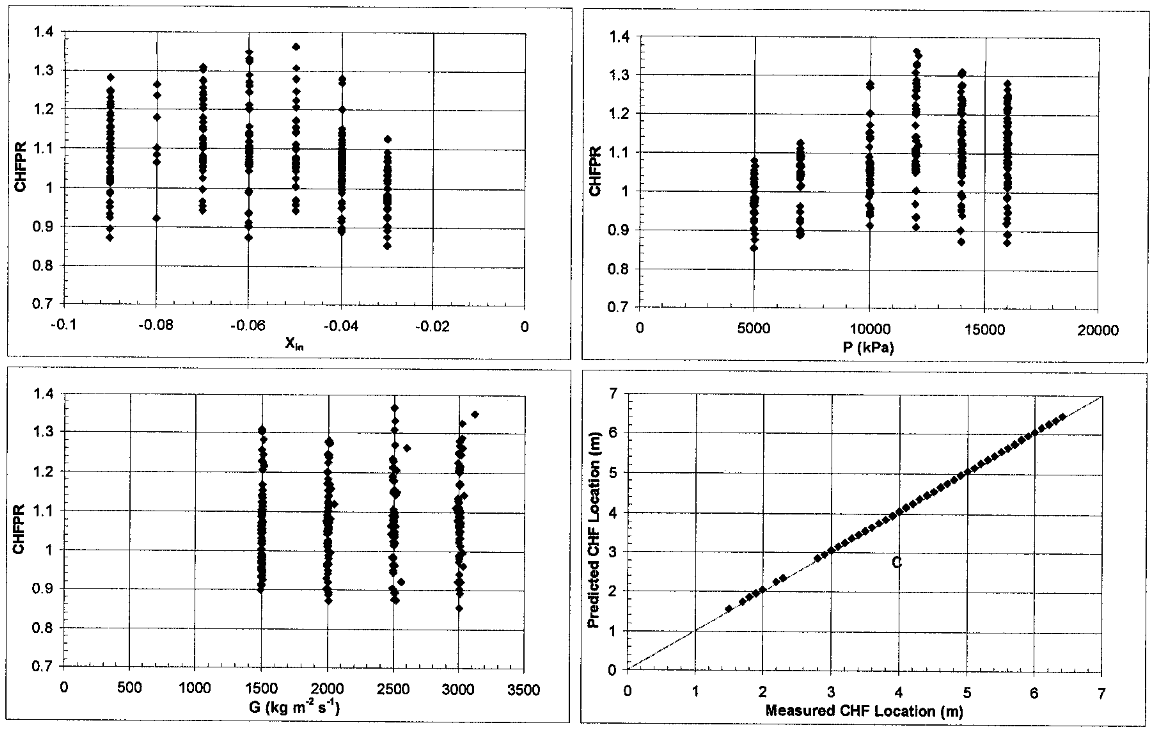

Figure 6.21 CHF Prediction Results by BLA_{OSV} Approach (Based on All Water Data Points).

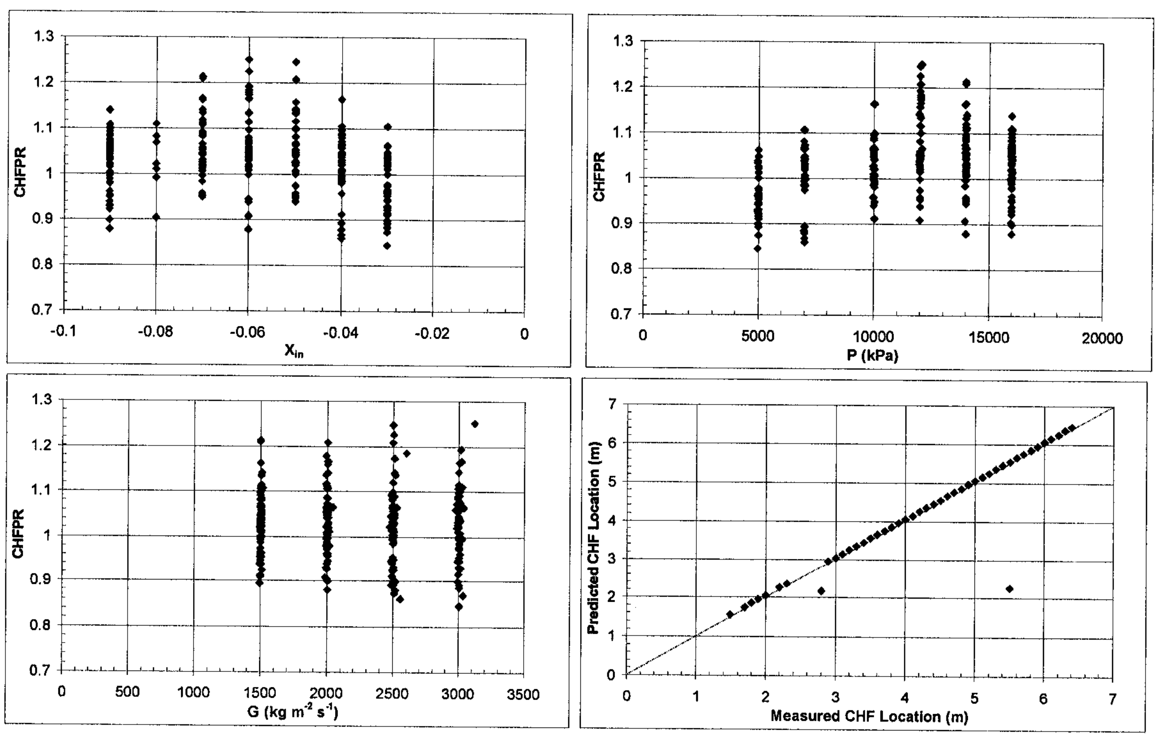

Figure 6.22 CHF Prediction Results by $BLA_{X=0}$ Approach (Based on All Water Data Points).

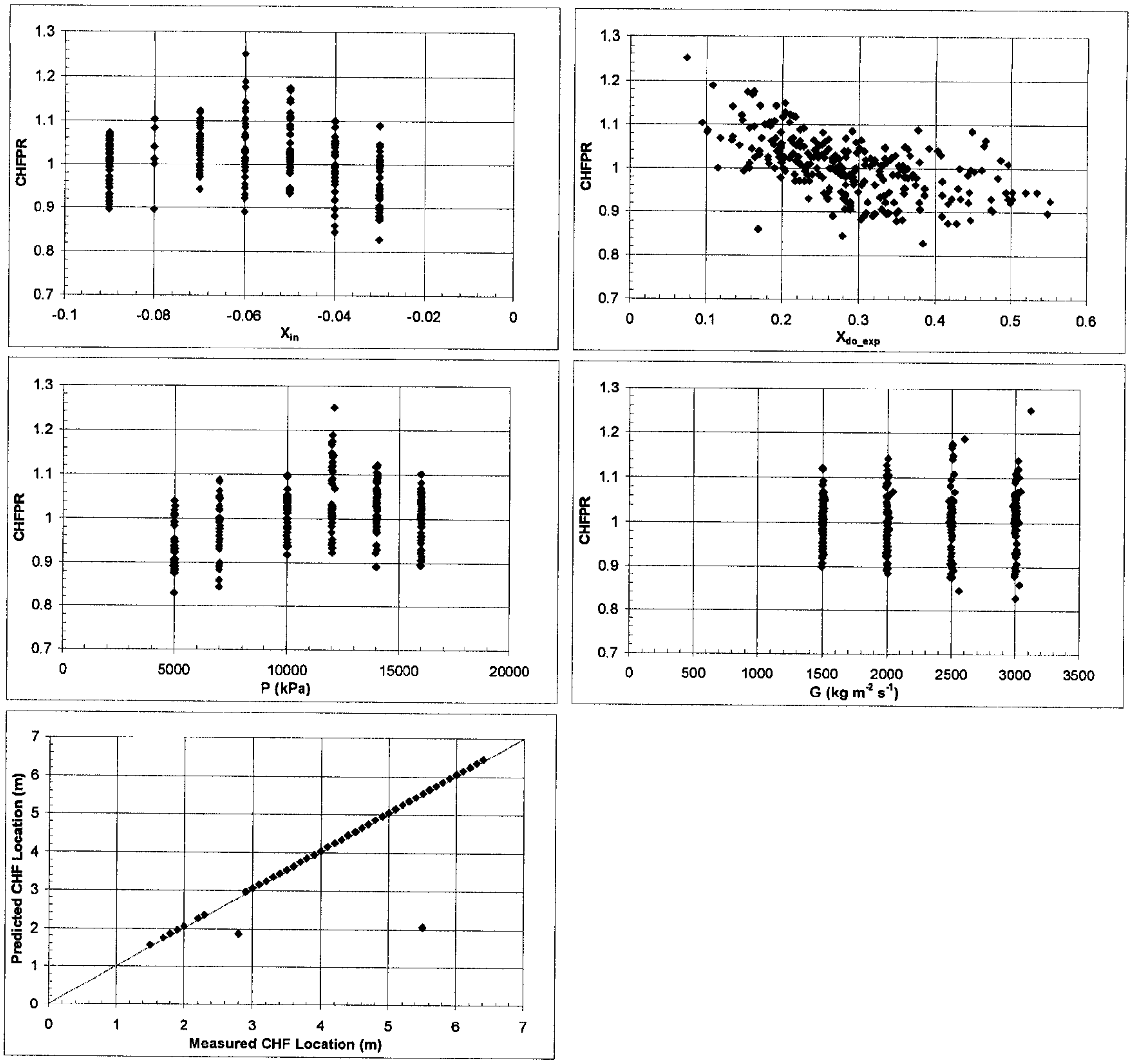

Figure 6.23 CHF Prediction Results by BLA_{OAF} Approach (Based on All Water Data Points).

In order to understand the non-uniform AFD shape effect on the prediction accuracy, the prediction errors for the critical power for each AFD profile by the BLA approach with boiling length starting point at the onset of annular flow are presented separately in Table 6.8. Plots of the prediction results by this method were also generated for each AFD profile separately, which are shown in Figures 6.24a to 6.24e. Generally, this method provides very good predictions for both critical power and CHF location for all the non-uniform AFD shapes. Looking closely, the outlet peak profile corresponds to the best prediction accuracy while the inlet peak profile results in the largest prediction error. The prediction accuracy for the middle peak profile is in between of the outlet peak and the inlet peak profiles. On the other hand, this method gives worse prediction accuracy for the inlet narrow peak profile and the middle narrow peak profile, when compared to that for the inlet peak profile and the middle peak profile, respectively.

Note that the prediction accuracy strongly depends on the accuracy of the relationship of CHF vs. X_{do} for uniform AFD, and this relationship in water was not obtained directly from the experiments using the tube of the same geometry as that of non-uniform AFD, but achieved from corrected look-up table by a limited amount of uniform CHF data. The uniform CHF data at higher dryout quality region is more numerous than the lower dryout quality data; therefore, the uniform AFD CHF values at higher dryout qualities from the corrected CHF look-up table are probably more accurate than the CHF values at lower dryout qualities.

Consider again the non-uniform AFD shapes. The non-uniform CHF data for the outlet peak profile basically has a longer length from the tube inlet to the CHF location than that for the inlet peak profile, and that for the middle peak profile falls in between. Note that all of the tests were performed with the same inlet subcooling (ΔT_{in} = 10 °C), thus, the CHF data with a longer length from the tube inlet to the CHF location will have a higher dryout quality and lower CHF value, i.e., the non-uniform CHF data for outlet peak profile basically has higher dryout quality and lower CHF value than those for inlet peak. This is the main reason that the prediction accuracy for the outlet peak profile is better than that for the inlet peak profile. That the inlet narrow peak profile and the middle narrow peak profile obtained worse prediction accuracy than that for the inlet peak

Table 6.8 Prediction Errors for Critical Power by BLA_{OAF} Approach for Each AFD (Based on Water Data Points)

Method		Average Error	RMS Error
BLA Approach with Boiling Length Starting Point at OAF	All Data (281)*	0.004	0.067
	Inlet Peak (24)	-0.021	0.076
	Middle Peak (80)	-0.004	0.67
	Outlet Peak (78)	0.019	0.034
	Inlet Narrow Peak (38)	-0.014	0.093
	Middle Narrow Peak (61)	0.017	0.076

* Value in ( ) is the number of data points.

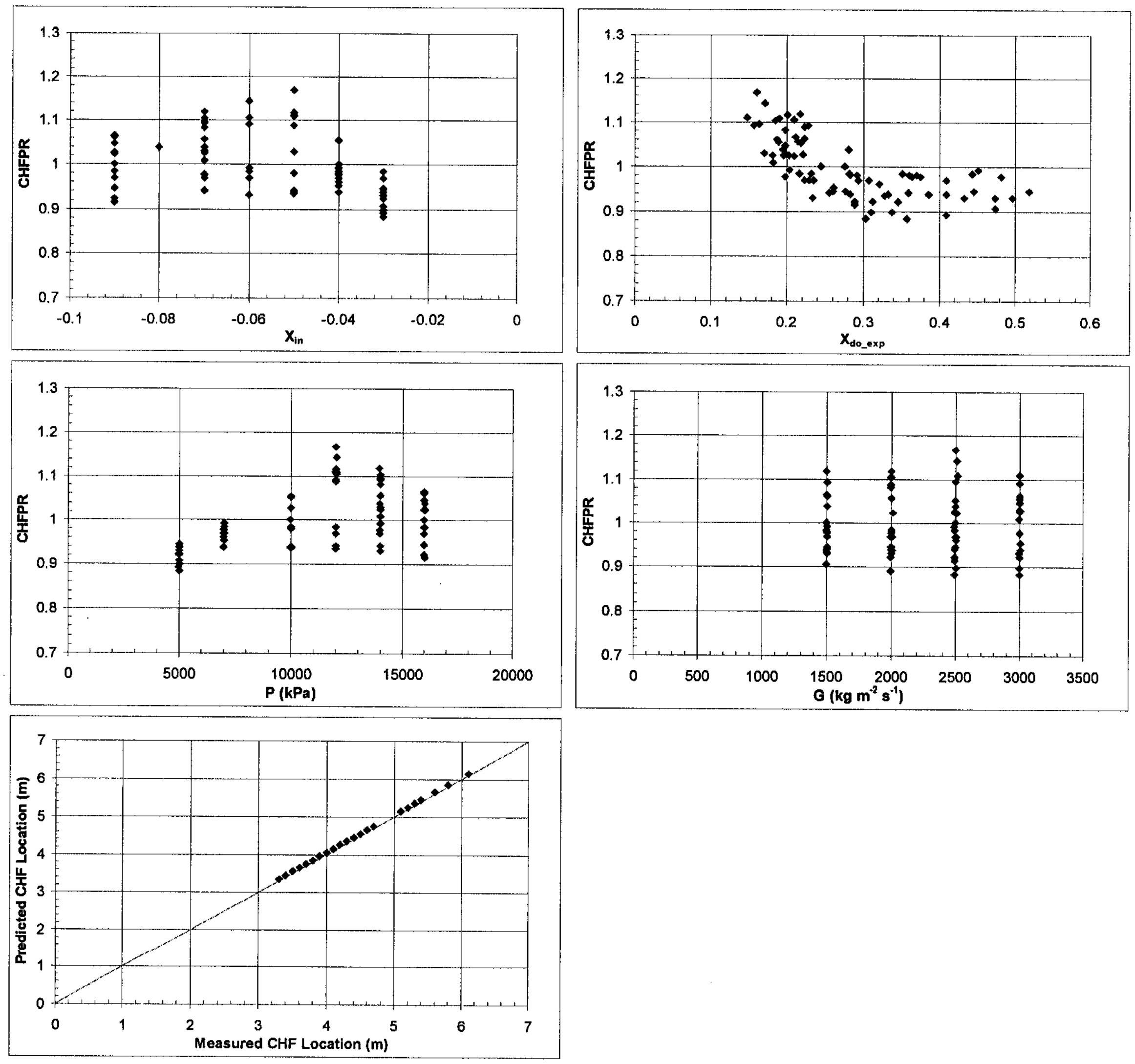

Figure 6.24a CHF Prediction Results by BLA_{OAF} Approach for Middle Peak AFD.

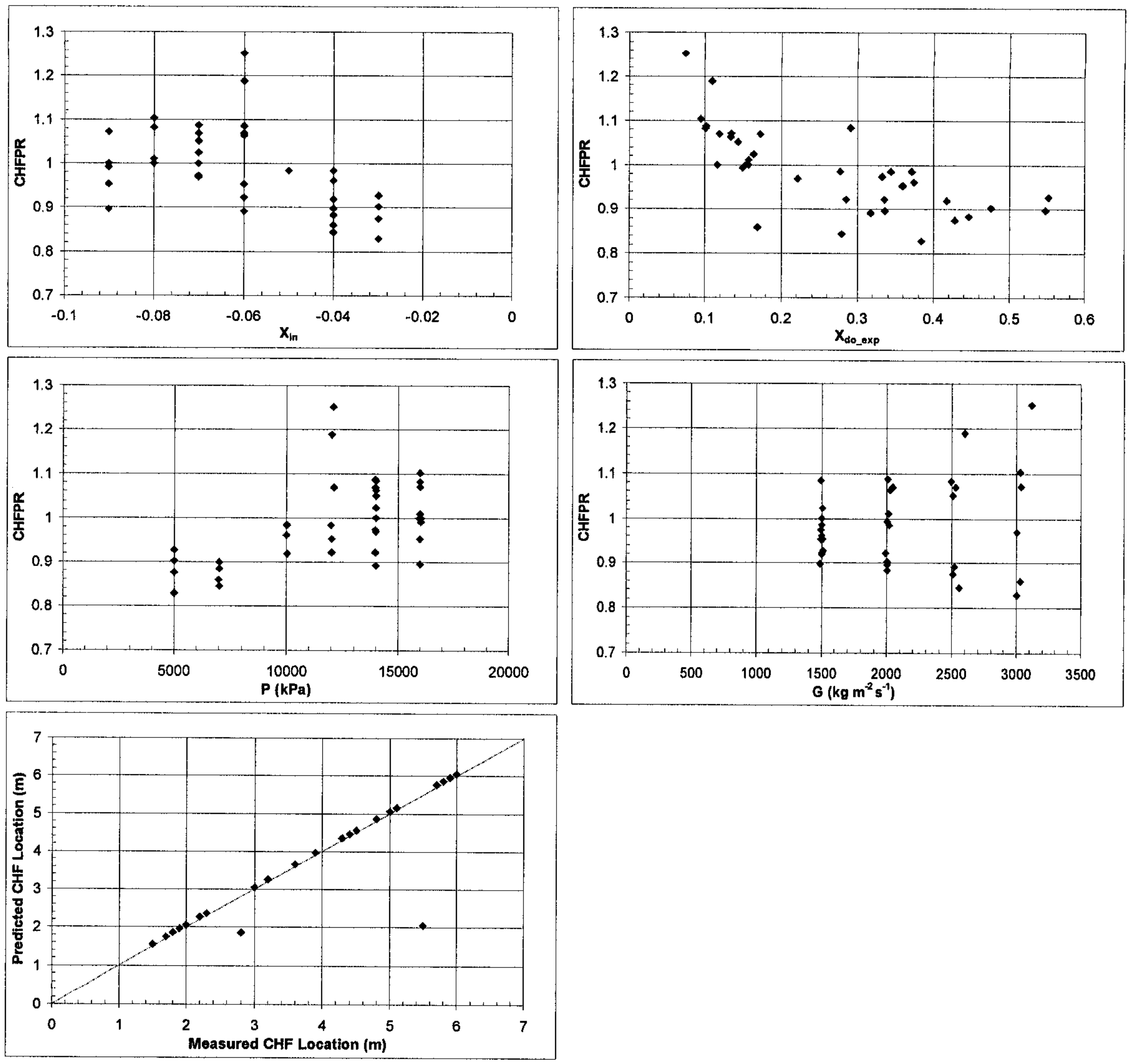

Figure 6.24b CHF Prediction Results by BLA_{OAF} Approach for Inlet Narrow Peak AFD.

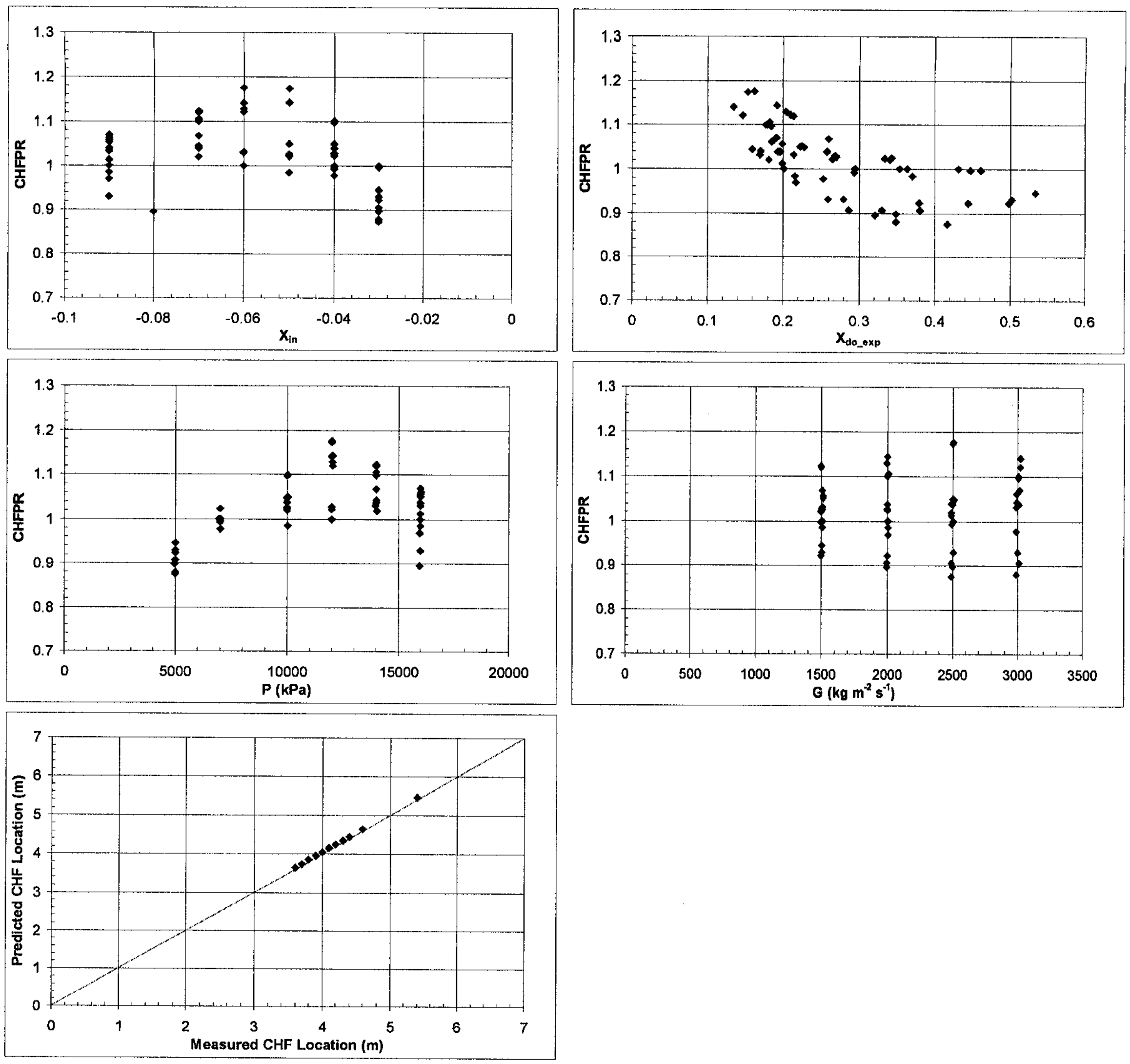

Figure 6.24c CHF Prediction Results by BLA_{OAF} Approach for Middle Narrow Peak AFD.

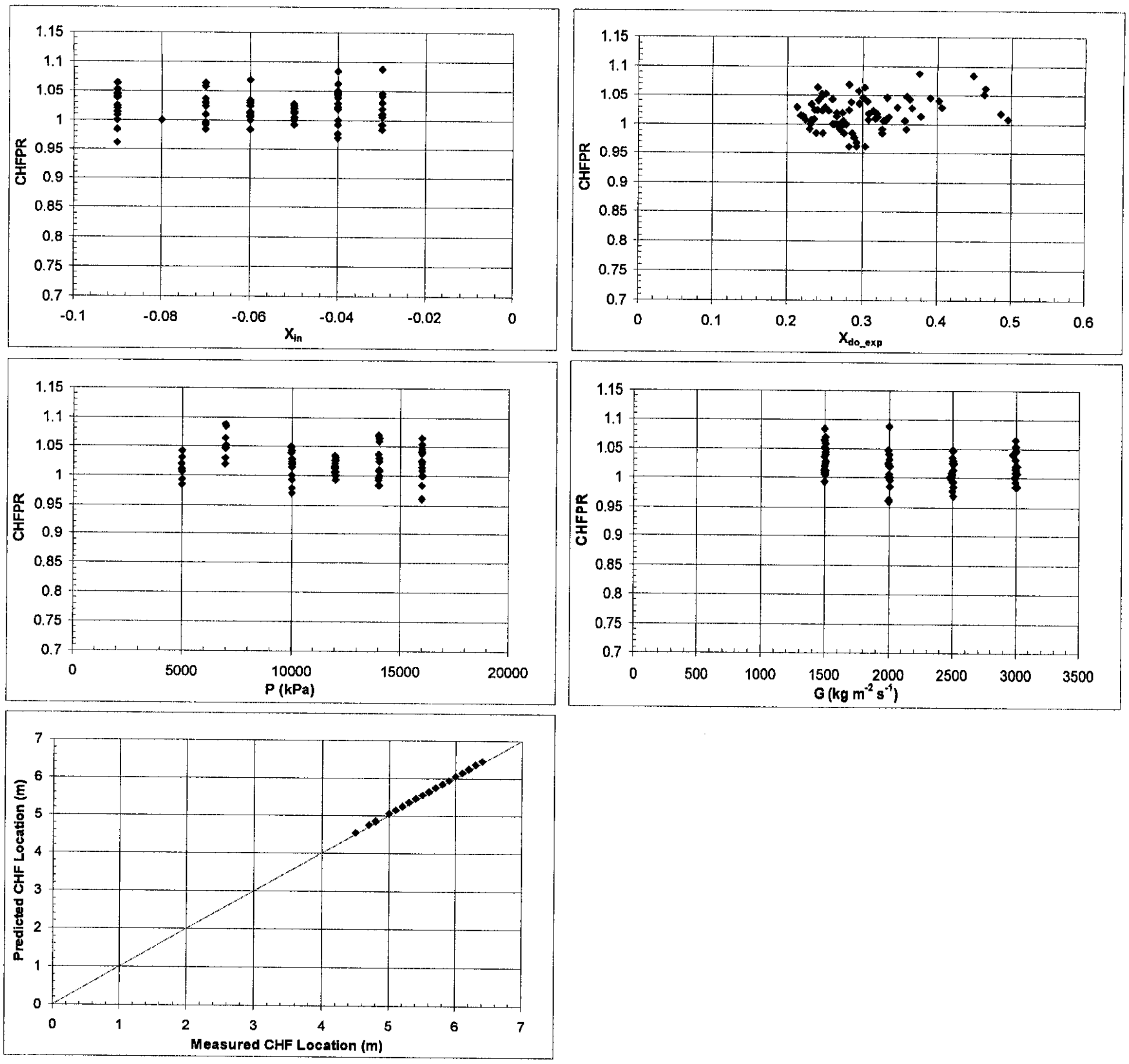

Figure 6.24d CHF Prediction Results by BLA_{OAF} Approach for Outlet Peak AFD.

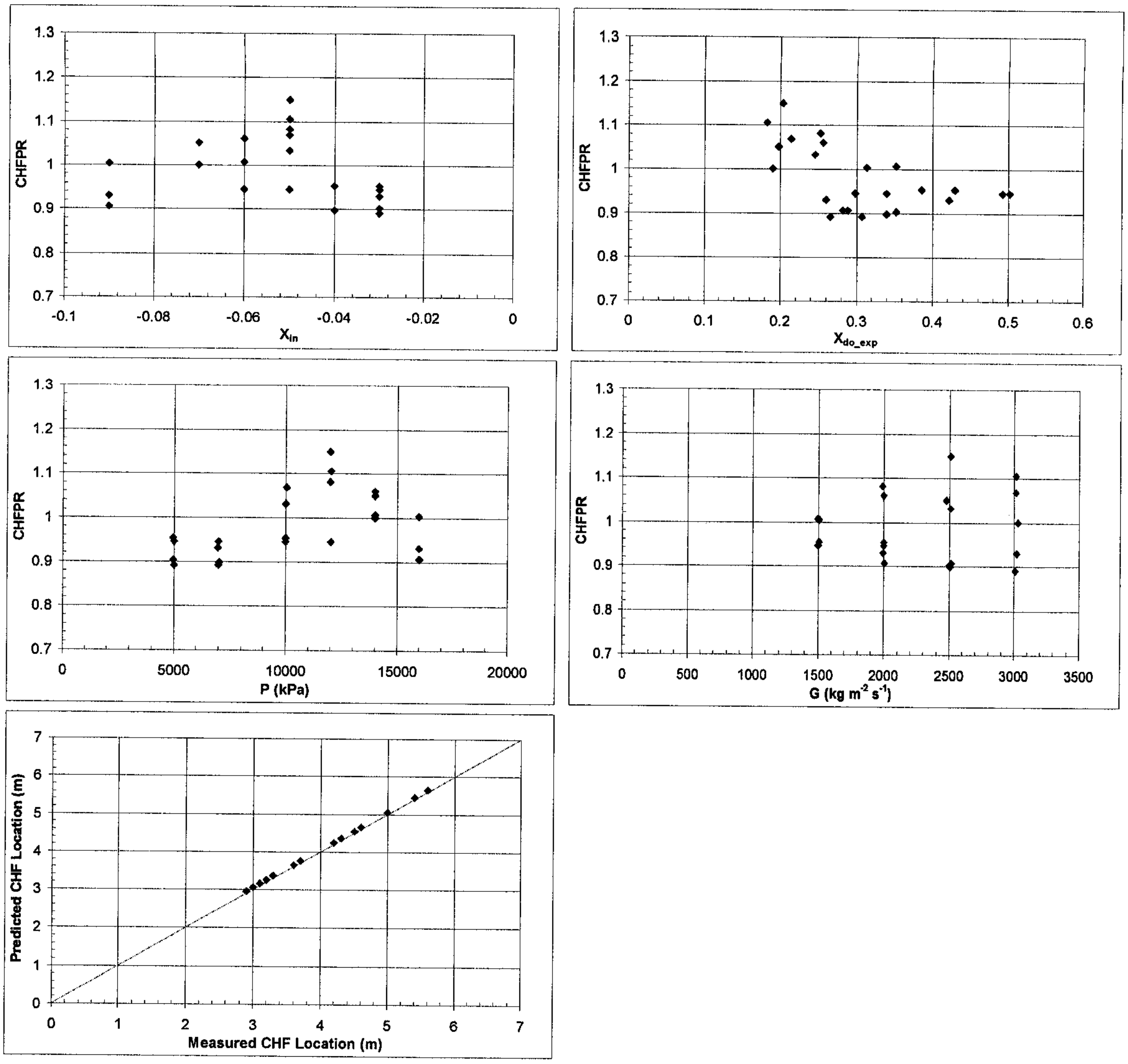

Figure 6.24e CHF Prediction Results by BLA_{OAF} Approach for Inlet Peak AFD.

profile and the middle peak profile, respectively, may be explained in the same way, i.e., the non-uniform CHF data for the narrow peak profile basically has lower dryout quality and higher CHF value than those for the normal peak.

Figures 6.24a to 6.24e also show that the CHF locations predicted by BLA_{OAF} approach are in good agreement with those measured. For a non-uniform AFD, CHF could occur at the tube exit as well as upstream of the tube exit depending on the flow conditions and particularly the AFD profile.

It is observed from Becker's AFD profiles (Figure 6.18) that the slope of the q''_{loc}/q''_{avg} vs. z curve near the potential CHF location basically increases along the flow direction, except that of the outlet peak AFD. Those of the TS No. 1 and TS No. 2 AFD profiles (Figures 4.2 and 4.3) have the opposite trend. This observation suggests that the point of tangency between the shortened AFD profile and the CHF curve (i.e. the CHF location) is more likely to occur at the tube exit for Becker's AFD profiles, compared to the TS No. 1 and TS No. 2 AFD profiles. With respect to Becker's outlet peak AFD profile, since for CHF analysis the tube was cut off at the location near the heat flux peak site, the CHF is also more likely to occur at the end of $L_{h,CHF}$.

The prediction results show that almost all of the predicted CHF locations are situated at the end of $L_{h,CHF}$, which agrees with the above argument.

Similar to that performed for HFC-134a data, here the effect of void fraction on the prediction accuracy for BLA approach was also investigated. The prediction results for critical power by BLA approach with boiling length starting point at different void fraction are shown in Table 6.9, while those by BLA approach with boiling length starting point at $X = X_{OAF} + \Delta X$ are shown in Table 6.10. Note that the calculated void fraction value at the onset of annular flow falls in the range of 0.12 to 0.55. Once again the value of void fraction, $\alpha = 0.3$, gives the lowest prediction errors, and these errors are slightly lower than those obtained by BLA_{OAF} (average error = 0.004, RMS error = 0.067). The errors provided by the optimum quality ($X_{opt} = X_{OAF} + 0.015$) are a little lower than those given by $X = X_{OAF}$ but a little higher than those given by $\alpha = 0.3$. Since the improvement in prediction accuracy is again marginal, the BLA approach with the

Table 6.9 Prediction Errors for Critical Power by BLA Approach with Boiling Length Starting Point at Different Void Fraction (Based on All 281 Water Data Points)

Method		Average Error	RMS Error
BLA Approach with Boiling Length Starting Point at	$\alpha = 0.10$	0.018	0.073
	$\alpha = 0.20$	0.009	0.067
	$\alpha = 0.30$	0.000	0.064
	$\alpha = 0.40$	-0.008	0.064
	$\alpha = 0.50$	-0.014	0.068
	$\alpha = 0.60$	-0.017	0.077

Table 6.10 Prediction Errors for Critical Power by BLA Approach with Boiling Length Starting Point at $X = X_{OAF} + \Delta X$ (Based on All 281 Water Data Points)

Method		Average Error	RMS Error
BLA Approach with Boiling Length Starting Point at $X = X_{OAF} + \Delta X$	$\Delta X = 0.005$	0.001	0.067
	$\Delta X = 0.010$	-0.002	0.066
	$\Delta X = 0.015$	-0.005	0.066
	$\Delta X = 0.020$	-0.007	0.067
	$\Delta X = 0.025$	-0.010	0.067

boiling length starting point at the onset of annular flow is again recommended for the CHF prediction for axially non-uniformly heated tubes.

In summary, the BLA approach with the boiling length starting point at the onset of annular flow is the optimum method for the CHF prediction for a tube with a non-uniform axial heat flux profile, regardless whether the working fluid is HFC-134a or water. The prediction accuracy strongly depends on the accuracy of the relationship of CHF vs. X_{do} for uniform AFD.

7. CONCLUSIONS AND FINAL REMARKS

The AFD experiments were performed using test sections with uniform, inlet peak, middle peak and outlet peak AFD profiles. The AFD effect on CHF was investigated. It was found that the AFD effect on the critical power for constant inlet conditions is generally small. However, the AFD has strong effect on the critical heat flux at high dryout qualities for constant local conditions. The CHF values for non-uniform AFDs can be up to 50% lower than those for uniform AFD depending on the pressure, mass flux and the shape of the AFD profile. The AFD effect on CHF decreases with the decrease in dryout quality.

The AFD effect on CHF with flow obstruction was also investigated (see Appendix A). The flow obstruction has a strong effect on CHF. It greatly enhances the CHF value, especially at high dryout qualities. There is no apparent AFD effect on CHF in the case where flow obstruction exists for constant local conditions. The flow obstruction greatly enhances the critical power at high inlet qualities. The enhancement decreases with an increase in inlet subcooling. The AFD effect on the critical power for the test section with flow obstruction appears to be stronger than that for the test section without flow obstruction especially at high inlet subcoolings. The AFD effect on the critical power decreases as the inlet quality increases, and disappears when the inlet quality is higher than approximately –0.4. At high inlet subcooling, the critical power for the non-uniform AFD test section with flow obstruction is higher than that for the uniform AFD test section with flow obstruction by an approximately constant value.

The CHF prediction methods for non-uniform AFD in tubes were assessed, and the optimum method was determined. The boiling length average approach with the boiling length starting point at the onset of annular flow was determined to be the optimum method for the CHF prediction for tubes with non-uniform axial heat flux profiles, regardless whether the working fluid is HFC-134a or water. This optimum method provides very good prediction for the critical power as well as for the CHF location.

7.1 AFD Effect on CHF

1. The critical power generally displays a linear relationship with inlet temperature or inlet quality except at high mass flux and very high inlet quality for uniform AFD.

2. To eliminate the effect of heated length on the critical power vs. inlet quality graphs, 2.4-m-equivalent values were used. This had the advantage of providing a much broader range of inlet temperature.

3. The effect of AFD on the critical power is small for all flow conditions and AFD profiles tested in this investigation.

4. At high inlet subcoolings, the non-uniform AFDs have the same critical power. At higher inlet qualities, the critical power for inlet peak AFD is slightly higher than that for outlet peak AFD profile (by 3 to 15%), and the critical power for middle peak AFD profile falls in between.

5. The critical power for the uniform AFD is slightly (0~5%) below that for the non-uniform AFDs at high inlet subcooling. The critical power for the uniform AFD test section approaches those for the non-uniform AFD profiles as inlet subcooling decreases and even exceeds those for the non-uniform AFDs as the inlet quality exceeds around -0.2. This phenomenon is more evident at high mass fluxes.

6. AFD has a strong effect on CHF at high dryout qualities. The CHF values for non-uniform AFDs can be up to 50% lower than that for uniform AFD depending on the pressure, mass flux and the shape of the AFD profile. The AFD effect on CHF decreases with the decrease in dryout quality. At low dryout qualities, the effect of AFD on CHF is small or non-existent. This observation implies that the local conditions hypothesis is only approximately valid at low dryout qualities. At a given dryout quality, the discrepancy of the CHF values between the uniform and non-uniform AFDs decreases as either the pressure increases or the mass flux increases.

7. The CHF location is affected by inlet subcooling and mass flux. The CHF location for the non-uniform AFDs tends to move downstream as either the inlet subcooling increases or the mass flux decreases.

7.2 CHF Prediction Methods for Non-Uniform AFD

1. Four CHF prediction methods for non-uniform AFD in tubes were assessed. These methods are the overall power approach, the local conditions approach, the F-factor approach and BLA approach. The variations of the BLA approach with different boiling length starting points were all evaluated as well.

2. The overall power approach generally under-predicts the critical power for a non-uniform AFD, especially at high inlet subcooling.

3. The local conditions approach generally over-predicts the critical power for a non-uniform AFD. At high inlet subcooling (X_{in}<-0.4), this method provides a good critical power prediction. The prediction accuracy decreases as the inlet subcooling decreases and/or the mass flux decreases.

4. F-factor approach is more accurate than the local conditions approach, but basically under-predicts the critical power, especially at high inlet subcooling. This is because the uniform CHF does not need to be corrected or the correction factor provided by the F-factor approach is stronger than that required in high inlet subcooled region. The CHF locations are reasonably predicted by this method.

5. The BLA approach with boiling length starting point at the channel inlet seriously under-predicts the critical power, and gives the largest prediction error compared with the other starting points. The prediction accuracy increases as the boiling length starting point shifts successively in the flow direction from the channel inlet to the points of the onset of nucleate boiling, the onset of significant void fraction, X=0 and the onset of annular flow.

6. The optimal method, the BLA approach with the boiling length starting point at the onset of annular flow, gives an average error of 0.9%, and an RMS error of 2.6% for the prediction of critical power for all of the 481 data points, which are much smaller than those predicted by overall power, local conditions and F-factor approaches. This method also gives a very good prediction for CHF location.

7. The measured CHF for non-uniform AFD is generally lower than the uniform CHF, especially at high qualities, while the boiling length average heat flux with the boiling length starting point at the onset of annular flow at the measured CHF location matches the uniform CHF very well in the whole dryout quality region. This is the explanation for the BLA approach with the boiling length starting point at the onset of annular flow giving an excellent CHF prediction for non-uniform AFD.

8. The optimum method, the BLA approach with the boiling length starting point at the onset of annular flow, derived from the experimental investigation using HFC-134a as working fluid, was confirmed by the experimental non-uniform AFD CHF data in water for five non-uniform AFD profiles for a wide range of flow conditions.

REFERENCES

Ahmad, S. Y. (1973). "Fluid to fluid modeling of critical heat flux: a compensated distortion model". Int. J. Heat Mass Transfer, 16, 641-661.

Becker, K.M., Ling, C.H, Hedberg, S., and Strand, G. (1983). "An experimental investigation of post dryout heat transfer". Rep. KTH-NEL-33, Sweden.

Becker, K.M., Askeljung, P., Hedberg, S., Soderquist, B., and Kahlbom, U. (1992). "An experimental investigation of the influence of axial heat flux distributions on post dryout heat transfer for flow of water in vertical tubes". Rep. KTH-NEL-54, Royal Institute of Technology, Sweden.

Bertoletti, S., Gaspari, G. P., Lombardi, C., Soldaini, G. and Zavattarelli, R. (1964). "Heat transfer crisis in steam-mixtures, experimental data in round tubes and vertical upflow obtained during the CAN 2 program". Centrol Inf. Studi Esperimenze Rep. CISE-R-90, Milan, Italy.

Bertoletti, S., Gaspari, G. P., Lombardi, C., Peterlongo, G., Silvestri, M. and Tacconi, F. A. (1965). "Heat transfer crisis with steam-mixtures". Energia Nucleare 12(3):121-172.

Casterline, J. and Matzer, B. (1964). "Burnout in long vertical tubes with uniform and cosine heating using water at 1000 psia". AECL report, TID-21031.

Coeling, K.J. (1978). "Effect of axial locations of spacers and hot spots on the CHF power of rods". WAPD-TM-1154, Westinghouse Electric Co.

Collier, J.G. and Thome, J. R. (1994). "Convective boiling and condensation". Oxford University Press, New York.

DeBortoli, R.A., Green, S.J., LeTourneau, B.W., Troy, M. and Weiss, A. (1958). "Forced-convection heat transfer burnout studies for water in rectangular channels and round tubes at pressures above 500 psia". Westinghouse Electric Corp. Report WAPD-188.

Doroshchuk, V.E., Levitan, L.L. and Lantzman, F.P. (1975). "Investigation into Burnout in Uniformly Heated Tubes" ASME Publication 75-WA/HT-22.

Fiori, M. P. and Bergles, A. E. (1970). "Model of critical heat flux in subcooled flow boiling". In Heat Transfer, 7, Paper B6.3 Elsevier Pub. Co., Amsterdam.

Frost, W. and Dzakowic, G. S. (1967). "An extension of the method of predicting incipient boiling on commercially finished surface". Paper 67-HT-61 presented at ASME-AIChE Heat Transfer Conference, Seattle, August.

Groeneveld, D.C. (1975). "The effect of non-uniform axial heat flux on the critical heat flux". Rep. AECL-4729, AECL.

Groeneveld, D.C. (1992). "A review of inverted annular film boiling, post dryout heat transfer". Editors: Hewit, Delhaye, and Zuber, Chapter 5, pp 327-366, Hemisphere Publishing Corporation (CRC Press)

Groeneveld, D.C., Blumenroehr, D., Cheng, S.C., Cheng, X., Doerffer, S., Erbacher, F.J., Tain, R.M. and Zeggel, W. (1992). "CHF fluid-to-fluid modelling studies in three laboratories using different modelling fluids". Proceedings of NURETH-5, Vol. 2, pp. 531-538, Salt Lake City, Sept. 21-24.

Groeneveld, D.C. (1996). "On the definition of critical heat flux". Nucl. Eng. and Des., 163 (1996) 245 - 247.

Groeneveld, D.C., Leung, L.K.H. et al. (1996). "The 1995 look-up table for critical heat flux in tubes". Nucl. Eng. and Des., Vol.163, pp. 1-33.

Groeneveld, D.C., Leung, L.K.H. et al. (1999). "A general method of predicting critical heat flux in advanced water cooled reactors". 9th Int. Topical Meeting on Nuclear Reactor T/H (NURETH-9), San Francisco, USA.

Groeneveld. D.C. (2003). Private communications.

Hewitt, G. F. et al. (1965). "Burnout and film flow in the evaporation of water in tubes". AERE-R 4864.

Hewitt, G. F. et al. (1966). "Studies of burnout in boiling heat transfer to water in round tubes with non-uniform heating". AERE-R 5076.

Keeys, R.K.F., Ralph, J.C. and Roberts, D.N. (1971). "Post burnout heat transfer in high pressure steam water mixtures in a tube with cosine heat flux distribution". UK Rep. AERE-R6411, AEA, Harwell, England.

Kinoshita, H., Nariai, H. and Yoshida, T. (1998). "Critical heat flux in sub cooled flow boiling with water in a tube with axially nonuniform heating". Heat Transfer, Japanese Research, Vol 27, No.2.

Kirby, G. J. (1966). "A new correlation of non-uniformly heated round tube burnout data". AEEW-R 500.

Kirby, G. J., Staniforth, R., and Kinneir, J. H. (1967). "A visual study of forced convection boiling. Pt. I". AEEW-R 281 (1965) and Pt. II. AEEW-R 506.

Kutateladze, S. S. and Leontev, A. I. (1966). "Some applications of the asymptotic theory of the turbulent boundary layer". Proceedings of 3rd International Heat Transfer Conference, Chicago, III.

Lee, D.H. and Obertelli, J.D. (1963). "An experimental investigation of forced convection boiling in high pressure water". UKAEA Report AEEW-R213.

Lee, D.H. (1966). "An experimental investigation of forced convection burnout in high pressure water, part 4. large diameter tubes at about 1600 psia". U.K, AEEW-R-479, AEEW, England.

Levy, S. (1966). "Forced convection subcooling – prediction of vapour volumetric fraction". General Electric Company, Report GEAP-5157.

Macbeth, R.V. (1963). "Burnout analysis, part 4: application of a local conditions hypothesis to world data for uniformly heated tubes and rectangular channels". AEEW-R-267.

Mortimore, E.P. and Beus, S.G. (1979). "Critical heat flux experiments with a local hot patch in an internally heated annulus". WAPD-TM-1419, Westinghous Electric Co.

Ornatskiy, A.P., Chernobay, V.A. and Vasil'yev, A.F. "Heat transfer crisis in annuli in which the rate of heat transfer varies longitudinally". Thermophysics and Heat Engineering, No. 24, pp70-73, (1973) [English translation. Heat Transfer - Soviet Research, Vol 7, No.4, 27-30, 1975].

Park, C., Groeneveld, D.C. and L. K. H. Leung, L.K.H. "A review and assessment of the axial heat flux distribution effect on CHF in tubes". Un-published paper.

Saha, P. and Zuber, N. (1974). "Point of net vapour generation and vapour void fraction in subcooled boiling". Proc. of the 5th Int. Heat Transfer Conference, Tokyo, Paper B4.7 (1974).

Semeria, R. and Hewitt, G. F. (1972). "Aspects of heat transfer in two-phase one-component flows". Seminar Recent Developments in Heat Exchangers, International Centre for Heat and Mass Transfer, Trogir, Yugoslavia, Lecture Session H53, September.

Silvestri, M. (1966). "On the burnout equation and on location of burnout points". Energia Nucleare, 13(9), 469-479.

Smith, O.G, Tong, L.S., and Rohrer, W.M. (1965). "Burnout in steam-water flows with axially non-uniform heat flux". ASME Paper No.65-WA/HT-33, ASME.

Stevens, G. F., Elliott, D. F., and Wood, r. w. (1965). "An experimental comparison between forced convection burnout in Freon 12 flowing vertically upwards through uniformly and non-uniformly heated round tubes". AEEW-R 426.

Swenson, H.S., Carver,J.R. and Kakarala, C.R. (1963). "The influence of axial heat flux distribution on the departure from nucleate boiling in a water cooled tube". ASME, 62-WA-297.

Taitel, Y., Bornea, D., and Dukler, A. E. (1980). 'Modelling flow pattern transitions for steady upward gas-liquid flow in vertical tubes'. AIChE J., Vol. 26, No. 3, pp. 354.

Thompson B. and Macbeth R.V. (1964). "Boiling water heat transfer burnout in uniformly heated round tubes: a compilation of world data with accurate correlations:. UKAEA, AEEW-R 359.

Todreas, N.E. and Rohsenow, W.M. (1965). "The effect of non-uniform axial heat flux distribution". Massachusetts Institute of Technology, Department of Mechanical Engineering report, No. 9843-37.

Tong, L.S., et al. (1966). "Influence of axially non-uniform heat flux on DNB". AIChE Chem. Eng. Prog. Symp. Ser. 62(64):35-40.

Tong, L.S. (1967). "Prediction of departure from nucleate boiling for an axially non-uniform heat flux distribution". J. Nuclear Energy 21:241-248.

Tong, L.S. and Tang, Y.S. (1997). "Boiling heat transfer and two-phase flow". Taylor & Francis, Washington, D. C.

Tong, L. S. (1968). "Boundary layer analysis of the flow boiling crisis". Int. J. Heat Mass Transfer, 11, 1208-1211.

Turner, J. M., and Wallis, G. B. (1965). "An analysis of the liquid film in annular flow". Dartmouth College: USAEC Report NYO-3114-13.

Weisman, J and Pei, B.S. (1983). "Prediction of critical heat flux in flow boiling at low quality conditions". Int. J. Heat Mass Transfer, vol 26, p. 1463.

Whalley, P.B. (1974). "The calculation of dryout in a heated annulus". AERE-M-2661.

Zenkevich, B.A., Kalinin, Yu. A., Remizov, C.V. and Subbotin, V.I. (1969). "Effect of non-uniform axial heat flux distribution in a tube on heat transfer crisis". Institute for Physics and Power Engineering report, No. FEI-150.

APPENDIX A: An Experimental Study of the Effect of Flow Obstruction on CHF in a Tube with Non-uniform Axial Heat Flux Distribution

A.1 Test Sections

Experiments of AFD effect on CHF in tubes with flow obstruction were also performed. These experiments were conducted in the uniform and one non-uniform AFD test section (TS No.1, reverse flow direction). A schematic drawing of the non-uniform AFD test section with 8 cylindrical obstacles (2.39 mm diameter, 10 mm long, $\varepsilon = A_{obstacle} / A_{test\_section} = 0.192$) is shown in Figure A.1. The uniform AFD test section, which has the same inner diameter, the same number of obstacles and the same distance from the exit to each obstacle as the non-uniform AFD test section, serves as the reference case. Thermocouples were installed on the test sections at the locations of (i) 8mm and 20mm (also 50mm and 100mm for the uniform AFD test section) before the upstream end of the upper power clamps; (ii) 1-2 mm before the upstream end of each obstacle; and (iii) 1-2 mm before the downstream end of each heat flux step for the non-uniform AFD test section.

A.2 Initial CHF Location

CHF always initially occurred at the downstream end of the heated length of the uniform test section, irrespective of the presence of flow obstructions. For the non-uniform test section with flow obstruction, however, the CHF could initiate at (i) the downstream end of the heat flux step, or (ii) the location just upstream of the flow obstacle, or at (iii) the downstream end of the heated length.

The experiment showed that, depending on the flow conditions, the initial CHF occurred at TC7&8, TC9&10 and TC11&12. The locations TC7&8 and TC9&10 are situated at the same heat flux step; hence they have the same heat flux but a different quality. The location TC11&12 has a higher heat flux than that of TC7&8 and TC9&10. Note, however, that TC9&10 are located just 15 mm downstream of TC11&12; therefore, the qualities at these two locations are almost the same (see Figure A.2).

Comparing these three locations, for the test section without flow obstruction, CHF occurs preferentially at either TC7&8 (because X is high) or TC11&12 (because q" is high). For the test section with obstacles, however, CHF is enhanced by the flow obstruction, and this enhancement decays along the flow direction, hence, the CHF enhancement at TC9&10 is weaker than that at TC11&12. As a result, CHF could also occur at TC9&10 provided that the flow obstruction exists.

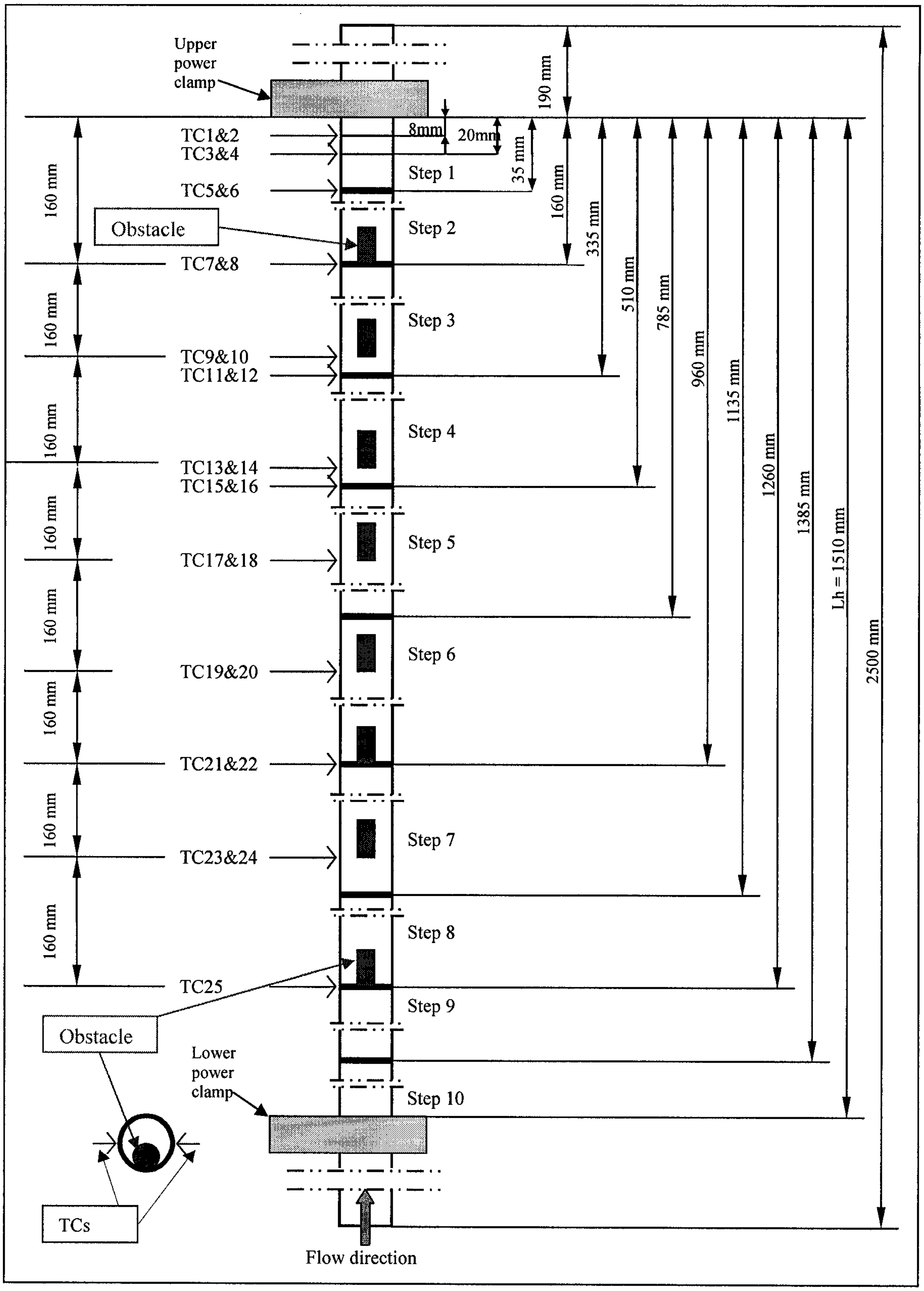

Figure A.1 Sketch of TS No.1 Test Section with Obstacles, Reverse Flow Direction.

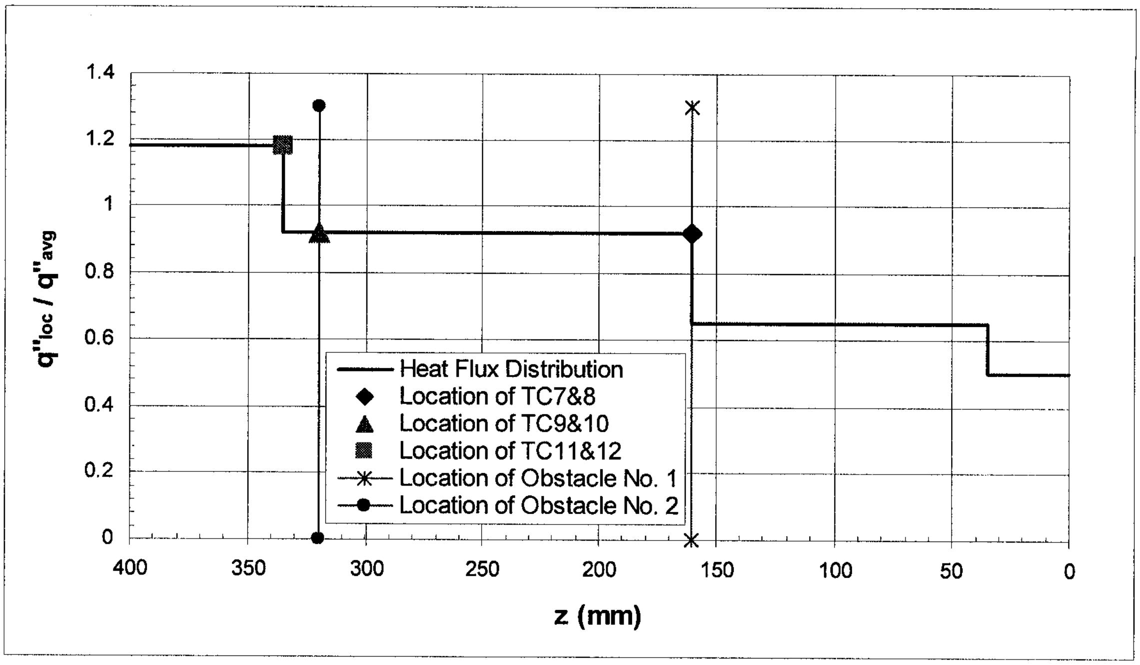

Figure A.2a Heat Flux Profile of the Test Section Near the Possible Initial CHF Location.

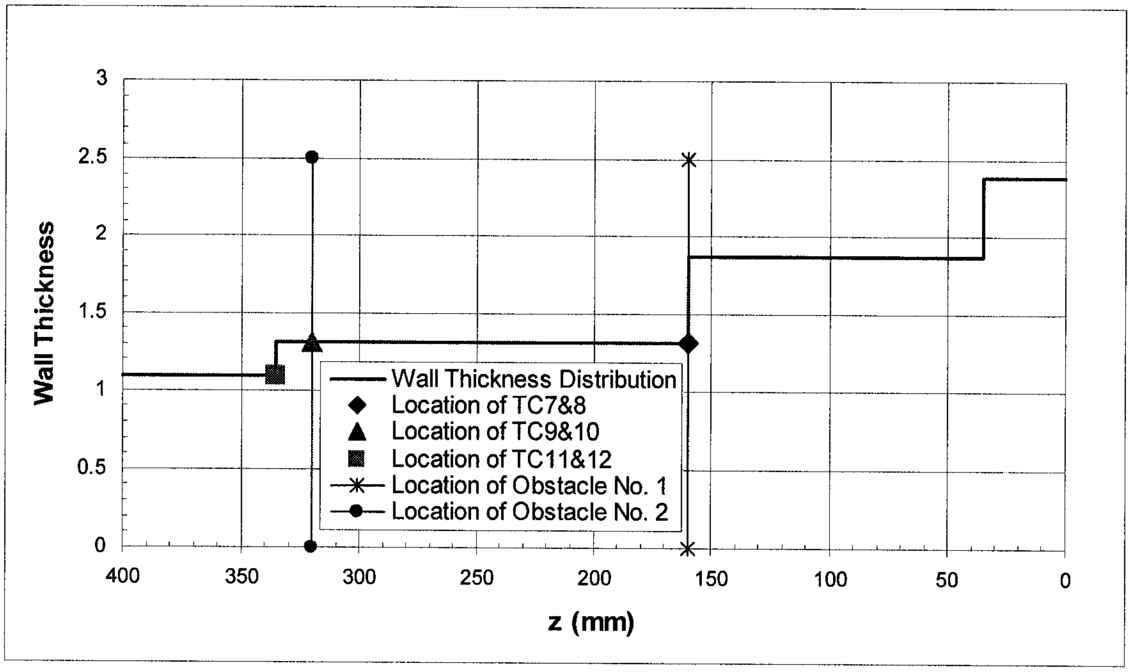

Figure A.2b Wall Thickness of the Test Section Near the Possible Initial CHF Location.

It was found during the experiment that CHF always occurred first at TC9&10 at high inlet qualities. The CHF location shifted or spread to TC11&12 as the inlet quality decreased, and could further shift to TC7&8 along with the decrease in the inlet quality at high mass flux. In order to obtain an understanding of the initial CHF spreading, extra runs were performed at high mass flux (G=3533 kg m^{-2} s^{-1}). The power was further increased after the initial CHF was detected at TC9&10, or TC7&8, until the CHF spread to TC11&12. The results are shown in Table A.1. It was observed that the extra power required for the CHF location spreading is quite small (around 1%). The main reason for the sudden shifts in the initial CHF location is the presence of a stepped heat flux profile. Improvement may be realized in future experimental study by moving the obstacle locations 15 mm downwards, thus, TC7&8 will be no longer at just upstream of the obstacle and the locations TC9&10 and TC11&12 will coincide with each other and the possible CHF locations would be reduced to only one.

Figure A.3 shows an example of the comparison among the critical heat flux for the uniform AFD test section with flow obstruction and the local heat fluxes at the locations of TC7&8, TC9&10 and TC11&12 at the CHF conditions for the non-uniform AFD test section with flow obstruction. The heat flux distribution in the length from TC11&12 to TC7&8 are presented as well in this plot. Figures A.4 to A.6 show the critical heat flux for the uniform AFD test section with flow obstruction, the initial CHF for the non-uniform AFD test section with flow obstruction, and the local heat fluxes at the locations of TC7&8, TC9&10 and TC11&12 at the CHF conditions based on local conditions. It is interesting to note that the local heat flux at TC11&12 always coincides with CHF for uniform AFD, even if the observed initial CHF occurred at other locations. This phenomenon may imply that TC11&12 is always the true initial CHF location.

A.3 Analysis Based on Local Conditions

Figures A.7 to A.9 show the curves of the critical heat flux versus dryout quality for uniform and non-uniform AFD bare tubes, and uniform and non-uniform AFD tubes with flow obstruction. Note that the initial CHF for the non-uniform AFD tubes with obstacles is assumed to always occur at TC11&12, while that for the non-uniform AFD tubes without obstacles is determined by the method described in Section 5.4.1. It is obvious that the flow obstruction has a strong effect on CHF and that it greatly enhances the CHF value, especially at high qualities. More importantly, the CHF vs. X_{do} curve for a non-uniform AFD test section with obstacles coincides almost perfectly with that for a uniform AFD test section with obstacles. This means that there is no apparent AFD effect on CHF in the case where flow obstruction exists. A possible explanation is that the large increase in local turbulence, induced by the flow obstruction, virtually destroys the effect of an upstream AFD. This implies that the local heat flux effect dominates.

Table A.1 Variation of the CHF Location along with the Change of Flow Conditions

P (kPa)	G (kg m^{-2} s^{-1})	T_{in} (°C)	Power (kW)	CHF Location
1667.2	3536	9.78	7.645	TC7&8
			7.74	TC7&8, TC9, TC11
1665.8	3541	20.50	6.915	TC8, TC9, TC11
1668.6	3533	30.29	5.916	TC9, TC11
1667.9	3539	40.15	4.939	TC9
			4.996	TC9, & TC11
1670.7	3538	50.06	4.35	TC9
			4.386	TC9, TC11

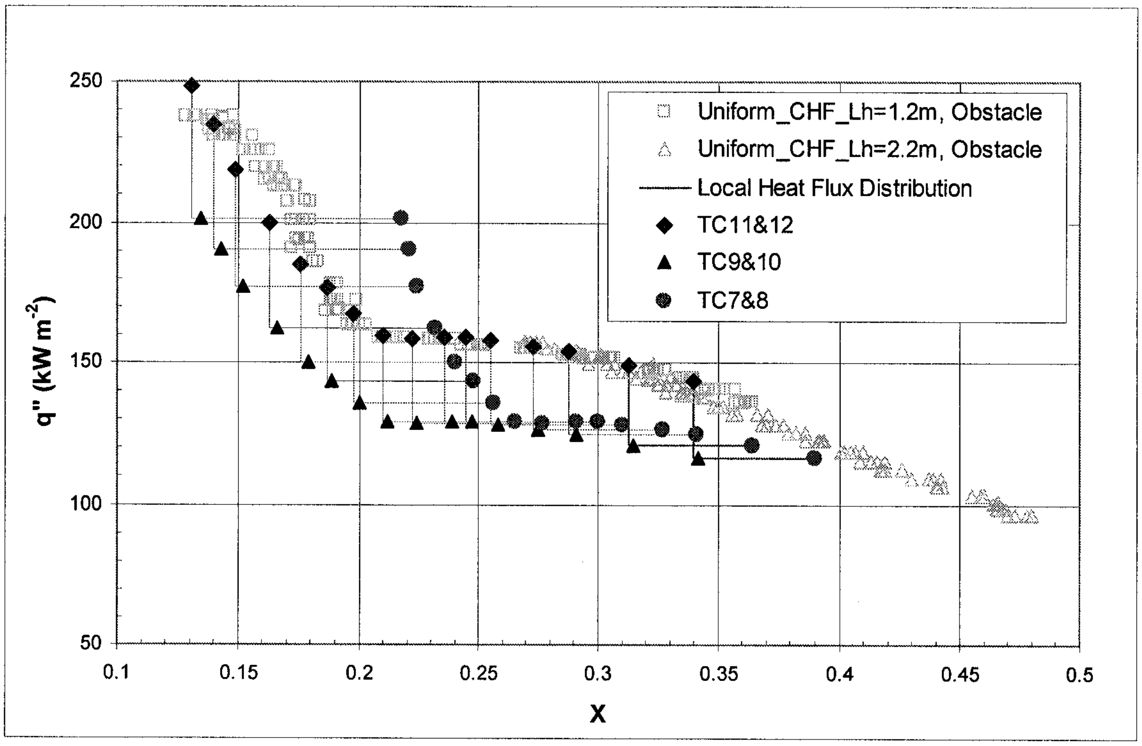

Figure A.3 Example of Local Heat Flux Distribution at Possible CHF Locations at CHF Conditions.

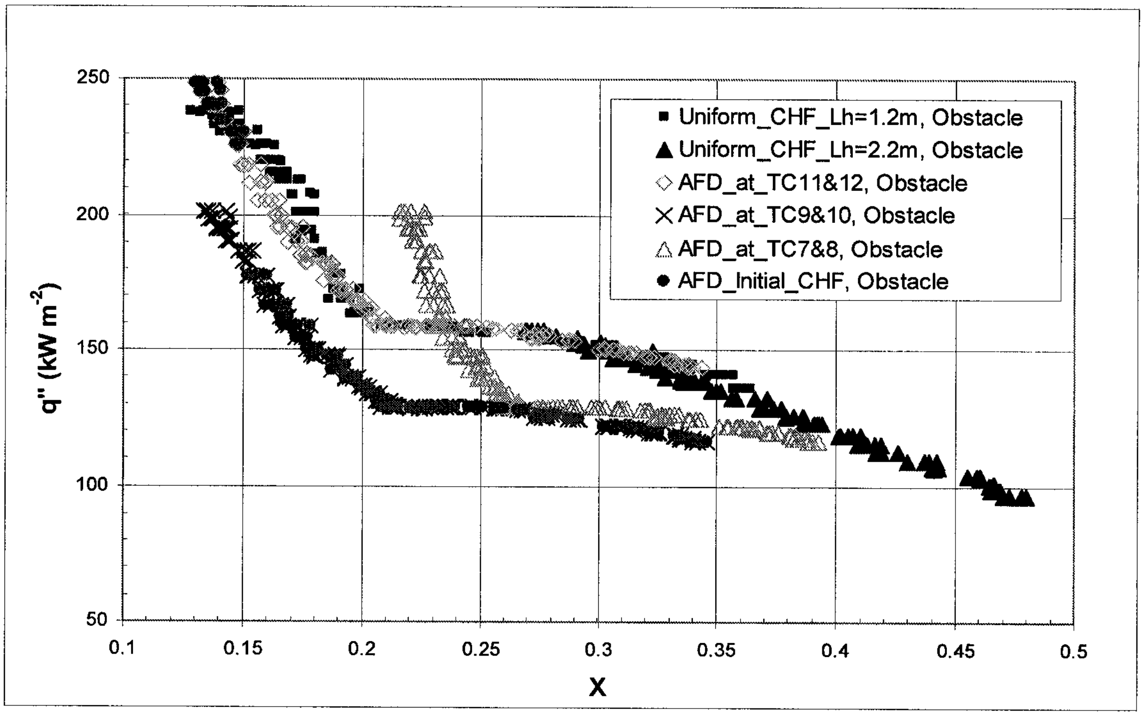

Figure A.4 Comparison of Local Heat Flux at Possible CHF Locations at CHF Conditions with Critical Heat Flux, P=1662 kPa, G=2120 kg m^{-2} s^{-1}.

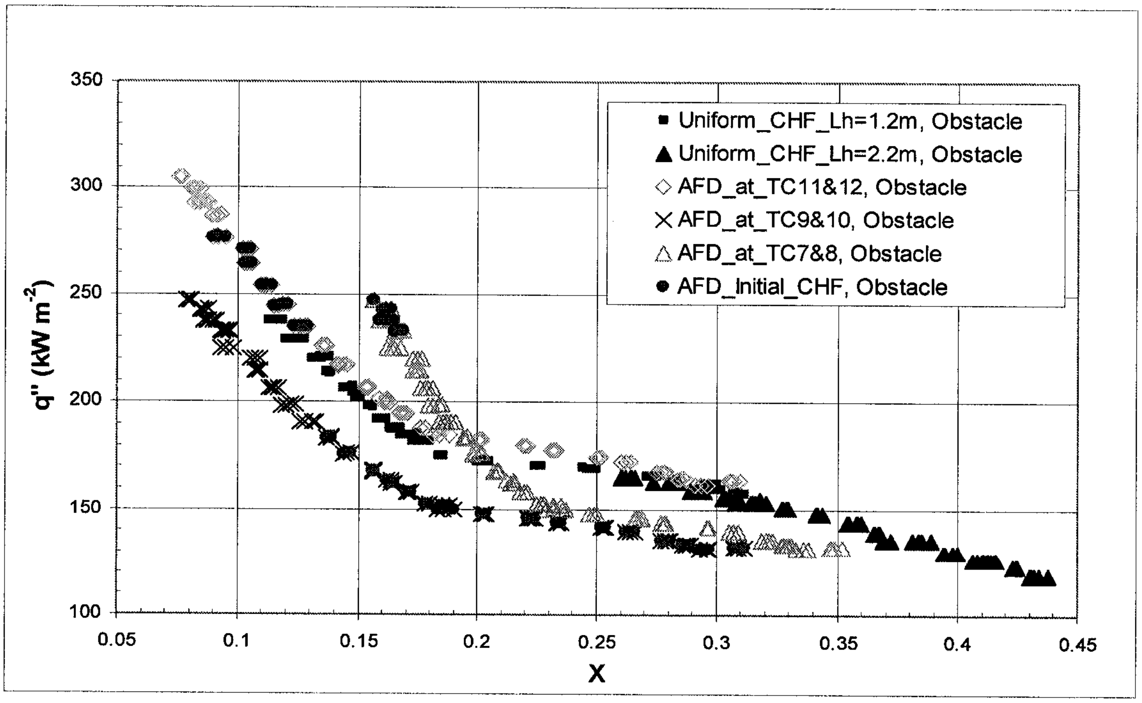

Figure A.5 Comparison of Local Heat Flux at Possible CHF Locations at CHF Conditions with Critical Heat Flux, P=1662 kPa, G=2826 kg m^{-2} s^{-1}.

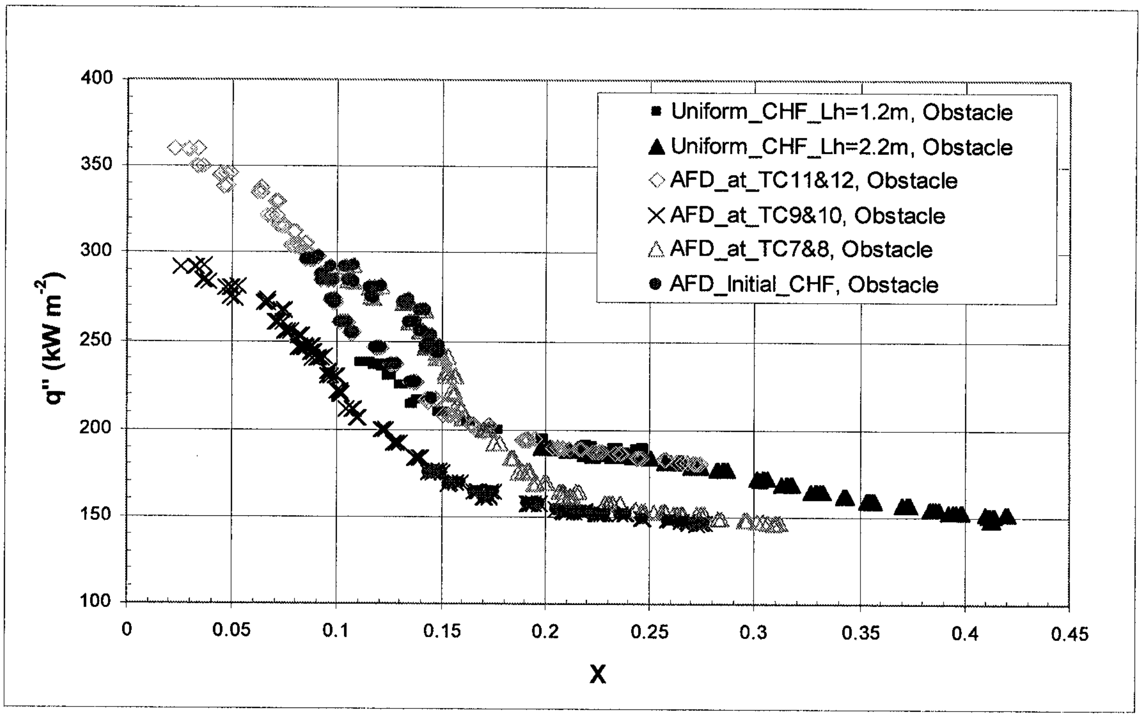

Figure A.6 Comparison of Local Heat Flux at Possible CHF Locations at CHF Conditions with Critical Heat Flux, P=1662 kPa, G=3533 kg m^{-2} s^{-1}.

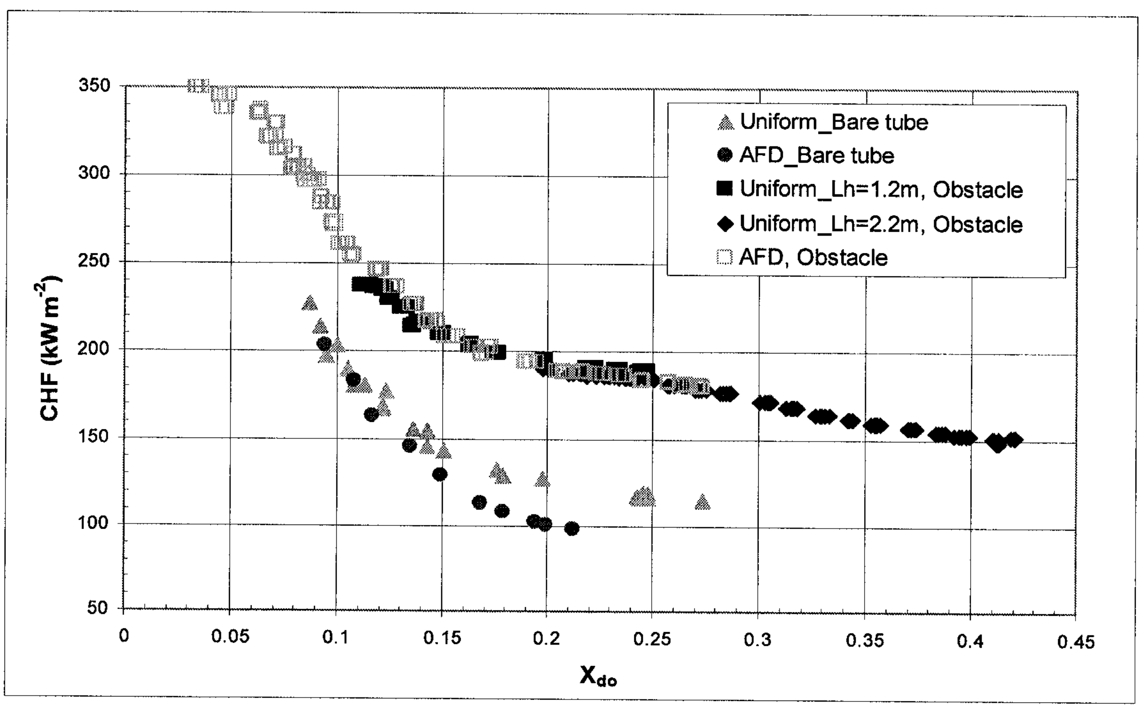

Figure A.7 CHF versus Dryout Quality, for Uniform and Non-uniform AFDs with and without Flow Obstruction, P=1662 kPa, G=3533 kg m^{-2} s^{-1}.

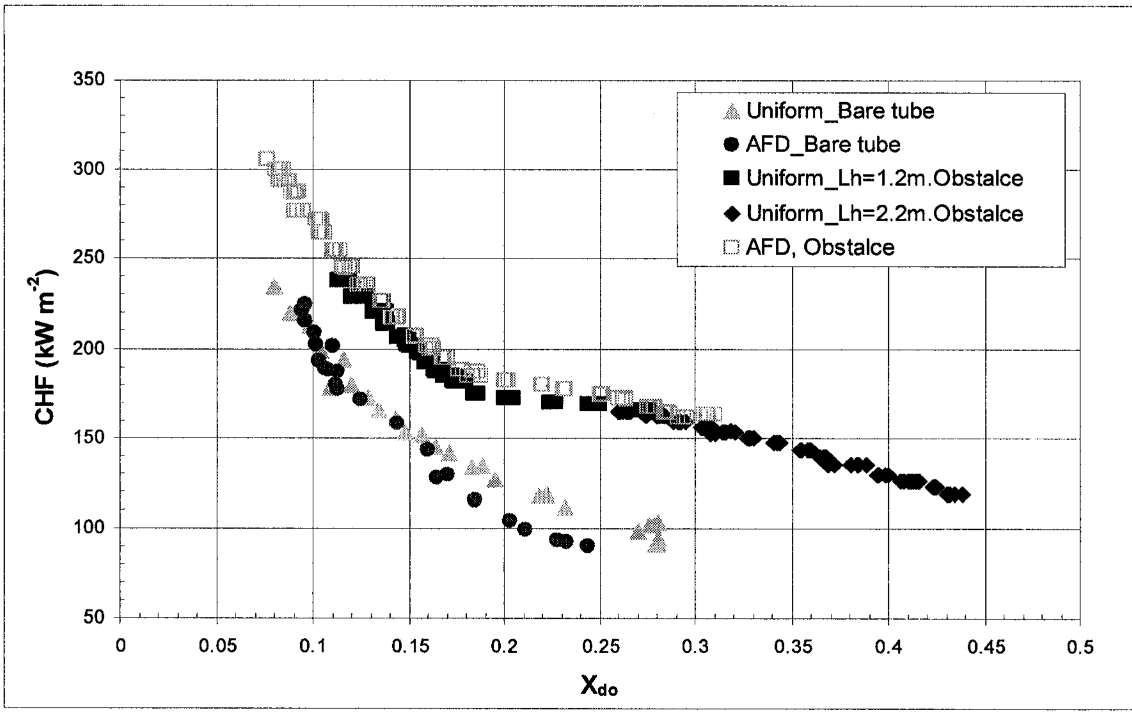

Figure A.8 CHF versus Dryout Quality, for Uniform and Non-uniform AFDs with and without Flow Obstruction, P=1662 kPa, G=2826 kg m^{-2} s^{-1}.

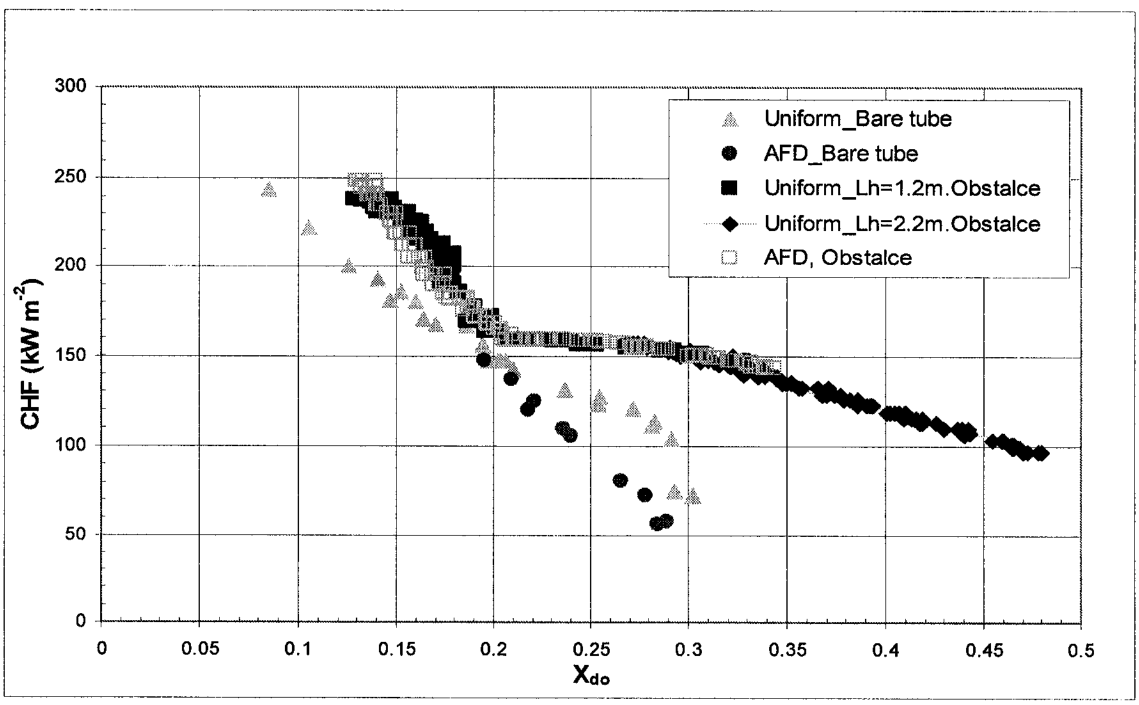

Figure A.9 CHF versus Dryout Quality, for Uniform and Non-uniform AFDs with and without Flow Obstruction, P=1662 kPa, G=2120 kg m^{-2} s^{-1}.

A.4 Analysis Based on Inlet Conditions

Figures A.10 to A.12 illustrate the flow obstruction effect on critical power at constant inlet conditions. Note that all of the data were converted to that of a 2-meter-equivalent heated length. Once again it was found that the flow obstruction has a strong effect on the critical power. The critical power for the test section with flow obstruction is up to 60% higher than that for the test section without flow obstruction at high inlet qualities. The discrepancy decreases with an increase in inlet subcooling. The critical power for the uniform test section with flow obstruction approaches that for the bare tube at high inlet subcoolings. The AFD effect on the critical power for the test section with flow obstruction appears to be stronger than that for the test section without flow obstruction especially at high subcoolings. The AFD effect decreases as inlet quality increases, and disappears when the inlet quality is higher than around –0.4. At high inlet subcooling, the critical power for the non-uniform AFD test section with flow obstruction is higher than that for the uniform AFD test section with flow obstruction by an approximately constant value.

Consider again the initial CHF location. At high inlet subcoolings, the initial CHF was detected at TC11&12 for a mass flux of 2120 kg m^{-2} s^{-1}, and at TC7&8 for mass fluxes of 2826 and 3533 kg m^{-2} s^{-1}. The initial CHF was always detected at TC9&10 at high inlet qualities, and at TC11&12 at moderate inlet qualities. Around 1% additional power (0.095 kW at T_{in}=9.78 °C, G=3533 kg m^{-2} s^{-1}; 0.057 kW at T_{in}=40.15 °C, G=3533 kg m^{-2} s^{-1}) was required to obtain subsequent CHF at TC11&12 in case the initial CHF occurrence was observed at TC7&8 or TC9&10. When looking closely at the plots, it is noticed that such small increases in power at the related regions will not affect the physical trend of critical power against inlet quality. This hence supports the assumption that the true initial CHF location is always at TC11&12.

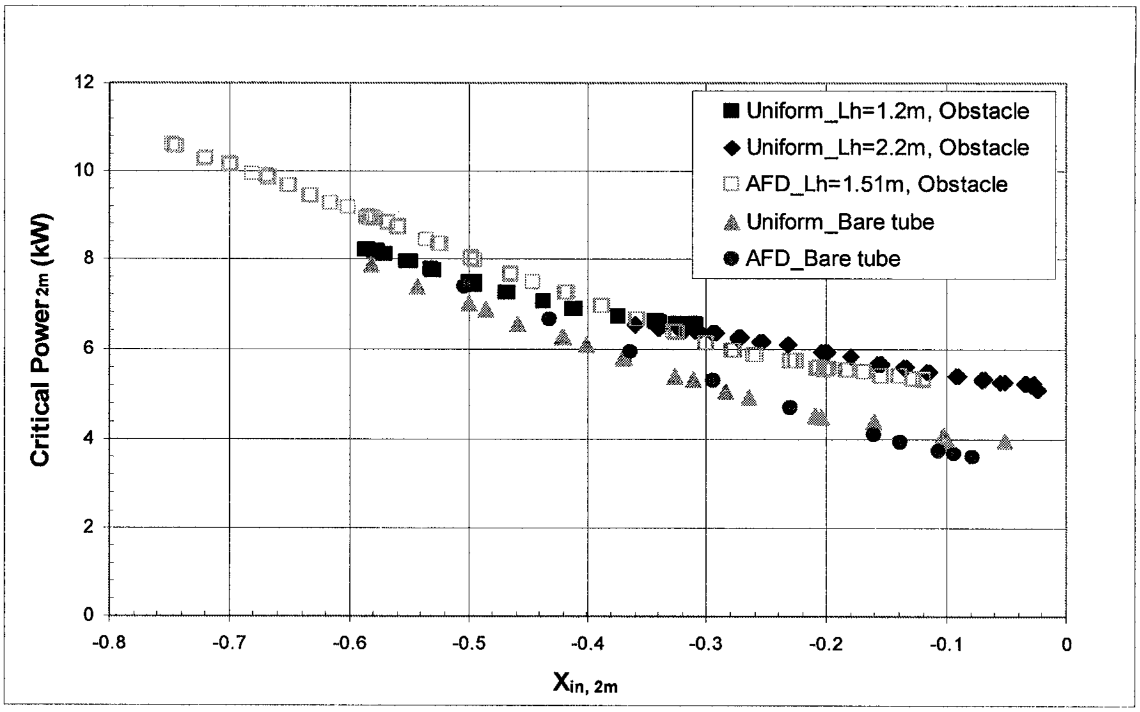

Figure A.10 Critical Power versus Inlet Quality, for Uniform and Non-uniform AFDs with and without Flow Obstruction, P=1662 kPa, G=3533 kg m^{-2} s^{-1}.

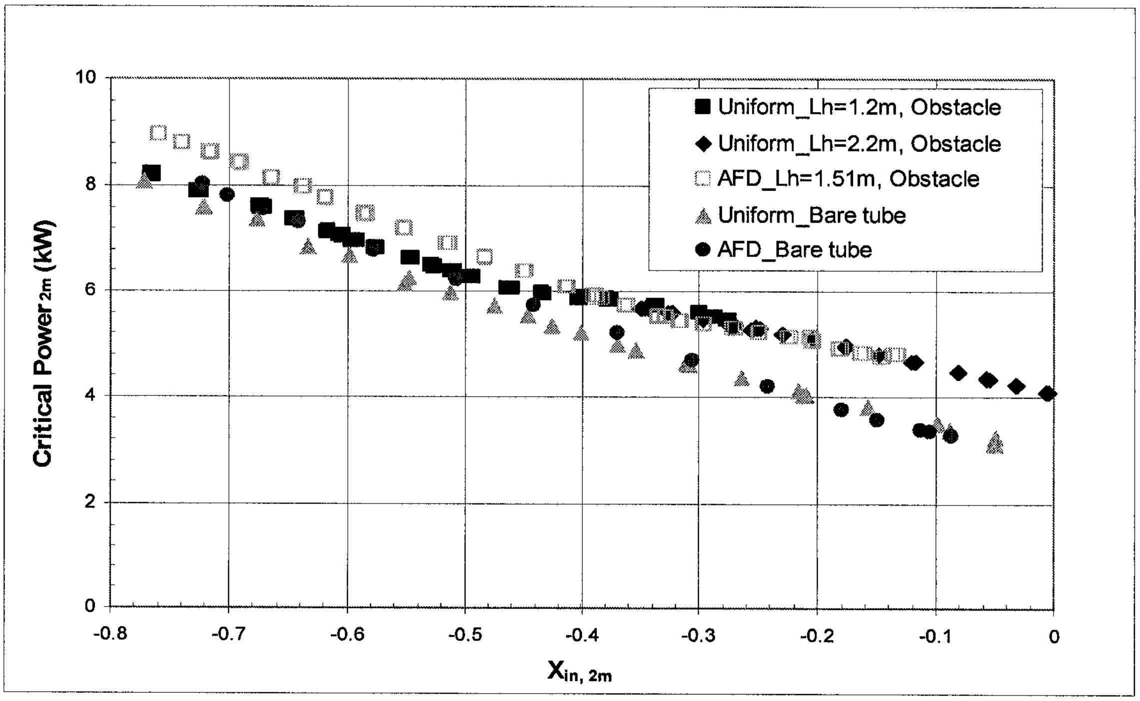

Figure A.11 Critical Power versus Inlet Quality, for Uniform and Non-uniform AFDs with and without Flow Obstruction, P=1662 kPa, G=2826 kg m^{-2} s^{-1}.

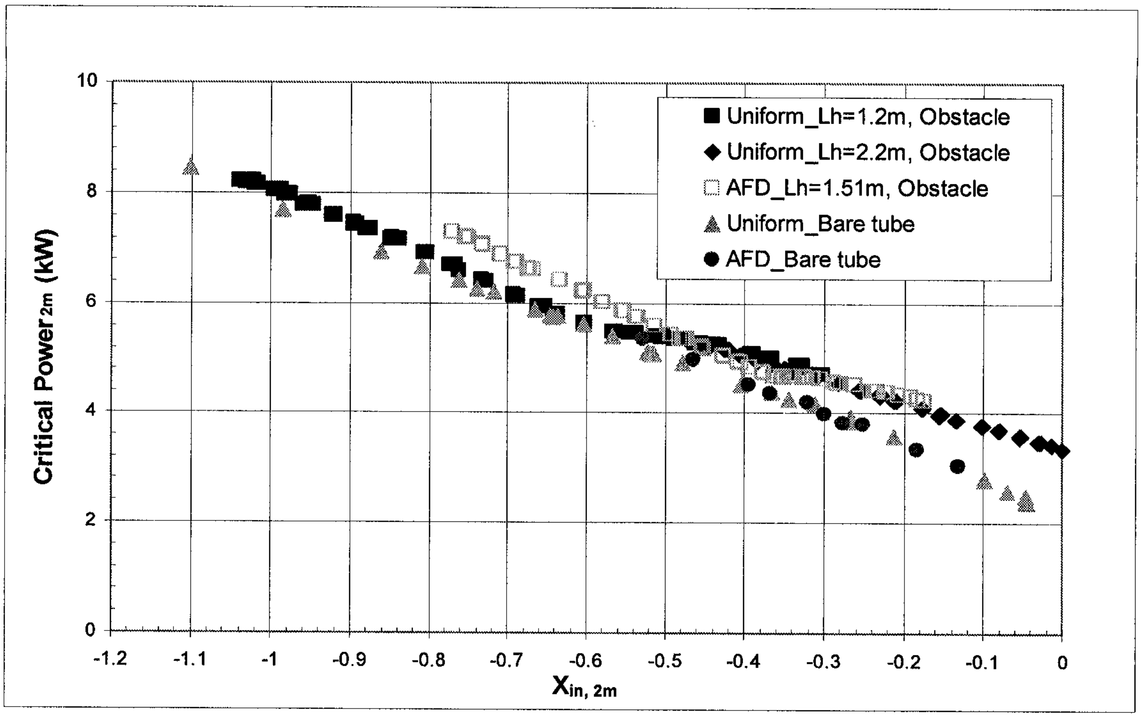

Figure A.12 Critical Power versus Inlet Quality, for Uniform and Non-uniform AFDs with and without Flow Obstruction, P=1662 kPa, G=2120 kg m^{-2} s^{-1}.

Appendix B: Quality Assurance of the Experiment

In order to assure the reliability of the experimental data, procedures of experiment preparations and repeatability, verifications were conducted, which are described in detail in the following sections.

B.1 Leakage Detection

Leakage detection was performed by filling the whole test loop with nitrogen at 400 psi. All of the potential leaking sites were checked using soapy water. Nitrogen remained in the loop for 24 hours after the soapy water checking. The system is considered as leak-proof if no pressure change is detected during this period.

B.2 Transient Temperature Test

This procedure was employed to check the response of the thermocouples by quickly turning on and off the power supply to the test section. The response speed of all of the thermocouples installed on the test section was acceptable.

B.3 Heat Loss Test

Heat loss test was performed by applying the power to the test section without insulation after evacuating the test loop. After all readings of the thermocouples installed at the test section showed that the surface temperatures had stabilized, the power supplied to the test section was recorded. In this case the power supplied to the test section was assumed to be equal to the heat loss from the outside tube surface to the environment in the CHF test for the same heated length and the same average outer surface temperature. Heat loss tests were perform at average outer surface temperatures of 56°C, 65°C and 77°C, which approximately correspond to the maximum average outer surface temperature in the runs of pressures 1662, 2022 and 2389 kPa. The results of the heat loss tests are shown in Figure B.1. The heat loss without insulation on the test section was very small (0.037 kW at an average thermocouple temperature equals to 77°C).

B.4 Heat Balance Test

Heat balance tests were conducted by supplying the power to the test section while a single-phase liquid flowed through the test section at a pressure of 2300 kPa, and mass flux of 4500 kg/m^2s. The power supplied to the test section was compared with the enthalpy rise of the fluid. The heat balance results are shown in Figures B.2a & B.2b. The

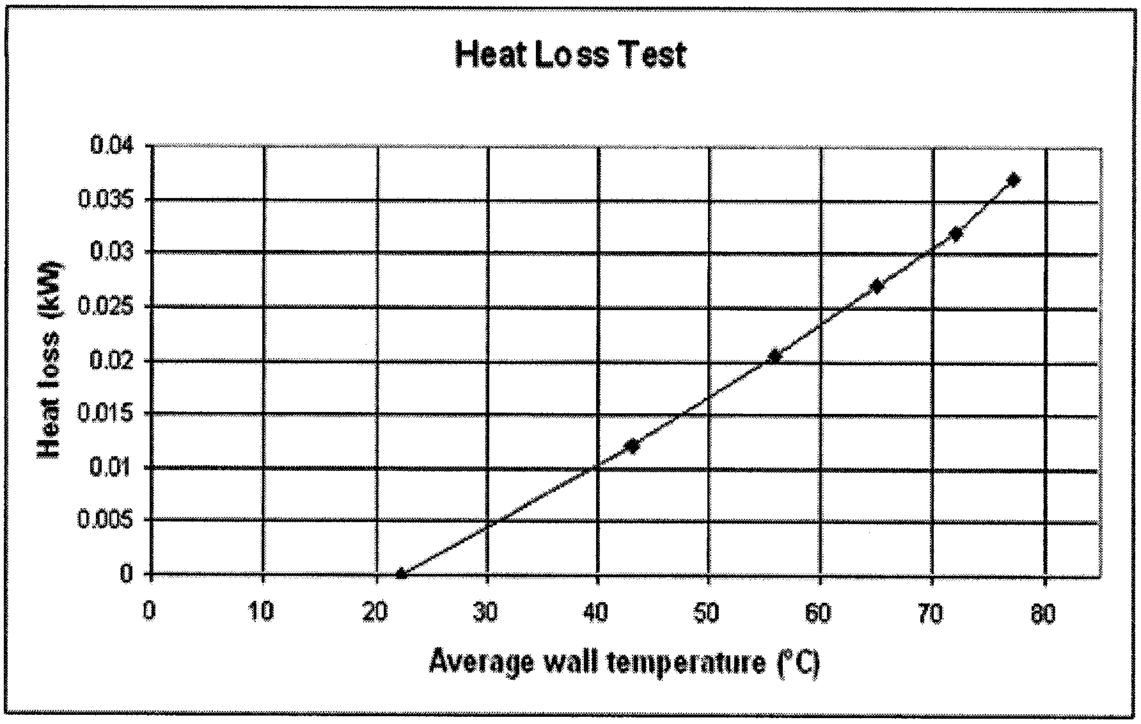

Figure B.1 **Result of Heat Loss Test.**

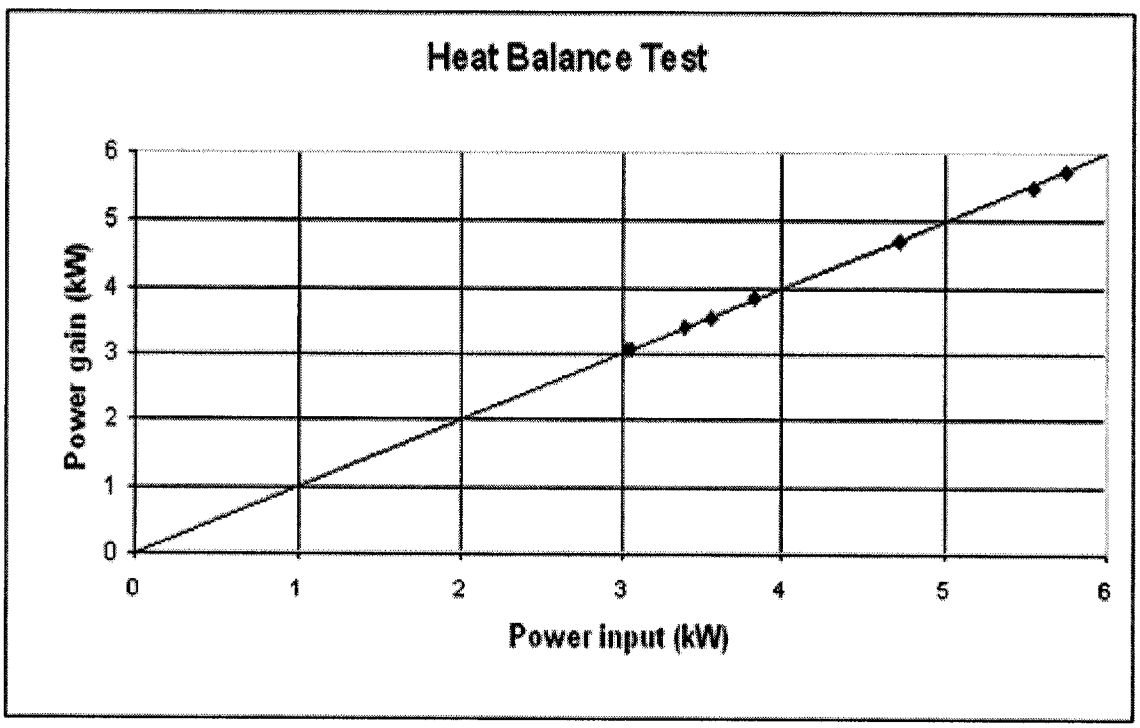

Figure B.2a **Result of Heat Balance Test.**

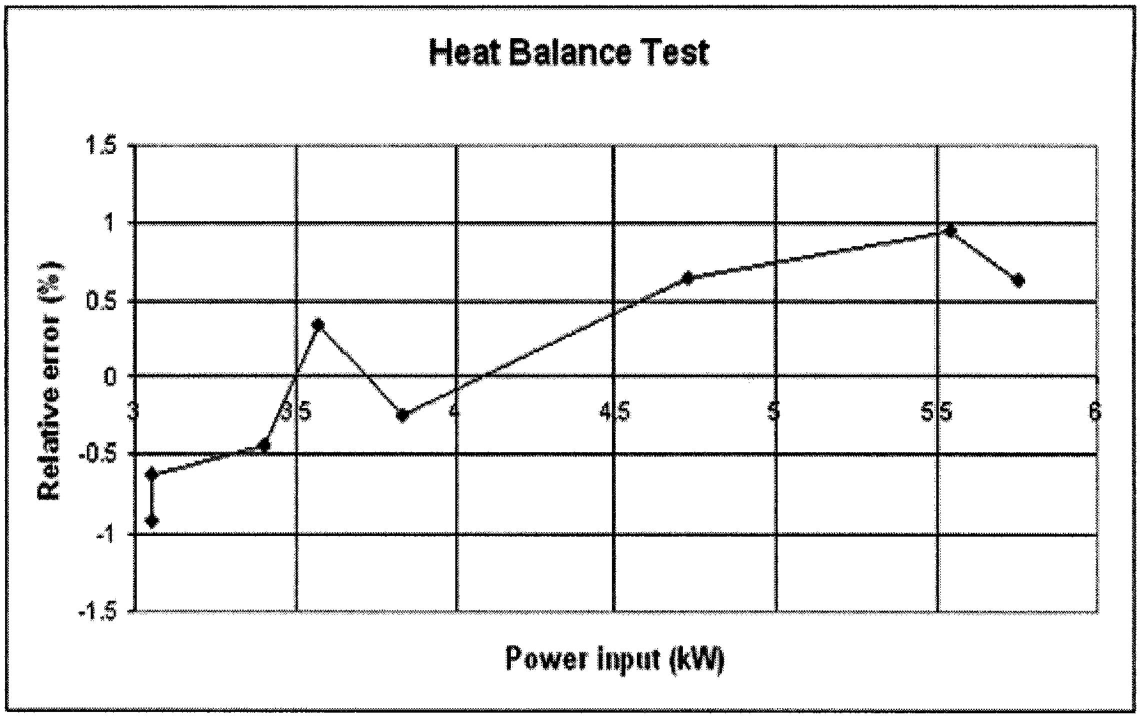

Figure B.2b   Result of Heat Balance Test.

difference between the power supplied to the test section and the enthalpy rise of the working fluid was less than 1%.

B.5 Calibration of RTD and Thermocouple

RTD for measuring inlet fluid temperature and thermocouples were calibrated by means of comparison with a standard mercury thermometer. The calibration results are shown in Figures B.3a & B.3b. The discrepancies between the mercury thermometer and the RTD and thermocouples were within 0.7% and 2%, respectively.

B.6 Calibration of Pressure

Pressure calibration was performed while the loop was filled with nitrogen. The pressure gauge mounted on the bottom of the test section (Pgauge) was treated as a standard. The values of the inlet and outlet pressures indicated by the DAS were recorded and compared with the values of the pressure gauge. The results are showed in Figures B.4a & B.4b. The discrepancies between the reading from the pressure gauge and the inlet and outlet pressures are less than 0.5%.

B.7 Calibration of Voltage and Current

Values of voltage and current indicated in DAS were compared with the readings of the voltage meter and the current meter mounted on the power supply. The results are shown in Figures B.5a, B.5b, B.6a and B.6b. Very good agreement was found in either the results of voltage calibration or that of current calibration. The differences between the voltages and the currents were within 0.35% and 0.1%, respectively.

B.8 Q/A Repeatability Test

Good repeatability is important in any experimental study, and is defined as the closeness of the agreement between the results of successive measurements of the same parameter carried out for the same flow conditions and the same test geometry. In this investigation, Q/A repeatability tests were performed. The quality assurance (Q/A) experimental point (at fixed flow condition P = 1670 kPa, G = 2000 kg m^{-2} s^{-1}, X_{do} = 0.2) was measured for the uniform AFD test section. The result was compared with the value of CHF in the look up table at the same condition after the conversion for fluid and geometry. The discrepancy of the two CHF values was around 3%. Certain CHF data points (P = 2389 kPa, G = 3576 kg m^{-2} s^{-1}, Tin = 50 °C) were repeated following the completion of the non-uniform AFD test for the whole range of the test matrix with each test section to assure the repeatability of the data. The discrepancy of critical power values for the previous run and the repeating run was in the range of 0.309% to 0.834%. This demonstrates that random errors are small. The repeatability test results are shown in Table B1.

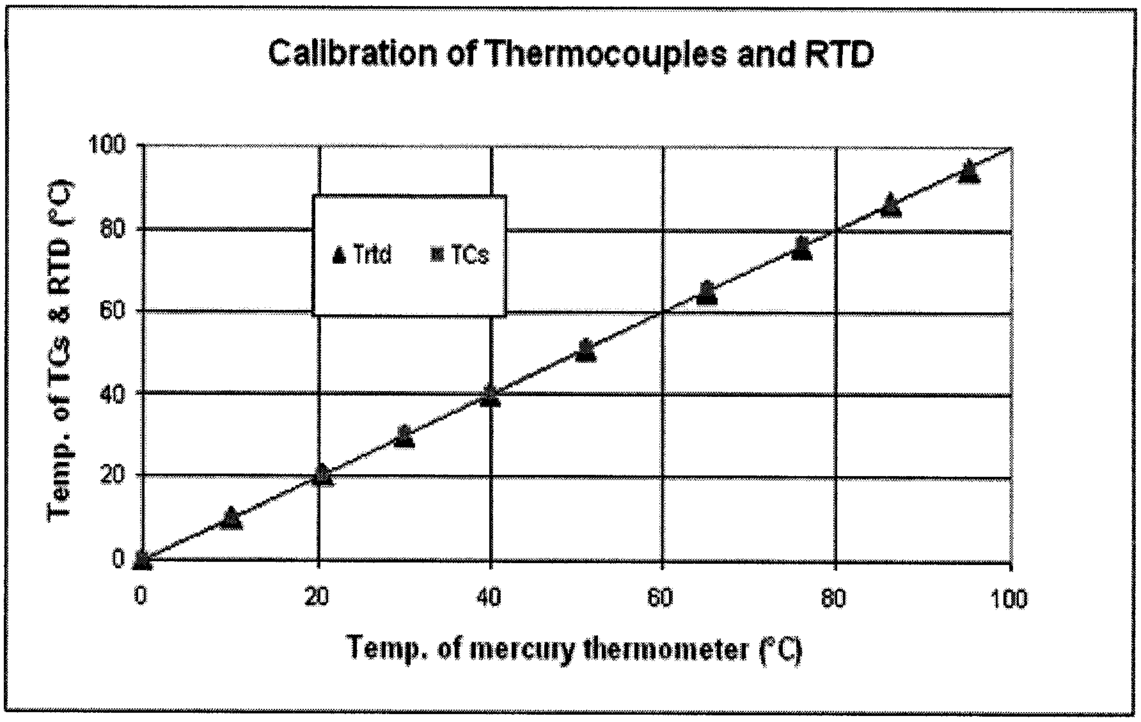

Figure B.3a Result of Calibration of Thermocouples and RTD.

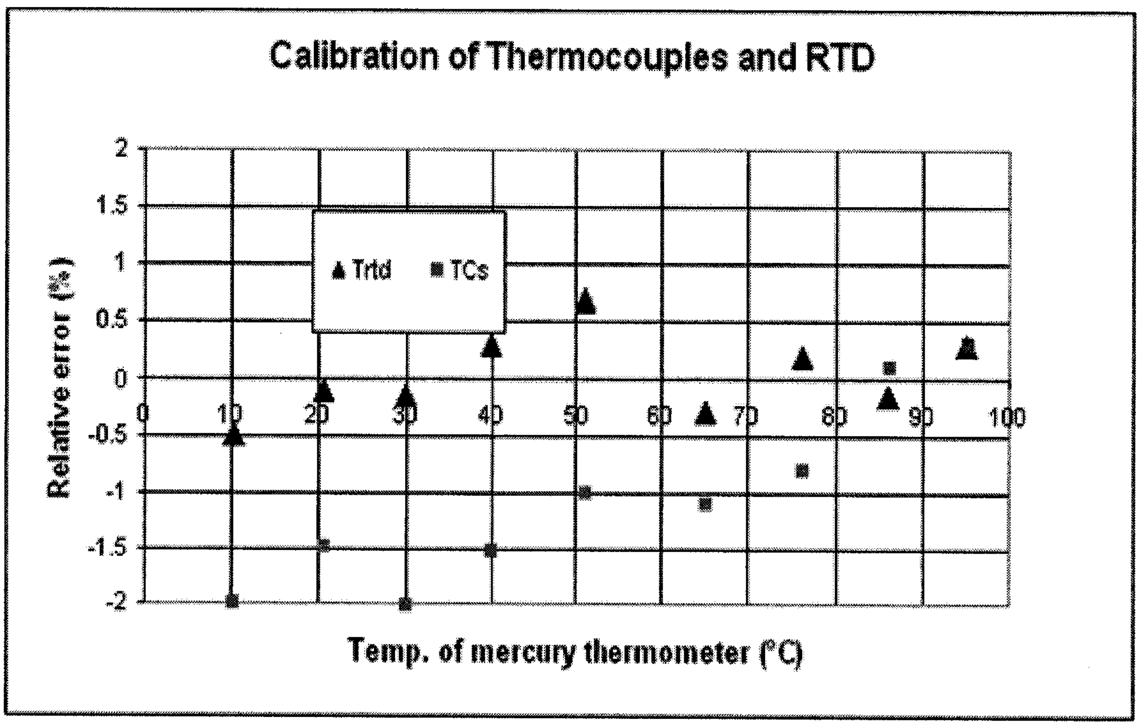

Figure B.3b Result of Calibration of Thermocouples and RTD.

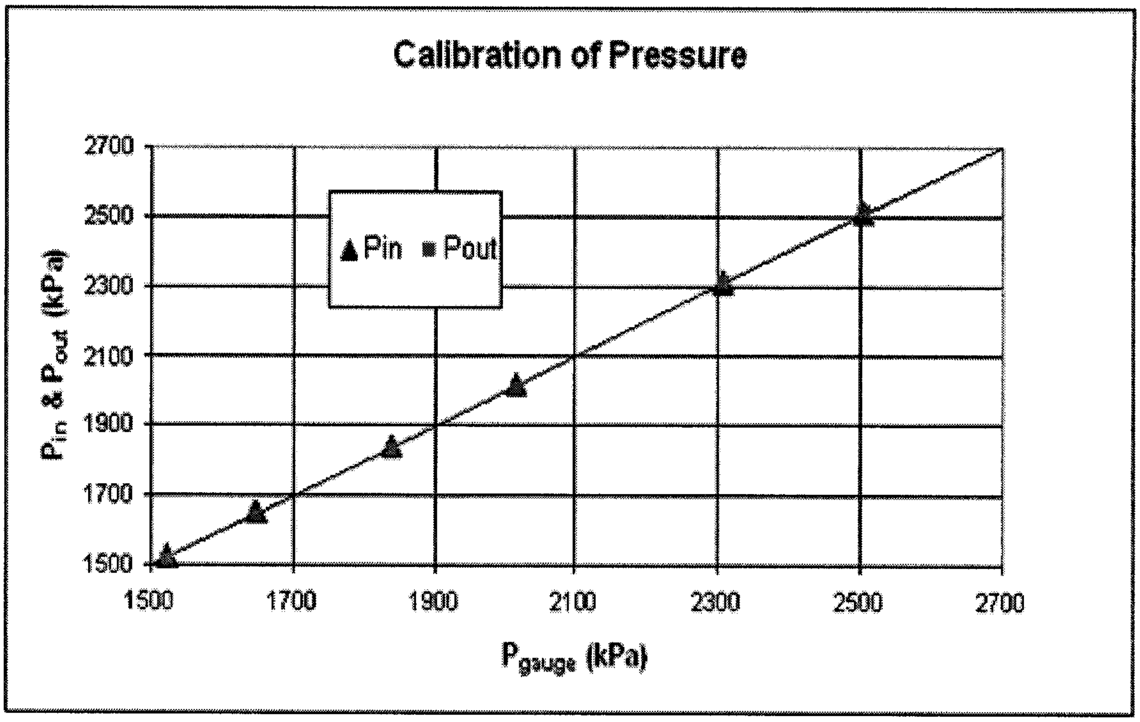

Figure B.4a Result of Calibration of Pressure.

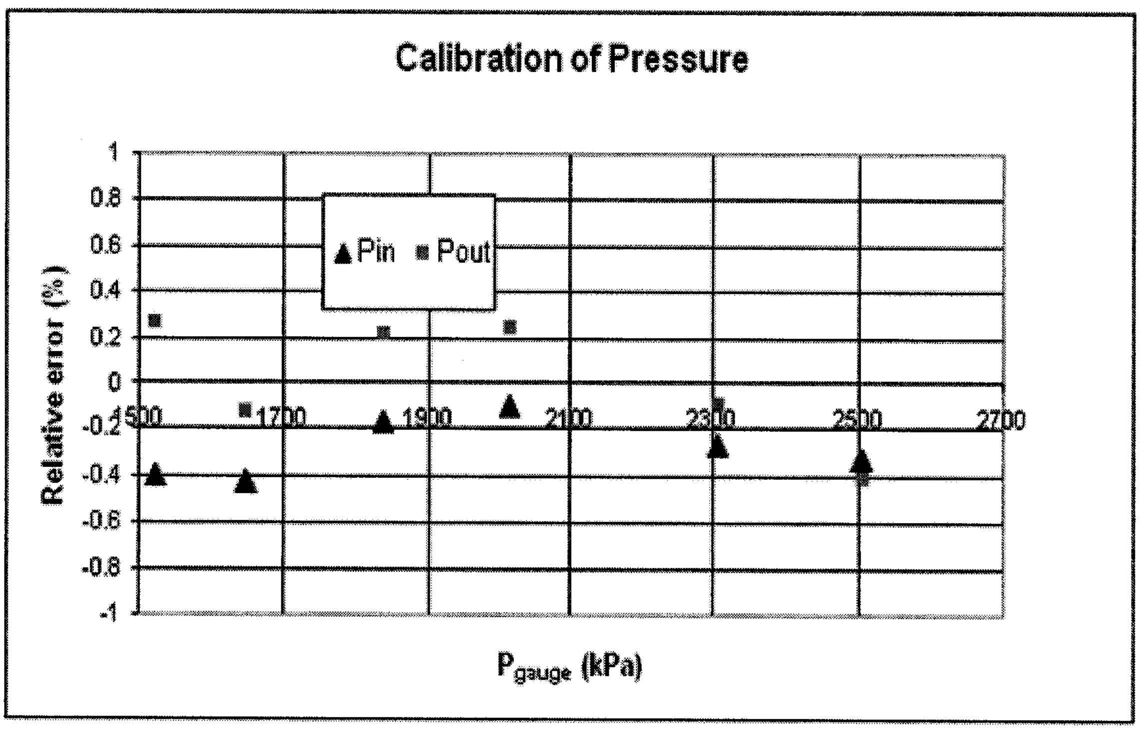

Figure B.4b Result of Calibration of Pressure.

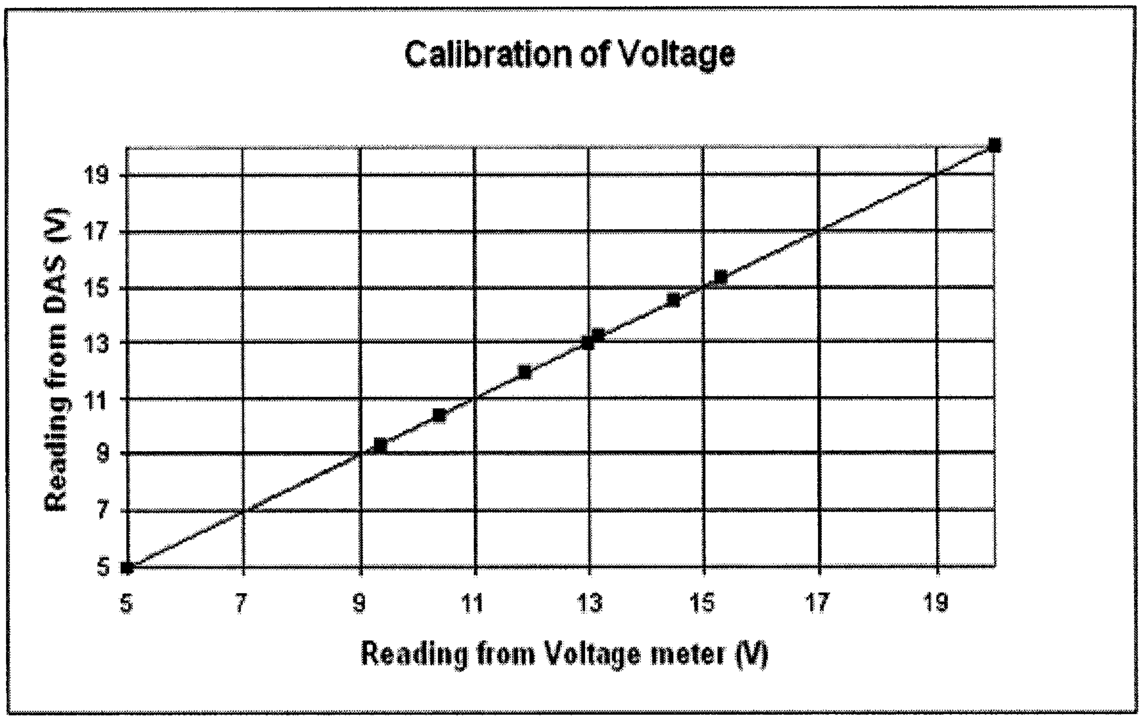

Figure B.5a Result of Calibration of Voltage.

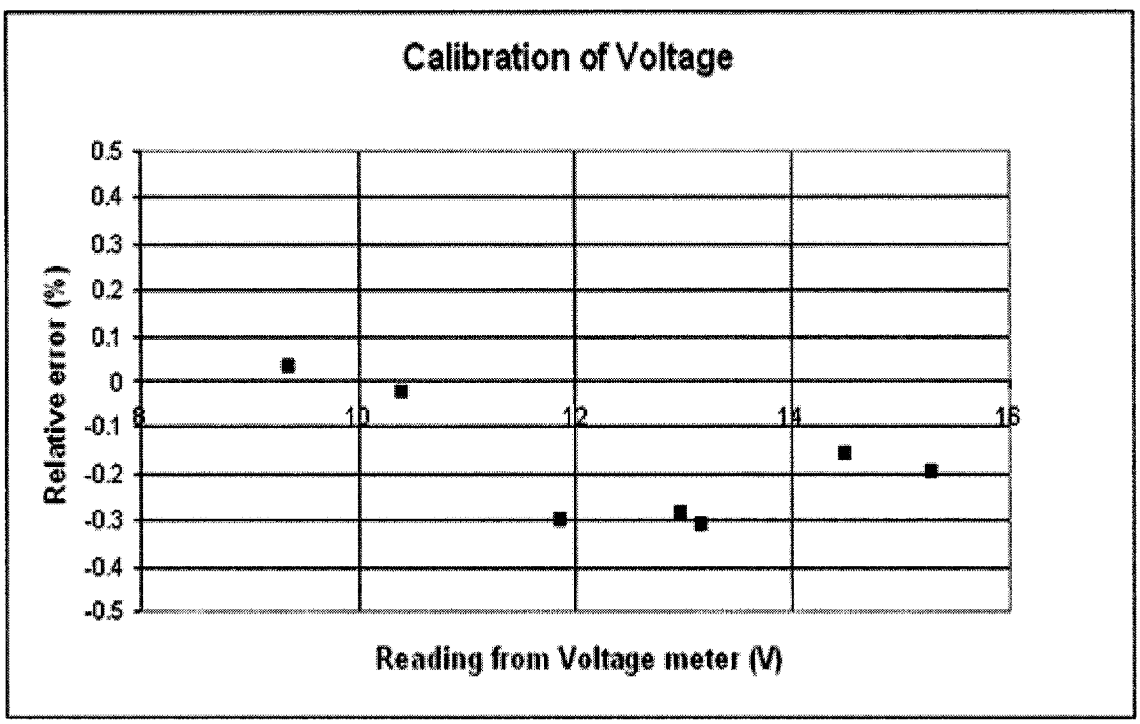

Figure B.5b Result of Calibration of Voltage.

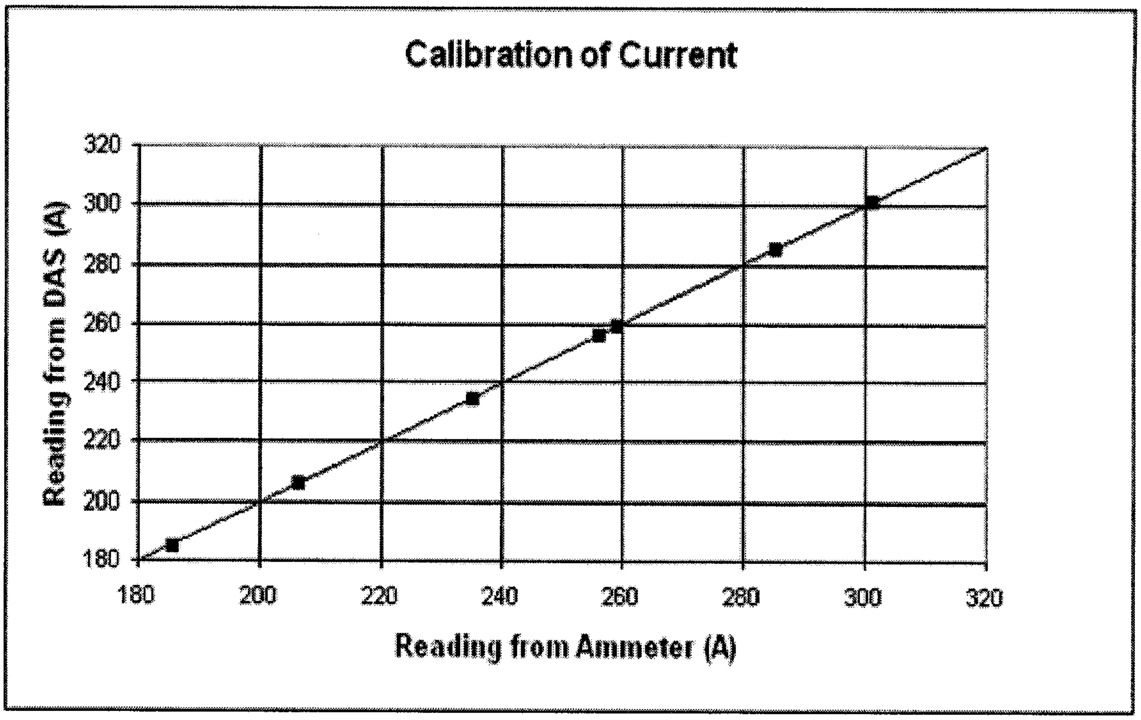

Figure B.6a Result of Calibration of Current.

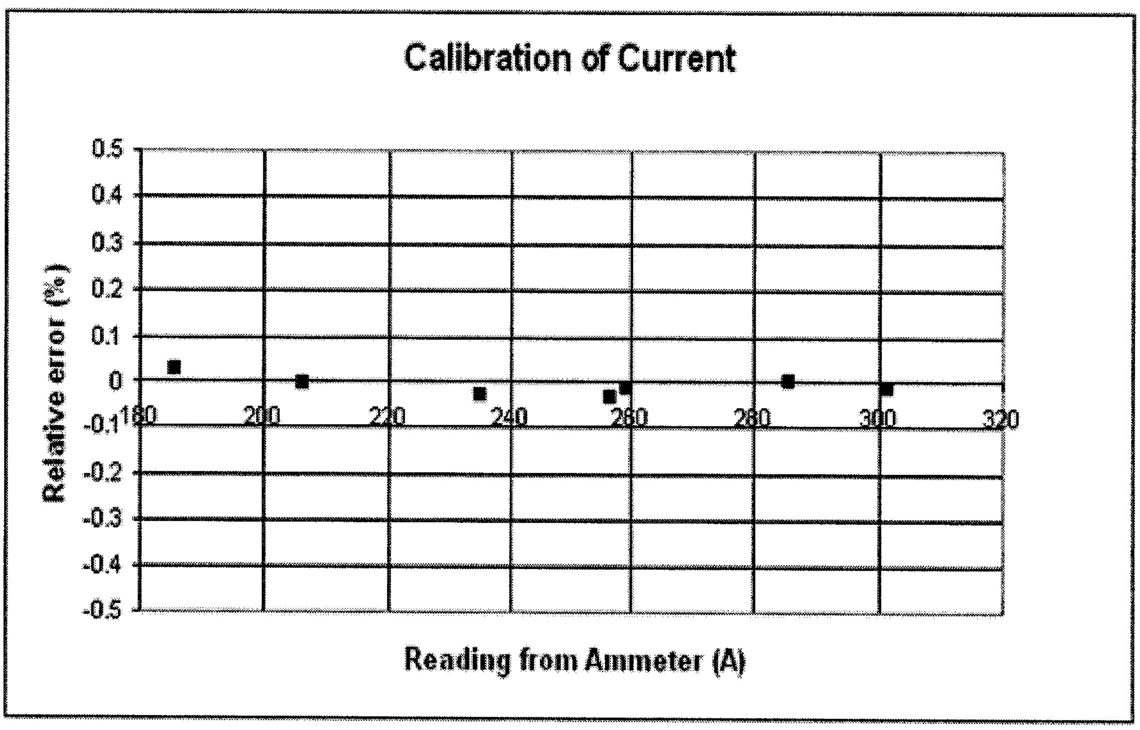

Figure B.6b Result of Calibration of Current.

Table B.1 Repeatability Test Results

Quality Assurance CHF Test, Uniform Test Section							
	P (kPa)	G (kg m^{-2} s^{-1})	X_{do}	CHF (kW m^{-2})	D_i (mm)	Lh (mm)	T_{in} (°C)
Look-up table	1670	2000	0.2	156.6	5.461		
	1670	2000	0.22	146.2	5.461		
Run 1	1640.93	1990.03	0.2202	140.99	5.461	1576	26.75
Run 2	1639.58	1985.63	0.2218	140.99	5.461	1576	26.75
Run 3	1657.76	2029.6	0.2101	142.25	5.461	1576	26.75
Run 4	1649.01	2025.2	0.2138	142.35	5.461	1576	26.75
Repeatability Test, Non-Uniform Test Section							
	D_i (mm)	Lh (mm)	T_{in} (°C)	P (kPa)	G (kg m^{-2} s^{-1})	Power (kW)	Error (%)
TS NO.1	5.461	1490	50.08	2394.4	3582.76	5.354	0.747
Forward Flow	5.461	1490	49.98	2390.5	3577.421	5.394	
TS NO.1	5.461	1510	49.66	2391.03	3573.964	5.173	-0.309
Reverse Flow	5.461	1510	49.86	2388.6	3576.352	5.157	
TS NO.2	5.461	1275	51.54	2389.01	3576.163	4.95	-0.687
Forward Flow	5.461	1275	51.74	2393.41	3580.321	4.916	
TS NO.2	5.461	1350	49.66	2389.01	3587.158	5.158	0.834
Reverse Flow	5.461	1350	49.32	2387.28	3579.542	5.201	

Appendix C: Analysis of Measurement Uncertainties

(N.B. In this section extensive quotes are taken from Tavoularis, 2001). The uncertainty of a measurement represents the interval with which the true value of a measurable property lies within a certain probability. Let v represents a measured value of a measurable property. Under the current international convention, the uncertainty U of this measurement is defined such that the experimenter is 95% confident that the true value of this property lies in the interval (v - U, v + U). Both bias (fixed or systematic) and precision (random) errors contribute to the uncertainty. Uncertainty can be specified as absolute, expressed in the same units as the measured property, or relative, expressed as a percentage.

When uncertainties are introduced by K different components or steps of the measuring process (for example by calibration, data acquisition or data processing), the total uncertainty is determined as

$$\frac{U_v^2}{v^2} = \sum_{k=1}^{K} \left(\frac{U_v}{v} \right)_k^2 \tag{C.1}$$

The uncertainty in a calculated result is a function of the uncertainty in each of the individual measurements used in calculating that result. A general outline of the method is given below.

Assuming a result, R, is a function of a number of independent variable, v_1, v_2, …, v_n, then

$$R = F(v_1, v_2, \dots, v_n) \tag{C.2}$$

The uncertainty on the result, U_R, becomes

$$U_R = \sqrt{\left(\frac{\partial R}{\partial v_1} \right)^2 U_1^2 + \left(\frac{\partial R}{\partial v_2} \right)^2 U_2^2 + \cdots + \left(\frac{\partial R}{\partial v_n} \right)^2 U_n^2} \tag{C.3}$$

where U_1, U_2, … U_n are the corresponding uncertainties of the v_1, v_2, …, v_n.

It can be written in non-dimensional form as

$$\frac{U_R^2}{R^2} = \sum_{i=1}^{n} \left(\frac{v_i}{R} \frac{\partial R}{\partial v_i} \right)^2 \left(\frac{U_i}{v_i} \right)^2 \tag{C.4}$$

The uncertainties in directly measured variables assessed by Eq. (D.1) are shown in Table D.1. The evaluation for the uncertainties in calculated results are described in detail in the following sections.

Uncertainty in Mass flux

The mass flux is calculated as follows:

$$G = \frac{4\dot{m}}{D^2\pi}$$

The uncertainty is given by

$$\frac{U_G}{G} = \sqrt{\left(2\frac{U_D}{D}\right)^2 + \left(\frac{U\dot{m}}{\dot{m}}\right)^2}$$

$$= \sqrt{\left(2\frac{0.0254}{5.461}\right)^2 + (0.006)^2 + (0.0006)^2 + \left(\frac{0.000666}{\dot{m}}\right)^2}$$

which ranged from $0.015 - 0.0127$ in this experiment ($G = 2826 - 4648$ kg m^{-2} s^{-1}).

Uncertainty in Power

The power is calculated as follows:

$$\text{Power} = U \times I$$

The uncertainty is given by

$$\frac{U_{Power}}{Power} = \sqrt{\left(\frac{U_U}{U}\right)^2 + \left(\frac{U_I}{I}\right)^2}$$

$$= \sqrt{(0.006)^2 + (0.006)^2} = 0.0085$$

Table C.1 Evaluation of Uncertainties for the Directly Measured Variable

Measured Variable	Symbol	Units	Error Source	Device Range	Used Range	Uncertainties
Test section inside diameter	D	mm	Measuring device accuracy ± 0.001" => ± 0.0254 mm.	5.461	5.461	$U_D = 0.0254$ mm
Test section heated length	Lh	m	Measuring device accuracy ± 1mm.	2.5	1.22 - 2.2	$U_{Lh} = 0.001$ m
Pressure	P	kPa	Viatran pressure transducer Model 245 0 - 500 psi, 0 - 3447 kPa, output 0 - 5 V accuracy ± 0.1% FSO (Full Scale Output), (3447 kPa => ± 3.447 kPa) connected to National Instrument DAS AT-MIO-16E-1 with SCXI-1121 and terminal block SCXI-1320 accuracy ±0.15% of full scale reading, (3447 kPa => ± 5.171 kPa).	0 - 3447	1662 - 2389	$(U_P)_{max}=4.31$ kPa $\frac{U_P}{P} = 0.0018$
Mass flow rate	ṁ	$kg\ s^{-1}$	Miro Motion mass flow sensor DS040S119SC with RFT9739 Transmitter, 0 - 20 kg min^{-1} (0.333 kg s^{-1}), output 4 - 20 mA accuracy ±0.2% FSO (Full Scale Output), (0.333 kg s^{-1} => ± 0.000666 kg s^{-1}) connected to National Instrument DAS AT-MIO-16E-1 with SCXI-1120 accuracy ± 0.6% of reading and terminal block SCXI-1327 accuracy ± 0.06% of reading (the range of mass flux during experiments are from 2826 kg m^{-2} s^{-1} => 0.0662 kg s^{-1} to 4648 kg m^{-2} s^{-1} => 0.1089 kg s^{-1}).	0 - 0.333	0.0937 - 0.1523	$(U_{\dot{m}})_{max} = 0.001134 kgs^{-1}$ $\frac{U_{\dot{m}}}{\dot{m}} = \sqrt{(0.006)^2 + (0.0006)^2 + \left(\frac{0.000666}{\dot{m}}\right)^2}$

(Continued)

Table C.1 Evaluation of Uncertainties for the Directly Measured Variable (Continued)

Measured Variable	Symbol	Units	Error Source	Device Range	Used Range	Uncertainties
Test section electrical voltage	U	V	Sorensen power supply DCR 40 - 300, 0 - 40 V, output 0 - 5 V connected to National Instrument DAS AT-MIO-16E-1 with SCXI-1120 accuracy ± 0.6% of reading and terminal block SCXI-1327 accuracy ± 0.06% of reading.	0 - 40	0 - 40	$(U_U)_{max}$=0.241 V $\frac{U_U}{U} = 0.006$
Test section electrical current	I	A	Sorensen power supply DCR 40 - 300, 0 - 320 A, remote current monitor (pins no. 11 and no. 17) output 0 - 2.24 V scaled with Labview to current 0 - 320 A, connected to National Instrument DAS AT-MIO-16E-1 with SCXI-1120 accuracy ± 0.6% of reading and terminal block SCXI-1327 accuracy ± 0.06% of reading.	0 - 320	0 - 320	$(U_I)_{max}$=1.93 A $\frac{U_I}{I} = 0.006$
Inlet temperature	Tin	°C	OMEGA 3-wire platinum RTD 1/8" probe accuracy ± 0.8 °C connected to National Instrument DAS AT-MIO-16E-1 with SCXI-1121 and terminal block SCXI-1320 accuracy ± 0.15% of full sacle reading (100 °C => ± 0.15 °C).	0 - 100	0 - 76	$(U_{Tin})_{max}$=0.813 °C $\frac{U_{Tin}}{Tin} = \sqrt{\left(\frac{0.8}{Tin}\right)^2 + \left(\frac{0.15}{Tin}\right)^2}$
HFC-134a property	–	–	UO property code for HFC-134a based on Tillner-Roth and Baehr (1994) formulation accuracy ± 0.5%.	–	–	$\frac{U_{Prop}}{Prop} = 0.005$

Appendix D: AFD CHF Experimental Data

	Measured HFC-134a Data							Water-equivalent Data for L_h = 2.4 m					
Run	D_i	L_h	P	G	T_{in}	X_{in}	Power	P	G	T_{in}	X_{in}	Power	Author
No.	m	m	kPa	kg m^{-2} s^{-1}	°C	-	kW	kPa	kg m^{-2} s^{-1}	°C	-	kW	-
Uniform.1.	0.00546	2.2	2392.4	4609.7	53.21	-0.330	7.16	14022.0	6442.0	266.27	-0.382	100.99	Yang2002
Uniform.2.	0.00546	2.2	2391.7	4625.1	50.28	-0.366	7.45	14019.0	6463.1	257.87	-0.420	105.02	Yang2002
Uniform.3.	0.00546	2.2	2391.0	4647.1	47.15	-0.407	7.73	14015.0	6494.2	248.24	-0.463	108.96	Yang2002
Uniform.4.	0.00546	2.2	2389.0	4649.3	43.60	-0.453	8.02	14004.0	6497.6	237.28	-0.511	113.08	Yang2002
Uniform.5.	0.00546	2.2	2391.7	4647.1	40.48	-0.498	8.34	14019.0	6493.9	226.56	-0.558	117.68	Yang2002
Uniform.6.	0.00546	2.2	2390.4	4647.1	36.73	-0.541	8.69	14011.0	6494.6	215.60	-0.604	122.57	Yang2002
Uniform.7.	0.00546	2.2	2391.7	4649.3	33.19	-0.586	9.11	14019.0	6496.9	204.27	-0.652	128.44	Yang2002
Uniform.8.	0.00546	1.5	2387.0	4614.1	65.37	-0.154	4.86	13994.0	6448.1	264.64	-0.388	100.56	Yang2002
Uniform.9.	0.00546	1.5	2393.1	4642.7	63.69	-0.181	5.04	14026.0	6487.8	257.58	-0.422	104.17	Yang2002
Uniform.10.	0.00546	1.5	2389.0	4649.3	61.38	-0.213	5.24	14004.0	6497.6	248.14	-0.463	108.47	Yang2002
Uniform.11.	0.00546	1.5	2389.0	4658.1	58.87	-0.248	5.45	14004.0	6509.9	237.91	-0.508	112.84	Yang2002
Uniform.12.	0.00546	1.5	2389.7	4651.5	54.89	-0.303	5.81	14008.0	6500.3	221.14	-0.581	120.09	Yang2002
Uniform.13.	0.00546	1.5	2387.0	4649.3	52.38	-0.336	6.04	13994.0	6497.2	210.52	-0.624	124.87	Yang2002
Uniform.14.	0.00546	1.5	2385.6	4649.3	50.28	-0.364	6.23	13987.0	6497.2	201.56	-0.661	128.97	Yang2002
Uniform.15.	0.00546	2.2	2028.1	4574.5	47.99	-0.252	6.50	12036.0	6435.4	261.46	-0.295	92.94	Yang2002
Uniform.16.	0.00546	2.2	2028.1	4616.3	44.23	-0.297	6.83	12036.0	6494.2	250.01	-0.342	97.72	Yang2002
Uniform.17.	0.00546	2.2	2024.7	4618.5	41.73	-0.325	7.05	12018.0	6497.3	242.38	-0.371	100.90	Yang2002
Uniform.18.	0.00546	2.2	2026.1	4627.3	38.60	-0.361	7.34	12025.0	6509.8	232.62	-0.409	104.99	Yang2002
Uniform.19.	0.00546	2.2	2022.0	4627.3	36.10	-0.388	7.61	12003.0	6510.1	224.85	-0.438	108.82	Yang2002
Uniform.20.	0.00546	2.2	2021.4	4618.5	32.98	-0.423	7.83	12000.0	6497.4	215.18	-0.475	112.06	Yang2002
Uniform.21.	0.00546	2.2	2025.4	4618.5	28.41	-0.476	8.35	12021.0	6497.7	200.51	-0.531	119.49	Yang2002
Uniform.22.	0.00546	2.2	2026.1	4616.3	25.09	-0.513	8.75	12025.0	6494.3	189.85	-0.571	125.19	Yang2002
Uniform.23.	0.00546	2.2	2022.7	4620.7	22.40	-0.541	9.09	12007.0	6500.6	181.32	-0.601	130.06	Yang2002
Uniform.24.	0.00546	1.5	2030.1	4614.1	58.66	-0.121	4.45	12047.0	6490.9	256.77	-0.315	93.44	Yang2002
Uniform.25.	0.00546	1.5	2026.8	4618.5	56.56	-0.147	4.62	12029.0	6497.2	248.49	-0.347	97.02	Yang2002
Uniform.26.	0.00546	1.5	2029.5	4616.3	53.63	-0.184	4.84	12044.0	6493.7	236.84	-0.394	101.45	Yang2002
Uniform.27.	0.00546	1.5	2026.1	4614.1	50.28	-0.224	5.11	12025.0	6491.3	223.21	-0.446	107.30	Yang2002
Uniform.28.	0.00546	1.5	2023.4	4625.1	45.69	-0.278	5.60	12010.0	6507.1	203.29	-0.520	117.58	Yang2002
Uniform.29.	0.00546	1.5	2026.1	4618.5	40.27	-0.342	6.22	12025.0	6497.4	178.73	-0.612	130.45	Yang2002
Uniform.30.	0.00546	2.2	1668.5	4559.1	40.06	-0.214	6.09	10043.0	6447.7	248.81	-0.251	88.22	Yang2002
Uniform.31.	0.00546	2.2	1661.8	4592.1	38.18	-0.231	6.24	10005.0	6495.0	243.34	-0.269	90.42	Yang2002
Uniform.32.	0.00546	2.2	1662.5	4600.9	34.85	-0.266	6.49	10009.0	6507.3	233.14	-0.305	93.99	Yang2002

Uniform.33.	0.00546	2.2	1662.5	4596.5	30.90	-0.307	6.80	10009.0	6501.1	220.93	-0.348	98.52	Yang2002
Uniform.34.	0.00546	2.2	1661.1	4596.5	27.58	-0.341	7.11	10001.0	6501.4	210.59	-0.383	102.98	Yang2002
Uniform.35.	0.00546	2.2	1662.5	4589.9	24.47	-0.372	7.49	10009.0	6491.8	200.62	-0.418	108.46	Yang2002
Uniform.36.	0.00546	2.2	1663.2	4594.3	20.95	-0.408	7.87	10013.0	6497.8	189.45	-0.455	113.97	Yang2002
Uniform.37.	0.00546	2.2	1661.1	4594.3	17.84	-0.438	8.25	10001.0	6498.3	179.54	-0.488	119.53	Yang2002
Uniform.38.	0.00546	1.5	1665.2	4576.7	49.66	-0.109	4.29	10024.0	6472.9	240.46	-0.280	91.16	Yang2002
Uniform.39.	0.00546	1.5	1666.5	4594.3	47.99	-0.128	4.42	10032.0	6497.4	233.98	-0.304	93.91	Yang2002
Uniform.40.	0.00546	1.5	1666.5	4589.9	45.69	-0.153	4.57	10032.0	6491.2	225.15	-0.335	96.97	Yang2002
Uniform.41.	0.00546	1.5	1665.2	4600.9	42.56	-0.186	4.81	10024.0	6507.1	212.77	-0.377	102.12	Yang2002
Uniform.42.	0.00546	1.5	1663.8	4594.3	40.27	-0.210	5.01	10017.0	6497.6	203.20	-0.409	106.47	Yang2002
Uniform.43.	0.00546	1.5	1664.5	4592.1	35.90	-0.256	5.46	10020.0	6494.9	184.20	-0.473	115.91	Yang2002
Uniform.44.	0.00546	1.5	1665.2	4592.1	30.49	-0.312	6.07	10024.0	6494.7	159.88	-0.554	128.84	Yang2002
Uniform.45.	0.00546	1.5	1665.8	4603.1	28.83	-0.330	6.28	10028.0	6510.0	152.28	-0.579	133.29	Yang2002
Uniform.46.	0.00546	2.2	2392.4	3578.4	66.84	-0.134	4.59	14022.0	5000.7	307.73	-0.178	64.78	Yang2002
Uniform.47.	0.00546	2.2	2387.0	3569.6	65.58	-0.151	4.61	13994.0	4988.4	304.32	-0.194	64.97	Yang2002
Uniform.48.	0.00546	2.2	2389.0	3585.0	63.48	-0.182	4.71	14004.0	5010.2	298.22	-0.227	66.45	Yang2002
Uniform.49.	0.00546	2.2	2390.4	3578.4	59.70	-0.237	4.94	14011.0	5001.0	286.98	-0.283	69.68	Yang2002
Uniform.50.	0.00546	2.2	2391.7	3571.8	56.98	-0.275	5.16	14019.0	4991.2	278.67	-0.324	72.76	Yang2002
Uniform.51.	0.00546	2.2	2391.7	3571.8	53.84	-0.318	5.40	14019.0	4991.2	269.05	-0.369	76.10	Yang2002
Uniform.52.	0.00546	2.2	2389.7	3574.0	50.28	-0.365	5.62	14008.0	4994.5	258.19	-0.418	79.33	Yang2002
Uniform.53.	0.00546	2.2	2389.7	3576.2	47.15	-0.407	5.87	14008.0	4997.6	248.43	-0.462	82.81	Yang2002
Uniform.54.	0.00546	2.2	2390.4	3576.2	45.06	-0.434	6.06	14011.0	4997.9	241.81	-0.491	85.48	Yang2002
Uniform.55.	0.00546	2	2383.6	3578.4	50.08	-0.365	5.40	13976.0	5000.9	244.59	-0.477	83.76	Yang2002
Uniform.56.	0.00546	2	2382.3	3587.2	50.08	-0.365	5.40	13969.0	5013.2	244.68	-0.476	83.76	Yang2002
Uniform.57.	0.00546	2	2385.6	3565.2	49.87	-0.369	5.41	13987.0	4982.2	243.75	-0.481	83.96	Yang2002
Uniform.58.	0.00546	2	2356.7	3582.8	54.89	-0.290	4.95	13830.0	5009.8	261.82	-0.391	76.82	Yang2002
Uniform.59.	0.00546	2	2443.6	3567.4	44.85	-0.461	5.97	14299.0	4979.8	224.47	-0.587	92.40	Yang2002
Uniform.60.	0.00546	2	2404.5	3578.4	40.06	-0.506	6.27	14088.0	4999.2	209.45	-0.636	97.21	Yang2002
Uniform.61.	0.00546	2	2404.5	3582.8	35.06	-0.569	6.73	14088.0	5005.4	191.98	-0.709	104.30	Yang2002
Uniform.62.	0.00546	2	2422.7	3519.0	30.70	-0.633	7.16	14186.0	4914.6	175.43	-0.785	110.87	Yang2002
Uniform.63.	0.00546	2	2423.4	3508.0	30.70	-0.633	7.16	14190.0	4898.9	175.30	-0.786	110.86	Yang2002
Uniform.64.	0.00546	2	2395.7	3596.0	25.09	-0.689	7.66	14040.0	5025.1	157.20	-0.847	118.90	Yang2002
Uniform.65.	0.00546	2	2384.3	3587.2	21.77	-0.723	7.93	13980.0	5012.9	145.97	-0.886	123.06	Yang2002
Uniform.66.	0.00546	2	2387.0	3567.4	21.57	-0.727	7.93	13994.0	4985.3	145.05	-0.891	123.06	Yang2002
Uniform.67.	0.00546	1.22	2401.1	3576.2	49.24	-0.384	4.69	14069.0	4996.9	155.74	-0.855	119.13	Yang2002
Uniform.68.	0.00546	1.22	2394.4	3571.8	54.68	-0.308	4.13	14033.0	4991.3	187.51	-0.723	105.06	Yang2002
Uniform.69.	0.00546	1.22	2389.0	3556.4	44.44	-0.442	5.05	14004.0	4970.2	130.37	-0.951	128.46	Yang2002
Uniform.70.	0.00546	2.2	2027.4	3552.0	42.56	-0.316	5.42	12033.0	4996.7	244.76	-0.362	77.54	Yang2002

Uniform.71.	0.00546	2.2	2026.1	3552.0	44.65	-0.291	5.24	12025.0	4997.0	251.33	-0.336	74.94	Yang2002
Uniform.72.	0.00546	2.2	2026.8	3552.0	49.03	-0.239	4.98	12029.0	4996.8	264.67	-0.282	71.17	Yang2002
Uniform.73.	0.00546	2.2	2024.1	3556.4	52.79	-0.193	4.73	12014.0	5003.3	276.12	-0.233	67.67	Yang2002
Uniform.74.	0.00546	2.2	2022.7	3556.4	56.56	-0.145	4.47	12007.0	5003.3	287.43	-0.183	63.88	Yang2002
Uniform.75.	0.00546	2.2	2028.8	3558.6	59.70	-0.108	4.29	12040.0	5006.0	296.42	-0.144	61.38	Yang2002
Uniform.76.	0.00546	2.2	2025.4	3558.6	62.43	-0.071	4.17	12021.0	5006.5	304.24	-0.107	59.62	Yang2002
Uniform.77.	0.00546	2.2	2028.8	3554.2	64.11	-0.050	4.09	12040.0	4999.8	308.84	-0.085	58.52	Yang2002
Uniform.78.	0.00546	2	2014.6	3547.6	50.28	-0.220	4.49	11963.0	4991.3	258.42	-0.304	70.72	Yang2002
Uniform.79.	0.00546	2	2008.6	3565.2	50.28	-0.218	4.49	11929.0	5016.9	258.67	-0.301	70.75	Yang2002
Uniform.80.	0.00546	2	2022.0	3563.0	50.49	-0.220	4.47	12003.0	5012.7	259.03	-0.303	70.38	Yang2002
Uniform.81.	0.00546	2	2032.8	3560.8	49.87	-0.231	4.59	12062.0	5008.8	256.34	-0.317	72.25	Yang2002
Uniform.82.	0.00546	2	1974.2	3545.4	54.68	-0.152	4.19	11740.0	4991.8	273.80	-0.230	66.06	Yang2002
Uniform.83.	0.00546	2	2086.0	3578.4	44.85	-0.311	5.04	12354.0	5029.1	237.93	-0.407	79.12	Yang2002
Uniform.84.	0.00546	2	2042.2	3571.8	40.27	-0.348	5.32	12114.0	5023.4	223.88	-0.448	83.68	Yang2002
Uniform.85.	0.00546	2	2053.0	3565.2	35.06	-0.413	5.80	12173.0	5013.3	205.39	-0.522	91.21	Yang2002
Uniform.86.	0.00546	2	2035.5	3525.6	30.49	-0.457	6.14	12077.0	4959.1	189.94	-0.574	96.60	Yang2002
Uniform.87.	0.00546	2	2036.2	3538.8	30.49	-0.458	6.13	12081.0	4977.4	190.08	-0.574	96.47	Yang2002
Uniform.88.	0.00546	2	2030.8	3558.6	24.88	-0.518	6.69	12051.0	5005.9	170.53	-0.643	105.18	Yang2002
Uniform.89.	0.00546	2	2033.5	3552.0	21.77	-0.553	7.01	12066.0	4996.3	159.25	-0.685	110.34	Yang2002
Uniform.90.	0.00546	2	2033.5	3558.6	21.57	-0.555	7.01	12066.0	5005.6	158.73	-0.687	110.28	Yang2002
Uniform.91.	0.00546	1.22	2057.7	3567.4	49.66	-0.243	3.80	12199.0	5016.0	187.82	-0.590	97.92	Yang2002
Uniform.92.	0.00546	1.22	2032.8	3571.8	54.68	-0.172	3.32	12062.0	5024.3	216.60	-0.473	85.68	Yang2002
Uniform.93.	0.00546	1.22	2030.1	3565.2	44.65	-0.292	4.22	12047.0	5015.4	161.74	-0.675	108.80	Yang2002
Uniform.94.	0.00546	1.22	2039.6	3571.8	37.56	-0.379	4.87	12099.0	5023.8	122.06	-0.821	125.63	Yang2002
Uniform.95.	0.00546	1.22	2031.5	3541.0	39.85	-0.349	4.59	12055.0	4980.9	135.96	-0.768	118.31	Yang2002
Uniform.96.	0.00546	1.22	2034.2	3578.4	39.85	-0.350	4.59	12070.0	5033.2	137.12	-0.765	118.29	Yang2002
Uniform.97.	0.00546	1.22	2024.7	3534.4	35.06	-0.401	5.05	12018.0	4972.2	108.56	-0.862	130.17	Yang2002
Uniform.98.	0.00546	2	1657.8	3512.4	50.49	-0.097	4.00	9983.0	4967.9	270.79	-0.166	63.73	Yang2002
Uniform.99.	0.00546	2	1652.4	3541.0	50.28	-0.098	4.01	9953.0	5008.6	270.46	-0.167	63.83	Yang2002
Uniform.100.	0.00546	2	1652.4	3545.4	50.28	-0.098	4.00	9953.0	5014.9	270.49	-0.166	63.79	Yang2002
Uniform.101.	0.00546	2	1654.4	3541.0	50.08	-0.101	4.02	9964.0	5008.6	269.75	-0.170	64.06	Yang2002
Uniform.102.	0.00546	2	1651.7	3516.8	50.08	-0.100	4.05	9949.0	4974.6	269.59	-0.170	64.47	Yang2002
Uniform.103.	0.00546	2	1658.4	3519.0	50.08	-0.102	4.05	9986.0	4977.5	269.40	-0.172	64.47	Yang2002
Uniform.104.	0.00546	2	1665.8	3530.0	50.08	-0.104	4.05	10028.0	4992.4	269.25	-0.174	64.45	Yang2002
Uniform.105.	0.00546	2	1659.8	3534.4	50.08	-0.102	4.08	9994.0	4999.0	269.28	-0.173	65.07	Yang2002
Uniform.106.	0.00546	2	1661.8	3541.0	50.08	-0.103	4.08	10005.0	5008.3	269.28	-0.173	64.97	Yang2002
Uniform.107.	0.00546	2	1673.9	3650.9	54.68	-0.055	3.95	10073.0	5162.9	283.27	-0.121	62.97	Yang2002
Uniform.108.	0.00546	2	1714.3	3569.6	44.85	-0.178	4.37	10299.0	5045.0	251.23	-0.253	69.53	Yang2002

Uniform.109.	0.00546	2	1681.3	3525.6	40.27	-0.216	4.54	10114.0	4985.4	237.53	-0.295	72.24	Yang2002
Uniform.110.	0.00546	2	1689.4	3536.6	35.06	-0.274	4.93	10160.0	5000.0	219.87	-0.359	78.40	Yang2002
Uniform.111.	0.00546	2	1669.2	3538.8	30.49	-0.314	5.33	10047.0	5004.5	204.74	-0.406	84.81	Yang2002
Uniform.112.	0.00546	2	1665.2	3552.0	24.68	-0.371	5.78	10024.0	5023.6	185.12	-0.470	92.02	Yang2002
Uniform.113.	0.00546	2	1660.5	3519.0	21.57	-0.401	6.09	9998.0	4977.1	173.97	-0.506	96.97	Yang2002
Uniform.114.	0.00546	1.22	1657.8	3536.6	46.32	-0.143	3.27	9983.0	5002.1	201.06	-0.415	85.38	Yang2002
Uniform.115.	0.00546	1.22	1673.9	3545.4	49.03	-0.119	3.06	10073.0	5013.7	214.60	-0.373	79.83	Yang2002
Uniform.116.	0.00546	1.22	1659.8	3532.2	54.47	-0.053	2.71	9994.0	4995.9	240.44	-0.279	70.78	Yang2002
Uniform.117.	0.00546	1.22	1669.2	3510.2	37.77	-0.238	3.98	10047.0	4964.1	154.62	-0.572	103.81	Yang2002
Uniform.118.	0.00546	1.22	1671.9	3549.8	40.06	-0.215	3.79	10062.0	5019.9	167.85	-0.530	98.87	Yang2002
Uniform.119.	0.00546	1.22	1663.8	3541.0	40.27	-0.210	3.79	10017.0	5007.9	168.55	-0.525	98.89	Yang2002
Uniform.120.	0.00546	1.22	1655.7	3543.2	35.06	-0.262	4.25	9971.0	5011.9	140.28	-0.614	110.99	Yang2002
Uniform.121.	0.00546	1.22	1665.2	3516.8	32.36	-0.293	4.48	10024.0	4973.8	124.56	-0.668	116.91	Yang2002
Uniform.122.	0.00546	1.22	1665.8	3556.4	29.86	-0.319	4.77	10028.0	5029.7	110.31	-0.714	124.50	Yang2002
Uniform.123.	0.00546	0.7	1669.2	3565.2	50.08	-0.105	2.38	10047.0	5041.8	146.46	-0.599	108.12	Yang2002
Uniform.124.	0.00546	0.7	1668.5	3582.8	55.10	-0.049	2.02	10043.0	5066.9	187.01	-0.465	91.74	Yang2002
Uniform.125.	0.00546	2.2	2391.7	2859.3	39.85	-0.502	5.30	14019.0	3995.6	225.02	-0.565	74.81	Yang2002
Uniform.126.	0.00546	2.2	2389.7	2863.7	42.98	-0.461	5.06	14008.0	4001.9	235.08	-0.521	71.40	Yang2002
Uniform.127.	0.00546	2.2	2388.3	2859.3	46.73	-0.412	4.79	14000.0	3996.2	246.96	-0.468	67.55	Yang2002
Uniform.128.	0.00546	2.2	2389.7	2859.3	49.66	-0.374	4.60	14008.0	3995.8	256.10	-0.428	64.88	Yang2002
Uniform.129.	0.00546	2.2	2391.7	2859.3	53.21	-0.327	4.35	14019.0	3995.6	267.14	-0.378	61.29	Yang2002
Uniform.130.	0.00546	2.2	2389.7	2859.3	61.17	-0.216	3.79	14008.0	3995.8	291.57	-0.260	53.51	Yang2002
Uniform.131.	0.00546	2.2	2389.0	2861.5	64.95	-0.161	3.54	14004.0	3999.1	302.84	-0.203	49.98	Yang2002
Uniform.132.	0.00546	2.2	2390.4	2859.3	67.68	-0.121	3.37	14011.0	3996.0	310.75	-0.161	47.48	Yang2002
Uniform.133.	0.00546	2.2	2388.3	2859.3	70.83	-0.072	3.14	14000.0	3996.2	319.76	-0.109	44.30	Yang2002
Uniform.134.	0.00546	2.2	2389.0	2861.5	73.36	-0.032	3.03	14004.0	3999.1	326.57	-0.068	42.80	Yang2002
Uniform.135.	0.00546	2	2375.5	2859.3	50.28	-0.359	4.29	13932.0	3996.7	245.53	-0.470	66.55	Yang2002
Uniform.136.	0.00546	2	2378.2	2859.3	50.28	-0.360	4.28	13947.0	3996.3	245.49	-0.471	66.49	Yang2002
Uniform.137.	0.00546	2	2389.7	2868.1	50.28	-0.365	4.32	14008.0	4008.1	245.10	-0.477	66.95	Yang2002
Uniform.138.	0.00546	2	2444.9	2850.5	45.06	-0.459	4.78	14306.0	3979.1	224.99	-0.586	74.03	Yang2002
Uniform.139.	0.00546	2	2407.9	2870.3	40.06	-0.507	5.08	14106.0	4009.8	209.02	-0.639	78.83	Yang2002
Uniform.140.	0.00546	2	2403.8	2841.7	35.27	-0.566	5.49	14084.0	3970.2	191.67	-0.710	85.07	Yang2002
Uniform.141.	0.00546	2	2401.1	2938.5	30.49	-0.625	5.87	14069.0	4105.9	175.95	-0.773	91.02	Yang2002
Uniform.142.	0.00546	2	2393.1	2868.1	25.09	-0.687	6.25	14026.0	4007.9	156.38	-0.849	96.98	Yang2002
Uniform.143.	0.00546	2	2385.6	2868.1	21.57	-0.726	6.47	13987.0	4008.0	144.51	-0.893	100.33	Yang2002
Uniform.144.	0.00546	1.22	2407.9	2863.7	49.87	-0.379	3.78	14106.0	4000.6	156.79	-0.854	96.08	Yang2002
Uniform.145.	0.00546	1.22	2396.4	2837.3	54.68	-0.309	3.40	14044.0	3964.7	183.96	-0.738	86.34	Yang2002
Uniform.146.	0.00546	1.22	2392.4	2854.9	44.65	-0.441	4.14	14022.0	3989.7	128.27	-0.961	105.28	Yang2002

Uniform.147.	0.00546	1.22	2397.8	2854.9	39.85	-0.505	4.52	14051.0	3989.3	100.38	-1.074	114.89	Yang2002
Uniform.148.	0.00546	1.22	2383.0	2854.9	39.85	-0.498	4.55	13972.0	3990.0	99.61	-1.068	115.86	Yang2002
Uniform.149.	0.00546	1.22	2393.7	2865.9	37.56	-0.532	4.72	14029.0	4005.0	87.09	-1.123	120.10	Yang2002
Uniform.150.	0.00546	2.2	2024.1	2843.9	41.52	-0.327	4.50	12014.0	4001.0	241.34	-0.375	64.42	Yang2002
Uniform.151.	0.00546	2.2	2026.8	2841.7	44.44	-0.294	4.30	12029.0	3997.6	250.42	-0.340	61.47	Yang2002
Uniform.152.	0.00546	2.2	2026.8	2839.5	48.61	-0.244	4.02	12029.0	3994.5	263.34	-0.287	57.52	Yang2002
Uniform.153.	0.00546	2.2	2027.4	2837.3	51.96	-0.204	3.84	12033.0	3991.3	273.49	-0.245	54.91	Yang2002
Uniform.154.	0.00546	2.2	2025.4	2843.9	56.14	-0.152	3.64	12021.0	4001.0	285.99	-0.190	52.12	Yang2002
Uniform.155.	0.00546	2.2	2027.4	2841.7	59.70	-0.107	3.37	12033.0	3997.5	296.58	-0.143	48.26	Yang2002
Uniform.156.	0.00546	2.2	2026.1	2837.3	62.01	-0.077	3.21	12025.0	3991.6	303.33	-0.111	45.94	Yang2002
Uniform.157.	0.00546	2.2	2026.8	2841.7	63.48	-0.058	3.07	12029.0	3997.6	307.62	-0.091	43.95	Yang2002
Uniform.158.	0.00546	2.2	2026.8	2837.3	65.58	-0.030	2.91	12029.0	3991.4	313.55	-0.061	41.66	Yang2002
Uniform.159.	0.00546	2	2018.7	2837.3	50.28	-0.221	3.64	11985.0	3991.8	258.06	-0.306	57.23	Yang2002
Uniform.160.	0.00546	2	2032.1	2848.3	49.45	-0.236	3.76	12058.0	4006.8	254.59	-0.324	59.18	Yang2002
Uniform.161.	0.00546	2	2094.1	2848.3	44.85	-0.314	4.15	12398.0	4002.6	236.86	-0.414	65.21	Yang2002
Uniform.162.	0.00546	2	2097.5	2797.7	44.85	-0.316	4.15	12417.0	3931.1	236.35	-0.417	65.15	Yang2002
Uniform.163.	0.00546	2	2047.6	2830.7	40.06	-0.353	4.45	12144.0	3980.7	221.70	-0.458	69.89	Yang2002
Uniform.164.	0.00546	2	2053.7	2824.1	35.06	-0.413	4.80	12177.0	3971.1	204.07	-0.527	75.49	Yang2002
Uniform.165.	0.00546	2	2036.9	2859.3	30.49	-0.458	5.11	12084.0	4021.9	189.09	-0.577	80.34	Yang2002
Uniform.166.	0.00546	2	2040.9	2824.1	24.68	-0.524	5.55	12107.0	3971.8	168.06	-0.656	87.28	Yang2002
Uniform.167.	0.00546	2	2038.2	2846.1	21.57	-0.557	5.81	12092.0	4003.0	157.27	-0.694	91.42	Yang2002
Uniform.168.	0.00546	1.22	2039.6	2857.1	46.52	-0.274	3.42	12099.0	4018.6	166.39	-0.661	88.16	Yang2002
Uniform.169.	0.00546	1.22	2061.8	2852.7	49.24	-0.249	3.25	12221.0	4010.9	179.68	-0.621	83.84	Yang2002
Uniform.170.	0.00546	1.22	2031.5	2815.3	54.89	-0.169	2.79	12055.0	3960.2	212.17	-0.489	71.93	Yang2002
Uniform.171.	0.00546	1.22	2044.3	2841.7	37.77	-0.378	4.05	12125.0	3996.5	116.96	-0.841	104.46	Yang2002
Uniform.172.	0.00546	1.22	2042.9	2839.5	40.06	-0.351	3.90	12118.0	3993.4	129.20	-0.797	100.57	Yang2002
Uniform.173.	0.00546	1.22	2065.1	2861.5	35.27	-0.415	4.34	12240.0	4022.8	100.12	-0.910	111.69	Yang2002
Uniform.174.	0.00546	1.22	2032.8	2835.1	32.57	-0.433	4.44	12062.0	3988.1	87.46	-0.940	114.62	Yang2002
Uniform.175.	0.00546	1.22	2034.2	2846.1	27.58	-0.489	4.84	12070.0	4003.2	59.12	-1.040	124.87	Yang2002
Uniform.176.	0.00546	0.7	2033.5	2835.1	49.66	-0.234	2.68	12066.0	3987.9	70.04	-1.001	120.37	Yang2002
Uniform.177.	0.00546	0.7	2038.2	2821.9	55.10	-0.169	2.29	12092.0	3969.0	119.41	-0.829	103.00	Yang2002
Uniform.178.	0.00546	0.7	2038.2	2835.1	55.10	-0.169	2.29	12092.0	3987.6	120.28	-0.826	103.00	Yang2002
Uniform.179.	0.00546	0.7	2032.1	2861.5	49.66	-0.233	2.68	12058.0	4025.3	71.76	-0.994	120.57	Yang2002
Uniform.180.	0.00546	0.7	2038.2	2854.9	55.10	-0.169	2.29	12092.0	4015.4	121.57	-0.822	103.00	Yang2002
Uniform.181.	0.00546	2	1653.7	2824.1	50.49	-0.096	3.52	9960.0	3994.7	269.20	-0.172	56.06	Yang2002
Uniform.182.	0.00546	2	1652.4	2839.5	50.49	-0.096	3.49	9953.0	4016.4	269.53	-0.170	55.55	Yang2002
Uniform.183.	0.00546	2	1651.7	2821.9	50.49	-0.095	3.48	9949.0	3991.6	269.45	-0.170	55.50	Yang2002
Uniform.184.	0.00546	2	1668.5	2821.9	51.33	-0.091	3.36	10043.0	3990.8	272.08	-0.164	53.56	Yang2002

Uniform.185.	0.00546	2	1661.1	2821.9	54.68	-0.051	3.10	10001.0	3991.4	283.39	-0.118	49.36	Yang2002
Uniform.186.	0.00546	2	1739.2	2813.1	54.89	-0.073	3.22	10438.0	3974.5	281.15	-0.144	51.20	Yang2002
Uniform.187.	0.00546	2	1685.4	2815.3	54.89	-0.056	3.10	10137.0	3980.7	283.29	-0.124	49.33	Yang2002
Uniform.188.	0.00546	2	1678.0	2808.7	54.68	-0.056	3.10	10096.0	3971.6	282.84	-0.124	49.37	Yang2002
Uniform.189.	0.00546	2	1686.0	2808.7	54.68	-0.059	3.13	10141.0	3971.2	282.48	-0.127	49.76	Yang2002
Uniform.190.	0.00546	2	1722.4	2865.9	45.06	-0.178	3.82	10344.0	4050.1	249.81	-0.261	60.74	Yang2002
Uniform.191.	0.00546	2	1678.0	2793.3	40.06	-0.217	4.03	10096.0	3949.8	234.33	-0.305	64.20	Yang2002
Uniform.192.	0.00546	2	1678.6	2830.7	40.27	-0.215	4.03	10099.0	4002.9	235.26	-0.302	64.20	Yang2002
Uniform.193.	0.00546	2	1678.0	2837.3	40.27	-0.215	4.04	10096.0	4012.0	235.33	-0.302	64.25	Yang2002
Uniform.194.	0.00546	2	1681.3	2848.3	35.06	-0.271	4.36	10114.0	4027.6	217.68	-0.365	69.42	Yang2002
Uniform.195.	0.00546	2	1663.2	2795.5	30.49	-0.312	4.62	10013.0	3953.7	202.29	-0.412	73.55	Yang2002
Uniform.196.	0.00546	2	1668.5	2817.5	24.68	-0.373	4.98	10043.0	3984.6	182.41	-0.481	79.38	Yang2002
Uniform.197.	0.00546	2	1669.9	2815.3	21.57	-0.404	5.21	10050.0	3981.6	171.46	-0.517	82.92	Yang2002
Uniform.198.	0.00546	1.22	1663.2	2815.3	46.11	-0.147	2.96	10013.0	3981.7	189.05	-0.457	77.32	Yang2002
Uniform.199.	0.00546	1.22	1679.3	2815.3	49.24	-0.118	2.79	10103.0	3981.0	204.06	-0.411	72.80	Yang2002
Uniform.200.	0.00546	1.22	1657.8	2828.5	55.31	-0.043	2.49	9983.0	4000.6	233.99	-0.301	64.90	Yang2002
Uniform.201.	0.00546	1.22	1674.6	2824.1	37.98	-0.238	3.47	10077.0	3993.6	146.56	-0.600	90.48	Yang2002
Uniform.202.	0.00546	1.22	1684.0	2819.7	40.06	-0.219	3.36	10130.0	3986.8	156.35	-0.572	87.61	Yang2002
Uniform.203.	0.00546	1.22	1618.0	2863.7	35.06	-0.248	3.61	9760.0	4052.6	135.75	-0.616	94.51	Yang2002
Uniform.204.	0.00546	1.22	1655.7	2819.7	32.36	-0.290	3.73	9971.0	3988.5	120.37	-0.678	97.36	Yang2002
Uniform.205.	0.00546	1.22	1667.2	2828.5	30.07	-0.317	4.05	10035.0	4000.4	102.48	-0.739	105.78	Yang2002
Uniform.206.	0.00546	1.22	1665.8	2873.2	24.68	-0.372	4.46	10028.0	4063.5	74.23	-0.829	116.43	Yang2002
Uniform.207.	0.00546	1.22	1658.4	2813.1	27.37	-0.342	4.15	9986.0	3979.1	90.00	-0.776	108.50	Yang2002
Uniform.208.	0.00546	1.22	1665.2	2835.1	21.57	-0.403	4.60	10024.0	4009.7	57.86	-0.880	120.10	Yang2002
Uniform.209.	0.00546	1.22	1659.8	2828.5	21.57	-0.400	4.60	9994.0	4000.6	57.78	-0.878	120.04	Yang2002
Uniform.210.	0.00546	1.22	1671.2	2868.8	18.25	-0.438	4.90	10058.0	4057.1	39.14	-0.942	128.01	Yang2002
Uniform.211.	0.00546	0.7	1673.3	2815.3	49.66	-0.111	2.16	10069.0	3981.4	121.77	-0.680	98.28	Yang2002
Uniform.212.	0.00546	0.7	1663.8	2815.3	54.89	-0.050	1.85	10017.0	3981.6	165.74	-0.534	83.97	Yang2002
TS NO.1 Forward.1.	0.00546	2.000	2390.4	4627.3	66.00	-0.149	5.95	14011.0	6466.9	312.08	-0.153	80.10	Yang2002
TS NO.1 Forward.2.	0.00546	2.000	2387.7	4611.9	65.16	-0.160	6.08	13998.0	6444.6	309.87	-0.165	81.92	Yang2002
TS NO.1 Forward.3.	0.00546	2.000	2387.0	4622.9	60.75	-0.224	6.41	13994.0	6460.4	297.76	-0.228	86.39	Yang2002
TS NO.1 Forward.4.	0.00546	2.000	2387.7	4682.3	55.51	-0.297	7.01	13998.0	6543.0	283.57	-0.299	94.46	Yang2002
TS NO.1 Forward.5.	0.00546	2.000	2392.4	4622.9	50.70	-0.361	7.42	14022.0	6460.4	269.65	-0.367	99.95	Yang2002
TS NO.1 Forward.6.	0.00546	2.000	2386.3	4691.1	45.27	-0.430	8.03	13990.0	6556.0	254.02	-0.436	108.25	Yang2002
TS NO.1 Forward.7.	0.00546	2.000	2405.8	4647.1	39.64	-0.512	8.75	14095.0	6492.3	236.98	-0.518	117.75	Yang2002
TS NO.1 Forward.8.	0.00546	2.000	2395.7	4653.7	35.06	-0.565	9.21	14040.0	6503.1	223.68	-0.572	124.09	Yang2002
TS NO.1 Forward.9.	0.00546	2.000	2392.4	4642.7	30.07	-0.626	9.89	14022.0	6488.1	208.93	-0.633	133.27	Yang2002
TS NO.1 Forward.10.	0.00546	1.490	2393.1	4629.5	46.73	-0.414	7.29	14026.0	6469.3	216.82	-0.600	128.59	Yang2002

TS NO.1 Forward.11.	0.00546	1.490	2392.4	4616.3	40.06	-0.500	8.09	14022.0	6451.2	191.04	-0.708	142.69	Yang2002
TS NO.1 Forward.12.	0.00546	1.490	2393.1	4638.3	35.06	-0.564	8.71	14026.0	6481.6	171.68	-0.787	153.63	Yang2002
TS NO.1 Forward.13.	0.00546	1.490	2389.0	4644.9	30.90	-0.614	9.07	14004.0	6491.5	156.76	-0.845	160.01	Yang2002
TS NO.1 Forward.14.	0.00546	1.490	2391.7	4642.7	23.43	-0.707	10.01	14019.0	6487.7	127.45	-0.964	176.57	Yang2002
TS NO.1 Forward.15.	0.00546	1.490	2374.2	4642.7	11.84	-0.836	11.49	13925.0	6489.5	83.00	-1.128	202.82	Yang2002
TS NO.1 Forward.16.	0.00546	1.490	2371.5	4664.7	10.40	-0.851	11.65	13910.0	6520.9	78.01	-1.146	205.70	Yang2002
TS NO.1 Forward.17.	0.00546	1.490	2384.3	4625.1	13.50	-0.822	11.34	13980.0	6463.4	88.47	-1.113	200.19	Yang2002
TS NO.1 Forward.18.	0.00546	1.490	2381.6	4605.3	19.08	-0.754	10.52	13965.0	6436.4	110.45	-1.025	185.73	Yang2002
TS NO.1 Forward.19.	0.00546	1.490	2355.3	4622.9	19.70	-0.732	10.37	13823.0	6464.2	114.39	-0.996	183.24	Yang2002
TS NO.1 Forward.20.	0.00546	2.000	2028.8	4497.5	63.90	-0.053	4.89	12040.0	6326.9	314.52	-0.056	66.85	Yang2002
TS NO.1 Forward.21.	0.00546	2.000	2023.4	4570.1	62.85	-0.065	5.00	12010.0	6429.8	311.91	-0.069	68.30	Yang2002
TS NO.1 Forward.22.	0.00546	2.000	2034.2	4552.5	60.33	-0.101	5.28	12070.0	6403.4	305.00	-0.105	72.08	Yang2002
TS NO.1 Forward.23.	0.00546	2.000	2029.5	4622.9	54.89	-0.168	5.79	12044.0	6503.0	290.24	-0.173	79.03	Yang2002
TS NO.1 Forward.24.	0.00546	2.000	2036.9	4664.7	50.70	-0.223	6.31	12084.0	6561.4	278.26	-0.227	86.23	Yang2002
TS NO.1 Forward.25.	0.00546	2.000	2034.8	4638.3	45.06	-0.289	6.84	12073.0	6524.4	262.16	-0.294	93.38	Yang2002
TS NO.1 Forward.26.	0.00546	2.000	2028.8	4620.7	40.48	-0.341	7.31	12040.0	6500.1	249.01	-0.346	99.88	Yang2002
TS NO.1 Forward.27.	0.00546	2.000	2030.8	4596.5	35.27	-0.401	7.91	12051.0	6465.9	233.66	-0.407	108.04	Yang2002
TS NO.1 Forward.28.	0.00546	2.000	2032.1	4627.3	29.86	-0.463	8.54	12058.0	6509.3	217.64	-0.469	116.62	Yang2002
TS NO.1 Forward.29.	0.00546	2.000	2032.8	4611.9	23.23	-0.537	9.39	12062.0	6487.4	197.92	-0.543	128.24	Yang2002
TS NO.1 Forward.30.	0.00546	1.490	2034.2	4636.1	40.06	-0.348	6.86	12070.0	6521.0	208.10	-0.506	122.68	Yang2002
TS NO.1 Forward.31.	0.00546	1.490	2026.1	4618.5	35.27	-0.399	7.31	12025.0	6497.4	190.51	-0.568	130.78	Yang2002
TS NO.1 Forward.32.	0.00546	1.490	2031.5	4642.7	30.49	-0.456	7.90	12055.0	6530.7	171.98	-0.638	141.41	Yang2002
TS NO.1 Forward.33.	0.00546	1.490	2030.8	4616.3	23.85	-0.529	8.73	12051.0	6493.8	145.98	-0.732	156.24	Yang2002
TS NO.1 Forward.34.	0.00546	1.490	2029.5	4614.1	12.26	-0.654	10.17	12044.0	6490.6	101.13	-0.890	181.93	Yang2002
TS NO.1 Forward.35.	0.00546	1.490	2034.8	4618.5	10.19	-0.679	10.49	12073.0	6496.6	92.55	-0.923	187.74	Yang2002
TS NO.1 Forward.36.	0.00546	1.490	2030.8	4611.9	13.70	-0.639	9.98	12051.0	6487.6	106.50	-0.872	178.55	Yang2002
TS NO.1 Forward.37.	0.00546	1.490	2028.8	4625.1	16.81	-0.605	9.54	12040.0	6506.3	119.25	-0.826	170.65	Yang2002
TS NO.1 Forward.38.	0.00546	1.490	2033.5	4614.1	18.46	-0.589	9.33	12066.0	6490.3	125.50	-0.806	166.84	Yang2002
TS NO.1 Forward.39.	0.00546	1.490	2034.2	4611.9	21.98	-0.551	8.91	12070.0	6486.9	138.87	-0.758	159.35	Yang2002
TS NO.1 Forward.40.	0.00546	2.000	1667.2	4493.2	54.05	-0.060	4.74	10035.0	6354.7	296.99	-0.063	65.53	Yang2002
TS NO.1 Forward.41.	0.00546	2.000	1663.8	4578.9	52.17	-0.080	4.87	10017.0	6475.8	292.02	-0.084	67.37	Yang2002
TS NO.1 Forward.42.	0.00546	2.000	1668.5	4567.9	50.08	-0.105	5.09	10043.0	6460.1	286.15	-0.109	70.44	Yang2002
TS NO.1 Forward.43.	0.00546	2.000	1668.5	4605.3	45.06	-0.160	5.57	10043.0	6513.0	272.11	-0.164	77.06	Yang2002
TS NO.1 Forward.44.	0.00546	2.000	1667.2	4603.1	40.27	-0.211	6.08	10035.0	6510.2	258.47	-0.215	84.04	Yang2002
TS NO.1 Forward.45.	0.00546	2.000	1663.2	4589.9	35.69	-0.258	6.53	10013.0	6491.6	245.35	-0.262	90.26	Yang2002
TS NO.1 Forward.46.	0.00546	2.000	1663.8	4587.7	30.28	-0.314	7.09	10017.0	6488.3	229.52	-0.319	98.12	Yang2002
TS NO.1 Forward.47.	0.00546	2.000	1661.8	4647.1	23.02	-0.387	7.92	10005.0	6572.8	208.18	-0.392	109.60	Yang2002
TS NO.1 Forward.48.	0.00546	1.490	1663.8	4609.7	35.27	-0.263	5.98	10017.0	6519.4	209.16	-0.389	108.28	Yang2002

TS NO.1 Forward.49.	0.00546	1.490	1665.2	4576.7	30.70	-0.310	6.51	10024.0	6472.9	191.69	-0.448	117.89	Yang2002
TS NO.1 Forward.50.	0.00546	1.490	1661.8	4589.9	24.05	-0.376	7.29	10005.0	6491.9	166.37	-0.531	132.11	Yang2002
TS NO.1 Forward.51.	0.00546	1.490	1663.8	4592.1	15.98	-0.457	8.33	10017.0	6494.5	134.92	-0.634	150.85	Yang2002
TS NO.1 Forward.52.	0.00546	1.490	1661.8	4589.9	16.81	-0.448	8.15	10005.0	6491.9	138.60	-0.622	147.58	Yang2002
TS NO.1 Forward.53.	0.00546	1.490	1662.5	4603.1	9.78	-0.517	9.12	10009.0	6510.4	110.70	-0.711	165.29	Yang2002
TS NO.1 Forward.54.	0.00546	1.490	1667.2	4598.7	10.60	-0.511	9.13	10035.0	6504.0	112.94	-0.706	165.38	Yang2002
TS NO.1 Forward.55.	0.00546	1.490	1669.2	4633.9	5.86	-0.558	9.77	10047.0	6553.2	94.84	-0.765	176.90	Yang2002
TS NO.1 Forward.56.	0.00546	1.490	1665.2	4576.7	13.50	-0.482	8.60	10024.0	6472.9	125.15	-0.666	155.79	Yang2002
TS NO.1 Forward.57.	0.00546	1.490	1668.5	4589.9	11.43	-0.504	8.98	10043.0	6491.2	116.55	-0.695	162.63	Yang2002
TS NO.1 Forward.58.	0.00546	2.000	2367.5	3580.6	72.52	-0.039	3.75	13888.0	5005.9	329.84	-0.042	50.59	Yang2002
TS NO.1 Forward.59.	0.00546	2.000	2391.7	3569.6	68.52	-0.109	4.07	14019.0	4988.1	319.27	-0.113	54.80	Yang2002
TS NO.1 Forward.60.	0.00546	2.000	2381.6	3582.8	64.32	-0.167	4.43	13965.0	5007.3	308.28	-0.172	59.70	Yang2002
TS NO.1 Forward.61.	0.00546	2.000	2382.3	3580.6	59.91	-0.231	4.80	13969.0	5004.0	296.13	-0.235	64.72	Yang2002
TS NO.1 Forward.62.	0.00546	2.000	2388.3	3582.8	55.10	-0.300	5.25	14000.0	5007.4	282.40	-0.305	70.76	Yang2002
TS NO.1 Forward.63.	0.00546	2.000	2389.7	3563.0	50.28	-0.365	5.70	14008.0	4979.2	268.51	-0.371	76.82	Yang2002
TS NO.1 Forward.64.	0.00546	2.000	2380.3	3519.0	45.69	-0.422	6.06	13958.0	4918.1	255.38	-0.428	81.70	Yang2002
TS NO.1 Forward.65.	0.00546	2.000	2394.4	3556.4	40.06	-0.501	6.74	14033.0	4969.7	238.47	-0.508	90.76	Yang2002
TS NO.1 Forward.66.	0.00546	2.000	2393.7	3582.8	35.48	-0.559	7.16	14029.0	5006.9	224.95	-0.566	96.43	Yang2002
TS NO.1 Forward.67.	0.00546	2.000	2389.7	3571.8	30.70	-0.616	7.79	14008.0	4991.5	210.82	-0.624	104.99	Yang2002
TS NO.1 Forward.68.	0.00546	2.000	2388.3	3541.0	23.23	-0.707	8.24	14000.0	4949.0	188.65	-0.716	110.99	Yang2002
TS NO.1 Forward.69.	0.00546	1.490	2389.7	3591.6	71.88	-0.056	3.35	14008.0	5019.1	309.90	-0.165	59.15	Yang2002
TS NO.1 Forward.70.	0.00546	1.490	2401.1	3591.6	65.37	-0.159	3.90	14069.0	5018.4	286.58	-0.288	68.83	Yang2002
TS NO.1 Forward.71.	0.00546	1.490	2396.4	3589.4	60.33	-0.230	4.36	14044.0	5015.6	268.22	-0.375	76.94	Yang2002
TS NO.1 Forward.72.	0.00546	1.490	2393.1	3556.4	55.51	-0.296	4.81	14026.0	4969.7	250.14	-0.456	84.83	Yang2002
TS NO.1 Forward.73.	0.00546	1.490	2394.4	3582.8	50.08	-0.370	5.35	14033.0	5006.6	229.38	-0.547	94.47	Yang2002
TS NO.1 Forward.74.	0.00546	1.490	2387.0	3574.0	45.27	-0.430	5.79	13994.0	4994.5	211.15	-0.622	102.12	Yang2002
TS NO.1 Forward.75.	0.00546	1.490	2395.7	3567.4	39.64	-0.507	6.35	14040.0	4985.1	188.79	-0.718	111.99	Yang2002
TS NO.1 Forward.76.	0.00546	1.490	2391.0	3565.2	35.48	-0.557	6.74	14015.0	4982.3	172.66	-0.782	118.99	Yang2002
TS NO.1 Forward.77.	0.00546	1.490	2394.4	3552.0	30.49	-0.621	7.23	14033.0	4963.6	152.96	-0.863	127.53	Yang2002
TS NO.1 Forward.78.	0.00546	1.490	2392.4	3569.6	23.85	-0.702	7.89	14022.0	4988.4	127.12	-0.965	139.19	Yang2002
TS NO.1 Forward.79.	0.00546	1.490	2373.5	3587.2	17.63	-0.767	8.45	13921.0	5014.4	104.29	-1.045	149.18	Yang2002
TS NO.1 Forward.80.	0.00546	1.490	2372.2	3574.0	18.46	-0.756	8.34	13914.0	4995.9	107.35	-1.032	147.24	Yang2002
TS NO.1 Forward.81.	0.00546	1.490	2378.9	3543.2	12.46	-0.831	8.89	13950.0	4952.4	83.77	-1.128	156.88	Yang2002
TS NO.1 Forward.82.	0.00546	1.490	2388.3	3578.4	18.25	-0.767	8.39	14000.0	5001.2	106.02	-1.046	148.06	Yang2002
TS NO.1 Forward.83.	0.00546	2.000	2032.1	3569.6	64.32	-0.048	3.66	12058.0	5021.4	315.56	-0.052	50.06	Yang2002
TS NO.1 Forward.84.	0.00546	2.000	2035.5	3554.2	60.12	-0.104	3.94	12077.0	4999.3	304.44	-0.108	53.79	Yang2002
TS NO.1 Forward.85.	0.00546	2.000	2037.5	3563.0	54.68	-0.174	4.35	12088.0	5011.5	289.48	-0.178	59.46	Yang2002
TS NO.1 Forward.86.	0.00546	2.000	2034.2	3563.0	50.70	-0.222	4.74	12070.0	5011.6	278.36	-0.226	64.70	Yang2002

TS NO.1 Forward.87.	0.00546	2.000	2043.6	3552.0	44.85	-0.295	5.32	12121.0	4995.7	261.31	-0.300	72.68	Yang2002
TS NO.1 Forward.88.	0.00546	2.000	2030.8	3580.6	39.64	-0.351	5.82	12051.0	5036.8	246.48	-0.356	79.50	Yang2002
TS NO.1 Forward.89.	0.00546	2.000	2034.2	3589.4	35.27	-0.403	6.23	12070.0	5048.7	233.56	-0.408	85.08	Yang2002
TS NO.1 Forward.90.	0.00546	2.000	2031.5	3552.0	30.70	-0.453	6.60	12055.0	4996.4	220.13	-0.459	90.14	Yang2002
TS NO.1 Forward.91.	0.00546	2.000	2032.1	3565.2	23.23	-0.536	7.35	12058.0	5015.2	197.91	-0.543	100.39	Yang2002
TS NO.1 Forward.92.	0.00546	1.490	2026.1	3580.6	64.95	-0.038	3.14	12025.0	5037.2	299.32	-0.130	56.11	Yang2002
TS NO.1 Forward.93.	0.00546	1.490	2030.8	3565.2	60.33	-0.100	3.49	12051.0	5015.2	283.05	-0.205	62.42	Yang2002
TS NO.1 Forward.94.	0.00546	1.490	2032.1	3571.8	54.68	-0.172	4.00	12058.0	5024.5	262.57	-0.292	71.60	Yang2002
TS NO.1 Forward.95.	0.00546	1.490	2034.2	3560.8	49.87	-0.232	4.41	12070.0	5008.5	245.04	-0.363	78.83	Yang2002
TS NO.1 Forward.96.	0.00546	1.490	2032.1	3547.6	44.44	-0.296	4.95	12058.0	4990.5	224.06	-0.444	88.63	Yang2002
TS NO.1 Forward.97.	0.00546	1.490	2033.5	3554.2	39.85	-0.350	5.41	12066.0	4999.4	206.27	-0.512	96.76	Yang2002
TS NO.1 Forward.98.	0.00546	1.490	2027.4	3543.2	35.69	-0.395	5.78	12033.0	4984.3	190.49	-0.569	103.42	Yang2002
TS NO.1 Forward.99.	0.00546	1.490	2026.8	3563.0	30.49	-0.454	6.33	12029.0	5012.3	169.95	-0.644	113.21	Yang2002
TS NO.1 Forward.100.	0.00546	1.490	2030.8	3554.2	23.85	-0.529	6.95	12051.0	4999.7	144.13	-0.738	124.40	Yang2002
TS NO.1 Forward.101.	0.00546	1.490	2028.8	3549.8	13.50	-0.640	7.89	12040.0	4993.6	104.15	-0.879	141.23	Yang2002
TS NO.1 Forward.102.	0.00546	1.490	2038.2	3554.2	10.60	-0.676	8.24	12092.0	4998.9	92.15	-0.926	147.44	Yang2002
TS NO.1 Forward.103.	0.00546	2.000	1663.2	3554.2	54.68	-0.052	3.67	10013.0	5026.7	298.79	-0.055	50.74	Yang2002
TS NO.1 Forward.104.	0.00546	2.000	1663.2	3538.8	52.59	-0.075	3.73	10013.0	5005.0	293.17	-0.079	51.61	Yang2002
TS NO.1 Forward.105.	0.00546	2.000	1668.5	3545.4	49.87	-0.108	4.01	10043.0	5014.0	285.56	-0.111	55.50	Yang2002
TS NO.1 Forward.106.	0.00546	2.000	1677.3	3543.2	45.27	-0.161	4.41	10092.0	5010.3	272.44	-0.165	60.90	Yang2002
TS NO.1 Forward.107.	0.00546	2.000	1672.6	3512.4	40.68	-0.209	4.81	10066.0	4966.9	259.46	-0.213	66.57	Yang2002
TS NO.1 Forward.108.	0.00546	2.000	1669.2	3527.8	35.48	-0.262	5.25	10047.0	4989.0	244.51	-0.267	72.60	Yang2002
TS NO.1 Forward.109.	0.00546	2.000	1668.5	3530.0	30.28	-0.316	5.72	10043.0	4992.2	229.32	-0.321	79.04	Yang2002
TS NO.1 Forward.110.	0.00546	2.000	1666.5	3534.4	23.43	-0.384	6.39	10032.0	4998.5	209.16	-0.390	88.35	Yang2002
TS NO.1 Forward.111.	0.00546	1.490	1663.2	3525.6	34.85	-0.267	4.95	10013.0	4986.3	204.88	-0.403	89.59	Yang2002
TS NO.1 Forward.112.	0.00546	1.490	1666.5	3541.0	30.49	-0.313	5.35	10032.0	5007.8	188.28	-0.460	96.90	Yang2002
TS NO.1 Forward.113.	0.00546	1.490	1665.8	3519.0	23.85	-0.380	5.97	10028.0	4976.8	162.29	-0.546	108.15	Yang2002
TS NO.1 Forward.114.	0.00546	1.490	1658.4	3538.8	15.56	-0.459	6.71	9986.0	5005.5	131.38	-0.644	121.50	Yang2002
TS NO.1 Forward.115.	0.00546	1.490	1658.4	3534.4	18.25	-0.433	6.46	9986.0	4999.3	141.43	-0.611	117.14	Yang2002
TS NO.1 Forward.116.	0.00546	1.490	1657.1	3512.4	19.91	-0.416	6.25	9979.0	4968.1	148.20	-0.589	113.24	Yang2002
TS NO.1 Forward.117.	0.00546	1.490	1666.5	3538.8	21.15	-0.407	6.19	10032.0	5004.7	152.48	-0.578	112.13	Yang2002
TS NO.1 Forward.118.	0.00546	1.490	1666.5	3530.0	21.57	-0.403	6.13	10032.0	4992.2	154.32	-0.572	111.12	Yang2002
TS NO.1 Forward.119.	0.00546	1.490	1659.1	3558.6	7.51	-0.538	7.59	9990.0	5033.4	99.33	-0.746	137.53	Yang2002
TS NO.1 Forward.120.	0.00546	1.490	1659.8	3538.8	9.57	-0.518	7.35	9994.0	5005.2	107.43	-0.721	133.16	Yang2002
TS NO.1 Forward.121.	0.00546	1.490	1665.2	3530.0	12.88	-0.488	6.90	10024.0	4992.5	120.90	-0.680	125.06	Yang2002
TS NO.1 Forward.122.	0.00546	1.490	1666.5	3549.8	17.43	-0.444	6.56	10032.0	5020.2	138.17	-0.625	118.78	Yang2002
TS NO.1 Forward.123.	0.00546	1.490	1666.5	3554.2	17.43	-0.444	6.56	10032.0	5026.4	138.18	-0.625	118.74	Yang2002
TS NO.1 Forward.124.	0.00546	2.000	2390.4	2865.9	71.88	-0.056	2.86	14011.0	4005.2	327.90	-0.060	38.55	Yang2002

TS NO.1 Forward.125.	0.00546	2.000	2387.7	2848.3	68.94	-0.101	3.02	13998.0	3980.2	320.48	-0.105	40.67	Yang2002
TS NO.1 Forward.126.	0.00546	2.000	2391.0	2865.9	64.74	-0.165	3.41	14015.0	4005.0	309.25	-0.169	45.90	Yang2002
TS NO.1 Forward.127.	0.00546	2.000	2391.0	2874.7	60.12	-0.231	3.75	14015.0	4017.3	296.54	-0.236	50.58	Yang2002
TS NO.1 Forward.128.	0.00546	2.000	2391.0	2865.9	54.26	-0.312	4.27	14015.0	4005.0	279.94	-0.318	57.53	Yang2002
TS NO.1 Forward.129.	0.00546	2.000	2389.7	2865.9	50.70	-0.360	4.56	14008.0	4005.0	269.73	-0.365	61.44	Yang2002
TS NO.1 Forward.130.	0.00546	2.000	2389.7	2881.3	45.06	-0.434	5.01	14008.0	4026.5	253.30	-0.440	67.54	Yang2002
TS NO.1 Forward.131.	0.00546	2.000	2391.0	2861.5	40.06	-0.499	5.37	14015.0	3998.9	238.56	-0.506	72.39	Yang2002
TS NO.1 Forward.132.	0.00546	2.000	2397.1	2863.7	35.48	-0.560	5.80	14048.0	4001.4	224.86	-0.568	78.09	Yang2002
TS NO.1 Forward.133.	0.00546	2.000	2385.6	2857.1	30.70	-0.614	6.18	13987.0	3992.7	210.95	-0.622	83.32	Yang2002
TS NO.1 Forward.134.	0.00546	2.000	2387.0	2857.1	23.23	-0.707	6.80	13994.0	3992.7	188.66	-0.715	91.55	Yang2002
TS NO.1 Forward.135.	0.00546	1.490	2388.3	2865.9	45.06	-0.434	4.71	14000.0	4005.4	209.86	-0.628	83.04	Yang2002
TS NO.1 Forward.136.	0.00546	1.490	2395.1	2846.1	40.89	-0.491	5.07	14037.0	3977.0	192.81	-0.701	89.36	Yang2002
TS NO.1 Forward.137.	0.00546	1.490	2399.1	2852.7	35.06	-0.567	5.54	14059.0	3985.8	169.69	-0.798	97.72	Yang2002
TS NO.1 Forward.138.	0.00546	1.490	2405.2	2865.9	30.49	-0.627	5.91	14091.0	4004.1	151.78	-0.873	104.29	Yang2002
TS NO.1 Forward.139.	0.00546	1.490	2402.5	2841.7	24.26	-0.702	6.39	14077.0	3970.3	127.17	-0.970	112.67	Yang2002
TS NO.1 Forward.140.	0.00546	1.490	2391.7	2846.1	11.84	-0.846	7.39	14019.0	3977.2	78.69	-1.155	130.46	Yang2002
TS NO.1 Forward.141.	0.00546	1.490	2385.0	2850.5	19.08	-0.756	6.75	13983.0	3983.7	107.94	-1.037	119.09	Yang2002
TS NO.1 Forward.142.	0.00546	1.490	2380.9	2868.1	5.86	-0.909	7.98	13961.0	4008.6	55.25	-1.240	140.90	Yang2002
TS NO.1 Forward.143.	0.00546	1.490	2390.4	2868.1	17.22	-0.781	6.95	14011.0	4008.3	100.56	-1.069	122.63	Yang2002
TS NO.1 Forward.144.	0.00546	1.490	2368.8	2863.7	10.19	-0.852	7.51	13896.0	4003.2	73.59	-1.162	132.55	Yang2002
TS NO.1 Forward.145.	0.00546	1.490	2380.3	2859.3	9.98	-0.861	7.55	13958.0	3996.1	72.13	-1.174	133.28	Yang2002
TS NO.1 Forward.146.	0.00546	2.000	2037.5	2817.5	65.16	-0.039	2.79	12088.0	3963.0	317.62	-0.042	38.05	Yang2002
TS NO.1 Forward.147.	0.00546	2.000	2026.1	2854.9	62.43	-0.071	2.90	12025.0	4016.3	310.81	-0.075	39.63	Yang2002
TS NO.1 Forward.148.	0.00546	2.000	2035.5	2846.1	60.12	-0.104	3.10	12077.0	4003.3	304.45	-0.108	42.33	Yang2002
TS NO.1 Forward.149.	0.00546	2.000	2032.1	2832.9	54.47	-0.175	3.56	12058.0	3985.1	289.00	-0.179	48.57	Yang2002
TS NO.1 Forward.150.	0.00546	2.000	2035.5	2843.9	50.28	-0.227	3.95	12077.0	4000.2	277.09	-0.232	53.93	Yang2002
TS NO.1 Forward.151.	0.00546	2.000	2029.5	2837.3	45.06	-0.287	4.39	12044.0	3991.2	262.24	-0.292	60.03	Yang2002
TS NO.1 Forward.152.	0.00546	2.000	2036.9	2848.3	39.85	-0.351	4.79	12084.0	4006.4	246.88	-0.357	65.48	Yang2002
TS NO.1 Forward.153.	0.00546	2.000	2038.2	2832.9	35.90	-0.397	5.11	12092.0	3984.5	235.24	-0.403	69.78	Yang2002
TS NO.1 Forward.154.	0.00546	2.000	2036.9	2837.3	31.32	-0.448	5.44	12084.0	3991.0	221.75	-0.455	74.25	Yang2002
TS NO.1 Forward.155.	0.00546	2.000	2039.6	2832.9	23.43	-0.537	6.05	12099.0	3984.5	198.25	-0.544	82.66	Yang2002
TS NO.1 Forward.156.	0.00546	1.490	2028.1	2817.5	40.68	-0.338	4.33	12036.0	3963.7	208.54	-0.502	77.46	Yang2002
TS NO.1 Forward.157.	0.00546	1.490	2028.1	2854.9	35.69	-0.395	4.71	12036.0	4016.2	189.85	-0.572	84.36	Yang2002
TS NO.1 Forward.158.	0.00546	1.490	2028.1	2830.7	30.28	-0.457	5.15	12036.0	3982.2	168.05	-0.651	92.24	Yang2002
TS NO.1 Forward.159.	0.00546	1.490	2026.8	2841.7	23.64	-0.530	5.69	12029.0	3997.6	142.10	-0.744	101.79	Yang2002
TS NO.1 Forward.160.	0.00546	1.490	2032.1	2821.9	17.63	-0.597	6.14	12058.0	3969.7	118.22	-0.831	109.85	Yang2002
TS NO.1 Forward.161.	0.00546	1.490	2038.9	2821.9	11.84	-0.663	6.63	12095.0	3969.2	95.10	-0.915	118.63	Yang2002
TS NO.1 Forward.162.	0.00546	1.490	2024.1	2841.7	11.22	-0.663	6.70	12014.0	3997.9	93.40	-0.915	119.89	Yang2002

TS NO.1 Forward.163.	0.00546	1.490	2029.5	2832.9	6.89	-0.711	7.13	12044.0	3985.0	75.04	-0.982	127.57	Yang2002
TS NO.1 Forward.164.	0.00546	2.000	1669.2	2843.9	56.35	-0.035	2.80	10047.0	4021.8	303.08	-0.037	38.74	Yang2002
TS NO.1 Forward.165.	0.00546	2.000	1661.8	2810.9	52.59	-0.075	3.08	10005.0	3975.7	293.18	-0.078	42.57	Yang2002
TS NO.1 Forward.166.	0.00546	2.000	1667.9	2815.3	49.87	-0.107	3.43	10039.0	3981.6	285.51	-0.111	47.43	Yang2002
TS NO.1 Forward.167.	0.00546	2.000	1668.5	2780.1	45.06	-0.160	3.85	10043.0	3931.7	271.98	-0.164	53.26	Yang2002
TS NO.1 Forward.168.	0.00546	2.000	1668.5	2797.7	39.64	-0.218	4.31	10043.0	3956.6	256.46	-0.223	59.62	Yang2002
TS NO.1 Forward.169.	0.00546	2.000	1671.2	2828.5	35.27	-0.265	4.64	10058.0	4000.0	243.72	-0.270	64.17	Yang2002
TS NO.1 Forward.170.	0.00546	2.000	1671.9	2832.9	30.28	-0.317	5.00	10062.0	4006.1	229.10	-0.322	69.16	Yang2002
TS NO.1 Forward.171.	0.00546	2.000	1670.6	2839.5	23.23	-0.388	5.51	10054.0	4015.7	208.33	-0.394	76.19	Yang2002
TS NO.1 Forward.172.	0.00546	1.490	1665.2	2824.1	36.10	-0.254	4.16	10024.0	3994.2	206.65	-0.398	75.37	Yang2002
TS NO.1 Forward.173.	0.00546	1.490	1663.8	2841.7	30.70	-0.310	4.55	10017.0	4018.9	186.52	-0.465	82.37	Yang2002
TS NO.1 Forward.174.	0.00546	1.490	1663.8	2819.7	23.43	-0.383	5.09	10017.0	3987.8	158.05	-0.559	92.23	Yang2002
TS NO.1 Forward.175.	0.00546	1.490	1666.5	2817.5	12.05	-0.497	5.89	10032.0	3984.6	114.47	-0.701	106.61	Yang2002
TS NO.1 Forward.176.	0.00546	1.490	1662.5	2821.9	19.08	-0.426	5.38	10009.0	3991.2	141.60	-0.612	97.49	Yang2002
TS NO.1 Forward.177.	0.00546	1.490	1659.1	2813.1	11.22	-0.502	6.02	9990.0	3979.0	110.44	-0.711	109.14	Yang2002
TS NO.1 Forward.178.	0.00546	1.490	1663.8	2815.3	10.81	-0.508	6.00	10017.0	3981.6	109.41	-0.716	108.66	Yang2002
TS NO.1 Forward.179.	0.00546	1.490	1660.5	2810.9	11.02	-0.505	5.96	9998.0	3975.6	110.43	-0.712	107.95	Yang2002
TS NO.1 Forward.180.	0.00546	1.490	1663.2	2799.9	8.13	-0.534	6.22	10013.0	3960.0	98.29	-0.751	112.71	Yang2002
TS NO.1 Reverse.1.	0.00546	1.510	2391.0	4662.5	67.47	-0.127	4.57	14015.0	6515.7	298.07	-0.228	76.40	Yang2002
TS NO.1 Reverse.2.	0.00546	1.510	2388.3	4666.9	64.95	-0.164	4.80	14000.0	6522.5	289.77	-0.269	80.31	Yang2002
TS NO.1 Reverse.3.	0.00546	1.510	2389.7	4644.9	71.67	-0.062	4.20	14008.0	6491.1	312.24	-0.152	70.20	Yang2002
TS NO.1 Reverse.4.	0.00546	1.510	2389.0	4669.1	70.20	-0.082	4.33	14004.0	6525.3	307.68	-0.177	72.41	Yang2002
TS NO.1 Reverse.5.	0.00546	1.510	2392.4	4658.1	60.54	-0.226	5.30	14022.0	6509.6	274.84	-0.342	88.59	Yang2002
TS NO.1 Reverse.6.	0.00546	1.510	2389.7	4666.9	54.89	-0.303	5.91	14008.0	6521.8	254.94	-0.433	98.86	Yang2002
TS NO.1 Reverse.7.	0.00546	1.510	2395.7	4638.3	50.28	-0.368	6.48	14040.0	6481.6	237.62	-0.512	108.39	Yang2002
TS NO.1 Reverse.8.	0.00546	1.510	2390.4	4640.5	44.65	-0.440	7.15	14011.0	6485.3	216.80	-0.599	119.50	Yang2002
TS NO.1 Reverse.9.	0.00546	1.510	2385.0	4640.5	40.06	-0.496	7.68	13983.0	6485.3	199.99	-0.667	128.42	Yang2002
TS NO.1 Reverse.10.	0.00546	1.510	2389.7	4684.5	35.06	-0.562	8.46	14008.0	6546.4	180.64	-0.749	141.39	Yang2002
TS NO.1 Reverse.11.	0.00546	1.510	2382.3	4721.8	29.45	-0.628	9.13	13969.0	6598.9	160.48	-0.827	152.70	Yang2002
TS NO.1 Reverse.12.	0.00546	1.510	2387.0	4752.6	25.71	-0.676	9.60	13994.0	6641.7	146.60	-0.885	160.59	Yang2002
TS NO.1 Reverse.13.	0.00546	1.510	2383.0	4728.4	22.19	-0.717	10.03	13972.0	6608.5	133.29	-0.936	167.67	Yang2002
TS NO.1 Reverse.14.	0.00546	1.510	2031.5	4629.5	62.22	-0.076	4.11	12055.0	6512.1	293.50	-0.158	69.72	Yang2002
TS NO.1 Reverse.15.	0.00546	1.510	2029.5	4627.3	60.75	-0.094	4.32	12044.0	6509.2	288.51	-0.180	73.18	Yang2002
TS NO.1 Reverse.16.	0.00546	1.510	2028.8	4620.7	55.10	-0.166	4.87	12040.0	6500.1	269.34	-0.263	82.53	Yang2002
TS NO.1 Reverse.17.	0.00546	1.510	2029.5	4640.5	50.49	-0.222	5.40	12044.0	6527.7	252.78	-0.331	91.60	Yang2002
TS NO.1 Reverse.18.	0.00546	1.510	2028.8	4605.3	44.44	-0.294	6.10	12040.0	6478.5	230.77	-0.417	103.35	Yang2002
TS NO.1 Reverse.19.	0.00546	1.510	2030.8	4625.1	40.27	-0.344	6.58	12051.0	6506.2	215.42	-0.477	111.62	Yang2002
TS NO.1 Reverse.20.	0.00546	1.510	2032.8	4649.3	35.27	-0.402	7.37	12062.0	6540.0	196.15	-0.550	124.96	Yang2002

TS NO.1 Reverse.21.	0.00546	1.510	2032.1	4618.5	29.45	-0.467	8.05	12058.0	6497.0	174.18	-0.630	136.55	Yang2002
TS NO.1 Reverse.22.	0.00546	1.510	2033.5	4620.7	23.85	-0.530	8.76	12066.0	6499.6	153.14	-0.707	148.57	Yang2002
TS NO.1 Reverse.23.	0.00546	1.510	1667.2	4598.7	57.19	-0.024	3.61	10035.0	6504.0	290.68	-0.090	61.90	Yang2002
TS NO.1 Reverse.24.	0.00546	1.510	1667.9	4600.9	56.56	-0.032	3.68	10039.0	6506.9	288.62	-0.098	63.12	Yang2002
TS NO.1 Reverse.25.	0.00546	1.510	1667.9	4605.3	53.21	-0.070	3.89	10039.0	6513.1	277.82	-0.142	66.79	Yang2002
TS NO.1 Reverse.26.	0.00546	1.510	1667.2	4592.1	50.08	-0.105	4.19	10035.0	6494.7	267.38	-0.182	72.00	Yang2002
TS NO.1 Reverse.27.	0.00546	1.510	1666.5	4596.5	45.48	-0.155	4.69	10032.0	6500.5	251.31	-0.241	80.56	Yang2002
TS NO.1 Reverse.28.	0.00546	1.510	1663.8	4596.5	40.27	-0.210	5.31	10017.0	6500.7	232.61	-0.308	91.09	Yang2002
TS NO.1 Reverse.29.	0.00546	1.510	1665.8	4592.1	34.85	-0.268	5.96	10028.0	6494.5	212.62	-0.378	102.29	Yang2002
TS NO.1 Reverse.30.	0.00546	1.510	1665.8	4581.1	30.28	-0.315	6.56	10028.0	6478.9	195.41	-0.436	112.59	Yang2002
TS NO.1 Reverse.31.	0.00546	1.510	1661.1	4598.7	25.51	-0.361	7.10	10001.0	6504.6	178.06	-0.493	121.91	Yang2002
TS NO.1 Reverse.32.	0.00546	1.510	1664.5	4598.7	21.98	-0.398	7.59	10020.0	6504.2	164.45	-0.539	130.34	Yang2002
TS NO.1 Reverse.33.	0.00546	1.510	2389.0	3545.4	71.88	-0.056	3.05	14004.0	4954.8	313.73	-0.144	51.02	Yang2002
TS NO.1 Reverse.34.	0.00546	1.510	2391.0	3578.4	69.99	-0.086	3.22	14015.0	5000.7	307.69	-0.177	53.83	Yang2002
TS NO.1 Reverse.35.	0.00546	1.510	2389.7	3574.0	65.16	-0.158	3.65	14008.0	4994.5	291.24	-0.262	61.02	Yang2002
TS NO.1 Reverse.36.	0.00546	1.510	2387.0	3582.8	59.91	-0.233	4.13	13994.0	5006.8	272.54	-0.351	69.11	Yang2002
TS NO.1 Reverse.37.	0.00546	1.510	2387.7	3574.0	55.31	-0.297	4.62	13998.0	4994.2	255.56	-0.430	77.16	Yang2002
TS NO.1 Reverse.38.	0.00546	1.510	2391.0	3574.0	49.66	-0.374	5.17	14015.0	4994.6	234.57	-0.523	86.50	Yang2002
TS NO.1 Reverse.39.	0.00546	1.510	2387.0	3569.6	45.06	-0.433	5.64	13994.0	4988.4	217.39	-0.595	94.24	Yang2002
TS NO.1 Reverse.40.	0.00546	1.510	2389.0	3574.0	39.43	-0.506	6.23	14004.0	4994.8	195.91	-0.686	104.10	Yang2002
TS NO.1 Reverse.41.	0.00546	1.510	2389.0	3574.0	34.85	-0.564	6.69	14004.0	4994.8	178.30	-0.758	111.81	Yang2002
TS NO.1 Reverse.42.	0.00546	1.510	2390.4	3569.6	29.45	-0.632	7.24	14011.0	4988.7	157.82	-0.842	121.07	Yang2002
TS NO.1 Reverse.43.	0.00546	1.510	2387.0	3571.8	22.81	-0.712	7.92	13994.0	4991.4	132.30	-0.942	132.48	Yang2002
TS NO.1 Reverse.44.	0.00546	1.510	2032.1	3549.8	65.58	-0.032	2.89	12058.0	4993.6	304.48	-0.107	48.99	Yang2002
TS NO.1 Reverse.45.	0.00546	1.510	2030.1	3560.8	62.64	-0.070	3.07	12047.0	5009.2	295.31	-0.150	52.04	Yang2002
TS NO.1 Reverse.46.	0.00546	1.510	2032.1	3534.4	59.28	-0.114	3.35	12058.0	4971.9	283.72	-0.202	56.74	Yang2002
TS NO.1 Reverse.47.	0.00546	1.510	2029.5	3576.2	54.68	-0.171	3.84	12044.0	5030.6	267.48	-0.271	65.11	Yang2002
TS NO.1 Reverse.48.	0.00546	1.510	2030.8	3545.4	50.70	-0.220	4.20	12051.0	4987.3	252.99	-0.330	71.28	Yang2002
TS NO.1 Reverse.49.	0.00546	1.510	2033.5	3556.4	45.06	-0.289	4.72	12066.0	5002.5	232.45	-0.412	80.09	Yang2002
TS NO.1 Reverse.50.	0.00546	1.510	2030.1	3585.0	39.64	-0.351	5.30	12047.0	5043.2	212.20	-0.489	89.93	Yang2002
TS NO.1 Reverse.51.	0.00546	1.510	2031.5	3571.8	34.85	-0.406	5.86	12055.0	5024.3	193.56	-0.559	99.39	Yang2002
TS NO.1 Reverse.52.	0.00546	1.510	2027.4	3556.4	30.07	-0.459	6.28	12033.0	5002.8	175.78	-0.623	106.51	Yang2002
TS NO.1 Reverse.53.	0.00546	1.510	2030.1	3569.6	23.64	-0.531	6.95	12047.0	5021.5	151.23	-0.713	117.82	Yang2002
TS NO.1 Reverse.54.	0.00546	1.510	1663.8	3532.2	57.40	-0.021	2.88	10017.0	4995.5	290.71	-0.089	49.47	Yang2002
TS NO.1 Reverse.55.	0.00546	1.510	1666.5	3565.2	56.14	-0.036	2.94	10032.0	5042.0	286.88	-0.105	50.48	Yang2002
TS NO.1 Reverse.56.	0.00546	1.510	1666.5	3534.4	52.59	-0.077	3.17	10032.0	4998.5	275.09	-0.152	54.40	Yang2002
TS NO.1 Reverse.57.	0.00546	1.510	1662.5	3552.0	55.10	-0.047	3.00	10009.0	5023.8	283.50	-0.118	51.52	Yang2002
TS NO.1 Reverse.58.	0.00546	1.510	1663.8	3585.0	50.91	-0.094	3.30	10017.0	5070.1	269.81	-0.172	56.70	Yang2002

TS NO.1 Reverse.59.	0.00546	1.510	1663.2	3549.8	45.48	-0.154	3.77	10013.0	5020.5	250.40	-0.244	64.76	Yang2002
TS NO.1 Reverse.60.	0.00546	1.510	1663.8	3538.8	40.48	-0.208	4.25	10017.0	5004.8	232.18	-0.309	73.03	Yang2002
TS NO.1 Reverse.61.	0.00546	1.510	1665.2	3536.6	34.85	-0.267	4.77	10024.0	5001.8	211.28	-0.382	81.87	Yang2002
TS NO.1 Reverse.62.	0.00546	1.510	1662.5	3543.2	29.45	-0.322	5.35	10009.0	5011.3	191.00	-0.450	91.77	Yang2002
TS NO.1 Reverse.63.	0.00546	1.510	1662.5	3549.8	23.43	-0.383	5.94	10009.0	5020.6	168.43	-0.525	101.93	Yang2002
TS NO.1 Reverse.64.	0.00546	1.510	2392.4	2859.3	72.73	-0.044	2.36	14022.0	3995.8	316.81	-0.127	39.43	Yang2002
TS NO.1 Reverse.65.	0.00546	1.510	2392.4	2859.3	70.20	-0.083	2.54	14022.0	3995.8	308.27	-0.175	42.39	Yang2002
TS NO.1 Reverse.66.	0.00546	1.510	2391.7	2859.3	65.37	-0.156	2.94	14019.0	3995.6	291.49	-0.261	49.07	Yang2002
TS NO.1 Reverse.67.	0.00546	1.510	2387.7	2863.7	59.70	-0.236	3.41	13998.0	4001.7	271.23	-0.358	57.00	Yang2002
TS NO.1 Reverse.68.	0.00546	1.510	2387.7	2868.1	54.89	-0.302	3.78	13998.0	4007.8	253.66	-0.438	63.27	Yang2002
TS NO.1 Reverse.69.	0.00546	1.510	2388.3	2863.7	50.70	-0.359	4.17	14000.0	4002.4	237.66	-0.509	69.71	Yang2002
TS NO.1 Reverse.70.	0.00546	1.510	2386.3	2854.9	44.85	-0.435	4.64	13990.0	3989.8	215.46	-0.603	77.54	Yang2002
TS NO.1 Reverse.71.	0.00546	1.510	2389.7	2861.5	40.06	-0.499	5.07	14008.0	3998.9	197.08	-0.681	84.69	Yang2002
TS NO.1 Reverse.72.	0.00546	1.510	2391.7	2865.9	34.85	-0.566	5.51	14019.0	4004.8	177.17	-0.764	92.06	Yang2002
TS NO.1 Reverse.73.	0.00546	1.510	2389.0	2857.1	29.66	-0.629	5.95	14004.0	3992.9	157.10	-0.844	99.45	Yang2002
TS NO.1 Reverse.74.	0.00546	1.510	2391.7	2863.7	22.81	-0.714	6.54	14019.0	4001.7	130.45	-0.952	109.40	Yang2002
TS NO.1 Reverse.75.	0.00546	1.510	2031.5	2835.1	64.53	-0.045	2.45	12055.0	3988.0	300.72	-0.125	41.46	Yang2002
TS NO.1 Reverse.76.	0.00546	1.510	2032.8	2843.9	62.43	-0.074	2.59	12062.0	4000.4	293.70	-0.158	43.96	Yang2002
TS NO.1 Reverse.77.	0.00546	1.510	2032.8	2848.3	59.91	-0.106	2.83	12062.0	4006.6	284.77	-0.198	47.97	Yang2002
TS NO.1 Reverse.78.	0.00546	1.510	2029.5	2835.1	55.31	-0.163	3.15	12044.0	3988.1	268.57	-0.266	53.41	Yang2002
TS NO.1 Reverse.79.	0.00546	1.510	2030.1	2848.3	49.45	-0.235	3.63	12047.0	4006.9	247.03	-0.354	61.56	Yang2002
TS NO.1 Reverse.80.	0.00546	1.510	2028.1	2843.9	44.85	-0.289	4.02	12036.0	4000.8	229.91	-0.421	68.21	Yang2002
TS NO.1 Reverse.81.	0.00546	1.510	2029.5	2835.1	40.27	-0.343	4.37	12044.0	3988.1	212.68	-0.487	74.13	Yang2002
TS NO.1 Reverse.82.	0.00546	1.510	2028.8	2828.5	35.48	-0.398	4.76	12040.0	3979.0	194.45	-0.555	80.75	Yang2002
TS NO.1 Reverse.83.	0.00546	1.510	2034.8	2850.5	30.07	-0.462	5.25	12073.0	4009.6	173.51	-0.634	89.01	Yang2002
TS NO.1 Reverse.84.	0.00546	1.510	2028.1	2848.3	24.05	-0.526	5.76	12036.0	4007.0	150.44	-0.715	97.65	Yang2002
TS NO.1 Reverse.85.	0.00546	1.510	2030.1	2830.7	13.08	-0.646	6.51	12047.0	3982.1	109.64	-0.860	110.39	Yang2002
TS NO.1 Reverse.86.	0.00546	1.510	2035.5	2819.7	18.46	-0.590	6.08	12077.0	3966.2	129.69	-0.792	103.04	Yang2002
TS NO.1 Reverse.87.	0.00546	1.510	1664.5	2819.7	57.40	-0.021	2.62	10020.0	3988.1	288.15	-0.099	45.00	Yang2002
TS NO.1 Reverse.88.	0.00546	1.510	1667.2	2821.9	55.93	-0.039	2.69	10035.0	3991.0	283.40	-0.119	46.18	Yang2002
TS NO.1 Reverse.89.	0.00546	1.510	1664.5	2832.9	55.31	-0.045	2.71	10020.0	4006.7	281.71	-0.125	46.54	Yang2002
TS NO.1 Reverse.90.	0.00546	1.510	1663.8	2835.1	52.38	-0.078	2.88	10017.0	4009.6	271.97	-0.163	49.42	Yang2002
TS NO.1 Reverse.91.	0.00546	1.510	1663.2	2804.3	50.08	-0.104	3.02	10013.0	3966.2	263.85	-0.194	51.79	Yang2002
TS NO.1 Reverse.92.	0.00546	1.510	1665.8	2815.3	45.27	-0.157	3.38	10028.0	3981.6	246.65	-0.258	57.94	Yang2002
TS NO.1 Reverse.93.	0.00546	1.510	1667.2	2826.3	40.27	-0.211	3.78	10035.0	3997.3	228.06	-0.325	64.86	Yang2002
TS NO.1 Reverse.94.	0.00546	1.510	1664.5	2821.9	35.27	-0.263	4.19	10020.0	3991.2	209.39	-0.388	71.88	Yang2002
TS NO.1 Reverse.95.	0.00546	1.510	1663.2	2819.7	29.45	-0.322	4.62	10013.0	3988.0	187.55	-0.462	79.30	Yang2002
TS NO.1 Reverse.96.	0.00546	1.510	1664.5	2835.1	23.85	-0.379	5.02	10020.0	4009.8	167.17	-0.530	86.13	Yang2002

TS NO.1 Reverse.97.	0.00546	1.510	1666.5	2826.3	18.05	-0.438	5.46	10032.0	3997.1	144.92	-0.603	93.69	Yang2002
TS NO.1 Reverse.98.	0.00546	1.510	1671.2	2830.7	12.67	-0.493	5.90	10058.0	4003.1	124.49	-0.670	101.18	Yang2002
TS NO.1 Reverse.99.	0.00546	1.510	1662.5	2830.7	10.19	-0.514	6.10	10009.0	4003.6	115.12	-0.697	104.78	Yang2002
TS NO.1 Reverse.100.	0.00546	1.510	1659.8	2819.7	7.51	-0.538	6.28	9994.0	3988.2	105.31	-0.728	107.89	Yang2002
TS NO.1 Reverse.101.	0.00546	1.510	1665.8	2832.9	5.86	-0.557	6.47	10028.0	4006.5	98.63	-0.751	110.98	Yang2002
TS NO.2 Forward.1.	0.00546	1.275	2389.0	4609.7	71.88	-0.059	3.97	14004.0	6442.3	301.52	-0.210	77.99	Yang2002
TS NO.2 Forward.2.	0.00546	1.275	2390.4	4647.1	69.99	-0.088	4.20	14011.0	6494.6	294.82	-0.244	82.46	Yang2002
TS NO.2 Forward.3.	0.00546	1.275	2387.0	4636.1	66.42	-0.139	4.61	13994.0	6478.8	280.81	-0.312	90.51	Yang2002
TS NO.2 Forward.4.	0.00546	1.275	2388.3	4647.1	62.22	-0.200	5.07	14000.0	6494.9	264.01	-0.391	99.41	Yang2002
TS NO.2 Forward.5.	0.00546	1.275	2391.0	4627.3	59.49	-0.240	5.38	14015.0	6466.6	252.45	-0.445	105.59	Yang2002
TS NO.2 Forward.6.	0.00546	1.275	2393.1	4647.1	55.10	-0.302	5.89	14026.0	6493.9	234.44	-0.525	115.59	Yang2002
TS NO.2 Forward.7.	0.00546	1.275	2386.3	4653.7	49.87	-0.369	6.53	13990.0	6503.7	212.53	-0.616	128.21	Yang2002
TS NO.2 Forward.8.	0.00546	1.275	2387.7	4658.1	44.65	-0.439	7.19	13998.0	6509.2	190.08	-0.710	141.02	Yang2002
TS NO.2 Forward.9.	0.00546	1.275	2391.0	4647.1	39.85	-0.502	7.77	14015.0	6494.2	169.07	-0.797	152.39	Yang2002
TS NO.2 Forward.10.	0.00546	1.275	2391.7	4653.7	35.06	-0.563	8.37	14019.0	6503.1	148.53	-0.880	164.25	Yang2002
TS NO.2 Forward.11.	0.00546	1.275	2390.4	4653.7	29.45	-0.632	9.02	14011.0	6503.8	124.49	-0.974	177.00	Yang2002
TS NO.2 Forward.12.	0.00546	1.275	2389.0	4671.3	26.13	-0.672	9.43	14004.0	6528.3	110.60	-1.029	185.11	Yang2002
TS NO.2 Forward.13.	0.00546	1.275	2389.7	4638.3	23.02	-0.711	9.79	14008.0	6481.9	97.03	-1.082	192.05	Yang2002
TS NO.2 Forward.14.	0.00546	1.275	2026.8	4614.1	67.05	-0.010	3.49	12029.0	6491.0	299.68	-0.129	69.36	Yang2002
TS NO.2 Forward.15.	0.00546	1.275	2028.8	4614.1	63.06	-0.064	3.87	12040.0	6490.8	284.95	-0.196	76.94	Yang2002
TS NO.2 Forward.16.	0.00546	1.275	2032.1	4627.3	60.33	-0.101	4.14	12058.0	6509.3	274.56	-0.242	82.32	Yang2002
TS NO.2 Forward.17.	0.00546	1.275	2029.5	4622.9	57.61	-0.134	4.48	12044.0	6503.0	263.35	-0.288	89.05	Yang2002
TS NO.2 Forward.18.	0.00546	1.275	2031.5	4627.3	54.47	-0.174	4.91	12055.0	6509.0	250.06	-0.342	97.62	Yang2002
TS NO.2 Forward.19.	0.00546	1.275	2030.1	4625.1	50.28	-0.225	5.36	12047.0	6506.4	233.09	-0.409	106.71	Yang2002
TS NO.2 Forward.20.	0.00546	1.275	2034.2	4622.9	46.11	-0.277	5.87	12070.0	6502.4	215.26	-0.479	116.83	Yang2002
TS NO.2 Forward.21.	0.00546	1.275	2033.5	4611.9	40.27	-0.345	6.56	12066.0	6487.2	190.42	-0.571	130.49	Yang2002
TS NO.2 Forward.22.	0.00546	1.275	2030.1	4618.5	35.27	-0.401	7.18	12047.0	6497.1	169.30	-0.647	142.87	Yang2002
TS NO.2 Forward.23.	0.00546	1.275	2033.5	4618.5	31.11	-0.449	7.67	12066.0	6496.5	151.45	-0.713	152.67	Yang2002
TS NO.2 Forward.24.	0.00546	1.275	2033.5	4618.5	26.96	-0.496	8.17	12066.0	6496.5	133.45	-0.778	162.62	Yang2002
TS NO.2 Forward.25.	0.00546	1.275	2032.1	4616.3	21.57	-0.555	8.87	12058.0	6493.9	109.80	-0.861	176.47	Yang2002
TS NO.2 Forward.26.	0.00546	1.275	1666.5	4594.3	57.40	-0.022	3.33	10032.0	6497.4	281.68	-0.126	67.02	Yang2002
TS NO.2 Forward.27.	0.00546	1.275	1664.5	4605.3	54.26	-0.057	3.60	10020.0	6513.5	270.35	-0.170	72.59	Yang2002
TS NO.2 Forward.28.	0.00546	1.275	1668.5	4592.1	50.70	-0.098	3.97	10043.0	6494.3	256.30	-0.223	80.05	Yang2002
TS NO.2 Forward.29.	0.00546	1.275	1666.5	4596.5	45.27	-0.157	4.63	10032.0	6500.5	234.40	-0.302	93.19	Yang2002
TS NO.2 Forward.30.	0.00546	1.275	1667.2	4592.1	40.06	-0.213	5.31	10035.0	6494.7	211.87	-0.381	106.96	Yang2002
TS NO.2 Forward.31.	0.00546	1.275	1669.2	4592.1	35.48	-0.262	5.89	10047.0	6494.1	192.25	-0.448	118.60	Yang2002
TS NO.2 Forward.32.	0.00546	1.275	1665.8	4589.9	31.11	-0.306	6.38	10028.0	6491.4	173.97	-0.508	128.47	Yang2002
TS NO.2 Forward.33.	0.00546	1.275	1665.2	4603.1	25.71	-0.361	7.06	10024.0	6510.2	150.73	-0.584	142.28	Yang2002

TS NO.2 Forward.34.	0.00546	1.275	1667.9	4592.1	22.19	-0.397	7.47	10039.0	6494.5	135.71	-0.633	150.46	Yang2002
TS NO.2 Forward.35.	0.00546	1.275	2392.4	3578.4	74.83	-0.010	2.73	14022.0	5000.7	314.12	-0.142	53.57	Yang2002
TS NO.2 Forward.36.	0.00546	1.275	2393.7	3585.0	71.25	-0.068	3.03	14029.0	5009.9	300.52	-0.216	59.48	Yang2002
TS NO.2 Forward.37.	0.00546	1.275	2388.3	3585.0	66.84	-0.133	3.42	14000.0	5010.4	283.42	-0.300	67.20	Yang2002
TS NO.2 Forward.38.	0.00546	1.275	2387.7	3585.0	62.22	-0.200	3.89	13998.0	5009.6	264.34	-0.390	76.25	Yang2002
TS NO.2 Forward.39.	0.00546	1.275	2391.0	3576.2	56.77	-0.278	4.44	14015.0	4997.6	240.89	-0.496	87.07	Yang2002
TS NO.2 Forward.40.	0.00546	1.275	2389.0	3576.2	51.54	-0.348	4.95	14004.0	4997.9	218.59	-0.591	97.15	Yang2002
TS NO.2 Forward.41.	0.00546	1.275	2393.1	3576.2	46.52	-0.417	5.45	14026.0	4997.4	196.69	-0.684	106.96	Yang2002
TS NO.2 Forward.42.	0.00546	1.275	2391.7	3571.8	40.68	-0.492	6.04	14019.0	4991.2	170.90	-0.790	118.51	Yang2002
TS NO.2 Forward.43.	0.00546	1.275	2391.7	3578.4	34.85	-0.566	6.56	14019.0	5000.4	146.09	-0.889	128.78	Yang2002
TS NO.2 Forward.44.	0.00546	1.275	2390.4	3571.8	29.66	-0.630	7.05	14011.0	4991.7	123.58	-0.978	138.44	Yang2002
TS NO.2 Forward.45.	0.00546	1.275	2391.0	3567.4	22.40	-0.719	7.80	14015.0	4985.3	91.58	-1.104	153.12	Yang2002
TS NO.2 Forward.46.	0.00546	1.275	2034.2	3558.6	67.05	-0.012	2.58	12070.0	5005.4	300.63	-0.126	51.31	Yang2002
TS NO.2 Forward.47.	0.00546	1.275	2032.8	3571.8	63.48	-0.060	2.86	12062.0	5024.3	287.46	-0.186	56.95	Yang2002
TS NO.2 Forward.48.	0.00546	1.275	2031.5	3552.0	60.12	-0.103	3.14	12055.0	4996.4	274.29	-0.243	62.56	Yang2002
TS NO.2 Forward.49.	0.00546	1.275	2031.5	3547.6	55.31	-0.164	3.64	12055.0	4990.2	253.99	-0.327	72.51	Yang2002
TS NO.2 Forward.50.	0.00546	1.275	2031.5	3558.6	49.87	-0.231	4.22	12055.0	5005.7	230.62	-0.419	83.89	Yang2002
TS NO.2 Forward.51.	0.00546	1.275	2031.5	3571.8	45.06	-0.288	4.68	12055.0	5024.3	210.41	-0.496	93.06	Yang2002
TS NO.2 Forward.52.	0.00546	1.275	2032.1	3567.4	40.89	-0.337	5.14	12058.0	5018.3	191.66	-0.566	102.36	Yang2002
TS NO.2 Forward.53.	0.00546	1.275	2033.5	3558.6	35.27	-0.402	5.70	12066.0	5005.6	167.08	-0.657	113.43	Yang2002
TS NO.2 Forward.54.	0.00546	1.275	2032.8	3556.4	29.66	-0.465	6.24	12062.0	5002.7	142.61	-0.745	124.15	Yang2002
TS NO.2 Forward.55.	0.00546	1.275	2033.5	3547.6	24.68	-0.521	6.69	12066.0	4990.1	120.98	-0.822	133.19	Yang2002
TS NO.2 Forward.56.	0.00546	1.275	2032.1	3549.8	20.74	-0.564	7.05	12058.0	4993.6	104.35	-0.880	140.27	Yang2002
TS NO.2 Forward.57.	0.00546	1.275	1667.2	3527.8	56.98	-0.027	2.63	10035.0	4989.4	279.63	-0.134	52.96	Yang2002
TS NO.2 Forward.58.	0.00546	1.275	1667.9	3534.4	53.63	-0.065	2.90	10039.0	4998.6	267.01	-0.183	58.40	Yang2002
TS NO.2 Forward.59.	0.00546	1.275	1666.5	3541.0	49.87	-0.107	3.27	10032.0	5007.8	251.60	-0.240	65.77	Yang2002
TS NO.2 Forward.60.	0.00546	1.275	1663.8	3527.8	45.48	-0.154	3.68	10017.0	4989.3	233.58	-0.304	74.18	Yang2002
TS NO.2 Forward.61.	0.00546	1.275	1663.8	3538.8	40.27	-0.210	4.19	10017.0	5004.8	211.68	-0.380	84.31	Yang2002
TS NO.2 Forward.62.	0.00546	1.275	1667.9	3545.4	35.69	-0.260	4.71	10039.0	5014.1	191.06	-0.451	94.90	Yang2002
TS NO.2 Forward.63.	0.00546	1.275	1666.5	3538.8	30.49	-0.313	5.25	10032.0	5004.7	167.83	-0.528	105.74	Yang2002
TS NO.2 Forward.64.	0.00546	1.275	1669.2	3536.6	25.30	-0.367	5.73	10047.0	5001.4	145.72	-0.601	115.38	Yang2002
TS NO.2 Forward.65.	0.00546	1.275	1666.5	3532.2	21.15	-0.407	6.14	10032.0	4995.3	127.52	-0.659	123.67	Yang2002
TS NO.2 Forward.66.	0.00546	1.275	2390.4	2861.5	72.94	-0.040	2.23	14011.0	3999.1	308.01	-0.176	43.72	Yang2002
TS NO.2 Forward.67.	0.00546	1.275	2391.7	2861.5	68.94	-0.102	2.52	14019.0	3998.7	292.46	-0.257	49.45	Yang2002
TS NO.2 Forward.68.	0.00546	1.275	2391.0	2861.5	63.90	-0.177	2.95	14015.0	3998.9	271.46	-0.358	57.87	Yang2002
TS NO.2 Forward.69.	0.00546	1.275	2390.4	2852.7	59.08	-0.245	3.36	14011.0	3986.8	250.66	-0.452	65.98	Yang2002
TS NO.2 Forward.70.	0.00546	1.275	2391.0	2865.9	54.47	-0.309	3.77	14015.0	4005.0	230.51	-0.541	74.00	Yang2002
TS NO.2 Forward.71.	0.00546	1.275	2391.7	2861.5	50.08	-0.369	4.16	14019.0	3998.7	210.87	-0.625	81.66	Yang2002

TS NO.2 Forward.72.	0.00546	1.275	2389.7	2868.1	45.27	-0.431	4.61	14008.0	4008.1	189.08	-0.714	90.37	Yang2002
TS NO.2 Forward.73.	0.00546	1.275	2390.4	2859.3	40.27	-0.496	5.02	14011.0	3996.0	166.64	-0.806	98.52	Yang2002
TS NO.2 Forward.74.	0.00546	1.275	2387.7	2857.1	35.27	-0.558	5.42	13998.0	3992.5	144.69	-0.893	106.35	Yang2002
TS NO.2 Forward.75.	0.00546	1.275	2392.4	2868.1	29.03	-0.638	5.91	14022.0	4008.1	117.75	-1.002	115.97	Yang2002
TS NO.2 Forward.76.	0.00546	1.275	2388.3	2861.5	25.71	-0.677	6.09	14000.0	3999.3	104.24	-1.053	119.61	Yang2002
TS NO.2 Forward.77.	0.00546	1.275	2389.7	2865.9	21.77	-0.726	6.47	14008.0	4005.0	86.49	-1.124	126.94	Yang2002
TS NO.2 Forward.78.	0.00546	1.275	2028.1	2841.7	67.26	-0.007	2.07	12036.0	3997.7	301.05	-0.122	41.24	Yang2002
TS NO.2 Forward.79.	0.00546	1.275	2033.5	2846.1	63.69	-0.057	2.32	12066.0	4003.4	287.46	-0.186	46.16	Yang2002
TS NO.2 Forward.80.	0.00546	1.275	2028.8	2839.5	59.70	-0.108	2.65	12040.0	3994.4	271.10	-0.255	52.72	Yang2002
TS NO.2 Forward.81.	0.00546	1.275	2028.8	2841.7	54.89	-0.168	3.05	12040.0	3997.5	251.03	-0.338	60.78	Yang2002
TS NO.2 Forward.82.	0.00546	1.275	2031.5	2846.1	49.45	-0.236	3.51	12055.0	4003.5	227.56	-0.431	69.78	Yang2002
TS NO.2 Forward.83.	0.00546	1.275	2030.8	2843.9	45.48	-0.283	3.84	12051.0	4000.5	210.12	-0.497	76.43	Yang2002
TS NO.2 Forward.84.	0.00546	1.275	2030.1	2846.1	39.85	-0.348	4.37	12047.0	4003.8	184.35	-0.592	86.89	Yang2002
TS NO.2 Forward.85.	0.00546	1.275	2032.8	2846.1	34.44	-0.412	4.81	12062.0	4003.5	160.36	-0.681	95.73	Yang2002
TS NO.2 Forward.86.	0.00546	1.275	2032.1	2852.7	29.86	-0.463	5.18	12058.0	4013.0	140.46	-0.752	103.16	Yang2002
TS NO.2 Forward.87.	0.00546	1.275	2032.1	2841.7	24.68	-0.520	5.61	12058.0	3997.5	117.34	-0.834	111.62	Yang2002
TS NO.2 Forward.88.	0.00546	1.275	2028.1	2841.7	21.15	-0.557	5.88	12036.0	3997.7	102.01	-0.886	117.08	Yang2002
TS NO.2 Forward.89.	0.00546	1.275	1664.5	2824.1	56.56	-0.031	2.46	10020.0	3994.3	273.89	-0.156	49.52	Yang2002
TS NO.2 Forward.90.	0.00546	1.275	1666.5	2824.1	52.79	-0.074	2.68	10032.0	3993.9	259.64	-0.211	54.01	Yang2002
TS NO.2 Forward.91.	0.00546	1.275	1666.5	2830.7	49.45	-0.112	2.93	10032.0	4003.3	245.89	-0.261	59.06	Yang2002
TS NO.2 Forward.92.	0.00546	1.275	1665.2	2824.1	45.27	-0.157	3.28	10024.0	3994.2	228.07	-0.324	66.04	Yang2002
TS NO.2 Forward.93.	0.00546	1.275	1665.8	2826.3	40.27	-0.211	3.63	10028.0	3997.2	207.04	-0.397	73.17	Yang2002
TS NO.2 Forward.94.	0.00546	1.275	1665.8	2826.3	34.44	-0.272	4.13	10028.0	3997.2	181.32	-0.483	83.20	Yang2002
TS NO.2 Forward.95.	0.00546	1.275	1667.9	2826.3	30.28	-0.316	4.47	10039.0	3997.2	162.87	-0.545	89.95	Yang2002
TS NO.2 Forward.96.	0.00546	1.275	1665.8	2819.7	25.71	-0.361	4.83	10028.0	3987.8	142.75	-0.610	97.36	Yang2002
TS NO.2 Forward.97.	0.00546	1.275	1668.5	2826.3	21.15	-0.408	5.21	10043.0	3997.1	122.57	-0.676	104.99	Yang2002
TS NO.2 Reverse.1.	0.00546	1.350	2389.0	4537.1	74.20	-0.021	3.73	14004.0	6340.9	311.05	-0.159	71.14	Yang2002
TS NO.2 Reverse.2.	0.00546	1.350	2391.0	4600.9	71.88	-0.059	4.11	14015.0	6429.7	302.29	-0.206	78.30	Yang2002
TS NO.2 Reverse.3.	0.00546	1.350	2390.4	4618.5	70.83	-0.073	4.33	14011.0	6454.6	297.61	-0.230	82.53	Yang2002
TS NO.2 Reverse.4.	0.00546	1.350	2387.7	4651.5	66.42	-0.139	5.07	13998.0	6500.0	278.88	-0.322	96.60	Yang2002
TS NO.2 Reverse.5.	0.00546	1.350	2388.3	4655.9	63.06	-0.188	5.34	14000.0	6507.2	266.42	-0.380	101.79	Yang2002
TS NO.2 Reverse.6.	0.00546	1.350	2392.4	4669.1	60.12	-0.232	5.58	14022.0	6525.0	255.31	-0.432	106.25	Yang2002
TS NO.2 Reverse.7.	0.00546	1.350	2389.0	4655.9	55.31	-0.297	5.98	14004.0	6506.8	236.89	-0.512	113.86	Yang2002
TS NO.2 Reverse.8.	0.00546	1.350	2392.4	4649.3	50.28	-0.366	6.61	14022.0	6497.3	215.34	-0.606	125.97	Yang2002
TS NO.2 Reverse.9.	0.00546	1.350	2390.4	4655.9	45.27	-0.432	7.26	14011.0	6506.9	194.15	-0.694	138.31	Yang2002
TS NO.2 Reverse.10.	0.00546	1.350	2389.7	4655.9	39.85	-0.501	7.95	14008.0	6506.5	171.07	-0.788	151.43	Yang2002
TS NO.2 Reverse.11.	0.00546	1.350	2389.0	4655.9	36.10	-0.549	8.45	14004.0	6506.8	154.57	-0.854	160.93	Yang2002
TS NO.2 Reverse.12.	0.00546	1.350	2389.7	4658.1	31.94	-0.601	8.92	14008.0	6509.6	137.19	-0.924	170.04	Yang2002

TS NO.2 Reverse.13.	0.00546	1.350	2391.7	4642.7	28.41	-0.646	9.38	14019.0	6487.7	121.68	-0.986	178.70	Yang2002
TS NO.2 Reverse.14.	0.00546	1.350	2393.7	4666.9	24.68	-0.692	9.83	14029.0	6521.9	106.27	-1.048	187.34	Yang2002
TS NO.2 Reverse.15.	0.00546	1.350	2389.0	4640.5	21.15	-0.733	10.26	14004.0	6485.3	91.07	-1.105	195.52	Yang2002
TS NO.2 Reverse.16.	0.00546	1.350	2028.8	4550.3	63.06	-0.064	4.41	12040.0	6401.1	281.51	-0.211	85.24	Yang2002
TS NO.2 Reverse.17.	0.00546	1.350	2032.1	4614.1	60.12	-0.103	4.66	12058.0	6490.8	271.26	-0.256	90.06	Yang2002
TS NO.2 Reverse.18.	0.00546	1.350	2031.5	4611.9	57.61	-0.135	4.86	12055.0	6487.4	261.93	-0.294	93.98	Yang2002
TS NO.2 Reverse.19.	0.00546	1.350	2028.8	4622.9	54.47	-0.173	5.04	12040.0	6503.2	250.76	-0.339	97.47	Yang2002
TS NO.2 Reverse.20.	0.00546	1.350	2028.8	4640.5	49.66	-0.232	5.37	12040.0	6528.0	233.28	-0.408	103.85	Yang2002
TS NO.2 Reverse.21.	0.00546	1.350	2031.5	4631.7	45.27	-0.286	5.90	12055.0	6515.2	215.19	-0.478	113.90	Yang2002
TS NO.2 Reverse.22.	0.00546	1.350	2032.8	4618.5	40.27	-0.345	6.54	12062.0	6496.7	193.65	-0.559	126.36	Yang2002
TS NO.2 Reverse.23.	0.00546	1.350	2029.5	4616.3	35.69	-0.396	7.15	12044.0	6493.7	173.79	-0.631	138.06	Yang2002
TS NO.2 Reverse.24.	0.00546	1.350	2032.8	4618.5	30.70	-0.454	7.84	12062.0	6496.7	151.86	-0.711	151.46	Yang2002
TS NO.2 Reverse.25.	0.00546	1.350	2029.5	4620.7	25.30	-0.512	8.50	12044.0	6499.9	129.02	-0.792	164.15	Yang2002
TS NO.2 Reverse.26.	0.00546	1.350	2029.5	4618.5	21.15	-0.558	9.02	12044.0	6496.8	111.12	-0.855	174.25	Yang2002
TS NO.2 Reverse.27.	0.00546	1.350	1662.5	4512.9	52.17	-0.080	4.31	10009.0	6382.9	259.18	-0.211	84.36	Yang2002
TS NO.2 Reverse.28.	0.00546	1.350	1663.8	4574.5	49.66	-0.108	4.56	10017.0	6469.6	250.06	-0.245	89.24	Yang2002
TS NO.2 Reverse.29.	0.00546	1.350	1661.8	4596.5	45.27	-0.156	4.78	10005.0	6501.3	234.91	-0.299	93.56	Yang2002
TS NO.2 Reverse.30.	0.00546	1.350	1665.2	4607.5	40.48	-0.208	5.11	10024.0	6516.4	217.33	-0.361	99.95	Yang2002
TS NO.2 Reverse.31.	0.00546	1.350	1663.8	4587.7	35.27	-0.263	5.75	10017.0	6488.3	195.34	-0.436	112.56	Yang2002
TS NO.2 Reverse.32.	0.00546	1.350	1665.8	4589.9	30.49	-0.313	6.40	10028.0	6491.4	174.72	-0.505	125.20	Yang2002
TS NO.2 Reverse.33.	0.00546	1.350	1664.5	4598.7	25.71	-0.361	7.05	10020.0	6504.2	153.91	-0.573	137.83	Yang2002
TS NO.2 Reverse.34.	0.00546	1.350	1665.8	4605.3	20.95	-0.409	7.67	10028.0	6513.1	133.41	-0.640	150.04	Yang2002
TS NO.2 Reverse.35.	0.00546	1.350	2389.0	3576.2	72.94	-0.039	3.36	14004.0	4997.9	304.01	-0.197	64.05	Yang2002
TS NO.2 Reverse.36.	0.00546	1.350	2390.4	3571.8	69.99	-0.086	3.51	14011.0	4991.7	293.74	-0.250	66.91	Yang2002
TS NO.2 Reverse.37.	0.00546	1.350	2390.4	3578.4	65.16	-0.158	3.86	14011.0	5001.0	275.22	-0.340	73.61	Yang2002
TS NO.2 Reverse.38.	0.00546	1.350	2386.3	3576.2	59.91	-0.232	4.24	13990.0	4997.8	255.18	-0.431	80.78	Yang2002
TS NO.2 Reverse.39.	0.00546	1.350	2389.7	3574.0	53.84	-0.317	4.70	14008.0	4994.5	231.00	-0.538	89.63	Yang2002
TS NO.2 Reverse.40.	0.00546	1.350	2389.0	3587.2	49.66	-0.373	5.16	14004.0	5013.2	212.94	-0.615	98.29	Yang2002
TS NO.2 Reverse.41.	0.00546	1.350	2389.7	3591.6	46.11	-0.420	5.53	14008.0	5019.1	197.62	-0.679	105.41	Yang2002
TS NO.2 Reverse.42.	0.00546	1.350	2392.4	3574.0	40.68	-0.492	6.10	14022.0	4994.6	173.46	-0.779	116.18	Yang2002
TS NO.2 Reverse.43.	0.00546	1.350	2388.3	3565.2	35.27	-0.559	6.65	14000.0	4982.8	149.87	-0.873	126.64	Yang2002
TS NO.2 Reverse.44.	0.00546	1.350	2387.7	3585.0	29.86	-0.626	7.24	13998.0	5009.6	126.34	-0.966	138.02	Yang2002
TS NO.2 Reverse.45.	0.00546	1.350	2386.3	3576.2	25.71	-0.676	7.65	13990.0	4997.8	108.19	-1.037	145.86	Yang2002
TS NO.2 Reverse.46.	0.00546	1.350	2390.4	3578.4	21.36	-0.731	8.09	14011.0	5001.0	89.43	-1.112	154.07	Yang2002
TS NO.2 Reverse.47.	0.00546	1.350	2027.4	3552.0	66.84	-0.013	3.01	12033.0	4996.7	297.14	-0.141	58.18	Yang2002
TS NO.2 Reverse.48.	0.00546	1.350	2030.8	3556.4	64.53	-0.045	3.23	12051.0	5002.8	288.01	-0.183	62.47	Yang2002
TS NO.2 Reverse.49.	0.00546	1.350	2026.8	3552.0	62.22	-0.074	3.37	12029.0	4996.8	279.82	-0.218	65.05	Yang2002
TS NO.2 Reverse.50.	0.00546	1.350	2029.5	3552.0	59.28	-0.113	3.58	12044.0	4996.5	268.68	-0.266	69.12	Yang2002

TS NO.2 Reverse.51.	0.00546	1.350	2026.1	3558.6	55.51	-0.160	3.82	12025.0	5006.3	254.78	-0.322	73.85	Yang2002
TS NO.2 Reverse.52.	0.00546	1.350	2028.1	3560.8	50.28	-0.224	4.13	12036.0	5009.3	235.10	-0.400	79.87	Yang2002
TS NO.2 Reverse.53.	0.00546	1.350	2025.4	3554.2	45.48	-0.281	4.48	12021.0	5000.3	216.30	-0.472	86.55	Yang2002
TS NO.2 Reverse.54.	0.00546	1.350	2025.4	3560.8	39.43	-0.352	5.13	12021.0	5009.6	190.09	-0.570	99.11	Yang2002
TS NO.2 Reverse.55.	0.00546	1.350	2026.8	3552.0	35.27	-0.400	5.59	12029.0	4996.8	171.64	-0.638	107.93	Yang2002
TS NO.2 Reverse.56.	0.00546	1.350	2026.8	3554.2	29.66	-0.463	6.19	12029.0	4999.9	146.72	-0.727	119.70	Yang2002
TS NO.2 Reverse.57.	0.00546	1.350	2026.1	3556.4	25.30	-0.511	6.66	12025.0	5003.2	127.50	-0.796	128.73	Yang2002
TS NO.2 Reverse.58.	0.00546	1.350	2024.7	3552.0	21.36	-0.554	7.08	12018.0	4996.9	110.25	-0.856	136.79	Yang2002
TS NO.2 Reverse.59.	0.00546	1.350	1665.2	3554.2	57.19	-0.024	3.13	10024.0	5026.7	276.97	-0.144	61.19	Yang2002
TS NO.2 Reverse.60.	0.00546	1.350	1665.2	3545.4	52.79	-0.074	3.44	10024.0	5014.3	260.54	-0.207	67.22	Yang2002
TS NO.2 Reverse.61.	0.00546	1.350	1665.8	3527.8	49.66	-0.109	3.68	10028.0	4989.2	248.12	-0.253	71.89	Yang2002
TS NO.2 Reverse.62.	0.00546	1.350	1664.5	3525.6	45.48	-0.154	3.91	10020.0	4986.4	232.87	-0.307	76.53	Yang2002
TS NO.2 Reverse.63.	0.00546	1.350	1662.5	3532.2	39.85	-0.214	4.28	10009.0	4995.8	211.39	-0.381	83.64	Yang2002
TS NO.2 Reverse.64.	0.00546	1.350	1666.5	3536.6	35.69	-0.259	4.64	10032.0	5001.6	194.22	-0.440	90.78	Yang2002
TS NO.2 Reverse.65.	0.00546	1.350	1663.8	3530.0	29.24	-0.325	5.21	10017.0	4992.4	167.55	-0.528	101.90	Yang2002
TS NO.2 Reverse.66.	0.00546	1.350	1660.5	3541.0	25.71	-0.359	5.61	9998.0	5008.2	151.79	-0.579	109.74	Yang2002
TS NO.2 Reverse.67.	0.00546	1.350	1663.8	3527.8	21.15	-0.406	6.03	10017.0	4989.3	132.16	-0.643	117.96	Yang2002
TS NO.2 Reverse.68.	0.00546	1.350	2389.7	2865.9	74.62	-0.012	2.45	14008.0	4005.0	311.77	-0.155	46.72	Yang2002
TS NO.2 Reverse.69.	0.00546	1.350	2389.0	2861.5	72.31	-0.049	2.60	14004.0	3999.1	303.17	-0.201	49.47	Yang2002
TS NO.2 Reverse.70.	0.00546	1.350	2389.7	2863.7	68.94	-0.102	2.81	14008.0	4001.9	290.54	-0.266	53.56	Yang2002
TS NO.2 Reverse.71.	0.00546	1.350	2389.7	2865.9	65.79	-0.149	3.01	14008.0	4005.0	278.28	-0.325	57.35	Yang2002
TS NO.2 Reverse.72.	0.00546	1.350	2388.3	2865.9	62.64	-0.194	3.25	14000.0	4005.4	265.53	-0.384	61.92	Yang2002
TS NO.2 Reverse.73.	0.00546	1.350	2391.7	2859.3	58.87	-0.249	3.48	14019.0	3995.6	250.75	-0.452	66.21	Yang2002
TS NO.2 Reverse.74.	0.00546	1.350	2388.3	2854.9	54.68	-0.305	3.74	14000.0	3990.1	233.82	-0.526	71.20	Yang2002
TS NO.2 Reverse.75.	0.00546	1.350	2389.7	2861.5	50.28	-0.365	4.03	14008.0	3998.9	216.08	-0.602	76.75	Yang2002
TS NO.2 Reverse.76.	0.00546	1.350	2389.0	2868.1	45.48	-0.428	4.49	14004.0	4008.3	194.49	-0.692	85.54	Yang2002
TS NO.2 Reverse.77.	0.00546	1.350	2388.3	2861.5	40.48	-0.493	4.97	14000.0	3999.3	171.66	-0.785	94.78	Yang2002
TS NO.2 Reverse.78.	0.00546	1.350	2390.4	2854.9	34.65	-0.567	5.50	14011.0	3989.9	145.11	-0.893	104.85	Yang2002
TS NO.2 Reverse.79.	0.00546	1.350	2391.0	2870.3	29.86	-0.627	5.92	14015.0	4011.2	124.32	-0.976	112.75	Yang2002
TS NO.2 Reverse.80.	0.00546	1.350	2388.3	2854.9	26.34	-0.669	6.21	14000.0	3990.1	108.66	-1.036	118.43	Yang2002
TS NO.2 Reverse.81.	0.00546	1.350	2390.4	2863.7	21.36	-0.731	6.62	14011.0	4002.2	87.21	-1.121	126.08	Yang2002
TS NO.2 Reverse.82.	0.00546	1.350	2028.8	2837.3	67.68	-0.002	2.34	12040.0	3991.3	300.27	-0.126	45.28	Yang2002
TS NO.2 Reverse.83.	0.00546	1.350	2027.4	2852.7	64.53	-0.044	2.57	12033.0	4013.0	288.40	-0.180	49.64	Yang2002
TS NO.2 Reverse.84.	0.00546	1.350	2028.8	2841.7	60.54	-0.097	2.86	12040.0	3997.5	272.56	-0.249	55.25	Yang2002
TS NO.2 Reverse.85.	0.00546	1.350	2027.4	2841.7	54.68	-0.170	3.23	12033.0	3997.5	249.81	-0.342	62.44	Yang2002
TS NO.2 Reverse.86.	0.00546	1.350	2027.4	2839.5	49.66	-0.232	3.54	12033.0	3994.4	229.79	-0.421	68.48	Yang2002
TS NO.2 Reverse.87.	0.00546	1.350	2025.4	2841.7	46.94	-0.264	3.71	12021.0	3997.9	219.27	-0.460	71.65	Yang2002
TS NO.2 Reverse.88.	0.00546	1.350	2026.1	2837.3	43.81	-0.301	3.93	12025.0	3991.6	206.20	-0.510	75.86	Yang2002

TS NO.2 Reverse.89.	0.00546	1.350	2026.1	2839.5	39.02	-0.356	4.26	12025.0	3994.7	186.28	-0.584	82.25	Yang2002
TS NO.2 Reverse.90.	0.00546	1.350	2026.8	2843.9	34.85	-0.404	4.65	12029.0	4000.7	167.50	-0.653	89.86	Yang2002
TS NO.2 Reverse.91.	0.00546	1.350	2025.4	2837.3	29.45	-0.465	5.10	12021.0	3991.8	143.86	-0.737	98.49	Yang2002
TS NO.2 Reverse.92.	0.00546	1.350	2026.8	2841.7	25.30	-0.511	5.42	12029.0	3997.6	126.19	-0.801	104.74	Yang2002
TS NO.2 Reverse.93.	0.00546	1.350	2024.7	2846.1	21.15	-0.556	5.76	12018.0	4003.9	108.05	-0.864	111.40	Yang2002
TS NO.2 Reverse.94.	0.00546	1.350	1665.2	2826.3	57.19	-0.024	2.63	10024.0	3997.3	275.13	-0.151	51.45	Yang2002
TS NO.2 Reverse.95.	0.00546	1.350	1665.8	2828.5	52.79	-0.074	2.82	10028.0	4000.3	259.29	-0.212	55.24	Yang2002
TS NO.2 Reverse.96.	0.00546	1.350	1665.8	2824.1	49.03	-0.116	3.06	10028.0	3994.0	244.71	-0.265	59.92	Yang2002
TS NO.2 Reverse.97.	0.00546	1.350	1663.8	2826.3	44.44	-0.165	3.44	10017.0	3997.2	225.40	-0.333	67.29	Yang2002
TS NO.2 Reverse.98.	0.00546	1.350	1662.5	2821.9	38.60	-0.227	3.85	10009.0	3991.2	201.27	-0.415	75.26	Yang2002
TS NO.2 Reverse.99.	0.00546	1.350	1661.8	2819.7	40.68	-0.205	3.68	10005.0	3988.2	210.29	-0.385	71.90	Yang2002
TS NO.2 Reverse.100.	0.00546	1.350	1663.8	2824.1	34.65	-0.269	4.09	10017.0	3994.1	185.43	-0.469	79.91	Yang2002
TS NO.2 Reverse.101.	0.00546	1.350	1666.5	2817.5	29.86	-0.319	4.44	10032.0	3984.6	165.09	-0.537	86.75	Yang2002
TS NO.2 Reverse.102.	0.00546	1.350	1665.2	2817.5	24.88	-0.369	4.77	10024.0	3984.8	144.65	-0.603	93.28	Yang2002
TS NO.2 Reverse.103.	0.00546	1.350	1663.8	2813.1	21.15	-0.406	5.07	10017.0	3978.5	128.29	-0.656	99.18	Yang2002

Appendix E: Computation Procedure of CHF Prediction for a Tube with Non-Uniform AFD Using CHF Look-up Table

E.1 Introduction

The objective is to predict the critical power and CHF location for a non-uniform AFD tube at given inlet conditions, channel geometry, heated length and AFD profile using CHF look-up table.

The given parameters are P, G, T_{in}, D_i, L_h. The non-uniform AFD profile is characterized by the ratio of local heat flux to average heat flux as a function of axial location, i.e.:

$$\frac{q''(z)}{q''_{avg}} = f(z). \tag{E.1}$$

Note that the actual f(z) used for CHF prediction in this study is different from those presented in Figures 4.2, 4.3 and 6.18 as was indicated in the titles of these figures. For Figures 4.2 and 4.3 the actual f(z) was based on the actual heated length used in the CHF measurement, while for Figure 6.18 it was based on the heated section upstream of the measured CHF location.

In the numerical computation, the heated length of the non-uniform AFD tube is divided into N zones about 0.05 m long. Eq (E.1) is re-written as

$$\frac{q''(k)}{q''_{avg}} = f(k), \ k = 1,2,\cdots N \tag{E.2}$$

where k is the zone number and q"(k) is the local heat flux at the end of zone k.

For a non-uniform AFD tube with a stepped AFD profile, the actual number of steps and the actual step length may be used for the computation.

The relationship of CHF as a function of local conditions for a uniform AFD tube, i.e.:

$$CHF = f(P, G, X_{do}, D_i) \tag{E.3}$$

is obtained from CHF look-up table.

The computation procedures for CHF using non-uniform AFD effect prediction methods are described in the following sections. These prediction methods are overall power approach, local conditions approach, F-factor approach and boiling length average approach.

E.2 Overall Power Approach

E.2.1 General

Using this method, the critical power for a non-uniform AFD tube is assumed to be the same as that for a uniform AFD tube of the same cross sectional geometry and heated length at given inlet conditions, i.e.,

$$Power_{non} = Power_{U} . \tag{E.4}$$

Since the initial CHF occurs always at the tube exit for a uniformly heated tube, the following relationship yields between X_{do} and CHF value for a uniform AFD:

$$X_{do} = X_{in} + \frac{4L_h}{D_i G i_{fg}} CHF . \tag{E.5}$$

The CHF value and X_{do} at given pressure and mass flux can be obtained by solving Eq (E.3) and Eq (E.4). The critical power can be obtained consequently by

$$Power_{non} = Power_{U} = \pi D_i L_h CHF . \tag{E.6}$$

E.2.2 Computation Procedure

The computation procedure is described as follows:

(i) Evaluate the fluid properties of i_l, i_f, i_g at given pressure of P.

(ii) Calculate X_{in} as

$$X_{in} = \frac{i_l - i_f}{i_g - i_f} . \tag{E.7}$$

(iii) Assuming the critical power for the uniformly heated tube equals arbitrarily to a value of W, i.e.:

$$Power_{U} = W \tag{E.8}$$

calculate the corresponded CHF value and X_{do} as

$$CHF = \frac{W}{\pi D_i L_h} \tag{E.9}$$

and

$$X_{do} = X_{in} + \frac{4L_h}{D_i G i_{fg}} CHF. \tag{E.10}$$

(iv) Compare this CHF value with that obtained from CHF look-up table, CHF_{TB}, at X_{do}. If

$$\left| \frac{CHF_{TB} - CHF}{CHF_{TB}} \right| \leq 0.005 \tag{E.11}$$

then the critical powers for the non-uniform and uniform AFDs equal to the assumed critical power, i.e.:

$$Power_{non} = Power_U = W. \tag{E.12}$$

(v) Otherwise, iterate (iii) and (iv) until Eq (E.11) is satisfied.

E.3 Local Conditions Approach

E.3.1 General

Using this method, the CHF conditions for a non-uniform AFD is supposed to be reached at a power at which the local heat flux vs. local quality curve of the non-uniform AFD becomes tangent to the curve of CHF vs. X_{do} of the uniform AFD at the same P, G and D_i.

E.3.2 Computation Procedure

The computation procedure is described as follows:

(i) Evaluate the fluid properties of i_l, i_f, i_g at given pressure of P.

(ii) Calculate X_{in} as

$$X_{in} = \frac{i_l - i_f}{i_g - i_f}. \tag{E.13}$$

(iii) Assuming the critical power for the non-uniformly heated tube equals arbitrarily to a value of W, i.e.:

$$Power_{non} = W \tag{E.14}$$

calculate the corresponded local heat flux value and local quality at the end of each zone according to Eq. (E.2) as

$$q''(k) = q''_{avg} f(k) = \frac{W}{\pi D_i L_h} f(k) \tag{E.15}$$

and

$$X(k) = X_{in} + \frac{\int_0^{z(k)} 4q''(z)dz}{GD_i(i_g - i_f)}. \tag{E.16}$$

(iv) Evaluate the CHF value for uniform AFD, $CHF_{TB}(k)$, at $X_{do} = X(k)$ using CHF look-up table.

(v) Calculate

$$\Delta q''(k) = CHF_{TB}(k) - q''(k). \tag{E.17}$$

(vi) Find the minimum of $\Delta q''(k), \Delta q''_{min}$, and the corresponding zone number, N_{min}. If

$$\left| \frac{\Delta q''_{min}}{CHF_{TB}(N_{min})} \right| \le 0.005 \tag{E.18}$$

then the critical power for the non-uniform AFD tube equals to W; the initial CHF location situates at $z(N_{min})$ and the initial CHF value equals to $q''(N_{min})$.

(vii) Otherwise, iterate (iii) to (vi) until Eq (E.18) is satisfied.

E.4 F-factor Approach

E.4.1 General

The F-factor approach modifies the CHF for a uniform AFD to predict the CHF value and CHF location for a non-uniform AFD as illustrated in Figure 3.1c.

The expression of F is given by

$$F = \frac{q''_{cr\_EU}}{q''_{cr\_non}} = \frac{C}{1-\exp(-Cz_{cr})}\int_0^{z_{cr}} \frac{q''(z)}{q''(z_{cr})}\exp[-C(z_{cr}-z)]dz \tag{E.19}$$

where

$$C = 0.15 \times \frac{(1-X(z_{cr}))^{4.31}}{(737.4631\times G/10^6)^{0.478}} (\text{inch}^{-1}). \tag{E.20}$$

E.4.2 Computation Procedure

(i) Evaluate the fluid properties of i_l, i_f, i_g at given pressure of P.

(ii) Calculate X_{in} as

$$X_{in} = \frac{i_l - i_f}{i_g - i_f}. \tag{E.21}$$

(iii) Assuming the critical power for the non-uniform AFD equals arbitrarily to a value of W, i.e.:

$$\text{Power}_{non} = W \tag{E.22}$$

calculate the corresponded local heat flux value and local quality at the end of each zone according to Eq. (E.2) as

$$q''(k) = q''_{avg}\, f(k) = \frac{W}{\pi D_i L_h} f(k) \tag{E.23}$$

and

$$X(k) = X_{in} + \frac{\int_0^{z(k)} 4q''(z)dz}{GD_i(i_g - i_f)}. \tag{E.24}$$

(iv) Calculate the coefficient, C, using the local quality at each zone end taking into account the unit conversion (1 m = 39.3701 inch, 1 kg m^{-2} s^{-1} = 737.4631 lb ft^{-2} h^{-1}) as

$$C(k) = 0.15 \times \frac{(1 - X(k))^{4.31}}{(737.4631 \times G / 10^6)^{0.478}} (\text{inch}^{-1}). \tag{E.25}$$

(v) Calculate the factor, F, for each zone end taking into account the unit conversion (1 m = 39.3701 inch) as

$$F(k) = \frac{C(k)}{1 - \exp(-Cz(k))} \int_0^{z(k)} \frac{q''(z)}{q''(k)} \exp[-C(k)(z(k) - z)] dz. \tag{E.26}$$

(vi) Evaluate the CHF value for uniform AFD, $CHF_{TB}(k)$, at X_{do} = X(k) using CHF look-up table.

(vii) Calculate the modified uniform CHF value at X_{do} = X(k) by

$$q''_{cr\_non}(k) = \frac{CHF_{TB}(k)}{F}. \tag{E.27}$$

(viii) Calculate

$$\Delta q''(k) = q''_{cr\_non} - q''(k). \tag{E.28}$$

(ix) Find the minimum of $\Delta q''(k)$, $\Delta q''_{min}$, and the corresponding zone number N_{min}. If

$$\left| \frac{\Delta q''_{min}}{CHF_{TB}(N_{min})} \right| \le 0.005 \tag{E.29}$$

then the critical power for the non-uniform AFD tube equals to W; the initial CHF location situates at $z(N_{min})$ and the initial CHF value equals to $q''(N_{min})$.

(x) Otherwise, iterate (iii) to (ix) until Eq (E.29) is satisfied.

E.5 Boiling Length Average Approach with Boiling Length Starting Point at the Onset of Annular Flow

E.5.1 General

The BLA approach modifies the local heat flux. This method is based on the hypothesis that the CHF for a non-uniform AFD is equal to the heat flux at the location where the $q''_{BLA,OAF}$ curve becomes tangent to the CHF curve for the uniform AFD at the same local conditions (see Figure 3.1d).

The boiling length average heat flux with the boiling length starting point at the onset of annular flow, $q''_{BLA,OAF}$, is defined as

$$q''_{BLA,OAF}(z_{cr}) = \frac{1}{L_B}\int_{z_{OAF}}^{z_{cr}} q''(z)dz \tag{E.30}$$

where the boiling length is obtained by

$$L_B = z_{cr} - z_{OAF}. \tag{E.31}$$

E.5.2 Computation Procedure

(i) Evaluate the fluid properties of i_l, i_f, i_g, ρ_f, ρ_g, σ at given pressure of P.

(ii) Calculate X_{in} as

$$X_{in} = \frac{i_l - i_f}{i_g - i_f}. \tag{E.32}$$

(iii) Assuming the critical power for the non-uniform AFD equals arbitrarily to a value of W, i.e.:

$$Power_{non} = W \tag{E.33}$$

calculate the corresponded local heat flux value and local quality at the end of each zone according to Eq (E.2) as

$$q''(k) = q''_{avg}\, f(k) = \frac{W}{\pi D_i L_h} f(k) \tag{E.34}$$

and

$$X(k) = X_{in} + \frac{\int_0^{z(k)} 4q''(z)dz}{GD_i(i_g - i_f)}. \quad (E.35)$$

(iv) Evaluate the local quality at OAF point as

$$X_{OAF} = \frac{3.09\rho_g^{0.5}\left[g(\rho_f - \rho_g)\sigma\right]^{0.25}}{G}. \quad (3.36)$$

(v) Evaluate the axial location of OAF point, z_{OAF}, by satisfying the following equation:

$$X_{OAF} = X_{in} + \frac{\int_0^{z_{OAF}} 4q''(z)dz}{GD_i(i_g - i_f)}. \quad (E.37)$$

(vi) Calculate $q''_{BLA,OAF}$ at each zone end after the OAF point as

$$q''_{BLA,OAF}(k) = \frac{1}{z(k) - z_{OAF}} \int_{z_{OAF}}^{z(k)} q''(z)dz. \quad (E.38)$$

(vii) Evaluate the CHF value for uniform AFD, $CHF_{TB}(k)$, at $X_{do} = X(k)$ using CHF look-up table.

(viii) Calculate

$$\Delta q''(k) = CHF_{TB}(K) - q''_{BLA,OAF}(k),\ k = N_{OAF,}\ N_{OAF,} + 1, N_{OAF,} + 2, \cdots N. \quad (E.39)$$

(ix) Find the minimum of $\Delta q''(k)$, $\Delta q''_{min}$, and the corresponded zone number N_{min}. If

$$\left|\frac{\Delta q''_{min}}{CHF_{TB}(N_{min})}\right| \le 0.005 \quad (E.40)$$

then the critical power for the non-uniform AFD tube equals to W; the initial CHF location situates at $z(N_{min})$ and the initial CHF value equals to $q''(N_{min})$.

(x) Otherwise, iterate (iii) to (ix) until Eq (E.40) is satisfied.